The Role of the Free Fatty Acid Receptor 4 (FFAR4)/GPR120 in Adipocyte Lipolysis

Emma Tripp

A thesis submitted to the University of Birmingham for the degree of DOCTOR OF PHILOSOPHY

Institute of Metabolism and Systems Research

College of Medical and Dental Sciences

University of Birmingham

August 2022

UNIVERSITY OF BIRMINGHAM

University of Birmingham Research Archive

e-theses repository

Abstract

Metabolites are intermediates or end products of metabolism. They are also building blocks for a variety of metabolic pathways and often function as intracellular and extracellular signalling molecules. Several G protein-coupled receptors (GPCRs) have the capacity to sense metabolites to control hormone secretion, or to regulate the metabolic activity of certain cell types. In metabolic diseases, such as diabetes and obesity, metabolites are dysregulated. Therefore, further understanding the mechanisms behind metabolite sensing GPCR signalling could help to identify novel therapeutic targets. Within this study, using bioluminescence resonance energy transfer (BRET) and other imaging-based approaches, I present evidence that the free fatty acid receptor 4 (FFAR4), a GPCR for long chain fatty acids (LCFA), is localised in close proximity to the lipid droplet membrane in adipocytes, where it can act as an intracrine negative-feedback regulator of lipolysis by inhibiting cyclic adenosine monophosphate (cAMP) production in response to the local concentration of intracellular FFAs. This intracrine signalling phenomenon is anticipated to assist the FFAR4 in its control of adipocyte metabolism.

Contents

Peer reviewed publications during candidacy

Husted, A.S., Ekberg, J. H., **Tripp, E**., Nissen, T. A. D., Meijnikman, S., O'Brien, S. L., Ulven, T., Acherman., Y., Bruin, S.C., Nieuwdorp, M., Gerhart-Hines, Z, Calebiro, D., Dragsted, L.O., Schwartz., T.W., 2020. Autocrine negative feedback regulation of lipolysis through sensing of NEFAs by FFAR4/GPR120 in WAT. *Molecular Metabolism,* **42**(101103), pp. 1-10.

Submitted publications during candidacy

*Grimes, J., ***Tripp, E**., *Mistry, R., and Calebiro, D., 2021. GPCR Signaling in Nanodomains: Lessons from Single-Molecule Microscopy. *Submitted to Wiley.*

Janane F. Rahbani, Charlotte Scholtes, Damien M. Lagarde, Mohammed F. Hussain, Anna Roesler, Christien B. Dykstra, Jakub Bunk, Bozena Samborska, Shannon L O'Brien, **Emma Tripp**, Alain Pacis, Anthony R. Angueira, Olivia S. Johansen, Jessica Cinkornpumin, Matthew D. Lynes, Yang Zhang, Andrew P. White, William A. Pastor, Maria Chondronikola, Samuel Klein, Aaron Cypess, Yu-Hua Tseng, Zachary Gerhart-Hines, Patrick Seale, Davide Calebiro, Vincent Giguère, and Lawrence Kazak*., 2022. Combined α- and β- adrenergic receptor activation triggers thermogenesis by the futile creatine cycle. *Submitted to Nature Metabolism.*

***Tripp, E**., O'Brien, S. L., and Calebiro, D., 2022. Modern methods investigating GPCR signalling in live cells. *Submitted to British Journal of Pharmacology.*

Abstracts/Posters

'The New Paradigm of GPCR Signalling at Intercellular Sites in Metabolic Diseases' at COMPARE Annual Research Symposium, Birmingham, 2019.

'Impact of Free Fatty Acid 4 Receptor internalisation on signalling' at Society for Endocrinology BES meeting, Brighton, November 2019.

Talks

'Endosomal Signalling of the Free Fatty Acid 4 Receptor' at COMPARE ECR GPCR Symposium, Online, September 2020.

'The Role of the FFAR4 in Adipocytes' at BPS, Online, September 2021 (invited speaker).

Acknowledgements

I would like to express my deepest gratitude to my primary supervisor, Professor Davide Calebiro. Thank you for your guidance and constant curiosity for this project! I really appreciate how excited you have been over data I have shown in meetings, or about ideas that we have come up with to test.

This endeavour would have been impossible without Dr Shannon O'Brien. Firstly, thank you for teaching me the ways of BRET, but also thank you for your constant support and optimism – even when I have been overly critical or pessimistic. I cannot express how much I have enjoyed discussing science and working with you over the last four years. Truly, thank you.

A big thanks must also go to the rest of the Calebiro lab group. To Yann, Tamara, Zsombor, Gab, Edalat, Ravi, and Jak. You have all been wonderfully encouraging and caring during my time in Birmingham. I wish you all the best of luck for the future and I hope our paths cross again.

Additional thanks must go to my secondary supervisors Professor Gareth Lavery and Professor Stephen Hill. Both of your invaluable ideas helped to shape parts of this work. Thank you for interesting discussions and brainstorming ideas.

To my family and friends. Thank you for always being on the other end of the phone when I needed to chat. Especially when writing up. Your support has been invaluable. A further thank you must go to my MRC PhD pub quiz friends. To Kim, Greg, Isaac, Georgiana, and Phil. Thank you for pub and quiz antics during our PhD studies. They helped to keep me sane!

Finally, a large thanks must go to William. I cannot imagine finishing a PhD without you by my side. Thank you for being there through all my stress over the last four years and for listening to my repeated complaints.

List of Figures

List of Tables

List of abbreviations

7TM: Seven-transmembrane

ABD: Abdominal

AC: Adenylyl cyclase

ACS: Acyl-CoA synthetase

AGS: Activator of G protein signalling

Ai: Atglistatin

AKAR: A-Kinase activity reporter

AMPK: AMP activated protein kinase

ANOVA: Analysis of variance

AP-2: Adaptor protein-2

AT$_1$R: Angiotensin II type 1 receptor

ATGL: Adipose triglyceride lipase

ATP: Adenosine triphosphate

AUC: Area under the curve

BAT: Brown adipose tissue

BAY: BAY 59-9435

BCS: Bovine calf serum

BERKY: BRET sensors based on an ER/K linker and YFP

BRET: Bioluminescence resonance energy transfer

C: Carboxyl

cAMP: cyclic adenosine monophosphate

CAMYEL: cAMP sensor using YFP-Epac-RLuc

CCP: Clathrin-coated pits

CD36: Cluster of differentiation 36

CGI-58: Comparative gene identification-58

CLR: Calcitonin receptor-like receptor

CoA: Coenzyme A

CpdA: Compound A

CREB: cAMP response element-binding protein

CRISPR: clustered regularly interspaced short palindromic repeats

CXCR4: C-X-C chemokine receptor type 4

D$_1$R: Dopamine 1 receptor

DAG: Diacylglycerol

Dex: Dexamethasone

DMEM: Dulbecco's Modified Eagle Medium

DNA: Deoxyribonucleic acid

DPBS: Dulbecco's phosphate-buffered saline

ECL: Extracellular loop

ER: Endoplasmic reticulum

ERK: Extracellular signal-regulated kinase

FABP: Fatty acid binding protein

FATP: Fatty acid transport protein

FBS: Foetal bovine serum

FFA: Free fatty acid

FFAR: Free fatty acid receptor

FFAR4L: Long isoform FFAR4

FFAR4S: Short isoform FFAR4

FKBP: FK506-binding protein

FICRhR: Fluorescein-labelled catalytic subunit and rhodamine-labelled regulatory subunit

FLR: Finger-loop region

FRB: FKBP-rapamycin binding domain of FRAP

FRET: Fluorescence resonance energy transfer

FSHR: Follicle stimulating hormone receptor

GAP: GTPase activating protein

GCMS: Gas chromatography mass spectrometry

GDP: Guanosine diphosphate

GEF: Guanine-nucleotide exchange factor

GIP: Gastric inhibitory peptide

GIRK: G protein-coupled inwardly rectifying potassium

GLP-1: Glucagon-like peptide 1

GLUT: Gluteofemoral

GLUT2: Glucose transporter 2

GLUT4:	Glucose transporter 4
GPCR:	G protein-coupled receptor
GRK:	G protein receptor kinase
GTP:	Guanosine-5'-triphosphate
H8:	Helix eight
HBSS:	Hanks' balanced salt solution
HCAR:	Hydroxycarboxylic acid receptor
HEK293:	Human embryonic kidney 293
HILO:	Highly inclined and laminated optical sheet
HSL:	Hormone sensitive lipase
IBMX:	Methylisobutylxanthine
ICL:	Intracellular loop
IP_3:	Inositol 1,4,5-triphosphate
IR:	Insulin receptor
IRS:	Insulin receptor substrate
kDa:	Kilodalton
KO:	Knock-out
LB:	Lennox broth
LCFA:	Long-chain fatty acid
LHR:	Luteinising hormone receptor
MAG:	Monoacylglycerol
MAPK:	Mitogen-activated protein kinase
MCFA:	Medium-chain fatty acid
MEK:	Mitogen-activated protein kinase kinase
MGL:	Monoacylglycerol lipase
$mGluR_2$:	metabotropic glutamate receptor 2
Mini-G:	Minimal-G
mM:	Millimolar
mm:	Millimetre
MT_1R:	Melatonin 1 receptor
MUFA:	Monounsaturated fatty acids
N:	Amino

NAM:	Negative allosteric modulator
NE:	Norepinephrine
NK$_1$R:	Neurokinin-1 receptor
NLuc:	Nanoluciferase
nm:	Nanometre
nM:	Nanomolar
NSIAD:	Nephrogenic syndrome of inappropriate antidiuresis
OMM:	Outer mitochondrial membrane
OR:	Opioid receptor
PAM:	Positive allosteric modulator
PCR:	Polymerase chain reaction
PDE:	Phosphodiesterase
PDE2A3:	PDE2A splice variant 3
PI3K:	Phosphatidylinositol 3-kinase
PI$_4$P:	Phosphatidylinositol-4-phosphate
PIP$_2$:	Phosphatidylinositol 4,5-bisphosphate
PIP$_3$:	Phosphatidylinositol (3,4,5)-trisphosphate
PKA:	Protein kinase A
PKC:	Protein kinase C
PLC:	Phospholipase C
PLIN:	Perilipin
PTH:	Parathyroid hormone
PUFA:	Polyunsaturated fatty acids
RGS:	Regulator of G protein signalling
RLuc:	*Renilla* luciferase
RPM:	Revolutions per minute
SAT:	Subcutaneous adipose tissue
SCFA:	Short-chain fatty acid
SFA:	Saturated fatty acid
SIM:	Structured illumination microscopy
T3:	Triiodo-L-Thyronine
TAG:	Triacylglycerol

TCA:	Tricarboxylic acid
TGN:	Trans-Golgi network
TIRF:	Total internal reflection fluorescence
TSH:	Thyroid-stimulating hormone
UCP1:	Uncoupling protein 1
V:	Volts
V$_2$R:	Vasopressin 2 receptor
VAT:	Visceral adipose tissue
WAT:	White adipose tissue
WT:	Wild-type
α**-AR**:	Alpha-adrenergic receptor
β**-AR**:	Beta-adrenergic receptor
μ**F**:	Microfarads (capacitance)
μ**m**:	Micrometre
μM:	Micromolar
ρ**M**:	Picomolar

Contribution by others to the thesis:

All work presented in this thesis is my own apart from the following exceptions:

Figure 4.11A&B, Figure 4.15A&B, Figure 4.22C&D, and Figure 4.23F were BRET experiments kindly performed by Dr Shannon O'Brien (Institute of Metabolism and Systems Research).

Figure 4.17 Fatty acid extraction was kindly performed by Adam Boufersaoui (Institute of Metabolism and Systems Research) using samples provided by myself.

Figure 4.18 Fatty acid extraction and GCMS was kindly performed and analysed by Adam Boufersaoui (Institute of Metabolism and Systems Research) using samples provided by myself.

G protein and mini-G protein schematics are modifications from schematics kindly provided by Professor Nevin Lambert (Augusta University), (Wan et al., 2018).

1.0 Chapter one: Introduction

1.1 G protein-coupled receptors

Complex organisms require intricate signalling mechanisms to permit physiological homeostasis. G protein-coupled receptors (GPCRs) are transmembrane proteins, mainly located at the plasma membrane, which control many different cellular pathways by interacting with a diverse repertoire of extracellular chemical messengers. These messengers include, but are not limited to, hormones, neurotransmitters, metabolites, photons, odorants, and ions (Wacker et al., 2017). Considering there are over 800 genes encoding for GPCRs in the human genome, they are the largest receptor family in humans (Hauser et al., 2017). Consequently, GPCRs are attractive drug targets, and it is currently estimated that approximately 35% of approved drugs target this receptor family (Sriram and Insel, 2018).

1.1.1 GPCR Structure and Classification

Crystallisation studies have greatly advanced our understanding of GPCR structures. In 2000, the first crystal structure of a GPCR, bovine rhodopsin, was characterised by X-ray crystallography (Palczewski et al., 2000). Due to significantly lower expression of non-visual GPCRs and difficulties in GPCR purification owing to the negative effects of detergents on membrane stability, it was an additional seven years before the first non-visual GPCR was purified, crystalised, and its structure resolved (Cherezov et al., 2007). Many GPCR structures have now been successfully resolved, including those that are bound by agonists and antagonists, as well as those in complex with or without G proteins and β-arrestins (Munk et al., 2019).

These high-resolution structures confirmed that GPCRs have seven-transmembrane (7TM) spanning α-helices, connected by three intracellular and three extracellular

loops (ICLs and ECLs) with an extracellular amino (N) terminus and an intracellular carboxyl (C) terminus. Family A GPCRs have an additional intracellular amphipathic α-helix (in the C tail), named helix eight (H8), which is a region containing palmitoylated cysteine residues that tether the helix to the plasma membrane (Goddard and Watts, 2012). Most commonly, the extracellular α-helices form a pocket which permits ligand interaction, whereas the C-terminal domain and ICLs are responsible for interaction with downstream signalling molecules e.g., G proteins, G protein receptor kinases (GRKs), β-arrestins, and other signalling partners (Zhang et al., 2015). The 7TM domain forms the structural core of a GPCR and, through conformational rearrangements controlled by ligand interaction, these domains transduce extracellular ligand binding into intracellular signalling. Whilst GPCRs share a conserved 7TM structure across the superfamily, there is great variation in sequence homology between different GPCRs. GPCRs are therefore classified into the family A-F system based upon shared characteristic motifs (Attwood and Findlay, 1994, Fredriksson et al., 2003). This classification system covers all GPCRs present in both vertebrates and invertebrates and includes GPCR families that are non-existent in humans.

The A-F system orders GPCRs into six classifications based on sequence homology and functional similarities: family A, rhodopsin-like receptors; family B, secretin receptors; family C, metabotropic glutamate receptors; family D, pheromone receptors; family E, cyclic adenosine monophosphate (cAMP) receptors; and family F, frizzled and smoothened receptors (Attwood and Findlay, 1994). Human GPCRs can be further classified into five families which share common origins of evolution. These families are glutamate, rhodopsin-like, adhesion, frizzled/taste2, and secretin

(GRAFS) (Fredriksson et al., 2003). The major difference between these two classification systems is that family B GPCRs are split into adhesion and secretin families within the GRAF system. The rhodopsin-like GPCRs (family A) form the main GPCR family, consisting of approximately 670 receptors, where a large proportion of these receptors are olfactory (Lagerstrom and Schioth, 2008). The secretin and adhesion receptors (family B) are a small group of GPCRs distinguished by their large extracellular N-terminal domain. The glutamate receptors (family C) are distinguished by two unique structural characteristics: firstly, they have a large extracellular domain, and secondly, this receptor family form constitutive dimers (Lagerstrom and Schioth, 2008). In family B and C, the large extracellular domain contains the ligand binding site.

1.1.2 GPCR activation

Ligand binding to GPCRs induces structural rearrangements that enable GPCRs to recruit G proteins or β-arrestins, initiating the activation of intracellular signalling pathways (Rasmussen et al., 2011). For class A GPCRs, when the receptor is an inactive state, there is a salt bridge/ 'ionic lock' in place between two highly conserved amino acids in TM3 and TM6, incorporating the E/DRY motif which stabilises the inactive conformation (Rasmussen et al., 2011). When the receptor is activated by ligand binding, the 'ionic lock' is broken, there is an upward movement of TM3, an inward movement of TM5, and a major outward movement and rotation of TM6 (Tehan et al., 2014). This movement exposes an intracellular cytoplasmic cavity for G protein and β-arrestin binding (Rose et al., 2014). Intriguingly, G protein binding has also been demonstrated to stabilise pre-active/active conformations of the receptor in the absence of agonist, which, in some cases, can even block agonist binding to the ligand

binding pocket (DeVree et al., 2016). This suggests a possible bidirectional control of GPCR conformational changes from the intracellular G protein/β-arrestin binding domain, and the extracellular ligand binding region.

In 1957, it was first proposed that receptors are in a dynamic equilibrium between resting and active states (R and R*, respectively) (Del Castillo and Katz, 1957). It is now understood that GPCRs can exist in multiple conformations. For example, the β_2-adrenoceptor (β_2AR) has been shown to occupy at least four distinct transient conformational states: two inactive states where the ionic lock is either intact or broken (Noel et al., 1993), an intermediate state where the receptor is in a partially active conformation, and a fully active state (Bokoch et al., 2010, Calebiro et al., 2021, Kim et al., 2013, Kofuku et al., 2012, Liu et al., 2012b, Manglik et al., 2015, Nygaard et al., 2013). Some GPCRs are understood to spontaneously adopt active conformations capable of generating downstream signals, without the presence of an agonist – a phenomenon known as constitutive activity (Cerione et al., 1984).

Ligands for GPCRs can therefore be thought of as conformational stabilisers that direct GPCRs into distinct conformations that either stimulate or supress downstream signalling, and as such, ligands are characterised into groups dependent on their influence on downstream signalling. A full agonist has maximum intrinsic activity, a partial agonist has submaximal intrinsic activity, an antagonist has no intrinsic activity, and an inverse agonist has negative intrinsic activity (Berg and Clarke, 2018). A fully active GPCR requires G protein binding, in combination with agonist binding, to elicit its maximal response (Manglik et al., 2015, Nygaard et al., 2013).

In addition to agonists that occupy the evolutionary conserved orthosteric site of a GPCR, there are compounds which bind to GPCRs via alternative binding pockets. These compounds are named allosteric modulators and since they bind to a region of a GPCR that is typically less conserved, they are generally more subtype selective than ligands that bind at the orthosteric site (Foster and Conn, 2017). Allosteric modulators help to stabilise GPCRs into discrete conformations that can enhance or supress GPCR signalling by modulating the affinity or efficacy (or both) of the orthosteric agonist (Gentry et al., 2015, Gregory et al., 2010). These compounds are termed positive allosteric modulators (PAM) or negative allosteric modulators (NAM). Importantly, PAMs and NAMs modulate GPCR signalling in response to endogenous physiological ligands despite having no intrinsic activity (Foster and Conn, 2017). It has been suggested that PAMs alter the equilibrium between GPCR conformational states and stabilise the active conformation of the receptor when already bound to orthosteric agonist. For instance, this concept has been demonstrated by measuring single molecule fluorescence resonance energy transfer (FRET) between metabotropic glutamate receptor 2 (mGluR$_2$) dimers in the presence and absence of glutamate (orthosteric agonist) and the presence and absence of BINA (PAM) (Cao et al., 2021). The mGluR$_2$ was shown to oscillate between inactive and active states in its un-liganded (apo) state. On the addition of glutamate, the equilibrium was shifted so that a greater proportion of receptors occupied an active state, but only in the presence of BINA or nucleotide free G protein were the full population of receptors able to occupy a stable active conformation (Cao et al., 2021). Allosteric modulators are not required to be a hormone/small molecule, but they can also be a protein. G proteins are the most familiar allosteric modulators related to GPCRs since G protein

coupling is positively cooperative with orthosteric agonist binding (Gregory et al., 2010).

1.1.3 G proteins

GPCRs interact with heterotrimeric guanine nucleotide-binding regulatory proteins (G proteins) to relay their activation (Syrovatkina et al., 2016) (Figure 1.1). G proteins are composed of three subunits: $G\alpha$; $G\beta$; and $G\gamma$. Within the human genome, there are 33 genes encoding G protein subunits (Calebiro et al., 2021). This includes 16 genes for $G\alpha$, 5 genes for $G\beta$, and 12 genes for $G\gamma$ (Downes and Gautam, 1999). The downstream signalling pathway initiated by a GPCR largely depends on the class of $G\alpha$ subunit activated within the G protein heterotrimer. The $G\alpha$ subunits are grouped into four main families based upon signalling similarities and sequence homology: $G\alpha_{s/olf}$; $G\alpha_{i/o}$; $G\alpha_{q/11}$; and $G\alpha_{12/13}$ (Weis and Kobilka, 2018). Since multiple G protein subunits belong to each family, the physiological responses regulated by GPCRs and G proteins are extremely diverse (Calebiro et al., 2021).
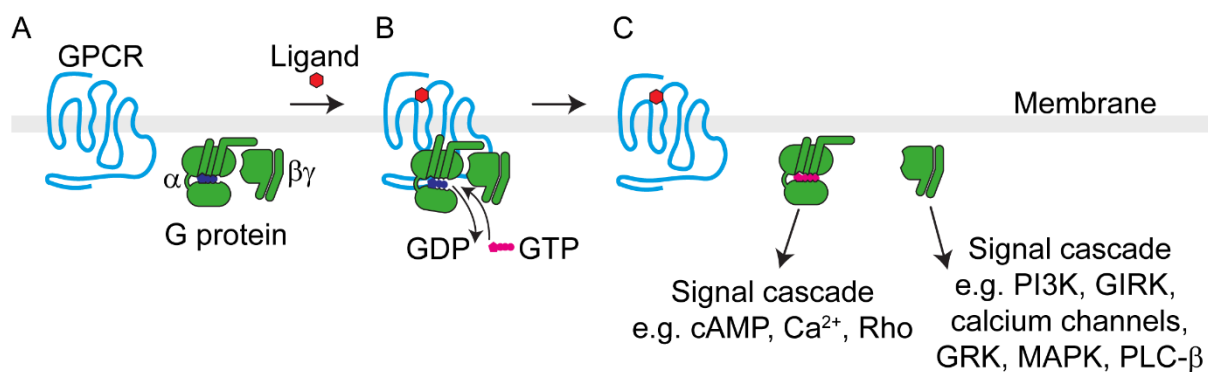
Figure 1. 1: GPCR mediated G protein activation.
Schematic illustrating classical GPCR and G protein activation. (**A**) A GPCR can interact with a heterotrimeric G protein upon ligand interaction. (**B**) Ligand interaction with a GPCR facilitates G protein binding. A conformational change occurs in the G protein which enables the exchange of GDP for GTP, and the G protein is activated.

(**C**) The G protein dissociates from the GPCR and the Gα subunit dissociates from the G$\beta\gamma$ subunit. This facilitates downstream signalling mediated through G proteins.

The G protein heterotrimer is anchored to membranes by lipid modifications of both Gα and G$\beta\gamma$ (Spiegel et al., 1991). G protein activity is controlled by guanosine-5'-triphosphate (GTP) and guanosine diphosphate (GDP). Gα consists of an alpha helical domain and a GTPase domain (Sprang, 1997). When inactive, Gα proteins are in complex with G$\beta\gamma$ subunits, and are GDP bound. Agonist binding to a GPCR promotes conformational rearrangements which increase the affinity of the receptor for G protein interaction (Lebon et al., 2011, Rasmussen et al., 2011, Rosenbaum et al., 2011, Xu et al., 2011). GDP bound G proteins bind to the exposed intracellular cytoplasmic cavity of a GPCR via the C-terminal region of the Gα subunit (Hamm et al., 1988). G protein binding to a GPCR triggers a rotation and displacement of the α5 helix of Gα (Oldham et al., 2006), which ultimately leads to the displacement of GDP (Alexander et al., 2014, Dror et al., 2015, Flock et al., 2015, Kaya et al., 2014, Sun et al., 2015, Van Eps et al., 2011). Since GTP is present at a higher concentration in the cytoplasm of the cell (Traut, 1994), this displacement facilitates the exchange of GDP for GTP. In this instance, the active GPCR acts as a guanine-nucleotide exchange factor (GEF) for G proteins. GTP binding to Gα promotes the dissociation of the G protein from the GPCR and the dissociation of Gα from G$\beta\gamma$. Once dissociated, G proteins can interact with their downstream effector proteins (Mahoney and Sunahara, 2016). Subsequently, G protein free active GPCR can further engage GDP bound G proteins to amplify its signal (Gurevich and Gurevich, 2019).

1.1.4 G protein dependent GPCR signalling

GPCR activation typically results in the downstream control of one, or more, of three major pathways. The $G\alpha_{s/olf}$ protein family couples to the stimulation of adenylyl cyclase (AC) to catalyse the production of cAMP from adenosine triphosphate (ATP) (Rasmussen et al., 2011, Sunahara and Taussig, 2002). On the contrary, the $G\alpha_{i/o}$ protein family couples to AC inhibition, principally AC5 and AC6 (Sunahara and Taussig, 2002). In some cases, persistent $G\alpha_{i/o}$ activation can lead to enhanced cAMP production (Watts and Neve, 2005). In this way, $G\alpha_{s/olf}$ and $G\alpha_{i/o}$ proteins help to control the production of cAMP to regulate the activation of protein kinase A (PKA) (Kim et al., 2007). The second major GPCR regulated signalling pathway is activated via the $G\alpha_{q/11}$ protein family. These G protein isoforms couple to phospholipase C (PLC) activation, an enzyme that breaks down membrane-associated phosphatidylinositol 4,5-bisphosphate (PIP_2) into inositol 1,4,5-triphosphate (IP_3) and membrane-associated diacylglycerol (DAG) (Rhee, 2001). After its production, IP_3 can bind to IP_3 receptors present on the endoplasmic reticulum (ER), inducing calcium release which facilitates, in concert with DAG, the activation of protein kinase C (PKC) (Rhee, 2001). Finally, GPCRs can couple to the $G\alpha_{12/13}$ protein family to stimulate Rho GEFs, leading to the activation of Rho family small GTPases to regulate the control of actin dynamics (Pierce et al., 2002). Originally GPCRs were only thought to couple to one G protein family, however, it is now understood that many GPCRs are promiscuous i.e., they can signal via multiple different G protein subtypes (Okashah et al., 2019).

In addition to the $G\alpha$ subunit, the $G\beta$ and $G\gamma$ subunits can also function as key signal transducers of GPCR signalling. The $G\beta$ and $G\gamma$ subunits have a close association and are considered as one functional unit (Syrovatkina et al., 2016). After the

disassociation of Gα and Gβγ proceeding receptor activation, Gβγ can interact with membrane proteins, receptors, or other downstream effectors to further diversify GPCR signalling. Gβγ is understood to regulate G protein-coupled inwardly rectifying potassium (GIRK) channels (Logothetis et al., 1987), GRKs (Koch et al., 1993, Pitcher et al., 1992b), calcium channels (De Waard et al., 1997, Herlitze et al., 1996), mitogen-activated protein kinases (MAPK) (Luttrell et al., 1997), PLC-β (Camps et al., 1992, Illenberger et al., 2003), and phosphatidylinositol 3-kinases (PI3K) (Vadas et al., 2013).

G proteins cannot enter a new cycle of activation until GTP hydrolysis has occurred, however, Gα proteins have weak intrinsic GTPase activity (Ross, 2008). This deactivation process can be enhanced by the regulator of G protein signalling (RGS) family. RGS proteins bind to Gα proteins via an 'RGS-box' domain to stabilise the Gα subunit into a confirmation that lowers the energy needed for GTP hydrolysis, returning the G protein to its inactive GDP-bound state (Berman et al., 1996). In addition to RGS proteins, activators of G protein signalling (AGS) influence G protein signalling in an independent manner from GPCR activation. AGS proteins can modulate G protein activity in three main ways: they can act as GEFs to facilitate the exchange of GDP for GTP, they can prevent guanine nucleotide disassociation, and they can interact with the βγ subunit (Blumer and Lanier, 2014).

1.1.5 GRKs and β-arrestins

After GPCR dependent G protein activation, a mechanism is required to stop further recruitment of G proteins to GPCRs (Gurevich and Gurevich, 2019). This process can be terminated in a two-step mechanism by the recruitment of GRKs and β-arrestins.

In humans, there are four GRKs (GRK2,3,5, and 6) known to be ubiquitously expressed, in addition to two β-arrestin isoforms (β-arrestin 1 and β-arrestin 2) (Matthees et al., 2021). After G protein disassociation from an active GPCR, GRKs bind, are allosterically activated, and phosphorylate GPCRs at intracellular serine/threonine residues located at the C-terminus or at ICLs (Gurevich and Gurevich, 2019, Krupnick and Benovic, 1998, Pitcher et al., 1992a) (Figure 1.2). These phosphorylations increase the affinity for β-arrestin to bind to the phosphorylated receptor (Krupnick and Benovic, 1998). β-arrestin engages to the active GPCR cavity via its finger-loop region (FLR) and inserts into the transmembrane helix bundle of the receptor (Kang et al., 2015). This "core" interaction is associated with high affinity arrestin binding and uncoupling of the G protein interaction with the GPCR, as it spatially blocks G protein binding (Kang et al., 2015). Recently, it has also been shown that the phosphorylated C-terminus of a GPCR can interact with the N-terminus of arrestin, without interaction of the FLR with the active GPCR cavity and transmembrane helix bundle (Nguyen et al., 2019, Thomsen et al., 2016). This "hanging" arrestin engagement can facilitate further GPCR-dependent activation of G proteins whilst still enabling β-arrestin to adopt an active conformation and increase receptor internalisation (Nguyen et al., 2019). The configuration of a GPCR with β-arrestin has been proposed mediated by the specific GRK subtypes that it interacts with (Drube et al., 2022).
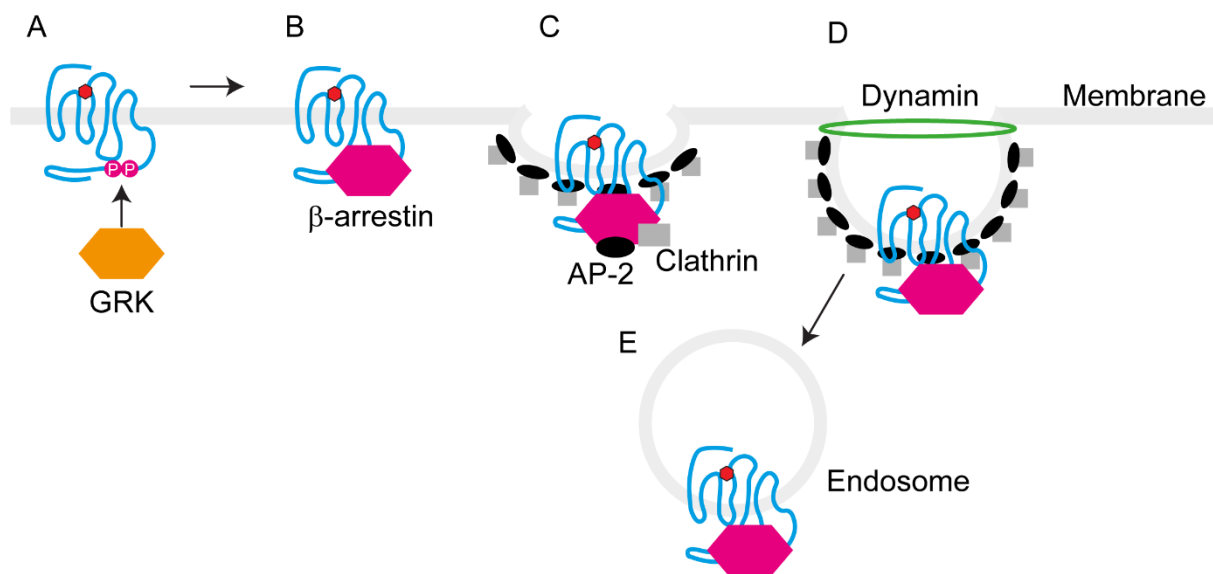
Figure 1. 2: GPCR internalisation upon interaction with GRK and β-arrestin.

Schematic illustrating classical GPCR internalisation. (**A**) The dissociation of a G protein from a GPCR enables GRK binding and phosphorylation of the receptor at the intracellular C-terminus. (**B**) C-terminal phosphorylation increase the affinity of the receptor for arrestin binding, which initiates the start of the internalisation complex. (**C**) Simply, β-arrestin acts as an AP-2 and clathrin adaptor to facilitate the formation of a clathrin coated pit. (**D**) The matured pit invaginates and is pinched off from the plasma membrane by dynamin. (**E**) The internalised clathrin-coated vesicle is uncoated, and typically fuses to a sorting endosome for degradation, recycling, or other, trafficking pathways.

1.1.6 β-arrestin mediated GPCR signalling

As well as impacting GPCR-G protein interactions, β-arrestins can function as GPCR-dependent signalling molecules. Upon binding of β-arrestin to an active and phosphorylated GPCR, a conformational change occurs within β-arrestin, which exposes its C-terminal domain (Matthees et al., 2021). The C-terminal domain contains motifs that permit binding of adaptor protein-2 (AP-2) and clathrin (Goodman et al., 1996), in addition to a phosphorylation site for mitogen-activated protein kinase

kinase (MEK). GPCR-dependent β-arrestin activation is known to activate the MAPK pathway. It has been hypothesised that when β-arrestin is bound to an agonist stimulated GPCR, it can recruit Raf and MEK. MEK phosphorylates β-arrestin at Thr[383] inducing a large conformational change in β-arrestin and the subsequent interaction with the GPCR C-terminal domain. Extracellular signal-regulated kinase (ERK) subsequently associates and is activated by MEK (Cassier et al., 2017). In doing so, β-arrestins function as scaffolds to facilitate the recruitment and activation of other proteins. β-arrestins have also been found to interact with members of the Src family of tyrosine kinases (Luttrell et al., 1999, Pakharukova et al., 2020), phosphodiesterases (PDEs) (Perry et al., 2002), and the DAG kinase family (Nelson et al., 2007).

1.1.7 GPCR internalisation and trafficking

GPCR function is tightly controlled by its trafficking profile (Wang et al., 2018a). Prolonged stimulation of a GPCR can lead to its internalisation from the plasma membrane into intracellular compartments (Pierce et al., 2002). There are several proposed mechanisms for this internalisation process, however, the best understood pathway is clathrin-mediated endocytosis. In the classical view, the agonist occupied receptor binds β-arrestin, which further interacts with AP-2 and clathrin to direct GPCRs into clathrin-coated pits (CCPs) (Krupnick and Benovic, 1998, Luttrell et al., 1999) (Figure 1.2). GPCRs subsequently endocytose after dynamin, a small GTPase, pinches off clathrin-coated vesicles from the plasma membrane and permits their entry into the cell (Doherty and McMahon, 2009). Once the GPCR has internalised into the endosomal compartment, it may be directed back to the plasma membrane, into lysosomes, or to the trans-Golgi network (TGN) via recycling, degradation, or

retrograde pathways, respectively (Calebiro and Godbole, 2018). Internalisation can decrease the strength or duration of GPCR signalling, however, a reduction in the number of surface receptors does not necessarily mean a decrease in the maximal response (Sorkin and von Zastrow, 2009).

Rab GTPases, the largest group of the Ras-related GTPase superfamily, (Wang and Wu, 2012), have distinct subcellular distributions to facilitate the correct trafficking of GPCRs, and other proteins, to specific subcellular compartments. In an inactive state, Rab GTPases are GDP bound, and after association with GTP, controlled by GEFs and GTPase activating proteins (GAPs), Rab proteins can interact with downstream effectors (Wang et al., 2018a).

Rab5 is the most well characterised Rab protein in terms of its involvement in GPCR trafficking. Rab5 has a role in the regulation of internalised GPCR trafficking into the early endosome compartment (Seachrist and Ferguson, 2003). Rab5 has also been proposed to have a role in the constitutive trafficking of certain GPCRs into the endosome compartment (Snyder et al., 2013). Internalisation into the early endosome compartment is a checkpoint in GPCR trafficking, and from this point, GPCRs are directed into recycling or degradation pathways.

Rab4 and Rab11 support the recycling of endosomal GPCRs back to the plasma membrane, either through rapid or slow mechanisms, respectively (Li et al., 2008, Wang et al., 2018a). Rab4 is present in fast recycling endosomes and aids in the control of the rapid recycling of several GPCRs from the endosomal network to the plasma membrane, including the β_2AR, and is often associated with rapid re-

14

sensitisation of GPCRs after agonist induced desensitisation (Yudowski et al., 2009).

On the other hand, Rab11 is present in the TGN, post-Golgi vesicles (Satoh et al., 2005), and recycling endosomes (Tower-Gilchrist et al., 2011), and helps to regulate the slow recycling of GPCRs back to the plasma membrane (Li et al., 2008). Rab7 and Rab9 have been demonstrated to aid in the transport of internalised GPCRs into late endosomes, slow recycling endosomes, the Golgi complex, and lysosomes. Typically, GPCR trafficking into Rab7 and Rab9 positive compartments is associated with receptor degradation (Wang et al., 2018a).

As well as trafficking via internalisation from the plasma membrane, GPCRs traffic anterogradely. After translation and assembly in the ER, GPCRs are transported from the ER to the Golgi (Wei et al., 2019). Following GPCR transportation through the Golgi complex, GPCRs are directed to the cell surface (Wei et al., 2019). Rab proteins also have roles in the regulation of anterograde GPCR trafficking. Rab1, Rab2, Rab6, and Rab8 all have roles in this process. Rab1 is thought to be essential in the trafficking of many GPCRs from the ER to the Golgi and subsequently onto the cell surface (Filipeanu et al., 2006). Loss of function mutations or inhibition of expression of Rab1 has been demonstrated to prevent the cell surface expression of the α_{1A} and α_{1B} adrenergic receptors (α_{1A}-AR/α_{1B}-AR) (Filipeanu et al., 2006), the β_1-AR, the β_2-AR (Dupre et al., 2006, Filipeanu et al., 2006, Li et al., 2010b), the angiotensin II type 1 receptor (AT$_1$R) (Filipeanu et al., 2004, Wu et al., 2003, Yin et al., 2011), the AT$_2$R (Zhang et al., 2009), and the human calcium sensing receptor (Zhuang et al., 2010). Such data imply that Rab1 is an essential mediator of anterograde trafficking of many GPCRs to the plasma membrane. Rab2 and Rab6 are suggested to coordinate the trafficking of GPCRs between the Golgi and the ER via anterograde and retrograde

transport mechanisms (Wang and Wu, 2012). Rab2 is principally localised to the ER-Golgi intermediate compartment, whereas Rab6 has a mainly Golgi localised expression (Hutagalung and Novick, 2011). The coordinated control of Rab2 and Rab6 are understood to be involved in the anterograde transport of proteins destined for the plasma membrane (Wu et al., 2003). Finally, Rab8 is localised in the TGN and has been suggested to regulate the post-Golgi trafficking of several GPCRs to the plasma membrane (Sato et al., 2007).

1.2 Compartmentalised GPCR signalling

Originally, GPCR localisation and signalling were considered restricted to the cell surface. Over the last twenty years, owing to the design of improved methods to investigate GPCR signalling, an expanse of evidence demonstrates that select GPCRs can be activated at different intracellular sites to generate distinct intracellular signals which might be of physiological relevance (Calebiro et al., 2009, Eichel and von Zastrow, 2018, Godbole et al., 2017, Irannejad et al., 2013, Yarwood et al., 2017). GPCR signalling and trafficking are no longer thought of as separate mechanisms, but a way for GPCRs to produce specific biological responses by signalling from unique intracellular locations. Intracellular GPCR signalling is proposed to be either internalisation dependent – where the receptor is activated at the plasma membrane, internalises, and is activated again in the endosomal or TGN to produce an intracellular 'second wave' of activity (Calebiro et al., 2009, Ferrandon et al., 2009, Godbole et al., 2017, Wright et al., 2021). Or internalisation independent – where pools of receptor are already present at intracellular sites, producing local responses after activation via cell-membrane permeable, membrane transported, or intracellularly produced, agonists (Irannejad et al., 2017, Suofu et al., 2017). GPCRs are now

proposed active at many intracellular compartments, including the endosomal network (Irannejad et al., 2013, Jensen et al., 2017, Kuna et al., 2013, Merriam et al., 2013, Slessareva et al., 2006, Sposini et al., 2020, Wan et al., 2018, White et al., 2020, Wright et al., 2021), lysosomes (Rozenfeld and Devi, 2008), the ER (Revankar et al., 2005, Vincent et al., 2016), nuclear membranes (Di Benedetto et al., 2014, Joyal et al., 2014, Re et al., 2010, Vincent et al., 2016), the mitochondria (Benard et al., 2012, Suofu et al., 2017), and the Golgi/TGN (Godbole et al., 2017, Irannejad et al., 2017, Nash et al., 2019, Wan et al., 2018). This has raised many questions in the field i.e., how do endogenous GPCR ligands access intracellular pools of GPCR? Which endogenous agonists activate intracellular GPCR pools? How do such agonists control whether a GPCR mediates a transient or sustained signalling response? Also, is intracellular GPCR signalling physiologically relevant?

1.2.1 Early evidence for compartmentalised GPCR signalling

Early evidence suggesting that GPCRs signal from intracellular compartments came from non-classical, G protein-independent, signalling mechanisms. β-arrestins, adaptor molecules of GPCR endocytosis, were found to act as GPCR associated scaffolds to facilitate the activation of MAPK at the endosomes (DeFea et al., 2000, Terrillon and Bouvier, 2004). Activation of MAPKs through β-arrestins was considered to be both spatially and temporally different from the activation of MAPKs through G protein dependent mechanisms (Cassier et al., 2017). For example, G protein mediated activation of ERK was demonstrated to be rapid and transient, reaching a maximum within minutes (Ahn et al., 2004, Shenoy et al., 2006). On the other hand, β-arrestin mediated activation of ERK was found to have a slower onset, typically taking 5-10 minutes to reach a maximum. In this way, β-arrestin dependent ERK

activation was suggested more persistent than G protein dependent ERK activation, where β-arrestin dependent ERK activation was demonstrated to last for more than an hour, mainly occurring in the cytosol (Ahn et al., 2004, Shenoy et al., 2006). It was proposed that an intracellular complex of β-arrestin and GPCR could mediate a 'second wave' of G protein independent activity from the endosomes, separate from GPCR activation at the plasma membrane (DeFea et al., 2000, Tohgo et al., 2003, Tohgo et al., 2002). However, although there is evidence that β-arrestins activate ERK independently of G protein signalling, contradictory results have shown β-arrestin isoforms are not always essential for ERK activation (O'Hayre et al., 2017). For example, O'Hayre et al. used small interfering RNA, or genome-editing, to deplete β-arrestin 1 and β-arrestin 2, where it was found that although β-arrestin 2 was essential for β_2-AR internalisation, both β-arrestin isoforms were superfluous for the activation of ERK (O'Hayre et al., 2017). In addition, a further study corroborated these findings by using gene-edited cells deficient in Gα or β-arrestin to show that ERK activation, for several GPCRs, requires G protein activation and not β-arrestin activation (Grundmann et al., 2018).

1.2.2 Evidence for intracellular G protein dependent GPCR signalling

It has since been discovered that G proteins are recruited to intracellular endocytic membranes to mediate endosomal GPCR signalling. A first potential indication of G protein dependent GPCR signalling at the early endosomes came from Slessareva et al. whilst investigating the Ste2 pheromone receptor in yeast (Slessareva et al., 2006). Using a constitutively active form of the Gα G protein subunit, Gpa_1, it was demonstrated that the active form of Gpa_1 accumulated at distinct sites within the cell, colocalising with Snf7, a marker of early endosomes. Furthermore, active Gpa_1 was

observed to interact with the endosomal PI3K Vsp34 catalytic subunit, increasing the availability of phosphatidylinositol 3-phosphate. Endosomal Ste2 receptor signalling was proposed to elicit functional differences in the yeast mating response compared to Ste2 receptor signalling at the plasma membrane (Slessareva et al., 2006). Shortly after, Boivin et al. demonstrated, using cell fractionation experiments in cardiomyocytes, that the β_1AR was present in the nuclear fraction where it could control $G\alpha_s$ dependent cAMP production (Boivin et al., 2006). These studies gave a first possible hint that some GPCRs might signal through G proteins on intracellular membranes.

More direct evidence for this intracellular signalling phenomenon came from two independent studies investigating the thyroid-stimulating hormone (TSH) (Calebiro et al., 2009) or the parathyroid hormone (PTH) receptors (Ferrandon et al., 2009). Calebiro et al. demonstrated in mouse thyroid follicles expressing a ubiquitous FRET reporter for cAMP, that activation of the TSHR with TSH generated persistent cAMP production which could not be supressed after agonist wash-out. Using subcellular fractionation methods, to assess AC activity in the absence of the plasma membrane, as well as inhibitors of endocytosis, to inhibit receptor internalisation, this persistent signal was found to be mediated by intracellular TSHR (Calebiro et al., 2009). A later follow-up study demonstrated that the TSHR traffics retrogradely to membranes of the TGN to activate a resident pool of $G\alpha_s$ and AC. The signalling of the TSHR at the TGN was demonstrated to control local cAMP production and PKA activation, a phenomenon proposed necessary for the efficient transcription of TSH-regulated genes (Godbole et al., 2017).

On the other hand, Ferrandon et al. demonstrated, again using a FRET reporter for cAMP, that the PTHR produces persistent, internalisation dependent, cAMP signals from the endosomes. Interestingly, sustained signalling of the PTHR was found reliant on the specific agonist used since it was stimulated by PTH_{1-34}, and not by human parathyroid related peptide ($PTHrP_{1-36}$). Agonist specific effects were suggested to be due to higher affinity of PTH_{1-34} binding to the receptor than $PTHrP_{1-36}$ (Ferrandon et al., 2009). Similar findings were revealed for the β_2-AR, where the receptor was discovered to signal from the early endosomes via active $G\alpha_s$, contributing to overall cAMP production, and assisting the efficient control of cAMP response element-binding (CREB) protein dependent transcription (Irannejad et al., 2013, Tsvetanova and von Zastrow, 2014). Conformation selective, fluorescently labelled, nanobody biosensors of active β_2-AR or active $G\alpha_s$ (Irannejad et al., 2013), and tools capable of initiating cAMP production specifically at the endosome compartment (Tsvetanova and von Zastrow, 2014), supported the demonstration of these findings. Similar approaches, using conformation specific nanobodies, subsequently revealed that a resident pool of β_1-AR can signal from the Golgi complex in response to adrenaline and other cell-impermeant agonists. It was further demonstrated that Golgi resident β_1ARs were able to access adrenaline by its transportation through the organic cation transporter 3 (Irannejad et al., 2017).

The duration and degree of intracellular GPCR signalling varies substantially between different GPCRs. Intracellular GPCR signalling can be either sustained, as for the PTHR (Ferrandon et al., 2009) and TSHR (Calebiro et al., 2009), or more transient, as for the β_2-AR (Irannejad et al., 2013) or the dopamine 1 receptor (D_1R) (Kotowski et al., 2011). This might be due to the affinity of ligands for specific GPCRs (Ferrandon

et al., 2009); however, it might also be due to interaction with β-arrestins. More recently, it has been proposed that β-arrestins may be involved in prolonged activation of G protein-dependent endosomal signalling, whereby GPCRs interact with both arrestins and G proteins at the endosomal compartment in a 'megaplex' (Cahill et al., 2017, Thomsen et al., 2016). Further structural evidence for this phenomenon was demonstrated by cryo-electron microscopy, where β-arrestin was demonstrated to bind to a GPCR via its 'tail' interaction, and not its 'core' interaction, which still facilitated the binding of $G\alpha_s$ to the receptor core (Nguyen et al., 2019). The ability of GPCRs to recruit β-arrestins or G proteins or both β-arrestins and G proteins at the endosomal compartment adds a new layer of complexity to GPCR signalling and is most likely a factor which strongly influences the intracellular signalling potential of many GPCRs.

1.2.3 Consequences of compartmentalised GPCR signalling

Evaluating the consequences of compartmentalised GPCR signalling is not without its challenges. Nevertheless, it has been proposed that endosomal signalling is functionally relevant to physiology. For example, sustained luteinising hormone receptor (LHR) dependent cAMP signalling after receptor internalisation was demonstrated required for oocyte meiosis in ovarian follicles (Lyga et al., 2016). In addition, endosomal signalling of the neurokin-1 receptor (NK_1R) (Jensen et al., 2017) and the calcitonin receptor-like receptor (CLR) (Yarwood et al., 2017) induced sustained spinal neuron excitation, a response required for nociception. To inhibit this effect, endosomally directed antagonists were designed to specifically attenuate endosomal signalling of these receptors, which offered improved pain relief in animal models of inflammatory pain compared to non-endosomally directed antagonists

(Jensen et al., 2017, Mai et al., 2021, Yarwood et al., 2017). Another study designed endosome directed lipoparticles containing delta opioid receptor (OR) agonist to specifically promote endosomal DOR signalling in primary mouse neurons. This approach again attenuated neuronal excitability and reduced pain responses (Jimenez-Vargas et al., 2020). Evidence also suggests that compartmentalised GPCR signalling is of pathophysiological relevance. For example, AP-2 σ-subunit mutations associated with familial hypocalciuric hypercalcemia type-3 have been found to impair endosomal signalling of the calcium-sensing receptor (Gorvin et al., 2018). In addition, β_1-AR signalling from the Golgi, and not the plasma membrane, has been suggested to mediate catecholamine-induced cardiac hypertrophy (Nash et al., 2019). These studies suggest that subcellular GPCR signalling is of physiological and pathophysiological relevance and highlight the potential therapeutic value of targeting spatially bias GPCR signals.

1.2.4 Genetically encoded methods detecting compartmentalised GPCR signalling

Genetically encoded tools, especially FRET/BRET-based biosensors, continue to be essential for the investigation of compartmentalised GPCR signalling. They have facilitated the research of GPCRs in living cells with higher spatiotemporal resolution compared to endpoint biochemical assays. Such tools bypass the need for cell lysis and facilitate the real-time detection of GPCR signalling in live cells. This not only gives better insight into the dynamics of GPCR signalling, but it also allows the measurement of real-time protein-protein interactions or conformational changes without membrane disruption. As such, these methods are commonly used in the field of GPCR research

to investigate the mechanisms of GPCR signalling, second messenger production, and GPCR trafficking.

1.2.4.1 The theory of FRET/BRET

FRET is a methodology that can be used to detect interactions between proteins or within a protein via fusion to donor and acceptor fluorophores (Figure 1.4A). In FRET, when a donor and an acceptor fluorophore are in close proximity, excitation of the donor fluorophore, aiding its transition into an 'excited state', enables the non-radiative energy transfer, through dipole-dipole coupling, from donor to acceptor fluorophore if three factors are met: (1) the emission spectrum of the donor fluorophore must overlap with the excitation spectrum of the acceptor fluorophore; (2) the distance between the donor and acceptor molecules must be typically less than 10 nm; and (3) there must be a favourable orientation of the donor and acceptor molecule dipoles in space (Sekar and Periasamy, 2003). Using FRET, protein-protein interactions and conformational rearrangements can be measured by microscopy methods and/or fluorimeters through tagging the proteins of interest with complimentary FRET pairs e.g., CFP and YFP (Sekar and Periasamy, 2003).
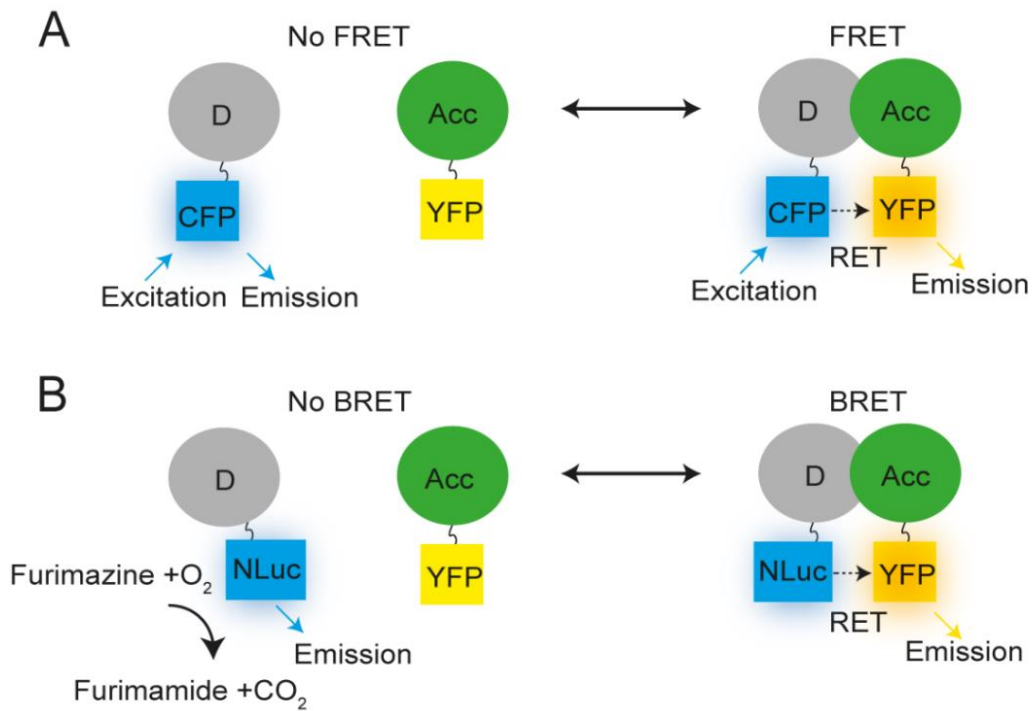
Figure 1. 3: FRET/BRET.

Schematic to illustrate the detection of protein-protein interaction using FRET and BRET. (**A**) To study protein-protein interaction using FRET, donor (D) and acceptor (Acc) proteins are fused to suitable fluorophores e.g., CFP and YFP. Upon excitation of the donor (CFP), non-radiative resonance energy transfer (RET) can occur from donor to acceptor fluorophores when proteins are in close proximity (typically less than 10 nm). (**B**) To study protein-protein interaction using BRET, donor (D) and acceptor (Acc) proteins are fused to suitable fluorophores e.g., NLuc and YFP. Furimazine, the luciferase substrate, is oxidised by NLuc to produce furimamide, CO_2, and light. The excited donor can non-radiatively transfer energy to the acceptor fluorophore if in close enough proximity.

BRET, similarly, to FRET, can be used to study protein-protein interactions and conformational changes (Figure 1.4B). However, no external light excitation of the donor molecule is required because the methodology harnesses bioluminescent luciferase enzymes (Pfleger et al., 2006). Through the years, there have been several improvements made to the luciferase enzymes used in BRET. *Renilla* Luciferase

(RLuc) and mutated RLuc8, isolated from the *Renilla Reniformis* sea pansy, have been widely used in the literature – particularly for use in GPCR research (Pfleger et al., 2006). NanoLuciferase (NLuc), a smaller, 19.1 Kilodalton (kDa) luciferase subunit derived from a larger, multi-subunit, luciferase isolated from the deep-sea shrimp *Oplophorus gracilirostris*, is becoming the new standard owing to its smaller size and increased brightness compared to RLuc (Hall et al., 2012). Both RLuc or NLuc, oxidise coelenterazine or furimazine substrates, respectively, in the presence of O_2 to produce light. In its excited state, the luciferase donor molecule has the capacity to non-radiatively transfer energy to an acceptor fluorophore in a manner like-to FRET (El Khamlichi et al., 2019).

1.2.4.2 FRET vs BRET

There are both advantages and disadvantages of using BRET and FRET techniques. Due to BRET reliance on bioluminescent luciferase enzymes as donor molecules, there is no excitation required from an external light source. Conversely, external light excitation, as required for FRET, can result in photobleaching, excitation of cellular autofluorescence, and light scattering (Hamdan et al., 2006). BRET bypasses such limitations. In addition, FRET can be susceptible to further complications because it is possible to excite both donor and acceptor fluorophores with one excitation wavelength. With BRET, the acceptor fluorophore is not excited with the addition of luminescent substrate, as such, acceptor excitation only arises from resonance energy transfer from the donor luciferase (Hamdan et al., 2006). Compared to FRET methods, BRET signals are very dim. As such, BRET imaging is more challenging, and it is harder to obtain spatial information of where resonance energy transfer occurs – which can be acquired more easily when using FRET microscopy methods. In addition, the

intensity or duration of external light excitation can be amplified to enable FRET detection in samples with low signal. This is not the case in BRET studies, which relies on sensitive instrumentation capable of measuring low-light levels (Hamdan et al., 2006).

1.2.4.3 Nanobodies

Conformational biosensors, based on nanobodies, have been crucial for the investigation of compartment specific GPCR signalling. Nanobodies, small (15 kDa), conformation specific, single-domain, camelid antibodies were principally designed to stabilise GPCRs into active conformations for crystallisation purposes (Rasmussen et al., 2011). However, nanobodies engineered to bind the active conformation of a specific GPCR can be used to detect spatiotemporal GPCR activation (Irannejad et al., 2013) (Figure 1.4A&B). In addition, nanobodies have also been designed to recognise nucleotide-free $G\alpha_s$ (e.g., Nb37) to detect GDP exchange from the $G\alpha$ subunit as a read-out of $G\alpha_s$ activation. Nanobody-based GPCR or $G\alpha_s$ conformational biosensors translocate from the cytoplasm to membranes containing active GPCR or active $G\alpha_s$, respectively (Irannejad et al., 2013). By fusing nanobodies with a fluorophore/luciferase, the ligand induced recruitment of the nanobody to its specific GPCR can be measured via imaging- or FRET/BRET-based approaches. In an elegant study, Irannejad et al., found that agonist treatment of the β_2-AR induced recruitment of Nb80, a nanobody specific for active $\beta-$ARs, and Nb37, a nanobody detecting $G\alpha_s$ activation, to the plasma membrane and subsequently to the early endosomes. This indicated active β_2-AR first at the plasma membrane, and then at the endosome compartment (Irannejad et al., 2013). A similar approach was used to detect endosomal activation of mu/delta OR signalling in neurons. Using Nb33, a

nanobody specific for active conformation ORs, activation of ORs with peptide agonists met-enkephalin and β-endorphin, were demonstrated to produce a first wave of OR activation at the plasma membrane, followed by an internalisation-dependent, second wave of activation from the endosomes (Stoeber et al., 2018). Interestingly, after stimulation of ORs with clinically relevant opioid drugs (i.e., morphine), a rapid, internalisation-independent, activation of ORs was detectable at the Golgi compartment – distinct from endosomal activation (Stoeber et al., 2018). A further study, again using a nanobody approach (Nb39), demonstrated ligand induced activation of the kappa OR from the Golgi compartment, however, there was no further investigation as to whether this activation was dependent on receptor internalisation (Che et al., 2020). Additional studies using nanobody approaches demonstrate the activation of internalised $G\alpha_s$ and $G\alpha_i$, coupled GPCRs across many endosomal compartments, including very early endosomes (Sposini et al., 2017), early endosomes (Sposini et al., 2020), and even late endosomes/lysosomes (Kunselman et al., 2021).
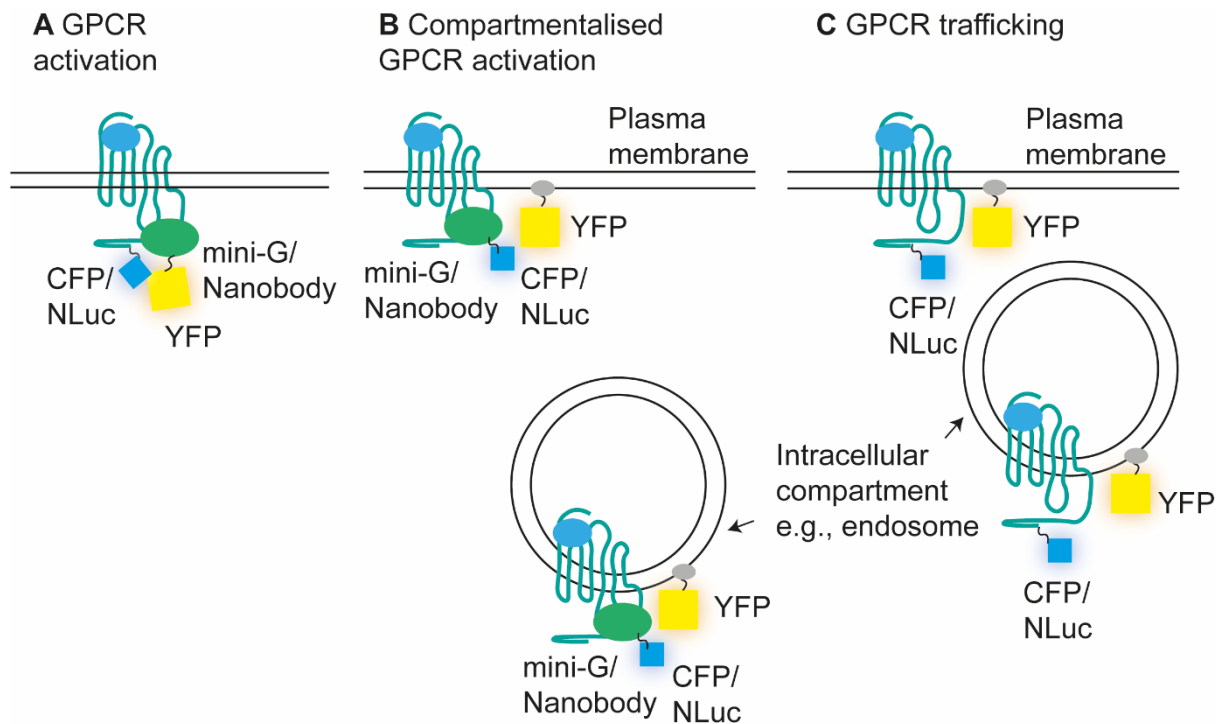
Figure 1. 4: Key resonance energy transfer methods to detect compartmentalised GPCR activation and GPCR trafficking.

Schematic to illustrate key genetically encoded resonance energy transfer methods to quantitatively detect (**A**) GPCR activation and (**B**) compartmentalised GPCR activation, using mini-G proteins and nanobodies, and (**C**) GPCR trafficking.

Intriguingly, nanobodies can be used to locally inhibit subcellular GPCR signalling. Irannejad et al. demonstrated that agonist stimulation of the β_1-AR induced Nb80 and Nb37 recruitment to GalT (a marker of the Golgi), indicative of β_1-AR activation and $G\alpha_s$ activation at the Golgi complex (Irannejad et al., 2017). Nb80 overexpression was found to block β-AR signalling at high concentrations, likely through steric occlusion of $G\alpha_s$ proteins to the β-ARs (Staus et al., 2014). Therefore, Nb80 was targeted to subcellular compartments to locally block β_1-AR signalling. By taking advantage of the FK506-binding protein (FKBP) and FKBP-rapamycin binding domain of FRAP (FRB) inducible dimerization system (Choi et al., 1996), Nb80 was specifically targeted to the

plasma membrane or the Golgi membranes. This inducible system was used to demonstrate that inhibiting β_1-AR signalling at the Golgi complex had a greater inhibitory effect on cAMP production than inhibiting β_1-AR signalling at the plasma membrane (Irannejad et al., 2017). Similar approaches have demonstrated that the D_1R is capable of signalling at the plasma membrane and the Golgi complex, where it stimulates cAMP production and local PKA activation through $G\alpha_s$ (Puri et al., 2022). With these studies in mind, nanobodies have been used with remarkable success to investigate subcellular GPCR activation.

1.2.4.4 Minimal-G probes

More recently, minimal-G (mini-G) probes, engineered $G\alpha$ subunits, were designed and have aided the investigation of subcellular GPCR signalling (Nehme et al., 2017, Wan et al., 2018). Originally, mini-G probes, like-to nanobodies, were designed to aid the crystallisation of GPCRs in their active conformation for structural investigations (Nehme et al., 2017). However, considering that mini-G probes translocate from the cytoplasm to a receptor after it transitions into an active conformation, mini-G probes are now commonly used to investigate: GPCR-G protein coupling; ligand pharmacology; and subcellular locations of GPCR activation (Wan et al., 2018) (Figure 1.4A&B). Mini-G probes are modified Ras-like domains of $G\alpha$ proteins, that contain: a truncated N-terminus to relieve membrane attachments and prevent interaction with the $\beta\gamma$-subunit; removal of the α-helical domain; mutations to improve *in vitro* stability; and a mutation to uncouple GPCR binding from nucleotide release to stabilise receptor-mini-G probe binding (Wan et al., 2018). In addition, mini-G probes have been engineered to be subtype specific ($G\alpha_s$, $G\alpha_{i/o}$, $G\alpha_q$, and $G\alpha_{12}$). In this way, mini-G probes have some advantage over nanobodies because they can be used to

investigate multiple GPCRs, and they not only indicate whether a receptor is in an active conformation, but they give further information about GPCR-G protein coupling specificity. This provides an indication of the likely second messengers of the GPCR in question. Mini-G probes can be fused to fluorescent, luminescent, and self-labelling protein tags to facilitate analysis using FRET, BRET, luminescence, and imaging methodologies (Wan et al., 2018).

As mentioned previously, mini-G probes can be used to detect subcellular GPCR activation. In the initial study by Wan et al., mini-$G\alpha_s$ was used to report β_2-AR activation at the early endosomes by measuring the resulting isoproterenol induced bystander BRET between Venus-tagged early endosome marker (Rab5) and NLuc-tagged mini-$G\alpha_s$ in the presence of the β_2-AR. This methodology has also been shown applicable for several other GPCRs. For example, Wright et al. used mini-G probes, in combination with imaging and BRET-based methods, to investigate the activation of several different $G\alpha_q$ coupled GPCRs at the early endosome compartment (Wright et al., 2021). Within this study, the group investigated endosomal activation of the AT$_1$R by measuring RLuc8-tagged mini-$G\alpha_q$, RLucII-tagged $G\alpha_q$, and RLucII-tagged p63RhoGEF translocation to a marker of the early endosomes (rGFP-FYVE) or the plasma membrane (rGFP-CAAX) after angiotensin II stimulation (Wright et al., 2021). Through the use of arrestin knock-out (KO) cells, to prevent receptor internalisation, in addition to compartment specific endosomal $G\alpha_q$ inhibition, it was found that AT$_1$R activation of $G\alpha_q$ at the plasma membrane enabled subsequent G protein activation at the endosomes (Wright et al., 2021). Mini-G probes have also been employed to detect activation of the glucagon-like peptide 1 (GLP-1) receptor at the endosomal compartment (Lucey et al., 2021).

As well as endosomal signalling, mini-G probes have been used to report select GPCR activation at the Golgi compartment. By measuring mini-G translocation after A_1-adenosine receptor stimulation with adenosine via imaging and BRET-based approaches, the A_1-adenosine receptor was found to recruit mini-Gα_i to the plasma membrane and the Golgi compartment, indicative of receptor activation from both sites (Wan et al., 2018). Mini-G recruitment to the Golgi apparatus had a delayed onset compared to mini-G recruitment to the plasma membrane (approximately 5 seconds) (Wan et al., 2018). A similar approach was also used to investigate Golgi activation of the β_1−AR in neonatal rat ventricular myocytes. Within this study, a pool of β_1-AR was detected at the Golgi compartment, where it was demonstrated to be activated in an internalisation-independent manner after dobutamine stimulation to promote phosphatidylinositol-4-phosphate (PI$_4$P) hydrolysis after PLC activation through Gα_s activation (Nash et al., 2019). This pool of intracellular β_1−AR was further suggested to have a possible role in the regulation of catecholamine-induced hypertrophy (Nash et al., 2019). In this way, mini-G probes have been used to evaluate the real-time activation of GPCRs from intracellular compartments, including endosomal and Golgi compartments. Thus, mini-G probes can be used to investigate spatiotemporal GPCR activity in a manner like-to nanobodies.

1.2.4.5 Genetically encoded biosensors measuring compartmentalised second messenger activity

Genetically encoded biosensors have been applicable for the investigation of compartmentalised GPCR-regulated second messenger production in live cells e.g., cAMP. Although such sensors do not directly measure GPCR activation, they can

indicate a preference of a GPCR for a particular G protein subtype and can help to examine the functional downstream effect of the receptor in question.

The evaluation of real-time second messenger production after GPCR activation was originally challenging. The first tool used to detect cAMP production in live cells was called FlCRhR (fluorescein-labelled catalytic subunit and rhodamine-labelled regulatory subunit). FlCRhR is a multimolecular FRET-based biosensor based on PKA – a heterotetramer that consists of two regulatory and two catalytic subunits that dissociate on cAMP binding to the regulatory subunits (Kim et al., 2007). By labelling the PKA catalytic subunits with fluorescein and the PKA regulatory subunits with rhodamine, real-time cAMP production could be measured by a decrease in FRET. Pioneering work with FlCRhR facilitated, for the first time, the visualisation of compartmentalised cAMP production in live cells (Adams et al., 1991, Bacskai et al., 1993, Hempel et al., 1996).

However, the use of FlCRhR was practically challenging since PKA subunits had to be purified, labelled *ex vivo*, and microinjected into live cells (Adams et al., 1991). The rise of fluorescent proteins and genetically encoded FRET biosensors based on FlCRhR bypassed this limitation and enabled direct cAMP and PKA imaging in single cell, and multicell, preparations (Janetopoulos et al., 2001, Lissandron et al., 2005, Zaccolo et al., 2000). However, these sensors still had some potential limitations: they were catalytically active, which could affect downstream signalling (Paramonov et al., 2015); the sensors were usually expressed in separate vectors, which led to challenges in equal subunit expression (Zaccolo et al., 2000); and high expression of

the sensors in living cells could cause the distortion of cAMP dynamics by the ability of the sensors to buffer endogenous cAMP (Paramonov et al., 2015).

These potential limitations were improved by the generation of new, unimolecular, cAMP sensors. A large number of these sensors were based on Epac – a cAMP-activated GEF for the small GTPase Rap1 (Calebiro and Maiellaro, 2014). Binding of cAMP to Epac provokes a conformational change that exposes a catalytic domain to aid the activation of Rap1 (Calebiro and Maiellaro, 2014). FRET sensors were created by sandwiching either the cAMP-binding domain of Epac, or full-length Epac, between two appropriate fluorophores, whereby a decrease in FRET could be measured after cAMP binding (DiPilato et al., 2004, Nikolaev et al., 2004, Ponsioen et al., 2004). These sensors had a faster response to cAMP binding than multimolecular sensors, increasing temporal resolution. Also, some of these sensors were catalytically inactive (Nikolaev et al., 2004, Ponsioen et al., 2004), reducing the risk of potential experimental contamination.

In addition to the measurement of cAMP, FRET-based A-Kinase activity reporters (AKARs), were designed to detect PKA activation. Such sensors comprise of a PKA substrate, and a phosphoamino acid binding domain sandwiched in between an appropriate FRET pair, for example CFP and YFP (Calebiro and Maiellaro, 2014, Zhang et al., 2001). Phosphorylation of the PKA substrate by PKA induces a conformational change prompting the PKA substrate to interact with the phosphoamino acid binding domain which can be measured by an increase in FRET (Calebiro and Maiellaro, 2014, Zhang et al., 2001).

These, and other, FRET-based cAMP/PKA sensors have helped in the detection of compartmentalised GPCR signalling. For this purpose, genetically encoded cAMP sensors, and sometimes also PKA sensors, have been targeted to many compartments: including the plasma membrane (DiPilato et al., 2004, Jimenez-Vargas et al., 2018, Suofu et al., 2017); mitochondria (DiPilato et al., 2004, Suofu et al., 2017); nucleus (DiPilato et al., 2004); cilia (Moore et al., 2016); and the Golgi (Godbole et al., 2017). For example, by targeting of Epac1-cAMP and AKAR2 cAMP FRET sensors to either the TGN or the plasma membrane in the presence and absence of internalisation inhibitors, Godbole et al. gave evidence that the TSHR has a late-stage, internalisation-dependent, signalling component at the TGN, distinct from signalling from the plasma membrane. The signalling of the TSHR in subdomains of the TGN was proposed to facilitate the efficient phosphorylation of CREB and gene transcription of TSH related genes via activation of Golgi resident $G\alpha_s$ proteins facilitating local cAMP production and PKA activation (Godbole et al., 2017).

As well as the detection of internalisation dependent GPCR signalling, targeting of cAMP sensors to intracellular compartments has also been used to measure GPCR signalling from subcellular compartments outside of the endosomal network. For example, a pool of melatonin 1 receptor (MT_1R) is situated in the outer mitochondrial membrane (OMM) and has been suggested to signal in response to intracellular melatonin (Suofu et al., 2017). Melatonin is synthesised inside the mitochondrial matrix, and it was proposed that this pool of melatonin may indeed be capable of reaching, and activating, mitochondrial MT_1R. Convincing evidence for this phenomenon was revealed by targeting FRET-based cAMP sensors to the OMM or the plasma membrane. Such targeting determined that the MT_1R inhibited cAMP

production more greatly at the OMM than at the plasma membrane (Suofu et al., 2017).

BRET-based cAMP sensors have helped in the detection of compartmentalised cAMP signalling; however, their use has not been commonly applied for the detection of compartmentalised GPCR signalling. The first BRET-based biosensor used to report cAMP production was based on PKA (Prinz et al., 2006). In this BRET-based sensor, the regulatory PKA subunits were fused with RLuc and the catalytic PKA subunits with GFP. Upon cAMP binding to the regulatory subunits, a reduction in BRET could be measured. Since multimolecular BRET biosensors had comparable disadvantages to their FRET alternatives, unimolecular BRET-based cAMP sensors, based upon Epac (Barak et al., 2008, Jiang et al., 2007), were designed. CAMYEL (cAMP sensor using YFP-Epac-RLuc) is a BRET-based cAMP biosensor that has been used in the literature for the investigation of compartmentalised cAMP signalling. By comparing cAMP production at the plasma membrane or cytosol using plasma membrane targeted CAMYEL compared to cytosolic CAMYEL, the role of cytosolic and membrane-bound PDE subtypes on cAMP compartmentalisation were investigated (Matthiesen and Nielsen, 2011).

In recent years, a NLuc-based cAMP BRET sensor has been designed. This sensor has been modified from a FRET-based cAMP sensor (Klarenbeek et al., 2011) where the donor fluorophore, mTurquoise, was substituted with NLuc (Masuho et al., 2015). The enhanced luminescence of NLuc compared to RLuc may both allow the application of this sensor hard to transfect cell types, as well as *in vivo* (Su et al., 2020). Targeting of BRET-based biosensors to subcellular compartments, like to FRET-

based biosensors, might also help to further advance our understanding of compartmentalised GPCR signalling.

1.2.4.6 Genetically encoded sensors monitoring GPCR trafficking

As well as evaluating compartmentalised GPCR signalling, it is also important to investigate the localisation of GPCRs since compartmentalised GPCR signalling and GPCR localisation are mutually supporting (Caengprasath and Hanyaloglu, 2019). Resonance energy transfer methods have been used to investigate the real-time subcellular trafficking and localisation of GPCRs with high spatiotemporal resolution in live cells (Figure 1.4C). One of the first studies to monitor protein translocation at the plasma membrane via FRET methods was by Zacharias et al. who monitored plasma membrane specific acylated protein clustering (Zacharias et al., 2002). Soon after, FRET methods were employed to monitor GPCR trafficking in live cells. For example, Drake et al. used FRET to monitor internalisation of CFP fused β_2-AR away from mYFP fused plasma membrane marker (Drake et al., 2008). As BRET methods can offer an improved signal-to-noise ratio compared to FRET, BRET approaches, rather than FRET approaches, have been favoured in the literature to quantify GPCR trafficking in live cells. Lan et al. measured ligand induced BRET changes to monitor the trafficking of RLuc8 fused β_2-AR away from Venus-K-ras (a marker of the plasma membrane) into Venus-Rab5 (a marker of early endosomes) (Lan et al., 2011). Later, by the addition of further Venus tagged subcellular compartment markers to the toolset, the same group demonstrated the applicability of this approach to follow GPCR trafficking to other compartments (Lan et al., 2012). Within a proof-of-concept study, BRET approaches were used to investigate β_2-AR trafficking through other endosomal compartments, in addition to the ER and the Golgi. The group also nicely

demonstrated the high sensitivity of BRET methods for the measurement of membrane topology – revealing that BRET is sensitive enough to show interactions of proteins at the OMM vs interactions of proteins at the inner mitochondrial membrane (Lan et al., 2012).

BRET methods have also been applied to investigate clinically relevant GPCR mutations and their effect on GPCR trafficking. For example, Tiulpakov et al. used BRET to demonstrate distinct differences in trafficking of the Vassopressin 2 receptor (V_2R) compared to mutant V_2R to gain further understanding into some of the possible mechanisms behind nephrogenic diabetes insipidus and nephrogenic syndrome of inappropriate antidiuresis (NSIAD) (Tiulpakov et al., 2016). Within this study, V_2R trafficking was investigated in combination with additional Venus-tagged intracellular compartment markers, including markers of recycling endosomes (Rab4, Rab11), ER to Golgi trafficking (Rab1a/Rab6), and TGN (Rab8) to gain yet more detailed clarity of GPCR trafficking in live cells in real-time (Tiulpakov et al., 2016).

More recently, BRET methods have been applied, using high-throughput approaches, to investigate compound dependent inhibition of GPCR trafficking into the endosome compartment (Giubilaro et al., 2021). Using this method, a novel inhibitor of Ras and ARF6 was discovered (Rasafarin) which was observed to block AT_1R internalisation, as well as the internalisation of other GPCRs. Rasafarin was further demonstrated to have anti-proliferative effects and may be applicable in the future for the inhibition of oncogenic cellular responses (Giubilaro et al., 2021).

The use of real-time FRET/BRET-based methods to monitor spatiotemporal GPCR activity, cAMP production, and GPCR trafficking has facilitated the understanding of GPCR mechanisms with much greater clarity. GPCR trafficking is now thought of as a way for GPCRs to signal in the right place at the right time. Furthermore, it has facilitated the notion that GPCRs which couple to the same G protein pathways are able to produce distinct responses from specific intracellular compartments. This adds further complexity to GPCR signalling and, with further understanding, may represent new therapeutic opportunities for the field of GPCR research.

1.3 Adipose tissue

1.3.1 Compartmentalised GPCR signalling in adipocytes

Owing to the growing evidence demonstrating that many GPCRs do not exclusively signal from the plasma membrane (Calebiro et al., 2009, Ferrandon et al., 2009, Godbole et al., 2017, Irannejad et al., 2013), it was hypothesised that intracellular signalling of GPCRs might be of particular relevance in metabolically relevant cell types e.g., adipocytes. In adipocytes, cAMP production is highly compartmentalised to tightly control several key functions, including lipolysis and adipogenesis (Kannabiran et al., 2020, Rogne and Tasken, 2014). In addition, adipocytes express GPCRs that are responsive to various metabolites, and the intracellular concentration of metabolites is sometimes of greater physiological relevance than the extracellular concentration (Husted et al., 2017). To date, the arrangement of metabolically relevant GPCRs within adipocytes is underappreciated. This raised an intriguing possibility that metabolite sensing GPCRs might be activated from intracellular compartments to regulate adipocyte metabolism in response to intracellular metabolites.

1.3.2 The role of adipose tissue in metabolism

In living organisms, the maintenance of energy homeostasis is tightly controlled to optimise the storage and breakdown of nutrients in response to fluctuations in metabolic requirements (Li et al., 2022). Dysregulation of this control is associated with the pathogenesis of metabolic diseases e.g., insulin resistance and type 2 diabetes. Adipose tissue is a metabolic organ highly involved in the systemic regulation of energy homeostasis. When in nutrient surplus, adipose tissue stores triacylglycerol (TAG) and acts as a caloric energy reservoir. When in nutrient deficit, adipose TAG stores are broken down to meet the energy requirements of surrounding organs (Luo and Liu, 2016). Adipose tissue can also secrete hormones (e.g., leptin and adiponectin), and is regarded as the largest endocrine organ in the human body (Kershaw and Flier, 2004). Although it is primarily composed of adipocytes, nonetheless pre-adipocytes, fibroblasts, endothelial cells, macrophages, and leukocytes also play important roles in the correct functioning of the tissue (Amisten et al., 2015).

1.3.3 Adipose tissue depots

In humans, the main adipose tissue depots are found around internal organs (visceral adipose tissue, VAT), or as subcutaneous adipose tissue (SAT). SAT is the largest adipose tissue depot, making up >80% of fat tissue in healthy adults, and can be categorised further into gluteofemoral (GLUT) and abdominal depots (ABD) (Amisten et al., 2015). An increase in GLUT fat depots is associated with a reduced risk of developing diabetes and cardiovascular disease (Manolopoulos et al., 2010), whereas an increase in ABD fat depots is associated with insulin resistance (de Mutsert et al., 2018). In addition, an increase in VAT is associated with increased risk of metabolic

and cardiovascular diseases (Despres, 2007, Grundy, 2004), as well as insulin resistance (de Mutsert et al., 2018).

1.3.4 Characteristics of adipose tissue

Adipose tissue is divided into white adipose tissue (WAT), brown adipose tissue (BAT), and beige/brite adipose tissue. WAT is the most prevalent type of fat and is predominantly located in SAT and VAT depots (Hwang and Kim, 2019). WAT is characterised by cells that contain large unilocular lipid droplets, which occupy approximately 95% of the cytoplasm, where the intracellular organelles of these cells are pushed to the edge of the cytoplasm (Choe et al., 2016). When the body is in energy deficit, WAT provides fuel through the breakdown of lipid droplets. The high capacity of WAT to store lipids also provides protection of organs from lipotoxicity (Slawik and Vidal-Puig, 2006). WAT has a second function as an endocrine organ. It secretes adipokines, including leptin and adiponectin, to regulate energy balance, and to regulate glucose homeostasis and inflammation (Coelho et al., 2013).

BAT is distinguished by multilocular lipid droplets, where lipid stores are smaller and spread throughout the cytoplasm (Fenzl and Kiefer, 2014). In addition, BAT is highly vascularised and dense with mitochondria, which gives it a distinctive 'brown' colour (Fenzl and Kiefer, 2014). BAT was found initially in hibernating and small mammals or human infants. However, it is now known to be localised in human adults where it can be found primarily in cervical, supraclavicular, axillary, paraspinal, and ABD regions (Leitner et al., 2017). One of the main functions of BAT is to dissipate energy as heat through a process termed non-shivering thermogenesis. Free fatty acids (FFAs) released into the cytoplasm from lipid stores during lipolysis are transported to the

mitochondria and are oxidised during β-oxidation to generate NADH, $FADH_2$, and acetyl-coenzyme A (CoA). Acetyl-CoA subsequently enters the tricarboxylic acid cycle (TCA) to produce further NADH and $FADH_2$. The generated electron carriers donate electrons to members of the electron transport chain located on the inner mitochondrial membrane which aids proton transport from the mitochondrial matrix into the intermembrane space. This creates a proton gradient which facilitates the transport of protons back into the mitochondrial matrix through ATP synthase to produce ATP. However, BAT expresses uncoupling protein 1 (UCP1), a proton transporter located on the inner mitochondrial membrane, which transports protons across the mitochondrial membrane, bypassing ATP synthase (Blondin et al., 2020). This mechanism releases considerable amounts of chemical energy as heat rather than as ATP.

More recently, a pool of adipose was discovered which is an interim between BAT and WAT. This adipose pool was named beige or brite (brown in white) adipose and is defined by brown-like adipocytes that appear in WAT depots (Wu et al., 2012). Under resting conditions, beige adipose tissue expresses very low levels of UCP1, bearing resemblance to WAT, however, the activation of cAMP production induces high UCP1 expression and high respiration rates, more reminiscent of BAT (Wu et al., 2012). Interestingly, WAT can be induced into beige adipocytes; as such, beige adipocytes are often referred to as inducible-brown adipocytes (Luo and Liu, 2016).

1.3.5 Fatty acids and lipid droplet formation

Adipose tissue stores large amounts of fatty acids in TAG stores called lipid droplets. Fatty acids are essential extracellular and intracellular signalling molecules that help

to regulate metabolism (Papackova and Cahova, 2015). High levels of intracellular fatty acid intermediates in tissues which do not normally store TAG causes lipotoxicity and cell death (Nishi et al., 2019), thus fatty acid concentration is carefully controlled. Fatty acids are carboxylic acids with long aliphatic carbon chains. They are grouped depending on the presence of double bonds: saturated fatty acids (SFA), containing no double bonds; monounsaturated fatty acids (MUFA), containing one double bond; and polyunsaturated fatty acids (PUFA), containing multiple double bonds (Papackova and Cahova, 2015). Fatty acids are also grouped according to their carbon chain length. Fatty acids with carbon chain lengths 1-5 are considered short-chain fatty acids (SCFAs), carbon chain lengths 6-12 are considered medium-chain fatty acids (MCFAs), and carbon chains of over 12 are considered long-chain fatty acids (LCFAs). A major characteristic of adipocytes is to store MCFAs and LCFAs as TAG in organelles called lipid droplets (Heid et al., 2014).

FFAs are delivered to the cell surface, transported in the blood mainly bound to albumin, and have been suggested to be transported across the plasma membrane via interaction with the lipid transporter, cluster of differentiation 36 (CD36) (Coburn et al., 2000, Goldberg et al., 2009, Mistry et al., 2021), and fatty acid transport proteins (FATPs) (Mistry et al., 2021). Furthermore, CD36 and FATPs are proposed to interact with plasma membrane associated fatty acid binding proteins (FABPs) to enable fatty acid desorption (Storch and Corsico, 2008). Cytoplasmic FABPs then shuttle fatty acids to subcellular organelles, including the mitochondria for β-oxidation, the ER for the synthesis of lipid droplets, or the nucleus to regulate transcription (Storch and Corsico, 2008).

Lipid droplet synthesis begins in the ER. The first step in this process is the synthesis of TAGs and sterol esters which require MCFAs and LCFAs. Fatty acids are inert and must first be activated by esterification to CoA, a reaction that is catalysed by acyl-coA synthetases (ACS), to produce fatty acyl-coA (Ellis et al., 2010). ACSs are located primarily at the plasma membrane, ER, TGN, and endosomes (Gargiulo et al., 1999). Inhibition of ACSs with triacsin C reduces the synthesis of TAG and prevents fatty acid dependent lipid droplet formation (Li et al., 2010a). Once bound to CoA, activated fatty acids are esterified to DAG or a sterol to produce TAG and sterol esters. The enzymes that catalyse this process, DAG acyltransferases and acyl-CoA:cholesterol O-acyltransferases, respectively, are localised to the ER (Olzmann and Carvalho, 2019). At first, neutral lipids (TAG and sterol esters) are distributed in the ER bilayer, but as their concentration rises, the neutral lipids coalesce and form a 'lens' (Khandelia et al., 2010). Expansion of this 'lens' results in lipid droplet budding from the ER membrane. Lipid droplets further expand by: fusion to other lipid droplets; the transfer of TAG from the ER membrane; or by TAG synthesis directly on the lipid droplet surface (Olzmann and Carvalho, 2019). As well as contact with the ER, lipid droplets also establish contacts with most subcellular organelles, including the endosomes, the Golgi, the mitochondria, the lysosomes, and the peroxisomes (Valm et al., 2017).

Ubiquitously expressed in cells, lipid droplets consist of a neutral lipid core surrounded by a phospholipid monolayer into which proteins are embedded (Olzmann and Carvalho, 2019). Lipid droplets are exceptionally dynamic, and alternate between periods of anabolism or catabolism. Proteomic studies have found 100-150 different proteins present on the membrane of lipid droplets in prototypical mammalian cells; some localise solely to this membrane whilst others are also found present at other

intracellular compartments (Yang et al., 2012). Perilipins (PLINs) are the most abundant proteins found on the surface of lipid droplets and they are well known as controllers of lipolysis – the breakdown of lipid droplets (Sztalryd and Brasaemle, 2017). There are five major PLIN proteins in mammals, with additional splice variants present at lower amounts. PLINs are either exclusively present at the lipid droplets (PLIN1&2), or they can exchange between the cytoplasm and lipid droplets (PLIN3-5). PLIN1&2 are rapidly degraded when not localised to the lipid droplets, whereas PLIN3-5 are stable in the cytoplasm and may have additional trafficking roles (Itabe et al., 2017). Intriguingly, PLIN3&5 have been found associated with micro lipid droplets and lipoprotein particles (Hashimoto et al., 2012, Sztalryd and Brasaemle, 2017). PLIN subtypes have a unique distribution across adipose depots and a possible unique role in lipid metabolism (Sztalryd and Brasaemle, 2017). PLIN1 has particular relevance in WAT in the control of lipolysis (Skinner et al., 2013), whereas PLIN5 has particular relevance in BAT, where it has been demonstrated to play a role in the trafficking of fatty acids to the mitochondria for β-oxidation and thermogenesis (Gallardo-Montejano et al., 2021, Wang et al., 2011).

1.3.6 Lipolysis

Lipolysis is the process by which intracellular TAG stores are broken down into FFAs and glycerol. In a state of energy demand, FFAs are released from adipocyte TAG stores during lipolysis and are transported by the blood for delivery to organs in metabolic demand (e.g., the liver, and skeletal/cardiac muscle) (Luo and Liu, 2016). In these organs, fatty acids function as energy substrates for ATP production by β-oxidation (Cucchi et al., 2019). Lipolysis is therefore tightly regulated to control energy homeostasis.

1.3.7 The mechanism of lipolysis

Lipolysis activation is largely regulated by the action of catecholamines on GPCRs. In high energy demand, sympathetic terminal nerve fibres which innervate fat cells are stimulated to release catecholamines i.e., norepinephrine (NE) or epinephrine, which bind to β−ARs (1-3) present in adipocytes (Carpene et al., 1998, Yang and Mottillo, 2020) (Figure 1.5). This initiates a signalling cascade mediated through $G\alpha_s$ proteins. $G\alpha_s$ proteins activate ACs to increase cAMP production, which binds and activates PKA (Kim et al., 2007). In adipocytes, PKA phosphorylates both PLINs and lipid droplet associated lipases, assisting conformational changes and translocations to facilitate the docking of these lipases to the lipid droplets via interaction with the PLIN family (Sztalryd and Brasaemle, 2017).
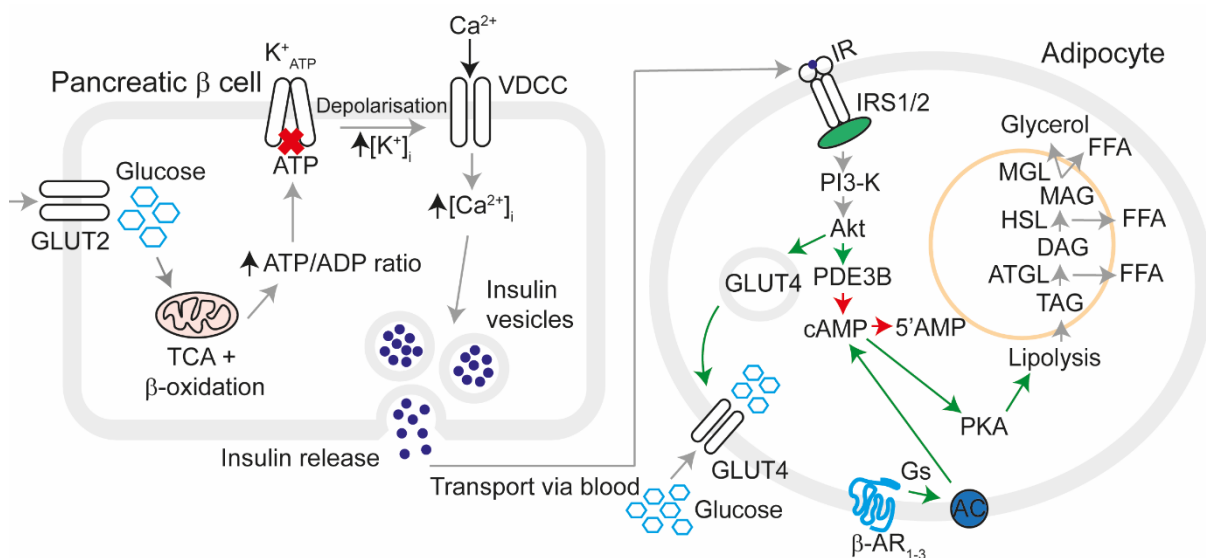
Figure 1. 5: Schematic to illustrate insulin release and its effects in adipocytes.
Glucose uptake through glucose transporter 2 (GLUT2) increases insulin release from pancreatic β cell islets which is transported to adipocytes in the blood. Upon binding of insulin to the insulin receptor (IR), a cascade is activated to inhibit lipolysis by enhancing cAMP breakdown. In addition, insulin increases glucose uptake by enhancing the expression of plasma membrane glucose transporter 4 (GLUT4).

There are three major lipases that are considered as the master controllers of lipolysis in adipose tissue (Figure 1.5). These lipases are adipose triglyceride lipase (ATGL), hormone sensitive lipase (HSL), and monoacylglycerol lipase (MGL). HSL was formerly believed to be the main lipase responsible for the overall control of lipolysis (Vaughan et al., 1964). However, HSL KO mice accumulated DAG and not TAG in multiple tissue types, including adipose, testis, and muscle (Haemmerle et al., 2002). In 2004, a new lipase was discovered and reported in the literature by three independent groups (Jenkins et al., 2004, Villena et al., 2004, Zimmermann et al., 2004) which was found to have profuse TAG hydrolase activity. This lipase, named ATGL, is now considered the master regulator of adipocyte lipolysis. ATGL is part of the patatin-like phospholipase domain-containing family which encompasses several lipid hydrolases (Wilson et al., 2006). ATGL is localised to the surface of lipid droplets and regulates the first step in lipolysis, catalysing the break-down of TAG into DAG and a FFA. For maximal hydrolase activity, ATGL also requires a co-activator, named comparative gene identification-58 (CGI-58) (Lass et al., 2006). Prior to activation of lipolysis, CGI-58 is bound to PLIN on the surface of lipid droplets. Upon the PKA dependent phosphorylation of PLIN, in combination with a possible additional phosphorylation of CGI-58, CGI-58 is released from PLIN to facilitate its interaction with ATGL (Brejchova et al., 2021). The combined interaction of CGI-58 with ATGL has been found to increase the hydrolysis of TAG by up to 20-fold (Lass et al., 2006). HSL is the rate-limiting lipase in the second step of lipolysis i.e., the breakdown of DAG into monoacylglycerol (MAG) and a FFA (Brejchova et al., 2021). HSL is activated after PKA-dependent phosphorylation, which facilitates the translocation of HSL from the cytoplasm to the surface of lipid droplets (Holm, 2003). Subsequently,

HSL hydrolyses DAG into MAG. Furthermore, MAG is hydrolysed to glycerol and a FFA by MGL (Taschler et al., 2011).

1.3.8 Inhibitors of adipocyte lipolysis

1.3.8.1 Hormones

Insulin is a hormone and is considered to be the main inhibitor of lipolysis (Li et al., 2022). In addition, insulin regulates the concentration of plasma glucose and inhibits hepatic gluconeogenesis (Lee et al., 2022). In the fed state, increases in plasma fatty acids, amino acids, and glucose stimulate insulin secretion into the plasma from secretory pancreatic β cell granules, located in the islets of Langerhans (Henquin, 2000) (Figure 1.5). In short, glucose uptake increases the production of ATP through oxidative phosphorylation in the mitochondria, increasing the ratio of ATP to ADP. This increase in ATP inhibits ATP sensitive K^+ transporters, increasing the concentration of intracellular K^+ and leading to depolarisation of the plasma membrane and the activation of voltage dependent calcium channels. Ca^{2+} is transported across the plasma membrane, increasing intracellular Ca^{2+} and facilitating the release of insulin into the blood. Insulin binds to insulin receptors (IR), dimeric receptor tyrosine kinases, located on the cell surface of adipocytes, skeletal muscle cells, and hepatocytes (Zhang and Liu, 2014). Insulin binding induces conformational changes in the IR, which bring the receptor's two kinase domains in close proximity, facilitating their efficient trans-autophosphorylation and activation (Uchikawa et al., 2019). This initiates the recruitment and docking of insulin receptor substrate 1 (IRS1) and IRS2 to activate PI3K. PI3K increases phosphatidylinositol (3,4,5)-trisphosphate (PIP_3) production, recruiting phosphoinositide-dependent kinase 1, and assisting the subsequent activation of Akt (Henquin, 2000). Akt has been proposed to

phosphorylate PDE3B, leading to cAMP hydrolysis and the concurrent inhibition of lipolysis since PKA activity is reduced (Kitamura et al., 1999). More recently, the role of Akt to fully control insulin's inhibitory effects on lipolysis have been challenged since serum fatty acid concentrations are unaffected in mice deficient in Akt (Koren et al., 2015) and mice with PDE3B mutations lacking Akt phosphorylation sites are able to supress lipolysis through insulin-dependent mechanisms (DiPilato et al., 2015). On the other hand, insulin dependent Akt activation is proposed to assist glucose transporter 4 (GLUT4) insertion into the plasma membrane, facilitating the subsequent absorption of glucose from plasma (Chang et al., 2004).

Additional hormones are also known to inhibit adipocyte lipolysis. For example, ghrelin, the 'hunger hormone', is an appetite stimulating hormone released by the stomach prior to food intake. Ghrelin binds the ghrelin receptor, a GPCR present on the surface of adipocytes, and inhibits adrenoceptor-stimulated lipolysis in WAT (Baragli et al., 2011, Muccioli et al., 2004). This has been proposed to occur through PI3K and PDE3B activation (Baragli et al., 2011). Similarly, adiponectin, a hormone secreted by adipocytes in response to insulin, inhibits lipolysis. For instance, adiponectin-KO mice exhibit increased lipolysis (Qiao et al., 2011). However, unlike insulin and ghrelin, adiponectin is considered to act by supressing PKA-dependent HSL activation, reducing lipolysis-induced fatty acid release. In this way, adiponectin is considered to potentiate the effects of insulin on lipolysis (Qiao et al., 2011).

1.3.8.2 Metabolite sensing GPCRs

In the last twenty years, it has been discovered that certain metabolites act as extracellular signalling ligands for specific GPCRs, working in a manner like-to

neurotransmitters and hormones (Husted et al., 2017). There are six metabolite sensing GPCRs highly expressed in adipose tissue which have been proposed to inhibit lipolysis through coupling to $G\alpha_{i/o}$ proteins (Husted et al., 2017). Such metabolite sensing GPCRs include: hydroxycarboxylic acid receptor 1 (HCAR1) (Ahmed et al., 2010); HCAR2 (Taggart et al., 2005); HCAR3 (Tunaru et al., 2003); GPR91 (He et al., 2004); free fatty acid receptor 2 (FFAR2) (Brown et al., 2003); and FFAR4 (Hirasawa et al., 2005).

The HCAR1 has been proposed to have a large control over insulin's inhibition of adipocyte lipolysis (~40%) (Ahmed et al., 2010). Insulin aids the uptake of glucose into adipocytes, which is broken down into pyruvate during glycolysis, and further metabolised into lactate (HCAR1 agonist) by pyruvate dehydrogenase. Both extracellular, and intracellular, concentrations of lactate increase after glucose uptake, and, in HCAR1-KO mice, insulin-induced lipolysis inhibition is seriously impaired (Ahmed et al., 2010). Therefore, the HCAR1 is partly responsible for the inhibitory effects of insulin on lipolysis through autocrine activation by lactate. The other members of the HCAR family are either sensitive to ketones (HCAR2) (Taggart et al., 2005) or β-hydroxyoctanoate (HCAR3) (Ahmed et al., 2009). Ketones and β-hydroxyoctanoate are products of LCFA fuelled β-oxidation in the mitochondria of hepatocytes, which transpires when intracellular glucose concentrations are not high enough for glycolysis and acetyl-CoA production. These metabolites are exported from the liver into the plasma in physiologically high enough concentrations to activate their respective receptors in adipose tissue (Blad et al., 2011). Adipose located HCA2 and HCA3 are most likely activated in an endocrine feedback mechanism to inhibit adipose tissue lipolysis when FFA release is sufficient in the liver to meet energy demand.

GPR91 is responsive to succinate, a metabolite produced in the mitochondria during the TCA cycle that only reaches physiologically relevant extracellular concentrations during hypoxia or metabolic stress. GPR91-KO mice are released from succinate-induced lipolysis inhibition (McCreath et al., 2015). It has therefore been proposed that GPR91 inhibits adipocyte lipolysis in an autocrine manner during times of metabolic stress (Husted et al., 2017).

Adipocytes also express the FFAR2 and the FFAR4 which are members of the FFAR family. The FFAR2 is activated during states of nutritional excess, via acetate production from pyruvate (Tang et al., 2015), or by SCFAs released from gut microbiota (Husted et al., 2017). Activation of the FFAR2 inhibits adipocyte lipolysis (Ge et al., 2008) and also controls adipokine production (Zaibi et al., 2010). The FFAR4 is activated in response to LCFAs which are obtained from the diet or TAG turnover (Husted et al., 2020). Both receptors are proposed activated in an autocrine manner to inhibit lipolysis.

1.3.8.3 Other GPCRs

The α_2-adrenoceptor (α_2-AR) is an inhibitory mediator of adipocyte lipolysis. Like the β-ARs, it is responsive to catecholamines, however unlike β-ARs, the α_2-AR couples predominantly to the $G\alpha_{i/o}$ protein family and inhibits adipocyte lipolysis (Ruohonen et al., 2018). The α_2-AR is more sensitive to catecholamines than the β-ARs, and at low catecholamine concentrations, the α_2-AR is proposed to prevail and inhibit lipolysis. When the concentration of catecholamine rises, lipolysis is then activated by the β-ARs (Mauriege et al., 1987). The mechanism and physiological relevance of this interplay is not well understood.

In addition, the adenosine receptors (A1, A2A) are also expressed in adipocytes and help to regulate lipolysis. Adenosine is persistently produced intracellularly and extracellularly by the dephosphorylation of AMP, a process regulated by intracellular or extracellular 5'-nucleotidases (Pardo et al., 2017). The A1 receptor is prevalent in WAT, coupling to $G\alpha_i$ and inhibiting lipolysis (Johansson et al., 2008). However, the A2A receptor is also expressed in adipocytes and is coupled to $G\alpha_s$, stimulating lipolysis through AC activation. Since the A2A receptor is activated by low concentrations of adenosine (Gnad et al., 2014), and the A1 receptor is activated by high concentrations of adenosine, it is likely that the A2A receptor is activated in states of energy demand (at low concentrations of ATP) to increase lipolysis, whereas the A1 receptor is activated when energy is sufficient (at high concentrations of ATP) (Braun et al., 2018, Li et al., 2022) to turn down lipolysis. In this way, these GPCRs help to regulate adipose lipolysis in response to energy requirements.

1.3.8.4 Intracellular mechanisms

Lipolysis is also controlled by intracellular systems. Evidence suggests that approximately 40% of fatty acids released during lipolysis are re-esterified back into TAG in humans, reducing extracellular fatty acid export (Reshef et al., 2003). In addition, lipolysis induced PKA activation indirectly activates AMP activated protein kinase (AMPK). AMPK is a serine/threonine kinase, which phosphorylates HSL in a position that attenuates HSL phosphorylation by PKA, inhibiting lipolysis (Kim et al., 2016). Furthermore, studies suggest that intermediary lipid metabolites (e.g., FFAs & long-chain acyl-CoAs) inhibit lipolysis. Part of this mechanism is proposed to be through fatty acid-dependent inhibition of ACs (Burns et al., 1978, Fain and Shepherd, 1975). AC and PKA activity are reduced by increasing the concentration of intracellular

FFAs by limiting extracellular albumin availability (Mottillo and Granneman, 2011). Additionally, when intracellular FFA concentrations rise, the concentration of LCFA acyl-CoAs would also be expected to rise. Recently, AMPK has been proposed activated via interaction with LCFA acyl-CoAs, generating a direct negative feedback loop on lipolysis (Pinkosky et al., 2020). Additionally, LCFA CoAs (e.g., oleoyl-CoA) have been suggested to non-competitively inhibit HSL and ATGL (Nagy et al., 2014) or interact with CGI-58 and PLIN proteins (Sanders et al., 2015) to inhibit lipolysis. Finally, mechanisms which increase PDE activity (Cheung et al., 2003, DiPilato et al., 2015), to increase cAMP hydrolysis, or protein phosphatase activity, to dephosphorylate lipases or PLINs (Kinney et al., 2010, Okumura et al., 2014), will also lead to the intracellular inhibition of lipolysis.

1.3.9 Insulin resistance and diabetes

Under normal metabolic conditions, lipolysis is tightly controlled by hormones and metabolites, which act via endocrine, autocrine, and paracrine mechanisms to control fatty acid storage and release (Li et al., 2022). Disruption to the balance of fat storage and mobilisation is associated with the development of obesity, insulin resistance, and type 2 diabetes (da Silva Rosa et al., 2020). Insulin resistance has dominant effects in adipose tissue, muscles, and the liver. During insulin resistance, insulin can no longer produce strong enough effects to enable sufficient glucose uptake, inhibit lipolysis, stimulate glycogen synthesis, or reduce hepatic gluconeogenesis (da Silva Rosa et al., 2020). This leads to hyperglycaemia. As a compensatory mechanism, pancreatic β cells secrete more insulin. Eventually pancreatic β cells become exhausted, cannot secrete adequate levels of insulin, and blood glucose levels are raised – a hallmark of type 2 diabetes (Cerf, 2013).

The mechanisms behind insulin resistance are not fully understood. However, insulin resistance is believed to be driven, in part, by the dysregulation of adipocyte lipolysis, leading to elevated levels of plasma FFAs. For example, mutations in PLIN1, an adipocyte specific lipid droplet coating protein, lead to unrestrained lipolysis and severe insulin resistance in humans (Gandotra et al., 2011a, Gandotra et al., 2011b). Furthermore, reductions in PDE3B expression, decreasing cAMP hydrolysis and thus increasing lipolysis, are implicated in insulin resistance. For instance, a decrease in ABHD15 expression, a protein highly expressed in adipose tissue known to stabilise PDE3B expression, is found decreased in humans with obesity and diabetes compared to obese humans with intact glucose tolerance (Xia et al., 2018). In addition, loss of ABHD15 expression in ABDH15-KO mice results in a failure of insulin to promote glucose uptake (Stockli et al., 2019, Xia et al., 2018). Furthermore, in adipose specific ATGL-KO mice, lipolysis is reduced, leading to a reduction in the concentration of extracellular plasma fatty acids and enhancing insulin sensitivity (Schoiswohl et al., 2015). In this way, insulin resistance is associated with the dysregulation of adipocyte lipolysis.

When the concentration of intracellular FFA is raised after lipolysis dysregulation, the concentration of intracellular fatty acid metabolites increases (e.g., DAG, fatty acyl-CoAs, or ceramides). Raised levels of fatty acid metabolites have been proposed to activate a serine/threonine kinase cascade, phosphorylating IRS-1 and IRS-2, leading to the failure of insulin-dependent PI3K activation, and reducing glucose uptake (Lee et al., 2022). Insulin resistance is also associated with increased plasma FFAs and enhanced accumulation of ectopic FFAs in insulin-responsive tissue types like the liver and skeletal muscle, leading to impaired insulin signalling in the muscles and liver (Lee

et al., 2022). In human patients with extreme obesity and type 2 diabetes, certain fatty acid species have been found significantly elevated. These include: eicosadienoic acid (C20:2); α-linolenic acid (C18:3n-3); docosahexaenoic acid (C22:6); arachidic acid (C20:0); myristic acid (C14:0); and eicosatrienoic acid (C20:3n-3) (Wrzosek et al., 2022). Since these fatty acid species are LCFAs which should act as agonists of the FFAR1 and FFAR4, and the FFAR4, and not the FFAR1, is highly expressed in adipose tissue, the role of the FFAR4 is further investigated within this thesis.

1.4 The FFARs

Five GPCRs are known activated in response to FFAs, where their selectivity depends on FFA carbon chain length: FFAR1/GPR40; FFAR2/GPR43; FFAR3/GPR41; FFAR4/GPR120; and GPR84. FFAR1 and FFAR4 are activated by LCFAs (Briscoe et al., 2003, Hirasawa et al., 2005), whereas FFAR2 and FFAR3 are activated by SCFAs (Brown et al., 2003). GPR84, although not part of the FFAR family, is activated by MCFAs (Wang et al., 2006) – however MCFAs are not considered to be the major endogenous agonists of this receptor, consequently GPR84 is not yet regarded as deorphanised (Mahmud et al., 2017). FFARs are characterized by their distinctive tissue expression, their affinity for fatty acids, their signalling properties, and their overall physiological function (Milligan et al., 2017b). FFAR signalling is involved in insulin secretion, incretin secretion, adipose tissue differentiation, the regulation of food intake, and many other metabolic actions (Kimura et al., 2020). Considering the impact of FFARs on energy regulation and thus their potential as therapeutic targets for metabolic disorders like type 2 diabetes and obesity, the FFARs are regarded as potentially valuable therapeutic targets (Kimura et al., 2020).

1.4.1 Physiological role of the FFAR4

The FFAR4/GPR120 is a class A GPCR that was deorphanized in 2005 where it was discovered activated in response to LCFAs (C13-C22) (Hirasawa et al., 2005). In particular, the FFAR4 was believed to have increased preference for MUFAs/PUFAs, since greater receptor activation was observed after stimulation with α-linolenic acid (PUFA) and palmitoleic acid (MUFA), than with SFAs; stearic acid and lauric acid (Hirasawa et al., 2005). The FFAR4 is now considered activated in response to a broad range of LCFAs, with potencies (EC_{50}) in the range of 1-30 μM (Christiansen et al., 2015).

Initially, the role of the FFAR4 was investigated in the gut. Within this study, LCFA-dependent activation of the FFAR4 increased the concentration of intracellular $[Ca^{2+}]$ and increased ERK activation (Hirasawa et al., 2005). Through this mechanism, the FFAR4 was proposed to promote secretion of GLP-1 from enteroendocrine cells. However, the FFAR4 is not only expressed within the intestine, but also across a variety of other tissue types, including adipose tissue, the hypothalamus, lungs, immune cells, pancreatic delta cells, and taste buds (Cornall et al., 2011, Gotoh et al., 2007, Hirasawa et al., 2005, Kimura et al., 2020, Tanaka et al., 2008). The physiological functionalities of the FFAR4 are consistent with its expression profile. The FFAR4 has been demonstrated to inhibit ghrelin secretion (Engelstoft et al., 2013, Gong et al., 2014), stimulate gastric inhibitory peptide (GIP) secretion (Iwasaki et al., 2015), and inhibit somatostatin secretion (Croze et al., 2021, Stone et al., 2014). In adipose tissue, the FFAR4 enhances adipogenesis (Gotoh et al., 2007, Hilgendorf et al., 2019, Song et al., 2016), enhances glucose uptake (Oh et al., 2010), inhibits lipolysis (Husted et al., 2020, Satapati et al., 2017), and promotes BAT activity by

increasing UCP1 activity (Quesada-Lopez et al., 2019, Schilperoort et al., 2018, Song et al., 2017). Other roles of the receptor include the inhibition of inflammation in macrophages (Oh et al., 2010), the reduction of airway resistance in the lungs (Prihandoko et al., 2020), the regulation of taste preference for fatty acids (Cartoni et al., 2010), and the regulation of food intake (Auguste et al., 2016).

1.4.2 FFAR4 signalling

In the literature, the FFAR4 has been suggested a predominantly $G\alpha_{q/11}$ coupled receptor, where receptor activation increases the concentration of intracellular $[Ca^{2+}]$ – a phenomenon that can be blocked by selective $G\alpha_{q/11}$ inhibition (Hudson et al., 2013). The FFAR4 is known to exist as multiple species-dependent splice variants with both "long" (FFA4L) and "short" (FFA4S) isoforms expressed in humans. Interestingly, the long variant has a 16 amino acid insertion in ICL3 which was demonstrated to uncouple the receptor from $G\alpha_{q/11}$ protein activation (Watson et al., 2012). In fact, this insertion is proposed to promote signalling bias of FFAR4L towards β-arrestin 2 recruitment and not $G\alpha_{q/11}$ protein recruitment (Watson et al., 2012). The coupling of the FFAR4S to $G\alpha_{q/11}$ has been demonstrated necessary for ERK activation (Prihandoko et al., 2016). Additionally, ligand induced activation of the FFAR4 induces phosphorylation of its C-terminal tail by GRK6, with a minor component mediated by PKC (Burns et al., 2014). PKC was found implicated in basal and heterologous FFAR4 phosphorylations (Burns et al., 2014). Ligand induced phosphorylations of the FFAR4 enabled the recruitment of β-arrestin 2 which has been found to stimulate strong FFAR4 internalisation and the G protein independent phosphorylation of Akt (Prihandoko et al., 2016). FFAR4 dependent β-arrestin 2 activation is considered important in the inhibition of inflammatory mediators in

macrophages (Oh et al., 2010). On the other hand, the FFAR4 has been found to couple to G$\alpha_{i/o}$ proteins. For example, FFAR4 activation inhibited ghrelin secretion in primary gastric mucosal cells (Engelstoft et al., 2013) and blocked glucose-induced somatostatin release from delta pancreatic islets (Stone et al., 2014). These effects were demonstrated pertussis toxin sensitive – indicating G$\alpha_{i/o}$ coupling. However, downstream signalling via this coupling through the measurement of cAMP has not yet been demonstrated in a simple cell model.

1.4.3 FFAR4 trafficking and compartmentalised signalling

FFAR4 trafficking has not been extensively investigated. Considering that trafficking is an essential component of compartmentalised GPCR signalling (Caengprasath and Hanyaloglu, 2019), it is important to understand where the FFAR4 localises and traffics before and after agonist induced stimulation. The FFAR4 rapidly internalises upon agonist stimulation, leading to increased receptor distribution at endosomal compartments and lysosomal compartments (Watson et al., 2012). This is indicative of both receptor recycling and receptor degradation (Wang et al., 2018a). More recently, using a FRET-based methodology, FFAR4 activation was shown to elicit receptor internalisation and increase the receptor's distribution in fast and slow recycling endosomes (Rab4 and Rab11), early endosomes (Rab5), and late endosomes (Rab7 and Rab9) (Flores-Espinoza et al., 2020). Yet, although FFAR4 trafficking was investigated in live cells within this study, it was investigated via single-cell analysis in combination with a small variety of compartment markers, which warrants the application of improved trafficking methods to enhance the spatiotemporal information gathered regarding FFAR4 trafficking. Within the literature,

there have been no studies, to my knowledge, investigating compartmentalised FFAR4 signalling.

1.4.4 The role and mechanisms of the FFAR4 in adipocyte metabolism

Many studies indicate that the FFAR4 has a critical role in the control of adipocyte metabolism. Firstly, the FFAR4 is highly expressed in adipocytes, across many adipose depots (including WAT and BAT) (Oh et al., 2010, Quesada-Lopez et al., 2016), and its expression increases during adipocyte differentiation (Gotoh et al., 2007, Oh et al., 2010, Song et al., 2016, Yamada et al., 2017). Furthermore, the FFAR4 has been implicated in the control of lipid droplet formation (Rohwedder et al., 2014). Reduction in FFAR4 expression by small interfering RNA was demonstrated to inhibit differentiation and lipid accumulation in 3T3-L1 adipocytes (Gotoh et al., 2007). In addition, stimulation of the FFAR4 with α-linolenic acid was found to promote 3T3-L1 adipocyte differentiation (Song et al., 2017, Song et al., 2016). Thus, the FFAR4 is considered an adipogenic receptor. The ability of the FFAR4 to promote intracellular increases in $[Ca^{2+}]$ (Song et al., 2016), presumably via $G\alpha_{q/11}$, or increase ciliary cAMP (Hilgendorf et al., 2019) have been suggested important in the control of this mechanism.

Secondly, the FFAR4 is implicated in the control of thermogenesis. Not only is the FFAR4 highly expressed in BAT, but the FFAR4 is strongly upregulated in mice in response to cold exposure (Quesada-Lopez et al., 2016). Activation of the FFAR4 was demonstrated to enhance thermogenesis by increasing the expression of BAT-specific proteins, including UCP1 (Quesada-Lopez et al., 2019, Song et al., 2017, Wang et al., 2018b). In addition, FFAR4 activation has been demonstrated to increase fatty acid

58

uptake and β-oxidation, alter mitochondrial respiration, and decrease fat mass in BAT (Christian, 2020, Schilperoort et al., 2018). These effects are proposed to be regulated via FFAR4 dependent activation of $G\alpha_{q/11}$, stimulating intracellular $[Ca^{2+}]$ accumulation (Christian, 2020).

Thirdly, the FFAR4 has been demonstrated to sensitise responses to insulin by enhancing glucose uptake via the translocation and insertion of GLUT4, a glucose transporter, into the plasma membrane in adipose tissue and 3T3-L1 adipocytes (Oh et al., 2010). In agreement with this study, knock-down of the FFAR4 was found to reduce GLUT4 expression and IRS-1 expression in 3T3-L1 adipocytes, suggesting that the FFAR4 is intricately associated with the mechanisms of insulin-induced glucose uptake (Liu et al., 2012a). Furthermore, by comparing between wild-type (WT) and FFAR4-KO mice, FFAR4 agonism with omega 3 fatty acids was demonstrated to have insulin-sensitising effects in *vivo* – improved insulin-stimulated glucose disposal and enhanced insulin sensitivity in the muscles and liver (Oh et al., 2010). These effects have again been proposed mediated through FFAR4-dependent activation of $G\alpha_{q/11}$, increasing intracellular $[Ca^{2+}]$ levels (Hudson et al., 2013, Oh et al., 2010).

Finally, the FFAR4 has been implicated in the control of lipolysis. In an elegant study by Satapati et al., after treatment with a specific FFAR4 agonist Compound B, mice were found to have reduced levels of plasma FFAs and plasma glycerol, with no change in plasma insulin concentration, suggesting direct lipolytic suppression by the FFAR4. This conclusion was further confirmed using FFAR4-KO mice, where Compound B administration dose-dependently supressed glycerol release in adipocytes from WT mice and not in FFAR4-KO mice (Satapati et al., 2017). A more

recent study demonstrates that the FFAs released after the induction of adipocyte lipolysis activate the FFAR4 in a $G\alpha_{i/o}$-dependent manner to inhibit cAMP production as part of an autocrine negative feedback loop to inhibit adipocyte lipolysis (Husted et al., 2020). As such, the ability of the FFAR4 to couple to $G\alpha_{i/o}$, rather than $G\alpha_{q/11}$, has been proposed necessary for the receptor's control over lipolysis.

1.4.5 Pathophysiological indication of the FFAR4 in adipocytes

Since the FFAR4 is intimately involved in adipocyte metabolism, it comes as no surprise that the receptor has been implicated in obesity and type 2 diabetes. Mice deficient in FFAR4 fed on a high-fat diet have been demonstrated to develop obesity, glucose intolerance, metabolic dysregulation, insulin resistance, and inflammation in adipose tissue (Ichimura et al., 2012). In human subjects, the expression of the FFAR4 in the adipose tissue of obese individuals was found significantly raised compared to the adipose tissue of lean individuals (Ichimura et al., 2012). In addition, a known FFAR4 variant (p.R270H) has been associated with both increased fasting glucose levels and an increased risk of obesity in humans (Bonnefond et al., 2015, Ichimura et al., 2012). The p.R270H variant has further been proposed to modulate the risk of type 2 diabetes in connection with dietary fat intake (Lamri et al., 2016).

1.4.6 Rationale

Since insulin resistance is associated with increased circulating levels of LCFAs released from adipocyte lipolysis (FFAR1 and FFAR4 agonists) (Wrzosek et al., 2022), and the FFAR4, and not the FFAR1, is highly expressed in adipocytes and heavily implicated in adipocyte metabolism (Husted et al., 2017), the role of the FFAR4 was investigated further within this thesis. Furthermore, the ability of the FFAR4 to signal

from intracellular compartments in both a simple cell model and a more complex adipocyte model was investigated using both imaging and BRET-based approaches.

2.0 Chapter Two: Materials and Methods

2.1 Materials

2.1.1 Plasmids

FFAR4-eYFP was kindly provided by Professor Graeme Milligan, University of Glasgow (Houthuijzen et al., 2017). FFAR4 was amplified from FFAR4-eYFP using primers incorporating restriction sites (BamHI and EcoRI) flanking the FFAR4, and a stop codon (TAG) on the reverse primer, under standard polymerase chain reaction (PCR) conditions. FFAR4 was subcloned into pcDNA3 by restriction digest to create WT FFAR4. To create FFAR4-NLuc, NLuc was amplified from NLuc-miniGα_i using primers incorporating restriction sites (EcoRI and XhoI) flanking NLuc and a stop codon (TAA) on the reverse primer, under standard PCR conditions. The FFAR4 stop codon (TAG) was mutated to a serine residue (TCG) by site-directed mutagenesis. Plasmids encoding NLuc-fused, YFP-fused, and Halo-fused mini-Gα probes (mGα_i, mGα_s, mGα_o, mGα_q, mGα_{12}) were kindly provided by Professor Nevin Lambert, Augusta University (Wan et al., 2018). Plasmids encoding Venus fused compartment markers (K-ras, Rab1a, Rab4, Rab5, Rab6, Rab7, Rab8, Rab9, and Rab11a/Rab11b) (Tiulpakov et al., 2016) and the AT$_1$R-RLuc8 (O'Brien et al., 2018) were kindly provided by Professor Kevin Pfleger, University of Western Australia. Plasmids encoding mCherry-fused PLIN1 and EGFP-fused PLIN1 were kindly provided by Professor David Savage, University of Cambridge (Rowe et al., 2016). Plasmids encoding mEmerald-Sec61β, mCherry-Sec61β, and Halo-Sec61β were a kind gift from Christopher Obara, Janelia Research Campus (Moore et al., 2021). Plasmids encoding CAMYEL and PDE2A3-CAMYEL were kindly provided by Professor Meritxell Canals, University of Nottingham (Matthiesen and Nielsen, 2011). CAMYEL was targeted to the ER by the addition of Sec61β (minimal sequence) or Rab1a (full protein) to the C-terminus of the sensor by Gibson assembly, creating CAMYEL-

Sec61β and CAMYEL-Rab1a, respectively. Sec61β and Rab1a fragments were amplified by PCR from mCherry-Sec61β and Venus-Rab1a, respectively. A plasmid encoding NLuc-Epac-VV, BRET cAMP sensor, was kindly provided by Professor Kirill Martemyanov, Scripps Research Institute (Masuho et al., 2015). NLuc-Epac-VV was targeted to the ER by the addition of Sec61β to the C-terminus of the sensor by Gibson assembly, creating NLuc-Epac-VV-Sec61β. NLuc-Epac-VV was targeted to the plasma membrane and the lipid droplets via the addition of PDE2A3 and PLIN1 to the N-terminus of the sensor via Gibson assembly, creating PDE2A3- and PLIN1-NLuc-Epac-VV. PDE2A3 and PLIN1 were amplified from PDE2A3- and PLIN1-CAMYEL sensors respectively, under standard PCR conditions. FRB-Nb80 and FKBP-GalT were kindly provided by Professor Mark von Zastrow, University of California San Francisco (Irannejad et al., 2017). FRB was amplified via PCR from FRB-Nb80 and N-terminally fused to Halo-mini-Gα proteins to create FRB-Halo-mini-Gα constructs by Gibson assembly. The Halo tag was subsequently replaced with NLuc (amplified from FFAR4-NLuc), via Gibson assembly. FKBP-Sec61β was created by amplifying FKBP from FKBP-GalT and Sec61β from NLuc-Epac-VV-Sec61β by PCR. FKBP was fused N-terminally to Sec61β in replacement of NLuc-Epac-VV by Gibson assembly. PLIN1 was amplified from PLIN1-NLuc-Epac-VV and fused to FKBP in replacement of Sec61β, creating FKBP-PLIN1. FKBP-K-ras was created by replacing Venus from Venus-K-ras with FKBP by restriction digest. FKBP was amplified from FKBP-GalT using primers incorporating restriction sites (BamHI and BsrGI) flanking FKBP. All other plasmids were taken from Calebiro lab stocks. All primer sequences for cloning are provided in the appendices.

2.2 Methods

2.2.1 Cell culture

2.2.1.1 Human embryonic kidney 293 cells

Human embryonic kidney 293 (HEK293) cells (ATCC) were cultured in Dulbecco's Modified Eagle Medium (DMEM) containing 10% foetal bovine serum (FBS), 100 U/ml penicillin, and 0.1 mg/ml streptomycin. Cells were incubated at 37 °C, 5% CO_2. For HILO imaging experiments, HEK293 cells were seeded at a density of 6.0×10^5 cells/well in a 6-well plate containing 24-millimetre (mm) round glass coverslips or at 7.0×10^5 cells/well in 6-well plates for BRET assays.

2.2.1.2 3T3-L1 cells

3T3-L1 cells (fibroblast cells isolated from mouse embryo) were purchased from ATCC (CL-173). They were cultured in preadipocyte expansion medium consisting of DMEM supplemented with 10% bovine calf serum (BCS), 100 U/ml penicillin, and 0.1 mg/ml streptomycin. 3T3-L1 cells were sub-cultured before reaching 70% confluence. For differentiation, 3T3-L1 cells were seeded in 6-well plates at density of 8×10^4 cells/well and grown for 48 hrs or until 100% confluency. After 48 hrs, the cells were fed with preadipocyte expansion medium. After another 48 hrs, media was replaced with preadipocyte expansion medium consisting of DMEM supplemented with 10% FBS, 1.0 µM Dexamethasone (Dex), 0.5 millimolar (mM) Methylisobutylxanthine (IBMX), 1.0 µg/mL bovine insulin, 100 U/ml penicillin, and 0.1 mg/ml streptomycin. Cells were incubated for another 48 hrs before the medium was replaced with adipocyte maintenance medium – DMEM supplemented with 10% FBS, 1.0 µg/mL bovine insulin, 100 U/ml penicillin, and 0.1 mg/ml streptomycin. Maintenance medium was replaced every 48 hrs and cells were fully differentiated within 7-15 days (Figure 2.1A).

Differentiated 3T3-L1 adipocytes were assessed by lipid droplet formation and verified by staining with LipidSpot™ 610 nm (biotium 70065-T) as per the manufacturers protocol (Figure 2.1B). Briefly, LipidSpot™ 610 nm was diluted (1:1000 dilution) in DMEM supplemented with 10% FBS. Cells were incubated with diluted LipidSpot™ 610 nm for 30 minutes, and subsequently washed with complete culture media three times.
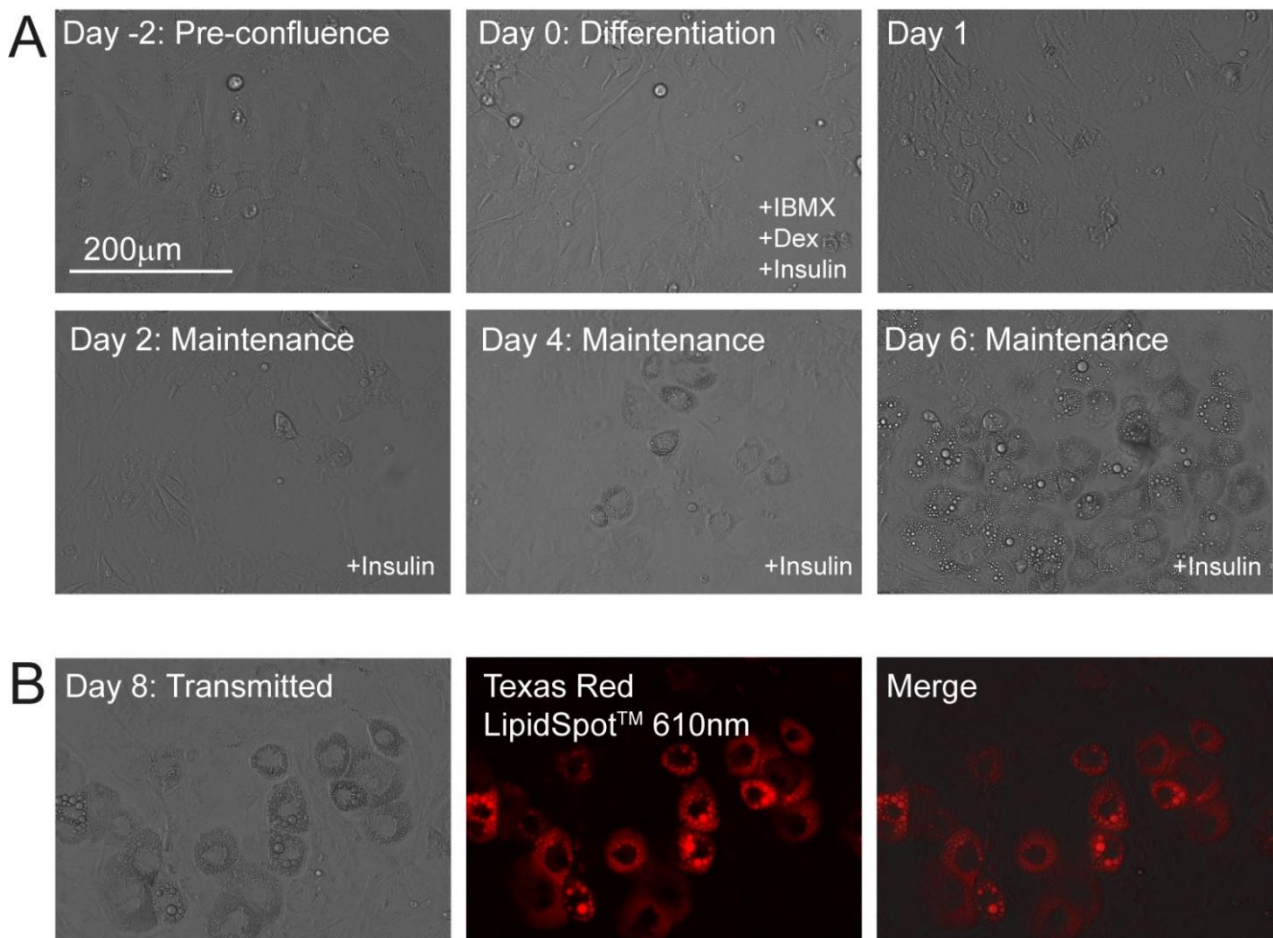
Figure 2. 1: Images showing the time course of 3T3-L1 differentiation.
(**A**) Differentiation time course of 3T3-L1 cells. Shown are the representative images of 3T3-L1 cell differentiation. Cells were treated with differentiation media (DMEM supplemented with 10% FBS, 0.5 mM IBMX, 1 µM Dex, and 1.0 µg/mL insulin) when confluence was reached. This marked the start of the differentiation process (Day 0). After 48hrs, the media was replaced with maintenance media (DMEM supplemented with 10% FBS and 1.0 µg/mL insulin) (Day 2). Maintenance media was refreshed

every 48 hrs until 3T3-L1 cells were differentiated. (**B**) Images to confirm lipid droplet presence in 3T3-L1 adipocytes. Shown are representative images of 3T3-L1 adipocytes stained with LipidSpot[TM] 610 nm. Images show transmitted light (left), Texas red (middle) or transmitted and Texas red images combined in a merged image (right) taken on an Evos fluorescence microscope. Lipid droplets are shown in red.

2.2.1.3 Immortalised brown preadipocytes

Immortalised brown preadipocytes (Harms et al., 2014, Sustarsic et al., 2018) were cultured in GlutaMAX™ DMEM (ThermoFisher), supplemented with 10% FBS, 100 U/ml penicillin, and 0.1 mg/ml streptomycin. Cells were incubated at 37 °C with 5% CO_2. Preadipocytes were sub-cultured before reaching confluence. For adipocyte differentiation, preadipocytes were either seeded into a 10 cm Petri dish at a density of 1.3×10^6 cells/dish, in a 6-well plate at a density of 5×10^5 cells/well onto 24mm glass coverslips (live-cell imaging) or 22-mm 1.5H thick glass coverslips (structured illumination microscopy), or into a 96-well plate at 6×10^4 cells/well (fatty acid quantification/glycerol quantification). Upon reaching 100% confluency, complete culture medium was replaced with differentiation medium, comprising of high glucose GlutaMAX™ DMEM supplemented with 500 μM IBMX, 1 μM Dexamethasome, 1 nM Triiodo-L-Thyronine (T3), 0.5 μM Rosiglitazone, 20 nM human Insulin, 100 U/ml penicillin, and 0.1 mg/ml streptomycin. After 48 hrs, the differentiation medium was replaced with maintenance medium, containing high glucose GlutaMAX™ DMEM supplemented with 1 nM T3, 20 nM Insulin, 100 U/ml penicillin, and 0.1 mg/ml streptomycin (Figure 2.2A). After 24 hrs the adipocytes were transfected for BRET/imaging assays. Adipocyte differentiation was assessed by the formation of lipid droplets, and further validated by transfection of PLIN1-mCherry – a protein which

localises to the surface of lipid droplets (Sztalryd and Brasaemle, 2017) (Figure 2.2B&C).
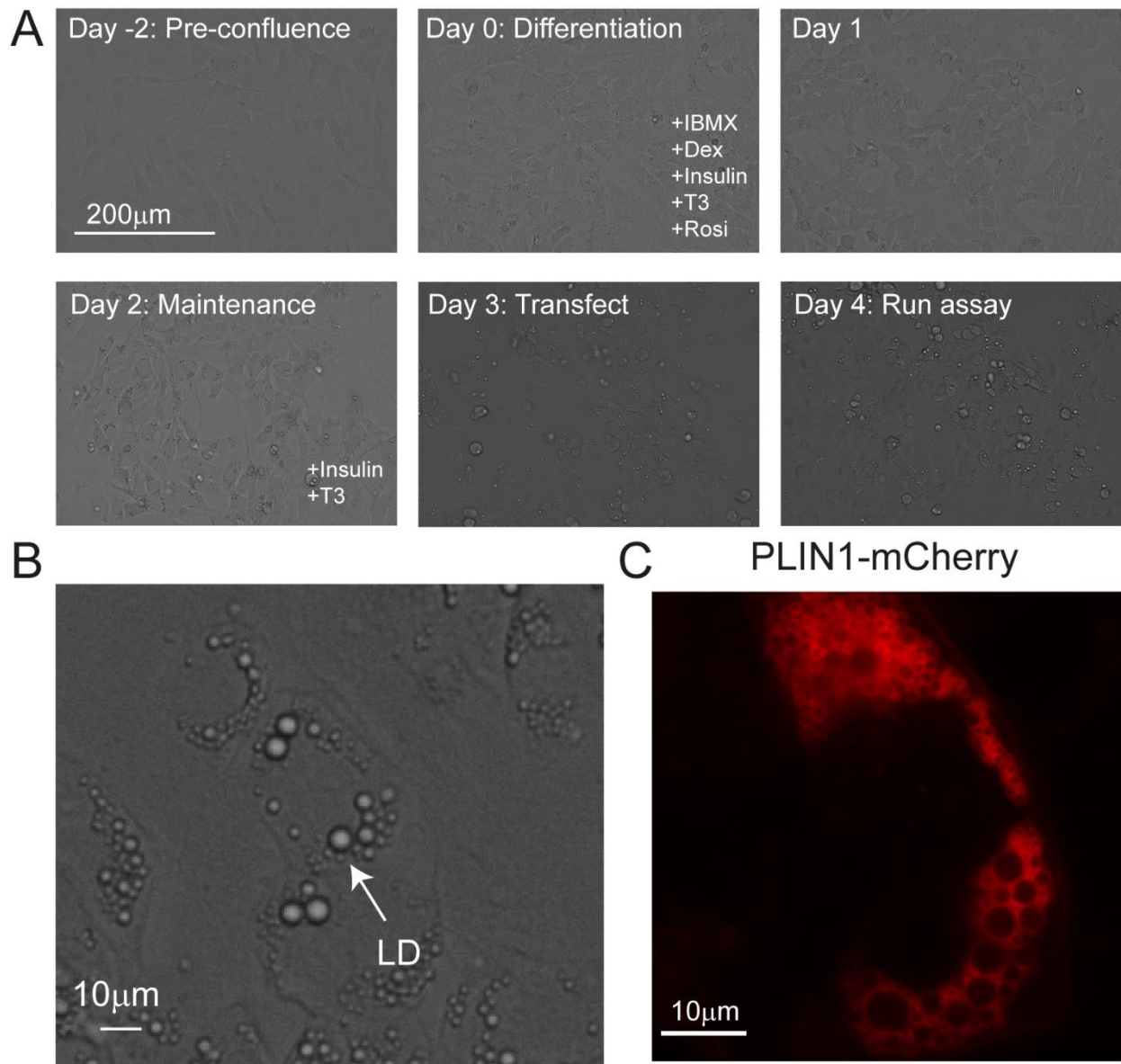
Figure 2. 2: **Images demonstrating the time course of immortalised brown adipocyte differentiation.**

(**A**) Differentiation time course of immortalised brown preadipocytes. Shown are representative images of immortalised brown adipocyte differentiation. Cells were treated with differentiation media (GlutaMAX™ DMEM supplemented with 10% FBS, 500 μM IBMX, 1 μM dexamethasone (Dex), 1 nM T3, 0.5 μM Rosiglitasone (Rosi), and 20 nM insulin) when confluence was reached. This marked the start of the differentiation process. After 48hrs, the media was replaced with maintenance media

(GlutaMAX™ DMEM supplemented with 10% FBS, 1 nM T3, and 20 nM insulin). (**B**) Zoomed in image representative of lipid droplet (LD) structure in transmitted light (at day 4). (**C**) Differentiated immortalised brown adipocytes transfected with PLIN1-mCherry as a marker of the lipid droplets.

2.2.2 Passaging

All cell types were passaged prior to reaching confluency. For passaging, cells were first washed with Dulbecco's phosphate-buffered saline (DPBS), and subsequently incubated at 37 °C with 0.25% trypsin-EDTA until fully detached from the culture vessel. Cells were transferred into a new culture vessel at the desired density in complete culture media

2.2.3 Labelling

For HaloTag® labelling, Janelia Fluor® HaloTag® 646 (Promega) was used. For ER labeling, ER-tracker Red^{TM} (ThermoFisher, E34250) was used. For mitochondria labeling, MitoTracker Red^{TM} CMXRos (ThermoFisher, M7512) was used. Cells were first washed with DPBS. The labels were diluted to 1 μM in fresh DMEM supplemented with 10% FBS (without antibiotic) and incubated with cells for 30 mins at 37 °C and 5% CO_2. The cells were then washed three times with fresh warm culture medium before live cell imaging.

2.3 Transfection

2.3.1 Lipofection

Lipofectamine™ 2000 transfection reagent (ThermoFisher Cat# 11668019) was used to introduce exogenous DNA for transient protein expression in HEK293 cells. Cells were seeded at 70-80% confluence in 6-well plates the day prior to transfection, with

transfections performed as per manufacturer's protocol. In short, per well of a 6-well plate, DNA (no more than 2 µg) was diluted in 100 µL Opti-MEM™ (ThermoFisher Cat# 31985070) and incubated for 5 minutes in sterile tubes. 3 µL of lipofectamine was added to the DNA:Opti-MEM™ mix and incubated for a further 20 minutes at room temperature to enable lipid:DNA complex formation. The final solution was gently pipetted into the 6-well plate, and the plate was incubated overnight at 37 °C with 5% CO_2. Typically, experiments were carried out 24-48hrs post transfection.

2.3.2 TransfeX

TransfeX (ATCC) was used to transfect 3T3-L1 preadipocytes for BRET assays. 3T3-L1 cells were seeded at a density of 9.0×10^4 cells/well in Nunc™ white F96 MicroWell™ plates. After 24hrs, cells were transfected with DNA plasmid using TransfeX, as per the manufacturer's protocol. Briefly, TransfeX was warmed to room temperature and mixed gently. Transfection master-mixes were composed in sterile tubes combining 20 µL Opti-MEM™, plasmid DNA, and 0.2 µLTransfeX per well of a 96-well plate. After each component addition, the tubes were gently mixed. DNA mixes were left to incubate at room temperature for 15-30 minutes. Transfection complexes were subsequently added to cells. Cells were then incubated at 37 °C with 5% CO_2 for a further 24 hrs prior to assay performance.

2.3.3 TransIT-X2

TransIT-X2 (Mirus) was used to transfect immortalised brown preadipocytes and differentiated immortalised brown adipocytes. TransIT-X2 was warmed to room temperature and vortexed gently. Transfection master-mixes were made up in sterile tubes combining 15 µL Opti-MEM™, plasmid DNA, and 0.45µL TransIT-X2 per well of

a 96-well plate. After each component addition, the tubes were gently vortexed. The master-mix was distributed into a Nunc™ white F96 MicroWell™ plate and left to incubate at room temperature for 15-30 minutes. Preadipocytes/differentiated brown immortalised adipocytes were trypsinized, counted, and seeded into 96-well plates at a density of 6×10^4 cell/well. Cells were then incubated at 37 °C with 5% CO_2 for 24 hrs prior to assay performance.

2.3.4 Electroporation

Undifferentiated 3T3-L1 cells were seeded in 35 mm x 10 mm round cell culture dishes (Corning® Cat# 430165). At approximately 90% confluency, the cells were washed twice with 1X DPBS before detachment with 0.25% trypsin-EDTA. Cells were resuspended in warmed compete culture medium and pelleted at 100 g for 3 minutes and the supernatant was discarded. The cells were washed twice with 1X DPBS and were subsequently resuspended in 240 µL 1X DPBS. 120 µL of cell suspension was added into each 4 mm cuvette alongside 40 µL of 1 µg/µL DNA (40 µg DNA total). The cells were electroporated at 320 V and 125 µF using a Gene Pulser Xcell™ Eukaryotic system (Bio-Rad Cat# 1652661). Following electroporation, 1 mL of warmed complete media was added to each cuvette and gently pipetted once. For imaging assays, 100 µL of electroporated cells was added to one well of a 6-well plate. Cells were subsequently differentiated into mature adipocytes where required.

2.3 Bacterial methods

2.3.1 Transformation of DH5α competent E. coli

High efficiency DH5α competent E. Coli (NEB, C29871) were transformed as per the manufacturer's protocol. Briefly, 1-100ng of plasmid DNA was added to 25 µL of

competent DH5α E. Coli. Cells and plasmid DNA were gently mixed and incubated on ice for 30 minutes and subsequently heat shocked at 42°C for 45 seconds. The mix was placed on ice for a further 5 minutes. 475 μL of Lennox broth (LB) outgrowth media was added, gently mixed, and incubated at 37 °C for 1 hour, shaking at 220 revolutions per minute (rpm). 50-100 μL of LB-competent cell mix was plated on agar containing appropriate selection antibiotic and was incubated overnight at 37 °C for 12-16 hours. Surviving colonies were used to inoculate 3-4 mL of LB outgrowth media containing appropriate selection antibiotic which was incubated at 37 °C for 1 hour, shaking at 220 rpm. This culture was used for mini preps, or to inoculate 100-250 mL of LB outgrowth media for maxi preps.

2.4 DNA methods

2.4.1 Mini prep

Small-scale plasmid production was completed using GeneJET™ Plasmid Miniprep Kit (ThermoFisher Scientific Cat# K0503) as per the manufacturer's instructions. 2 mL of inoculated bacterial culture was harvested at 6800 g in a microcentrifuge tube for 2 minutes at room temperature. The created pellet was resuspended, lysed, and DNA was precipitated. The supernatant was transferred into a ThermoFisher Scientific GeneJET™ Spin column, centrifuged, subjected to a series of washes, and plasmid DNA was eluted in HyClone™ Molecular Biology Grade Water (Fisher Scientific Cat# 10307052).

2.4.2 Maxi prep

Large-scale plasmid preparation was achieved using GeneJET™ Plasmid Maxiprep kit (ThermoFisher Scientific Cat# K0491) as per the manufacturer's instructions. 100-

250mL of bacterial culture was pelleted by centrifugation at 4°C for 10 minutes. The pellet was resuspended, lysed, and DNA was precipitated. The remaining supernatant was transferred into a GeneJET™ Maxi purification column and centrifuged. The purification column was subjected to a series of washes before final DNA plasmid elution in HyClone™ Molecular Biology Grade Water. All plasmid DNA was stored at -20°C.

2.4.3 DNA quantification

The concentration of plasmid DNA was quantified using a NanoDrop ND-2000c spectrophotometer. Concentrations were estimated by measuring the absorbance of plasmid DNA at 260 nm. The absorbance at 280nm was also measured to assess DNA purity. A DNA solution with a 260/280 ratio between 1.7 – 2.0 nm was considered pure enough for use.

2.4.4 PCR

For cloning purposes, restriction sites were incorporated into primers and DNA fragments were expanded using PCR. Primers were designed to have lead sequences, Kozak sequences, restriction sites, hybridisation sequences and stop codons (where necessary). The hybridisation sequence was 18-21 bp in length to avoid off target binding and the overall primer was designed to have 40-60% GC content with minimal secondary structure/self-dimerization. A GC 3' clamp was incorporated where possible. The PCR reaction was set up to the following cycling conditions:

PCR Stage	Temperature (°C)	Time (S)	Cycles
Initial denaturation	98	30	1x
Denaturation	98	10	30x
Annealing	~50-68	20	
Extension	72	s/kb	
Final extension	72	120	1x

Table 1. 1: Table to demonstrate the PCR conditions used to amplify DNA fragments from plasmid DNA.

PCR reactions were performed in 25 µL volumes using the following reagents and concentrations:

Component	Final Concentration	Stock Concentration	Dilution	Volume (mL)
HyClone™ water	-	-	-	11.25
Q5® reaction buffer (NEB B9027S)	1x	5x	5	5.00
dNTP mix (ThermoFisher)	200 mM	10 mM	50	0.50
Reverse primer	0.5 mM	10 mM	20	1.25
Forward primer	0.5 mM	10 mM	20	1.25
Template DNA	0.02 ng/mL	1 ng/mL	50	0.50
GC enhancer (NEB B9027S)	1x	5x	5	5.00
Q5® polymerase (NEB M0491S)	0.02 units/mL	2 units/mL	100	0.25

Table 1. 2: Table to demonstrate components and concentrations of the PCR buffer used to amplify DNA fragments from plasmid DNA.

2.4.5 PCR clean-up

PCR product was purified using Nucleospin® Gel and PCR clean-up (MACHERY-NAGEL Cat# 740609.10) as per the manufacturer's protocol. Briefly, PCR product was mixed in a 1:2 ratio with buffer NT1 and subsequently loaded into a NuleoSpin® and

PCR clean-up column where it was subjected to a series of spins and washes. All spins were performed at 14,000 g. The membrane was dried, and DNA was eluted in HyClone™ Molecular Biology Grade Water.

2.4.6 Restriction digestion

All restriction enzymes were used as to the manufacturer's protocol (NEB). In short, 1 µg of DNA was digested using 1 µL of restriction enzyme in 1X NEB cutsmart buffer for 1hr at 37 °C. Digested DNA was resolved, excised, and quantified before vector ligation.

2.4.7 Agarose gel electrophoresis

DNA fragments and digested DNA were separated using a 0.8 % agarose gel in 1X Tris-Acetate-EDTA buffer containing 1X GelRed DNA stain (ThermoFisher Scientific Cat# 41003-T). DNA samples were resuspended with a 1X purple loading dye (NEB) and loaded alongside a 1 kb DNA ladder. Digested DNA was resolved at 100 V. Fragments were subsequently visualised under UV illumination.

2.4.8 Recovery

DNA was extracted from the 0.8 % agarose gel using a GeneJET Gel Extraction Kit (ThermoFisher Scientific Cat# K0691) as per the manufacturer's protocol. DNA bands of interest were excised from the agarose gel using a scalpel. Excised bands were weighed and dissolved at 50-60 °C in 1:1 ratio with binding buffer. Fragments were purified using GeneJET purification columns, washed, and eluted in HyClone™ Molecular Biology Grade Water. Purified DNA was stored at -20°C.

2.4.9 DNA Ligation

DNA ligation was performed using T4 DNA Ligase (NEB Cat# M0202) as to the manufacturer's protocol. In general, a 3:1 ratio for vector: insert (determined using the NEBioCalculator™) was mixed with T4 DNA ligase and 1X T4 DNA Ligase Buffer. The solution was mixed at room temperature for 10 minutes and heat inactivated at 65°C for 10 minutes. The mix was chilled on ice and 1-5 µl of ligated DNA plasmid was transformed in 25 µl of competent DH5α E. Coli (high efficiency), as described previously.

2.4.10 Gibson assembly

Primers were designed with complementary ends to amplify the desired fragments from template plasmid DNA using PCR cloning primer design software (Sun et al., 2013). Fragments were amplified by PCR and run on an agarose gel to determine whether the correct size of fragment had been amplified during the PCR, as described previously. Template DNA from successful reactions was digested using Dpn1 (NEB R0176S) at 37 °C for 1 hr, leaving the PCR product for Gibson assembly. The PCR product was purified using Nucleospin® Gel and PCR clean-up (MACHERY-NAGEL Cat# 740609.10) as per the manufacturer's protocol. 2.5 μL of fragment DNA was added to 7.5 μL Gibson assembly mastermix. Gibson assembly mastermix was prepared using 320 μL of 5X isothermal reaction buffer (25% PEG-8000, 500 mM Tris-HCl pH 7.5, 50 mM $MgCl_2$, 50 mM DTT, 1 mM each of the four dNTPs, and 5 mM NAD) with the addition of 160 μL of 40 U/μL Taq DNA Ligase (NEB M0208L), 20 μL of 2 U/μL Phusion high-fidelity DNA polymerase (NEB M0530S), and 0.64 μL of 10 U/μL of T5 Exonuclease (NEB M0663S) made up to a final volume of 1.2 mL in HyClone™ Molecular Biology Grade Water (Gibson et al., 2009). Gibson assembly

was conducted for 10 mins at 50°C followed by 1 hr at 37 °C. 5 µL of solution was added in a 25 µL reaction of high efficiency competent cells for bacterial transformation (as described previously).

2.4.11 DNA sequencing

All cloned constructs were verified by sequencing. DNA sequencing was performed by Source BioScience. A total of 500 ng of plasmid DNA was submitted alongside 3.2 ρmol/μl of primer. All sequencing was performed using the Sanger method.

2.5 Fatty acid and glycerol quantification

2.5.1 Sample collection

Media samples were collected from differentiated immortalised brown adipocytes for fatty acid quantification, glycerol quantification, and gas chromatography mass spectrometry (GCMS) analysis. To collect samples, immortalised brown preadipocytes were differentiated in 96-well plates (as described previously), serum starved (2 hrs), and washed twice with DPBS. Cell media was replaced with Krebs-Ringer buffer (pH 7) supplemented with 0.1% fatty acid free bovine serum albumin (BSA) (unless specified). After treatment with agonists, antagonists, or vehicle control, 50-100 μL of media was collected at desired time points. Samples were frozen and stored at -80°C prior to quantification.

2.5.2 Glycerol quantification

From collected samples, total glycerol concentration was quantified using the luminescence Glycerol-Glo^{TM} assay (J3151, Promega). Using this assay, light production is proportional to the concentration of glycerol in the sample.

Kit reagents included glycerol detection solution, pro-luciferin reductase substate, kinetic enhancer, and glycerol standard. Reagents were thawed to room temperature, mixed by inversion, and the kinetic enhancer and pro-luciferin reductase substrate were placed on ice. Together, frozen samples for glycerol quantification were thawed to room temperature. When reagents were defrosted, glycerol detection reagent was prepared by adding 10 μL reductase substrate per mL of glycerol detection reagent. After 1hr, 10 μL of kinetic enhancer was added to the glycerol detection solution and was mixed by inversion. Defrosted samples and glycerol standard were aliquoted, in at least duplicate, into a Nunc™ white F96 MicroWell™ plate (50 μL). Glycerol standard was diluted in Krebs-Ringer buffer (pH 7) supplemented with fatty acid free BSA as specified. 50 μL of prepared glycerol detection reagent was added onto the samples. The plate was then incubated at room temperature and protected from light. After 1 hr, luminescence was read using a PHERAstar® plate reader.

The concentration of glycerol in the collected samples was calculated in Excel using the following equation:

Glycerol (μM) = Standard (μM) × (Sample luminescence – Background luminescence) / (Standard luminescence – Background luminescence)

Luminescence values from typical standards are shown below.
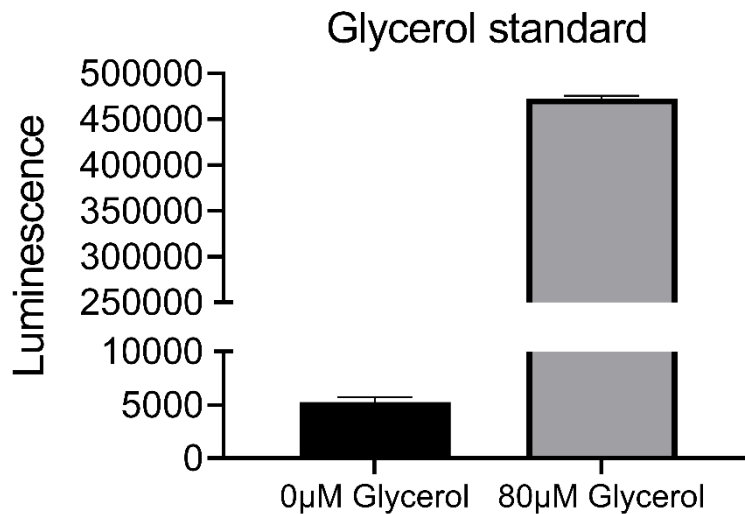
Figure 2. 3: Glycerol-Glo^{TM} standard.

Typical standard values produced from Glycerol-Glo^{TM} detection assay. Shown are the resulting luminescence values from glycerol standards of 0- and 80 μM using the Glycerol-Glo^{TM} assay.

2.5.3 Fatty acid quantification

The total fatty acid concentration from collected samples was quantified using colorimetric FFA quantification kit (MAK044, Sigma Aldrich). The FFA kit detects FFA (C8 and longer) through a coupled enzyme assay which produces a colorimetric product proportional to fatty acid content.

Reagents and samples for fatty acid quantification were defrosted and mixed. Palmitic acid standard (0-, 40-, 80-, 120-, 160-, 200 μM), or sample, were aliquoted (50 μL), in at least duplicate, into a clear-bottomed 96-well plate. Standards were diluted to the appropriate concentration in Krebs-Ringer buffer (pH 7) supplemented with fatty acid free bovine serum albumin (BSA) when required. 2 μL of ACS reagent was added to

each well and the plate was incubated for 30 minutes at 37 °C. A master reaction mix was created according to the total volume required for each reaction (Table 3).

Reagent	Volume (μL)
Krebs-Ringer buffer (pH 7)	44
Fatty acid probe	2
Enzyme mix	2
Enhancer	2

Table 1. 3: Table to demonstrate fatty acid quantification master mix volumes required for one well of a 96-well plate.

50 μL fatty acid quantification master mix was added to each sample/standard, mixed by shaking, and incubated at 37 °C for a further 30 minutes. To assess fatty acid concentration, the absorbance (at 570 nM) was measured using a PHERAstar® plate reader. Standard values were plotted on a standard curve with GraphPad prism using a linear-regression curve fit. Sample values were corrected by subtracting background values (0 μM palmitic acid standard). Fatty acid concentration was quantified by comparing the unknown samples to the standard curve. Absorbance values from a typical standard curve are shown below (Figure 2.4).
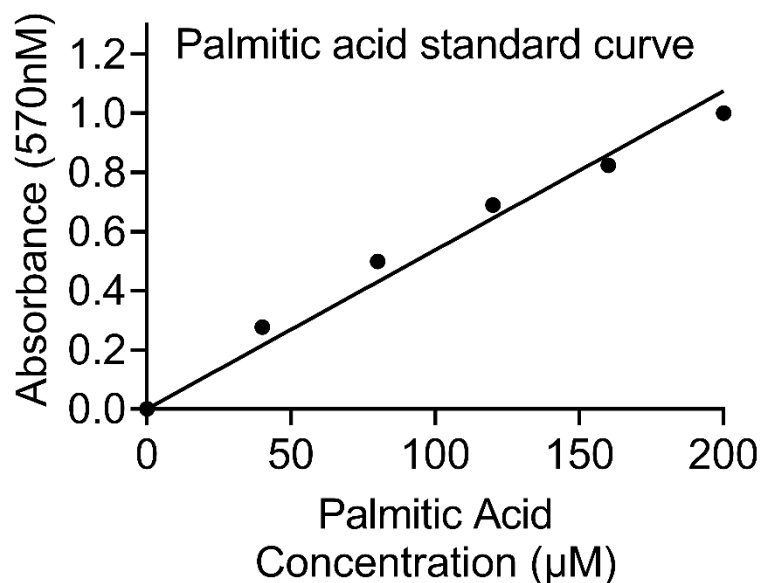
Figure 2. 4: Fatty acid kit standard curve.

Typical standard curve produced using FFA kit detection assay. Shown are typical palmitic acid standard (0-, 40-, 80-, 120-, 160-, 200 μM) absorbance values quantified for total fatty acid content. Absorbance (at 570 nM) was measured using a PHERAstar® plate reader.

2.5.4 Fatty acid extraction

Adipocytes were differentiated in a 6-well plate, serum starved (2 hrs), and washed with DPBS. Culture media was replaced with Krebs-Ringer buffer (pH 7) supplemented with BSA where indicated. Upon stimulation with agonist or vehicle, 1 mL of media sample was collected for fatty acid extraction at desired time points. Collected samples, or palmitic acid standard, were resuspended in Krebs-Ringer buffer (at a known concentration) and total fatty acid content was extracted. Fatty acids were extracted from larger media samples and concentrated into a smaller volume to increase the detection limit of the fatty acid quantification kit (MAK044, Sigma Aldrich).

Media samples (1 mL) were added to glass tubes. Methanol (1 mL) was subsequently added followed by hexane in excess (2 mL). The samples were quickly vortexed and

then centrifuged for 20 mins (at 4 degrees) until clear biphasic separation was observed. The top fraction of sample, containing lipids, was removed with a glass Pasteur pipette, and transferred into a clean glass tube. Hexane solvent was subsequently evaporated using a nitrogen condenser and the remaining extracted fatty acid sample or standard was resuspended in fatty acid buffer (from fatty acid quantification kit MAK044, Sigma Aldrich) for quantification.

2.6 Fluorescence imaging

2.6.1 Highly inclined and laminated optical sheet (HILO) microscopy

Live-cell imaging was performed on a custom system (CAIRN Research) total internal reflection fluorescence (TIRF) microscope equipped with an Eclipse Ti2 microscope (Nikon, Japan), an 100x oil-immersion objective, 405-, 488-, 561-, and 637 nm diode lasers (Coherent, Obis), an iLas2 TIRF illuminator (Gataca Systems), quadruple band excitation and dichroic filters, a quadruple beam splitter, and four EMCCD cameras (iXon Ultra 897, Andor). Coverslips were mounted in a microscopy chamber filled with Hanks' balanced salt solution (HBSS) supplemented with 10 mM HEPES (pH 7.5) and were maintained at 37 °C using a temperature-controlled enclosure throughout experiments. Images were acquired using MetaMorph multi-dimensional acquisition software and dual colour images were taken sequentially to minimise bleed through. The addition of post-acquisition image pseudocolours were added using ImageJ (https://imagej.nih.gov.ij/). Co-localisation analysis was performed in ImageJ using the JACoP plugin.

2.6.2 Structured illumination microscopy (SIM)

2.6.2.1 Sample preparation

Differentiated adipocytes were fixed in 4% PFA (ampoules Electron Microscopy sciences) diluted in PEM buffer (0.1 M PIPES (pH 6.95), 2 mM EGTA, 1 mM $MgSO_4$) for 15 minutes. Coverslips were washed three times with DPBS, quenched with 50 mM ammonium chloride, and washed again three times with DPBS. The coverslips were subsequently air dried and mounted on slides with prolong diamond (ThermoFisher) and sealed using clear nail polish. Slides were cured at room temperature for 48 hrs before imaging.

2.6.2.2 SIM imaging

Images were acquired using a SIM microscope equipped with an Eclipse Ti2 microscope (Nikon, Japan), an 100x oil-immersion objective, 405-, 488-, 561-, and 640 nm diode lasers, a moveable diffraction grating incorporated within the excitation beam path, and EMCCD cameras. Two-dimensional (2D) SIM used three translations and three rotations of the diffraction grating, creating 9 raw images, and 3D SIM used 5 translations and 3 rotations of the diffraction grating, creating 15 raw images for each Z plane (taken in 0.05 nm sections). 2D and 3D raw images were reconstructed in NIS-Elements. Reconstructed 3D-images were then visualised in ARIVIS.

2.7 BRET

2.7.1 BRET assays

For BRET assays, HEK293 cells were resuspended in FluoroBrite™ DMEM (Life Technologies, Cat# A1896701) phenol red-free medium supplemented with 5% FBS, 10% L-Glutamine, and re-seeded in poly-D-lysine coated Nunc™ white F96 MicroWell™ plates at 1×10^5 cells/well. 3T3-L1 preadipocytes or immortalised brown adipocytes were transfected with TransfeX (ATCC) or TransIT-X2 (Mirus) (as mentioned previously) in Nunc™ white F96 MicroWell™ plates, respectively.

On the day of the assay, 48 hrs post transfection, the cell medium was replaced with HBSS (ThermoFisher Cat# 14025092) containing 1 μM furimazine/Nano-Glo® Luciferase Assay Substrate (Promega Cat #N113A) or 5 μM coelenterazine-h (Promega #S201A) supplemented with HEPES (10 mM). Furimazine was used when NLuc was used as the donor molecule and coelenterazine-h was used when RLuc or RLuc8 was the donor molecule. BRET measurements were taken at 37 °C using a PHERAstar® plate reader with a dual luminescence BRET1 plus filter – reading the emissions at 460-490 and 520-550 nm. Following four baseline reads, agonist or vehicle was administered to the cells and the BRET signal was measured every two minutes over the course of 1 hr. The BRET ratio was calculated by dividing the measured acceptor emission by the measured donor emission. The results were normalised to vehicle and the baseline values. Either the area under the curve (AUC) or the max BRET response minus minimum BRET response was calculated to compare between conditions.

2.8 Statistics

Statistical analysis was performed using GraphPad Prism 9 software. Values are given as mean ±S.E.M. Differences between two groups were assessed by a two-tailed student's t-test. Differences between three or more groups were assessed by one-way or two-way analysis of variance (ANOVA), as suitable, followed by Dunnett's or Holm-Šídák test for multiple comparisons between groups. Differences were considered significant for P values <0.05.

3.0 Chapter Three: Evaluation of FFAR4 signalling and

trafficking in a simple cell model

3.1 Aims of this study

The primary objective of this study was to characterise the signalling and trafficking profile of the FFAR4 in a simple cell model. Since the FFAR4S, and not the FFAR4L, is thought to couple to G proteins, the FFAR4S was studied within this thesis.

The G protein-coupling specificity of the FFAR4 is generally debated. Previous studies have investigated the coupling specificity of the FFAR4 by investigating the receptor's impact on downstream signalling pathways (cAMP and Ca^{2+}). Within this study, the trafficking and signalling profile of the FFAR4 was investigated. This not only delineated the primary coupling specificity of the FFAR4, but also interrogated the receptor's ability to signal from intracellular compartments. Furthermore, the function of the FFAR4 was assessed on second messenger activity using BRET-based methods.

3.2 Results

3.2.1 The FFAR4 is predominantly coupled to $G\alpha_{i/o}$ proteins in a simple cell model

To further investigate the coupling specificity of the FFAR4, mini-G probes, engineered GTPase domains of the $G\alpha$ subunit of a G protein (Nehme et al., 2017), were used. Mini-G probes rapidly translocate from the cytoplasm to active GPCRs upon receptor activation. This translocation can be quantified by imaging and BRET-based methods (Wan et al., 2018).

For this purpose, real-time BRET measurements were performed between FFAR4 carrying NLuc (FFAR4-NLuc) and Venus fused mini-G probe subtypes (mGα_i, mGα_o, mGα_s, mGα_q, or mGα_{12}) (Figure 3.1A). Three agonists were chosen to activate the FFAR4: TUG-891; Compound A (CpdA); and α-linolenic acid. TUG-891 (Hudson et al., 2013) and CpdA (Oh et al., 2014) are potent synthetic agonists of the FFAR4, and α-linolenic acid is an essential LCFA supposed to endogenously activate the FFAR4 (Hirasawa et al., 2005, Sanchez-Reyes et al., 2014). Agonist stimulation induced a major increase in BRET between the FFAR4 and mGα_i and mGα_o (Figure 3.1B&C). A minor increase in BRET was detectable between the FFAR4 and mGα_q. A small response was also detectable between the FFAR4 and mGα_s and Gα_{12} subtypes (Figure 3.1B&C). These results suggest that the FFAR4 is predominantly G$\alpha_{i/o}$ coupled in a simple cell model.
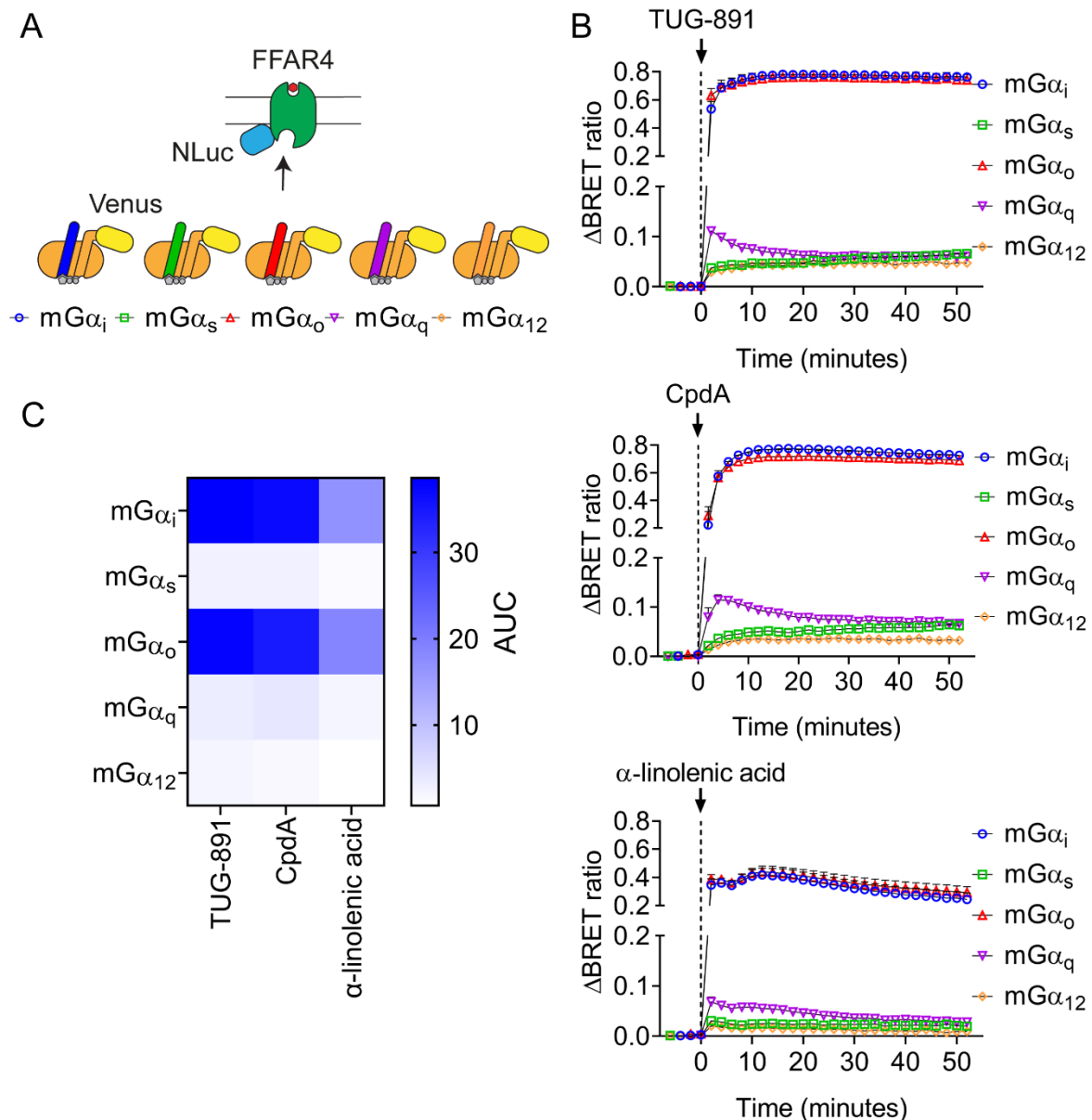
Figure 3. 1: BRET assay delineating the coupling specificity of the FFAR4 using FFAR4-NLuc and Venus-mini-G probes.

(**A**) Schematic to illustrate the BRET assay used to detect the G protein coupling specificity of the FFAR4 using mini-G probes. (**B**) Real-time BRET measurements of Venus fused mini-G probe (mGα_i, mGα_s, mGα_o, mGα_q, or mGα_{12}) recruitment to the FFAR4-NLuc upon TUG-891 (top), CpdA (middle), and α-linolenic acid (bottom) (10 μM) stimulation. (**C**) Corresponding AUC values are presented on a heat map. Data represent mean ± S.E.M. compiled from three independent experiments performed in triplicate.

To validate whether the BRET assay performed better with FFAR4 carrying NLuc or YFP, an analogous assay was designed. Within this assay, the real-time BRET between FFAR4 carrying YFP and NLuc-fused mini-G probes (mGα_i, mGα_s, mGα_q, or mGα_{12}) (Figure 3.2A) was measured after stimulation with FFAR4 agonists (TUG-891, CpdA, and α-linolenic acid). Agonist stimulation induced a major increase in BRET between the FFAR4 and mGα_i (Figure 3.2B&C). A minor increase in BRET was detectable between FFAR4 and mGα_q. Again, a virtually negligible response was detectable between the FFAR4 and mGα_s or mGα_{12} subtypes (Figure 3.2B&C). Compared to the previous assay, where BRET was measured between FFAR4-NLuc and Venus-mini-G probes (Figure 3.1), the agonist induced BRET between NLuc fused mini-G probe and FFAR4-YFP was considerably lower. In addition, the recruitment of mGα_q to the receptor was reduced. These results suggest that measuring the ligand induced BRET between FFAR4-NLuc and Venus fused mini-G probes is superior to measuring the ligand induced BRET between FFAR4-YFP and NLuc fused mini-G probes. Therefore, when further testing the coupling specificity of the FFAR4, FFAR4-NLuc was used in combination with Venus fused mini-G probes. Despite the alternative tag orientation, these data again suggest that the FFAR4 is a predominantly G$\alpha_{i/o}$ coupled receptor in a simple cell model.
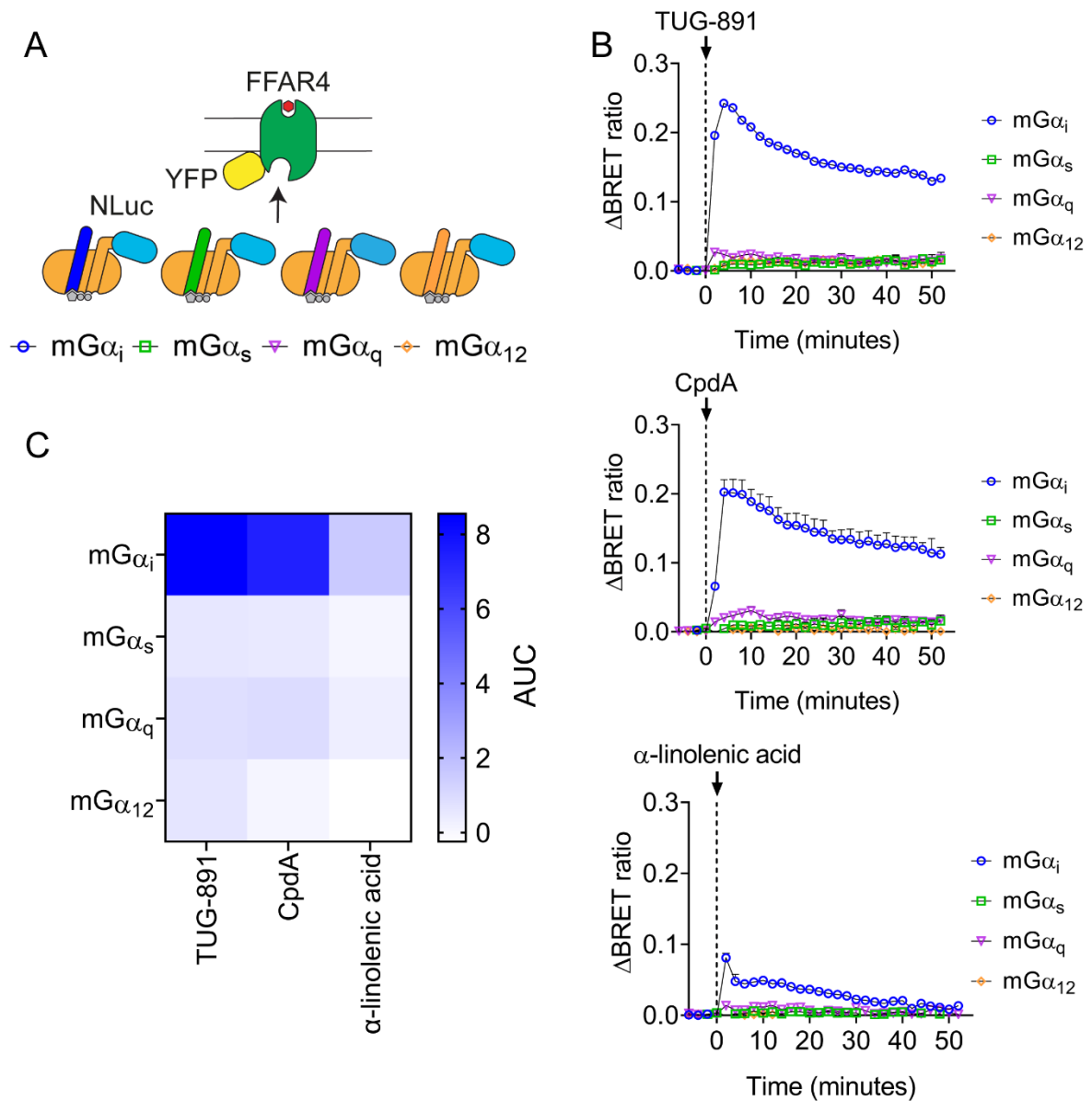
Figure 3. 2: BRET assay delineating the coupling specificity of the FFAR4 using FFAR4-YFP and NLuc-mini-G probes.

(**A**) Schematic to illustrate the BRET assay used to detect the G protein coupling specificity of the FFAR4 using mini-G probes. (**B**) Real-time kinetics of NLuc fused mini-G probe (mGα_i, mGα_s, mGα_q, or mGα_{12}) recruitment to the FFAR4-YFP upon TUG-891 (top), CpdA (middle), and α-linolenic acid (bottom) (all 10 μM) stimulation. (C) Corresponding AUC values displayed on a heat map. Data represent mean ± S.E.M. compiled from one independent experiment performed in triplicate.

3.2.2 Mini-G probes can be used to detect predominantly $G\alpha_{q/11}$ coupled GPCRs.

Considering that the FFAR4 is often considered a predominantly $G\alpha_{q/11}$ coupled receptor, and not a predominantly $G\alpha_{i/o}$ coupled receptor, the coupling specificity of a prototypical $G\alpha_{q/11}$ coupled receptor was also tested using mini-G probes. This was conducted to further validate that mini-G probes can detect when a GPCR is predominantly $G\alpha_{q/11}$ coupled rather than when a GPCR is predominantly $G\alpha_{i/o}$ coupled. The angiotensin type 1 receptor (AT$_1$R) was used in this assay since it has been shown in the literature to couple principally to $G\alpha_{q/11}$ proteins (Galandrin et al., 2016). Within this assay, the AT$_1$R-RLuc8 was co-transfected with mini-G probes and stimulated with angiotensin II (Figure 3.3A). Agonist stimulation induced a major increase in BRET between AT$_1$R and mGα_q (Figure 3.3B&C). A minor increased in BRET was detectable between mGα_i and the AT$_1$R. A virtually negligible response was detectable between the AT$_1$R and mGα_s and Gα_{12} subtypes. These results suggest that the AT$_1$R is a predominantly $G\alpha_{q/11}$ coupled receptor, with a partial coupling to $G\alpha_i$, in agreement with the literature (Galandrin et al., 2016) (Figure 3.3B&C). This indicates that mini-G probes maintain coupling specificity for $G\alpha_{q/11}$ coupled GPCRs and suggests that the FFAR4 is indeed a predominantly $G\alpha_{i/o}$ coupled receptor, rather than a predominantly $G\alpha_{q/11}$ coupled receptor.
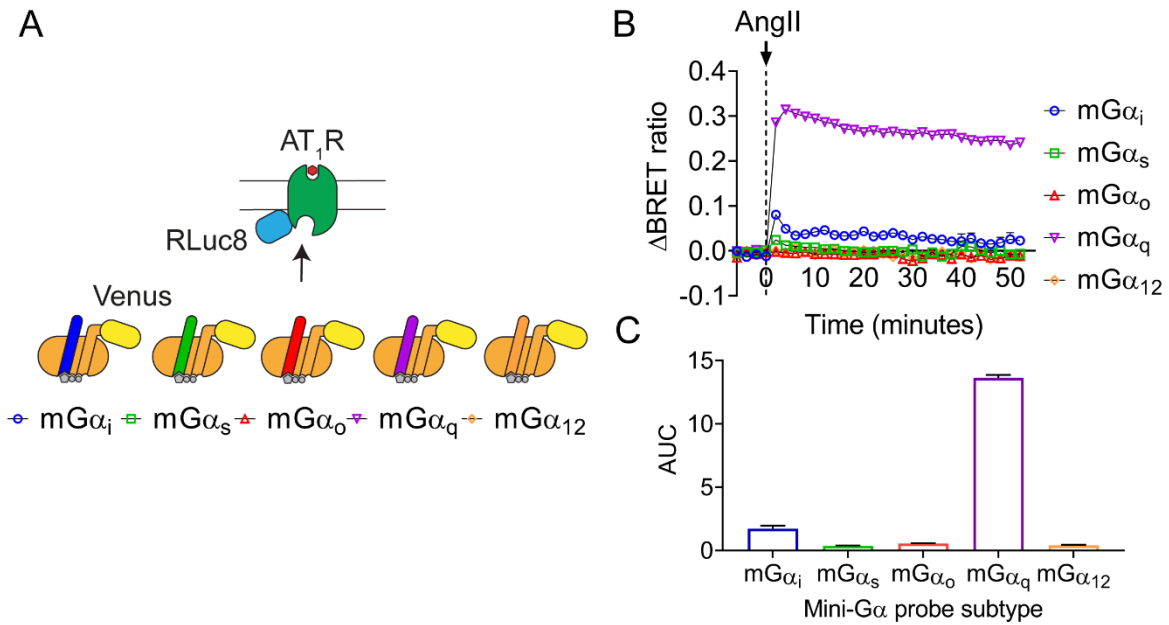
Figure 3. 3: BRET assay confirming the G protein coupling specificity of the AT₁R using AT₁R-RLuc8 and Venus-mini-G.

(**A**) Schematic to illustrate the BRET assay used to detect the G protein coupling specificity of the AT₁R using mini-G probes. (**B**) Real-time kinetics of Venus fused mini-G probe (mGα$_i$, mGα$_s$, mGα$_o$, mGα$_q$, or mGα$_{12}$) recruitment to the AT₁R-RLuc8 upon angiotensin II (AngII), 10 μM, stimulation. (**C**) Corresponding AUC values are presented on a bar graph. Data represent mean ± S.E.M. compiled from one independent experiment performed in triplicate.

3.2.3 Mini-G probe recruitment to the FFAR4 is specific

To validate that the detected ligand induced BRET responses were specific to FFAR4 activation, a selective FFAR4 NAM, AH7614 (Watterson et al., 2017), was used. AH7614 was hypothesised to reduce mini-G probe recruitment to the FFAR4. To test this hypothesis, the agonist induced BRET between Venus fused mini-G probe and FFAR4-NLuc was measured after stimulation with TUG-891 or CpdA, in the presence and absence of FFAR4 NAM, AH7614. After TUG-891 stimulation, AH7614 significantly reduced BRET between the FFAR4 and mGα$_i$, mGα$_o$, and mGα$_q$ probes (Figure 3.4A). A similar trend was also observed after CpdA stimulation, however,

AH7614 significantly reduced BRET between the FFAR4 and $mG\alpha_i$ and $mG\alpha_o$, and not $mG\alpha_q$, probes (Figure 3.4B). From these data, mini-G probe recruitment to the FFAR4 was considered specific and a valuable method to detect both FFAR4 activation and to identify the coupling specificity of the FFAR4 in live cells.
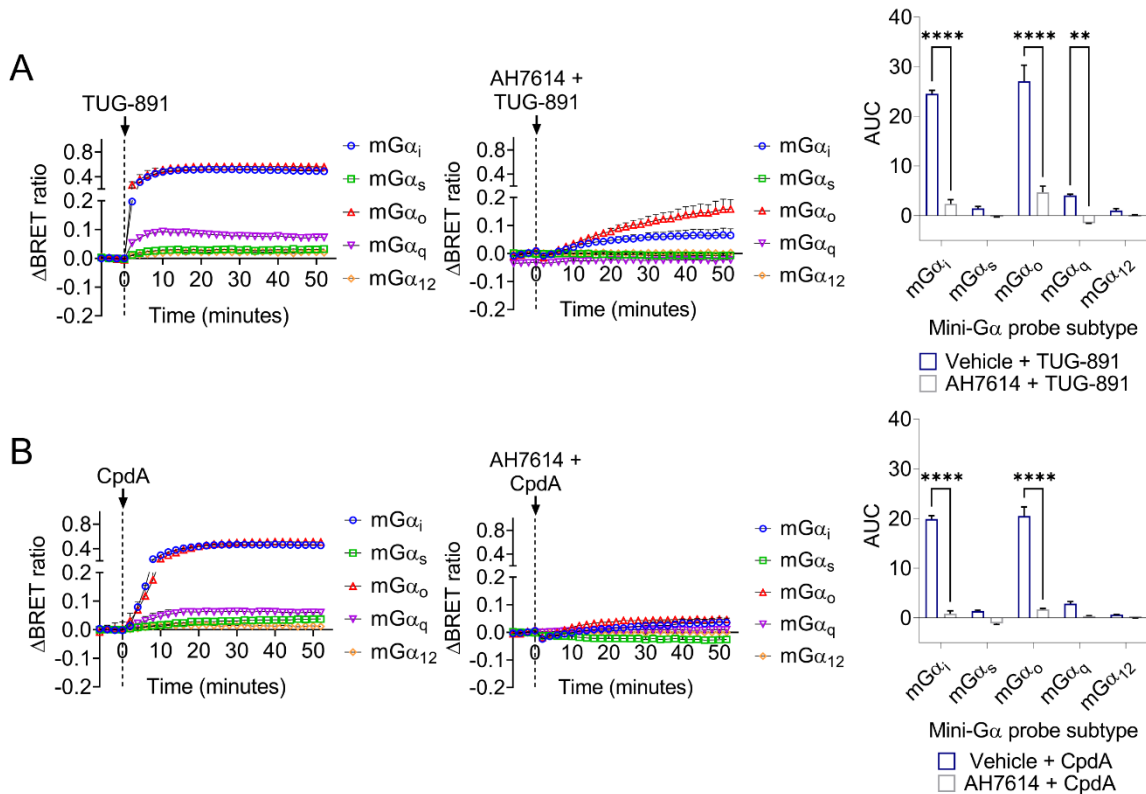
Figure 3. 4: BRET assay to confirm the specificity of Venus fused mini-G probe recruitment to FFAR4-NLuc.

(**A**) TUG-891 dependent increases in Venus fused mini-G probe recruitment to the FFAR4-NLuc in the presence or absence of FFAR4 NAM, AH7614. Shown are the real-time BRET responses after TUG-891 (1 μM) (left) stimulation with and without AH7614 (10 μM) preincubation (30 mins) (middle) in HEK293 cells. Corresponding AUC values (right) are displayed on a bar graph. (**B**) CpdA dependent increases in mini-G probe recruitment to the FFAR4-NLuc in the presence or absence of FFAR4 NAM, AH7614. Shown are the real-time BRET responses between FFAR4-NLuc and Venus fused mini-G probe after CpdA (1 μM) stimulation (left) with and without AH7614 (10 μM) preincubation (30 mins) (middle). Corresponding AUC values (right) are displayed on a bar graph. Differences are statistically significant by two-way ANOVA. **** $p < 0.0001$, ** $p < 0.01$ with Sidak's multiple comparison post hoc test. Data

represent mean ± S.E.M. and are compiled from one independent experiment performed in triplicate.

Having established a specific and dynamic method to evaluate the activation and the coupling specificity of the FFAR4 in a simple cell model, the efficacy of FFAR4 agonists (TUG-891, CpdA, and α-linolenic acid) were subsequently evaluated. For this purpose, the ligand induced bystander BRET was measured between NLuc fused mini-G probe and Venus-K-ras (a marker of the plasma membrane) in the presence of WT FFAR4 (Figure 3.5A). This was also achieved to ensure that the WT FFAR4 construct was functional. TUG-891 was found to have the strongest efficacy (EC_{50}: 6.397×10^{-7} M), followed by CpdA (EC_{50}: 1.864×10^{-6} M), and then by α-linolenic acid (EC_{50}: 2.199×10^{-5} M) (Figure 3.5B). 10 μM stimulations, for each FFAR4 agonist, was found to elicit strong FFAR4 activation, therefore, this concentration was used for future experiments.

In addition, the same assay design was used to assess the effect of AH7614, FFAR4 NAM, on TUG-891 stimulation (Figure 3.5C) (Watterson et al., 2017). Within this experiment, AH7614, at 10 μM and 100 μM, reduced the Emax of TUG-891, but did not alter its potency/EC_{50}. This further validates that AH7614 does not act competitively to TUG-891 (Watterson et al., 2017).
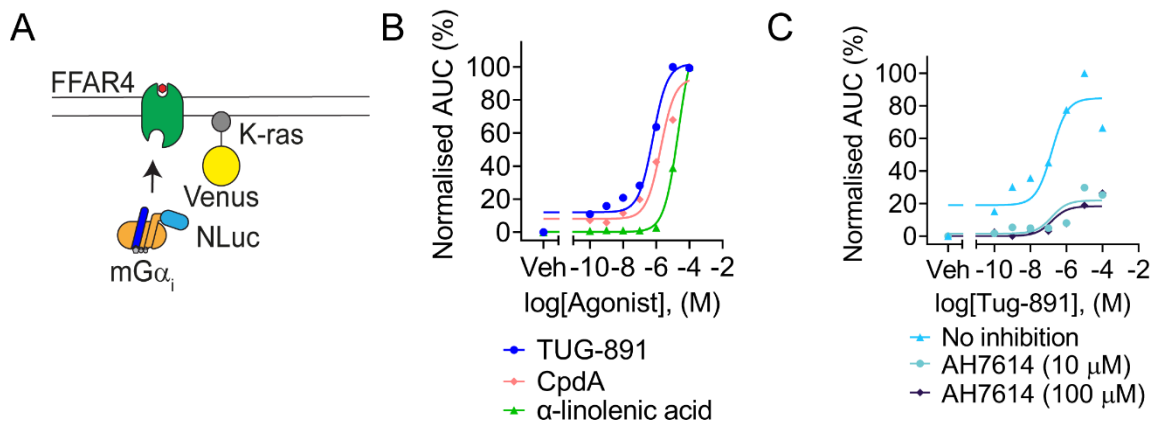
Figure 3. 5: BRET assay to evaluate the pharmacology of FFAR4 agonists and AH7614.

(**A**) Schematic to illustrate the BRET assay used to detect FFAR4 activation by measuring the bystander BRET between NLuc fused mini-Gα_i and Venus fused K-ras (plasma membrane marker). (**B**) Dose response curve measuring the ligand induced BRET between NLuc-mGα_i and Venus-K-ras in the presence of WT FFAR4 after stimulation with increasing concentrations of TUG-891, CpdA, or α-linolenic acid. (**C**) Dose response curve measuring the ligand induced BRET between NLuc-mGα_i and Venus-K-ras in the presence of FFAR4 after stimulation with increasing concentrations of TUG-891 in the presence or absence of AH7614 (10 μM and 100 μM, preincubation 30 mins). Data represent mean ± S.E.M. and are compiled from one independent experiment performed in triplicate.

3.2.4 The FFAR4 rapidly internalises to intracellular compartments in a simple cell model

After investigating the coupling specificity of the FFAR4, the localisation and trafficking profile of the receptor was investigated in a simple cell model. Within the literature, FFAR4 stimulation has been demonstrated to rapidly induce FFAR4 internalisation to endosomal and lysosomal compartments (Watson et al., 2012). Firstly, agonist induced receptor internalisation was recapitulated using a live-cell imaging approach. FFAR4-YFP was transfected into HEK293 cells and imaged using HILO microscopy,

a method especially suited for visualising dynamic trafficking and signalling events in live cells. Under basal conditions, the FFAR4 was localised predominantly at the plasma membrane, with a small amount localised at intracellular compartments (Figure 3.6). Upon stimulation with TUG-891, the FFAR4 rapidly internalised. This internalisation was inhibited in the presence of Dyngo4a – an antagonist that prevents receptor internalisation by dynamin inhibition (McCluskey et al., 2013) (Figure 3.6). Since agonist stimulation of the FFAR4 with TUG-891 appeared to stimulate FFAR4 internalisation into an endosomal-like compartment, and possibly to other compartments, this observation was further validated in combination with a marker of the early endosome compartment – Rab5-mCherry (Figure 3.7). From this experiment, the FFAR4 was demonstrated to rapidly internalise to the early endosomes.

This method of trafficking analysis does not give easily quantitative information on receptor trafficking. In addition, it does not give detail about other compartments that the FFAR4 might be trafficking to without further extensive imaging analysis in combination with other subcellular compartment markers. Therefore, a BRET-based assay was designed to both give quantitative data on FFAR4 trafficking and to reveal further information about FFAR4 trafficking to other intracellular compartments in real-time.
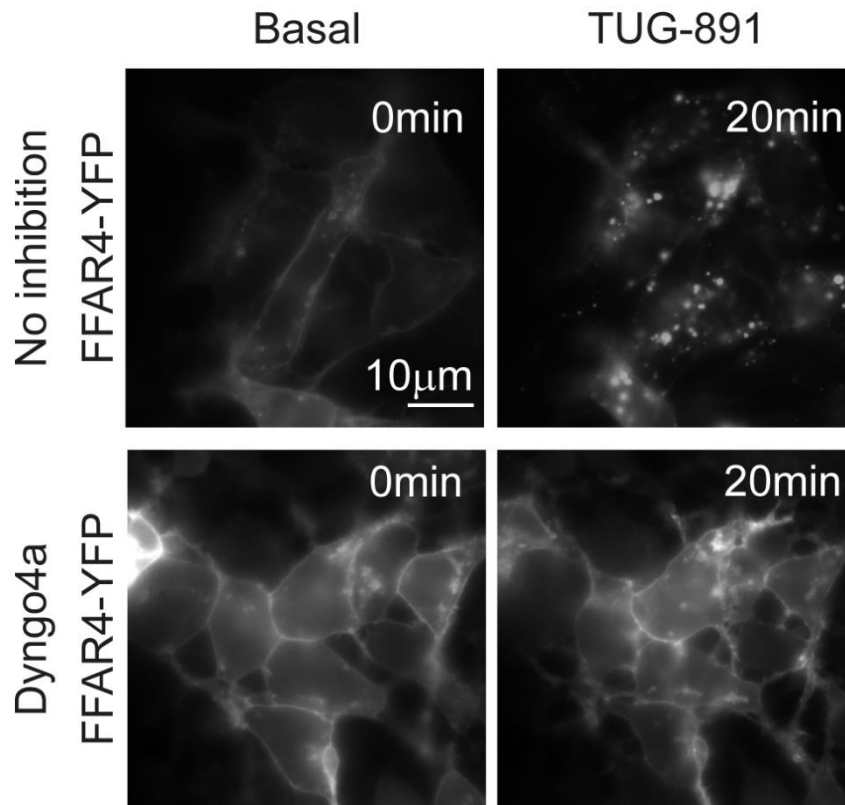
Figure 3. 6: The FFAR4 rapidly internalises to intracellular compartments after TUG-891 stimulation in a dynamin dependent manner.

Effect of TUG-891 stimulation on FFAR4 localisation. Shown are selective images of live cell HILO imaging of HEK293 cells transfected with FFAR4-YFP. Cells were preincubated with Dyngo4a (50 μM) or vehicle for 30 minutes and subsequently stimulated with TUG-891 (10 μM), selective FFAR4 agonist. Data are representative of at least three independent experiments.
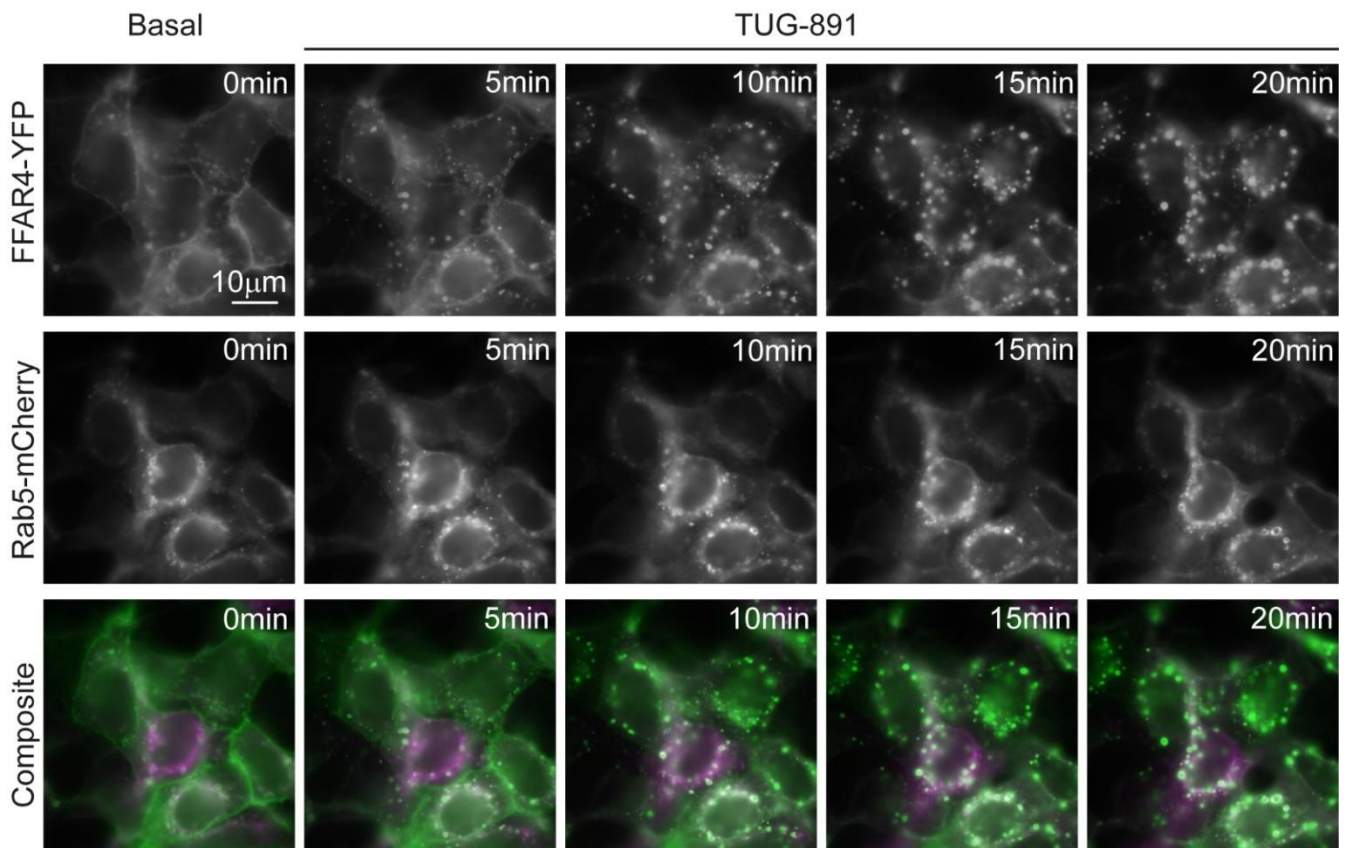
Figure 3. 7: The FFAR4 rapidly internalises to the early endosomes after agonist stimulation.

Effect of TUG-891 stimulation on FFAR4 internalisation to the early endosomes. Shown are selective frames representative of FFAR4 internalisation after TUG-891 (10 μM) stimulation in combination with an early endosome marker, Rab5. Images display FFAR4-YFP (top), Rab5-mCherry (middle), and a composite image of the two channels (bottom). Green pseudocolour indicates FFAR4-YFP and magenta pseudocolour indicates Rab5-mCherry. White colour indicates co-localisation. Data are representative of at least three independent experiments.

3.2.5 BRET-based approach monitoring FFAR4 localisation and trafficking

To quantify the localisation and trafficking profile of FFAR4 more precisely, a bystander BRET assay was performed to monitor, in real-time, the proximity between the FFAR4 and various previously validated Venus fused subcellular compartment markers (Figure 3.8A) (Tiulpakov et al., 2016). This was achieved using a method modified from the bystander BRET approach used to evaluate the trafficking profile of the V_2R-RLuc8 compared to clinically relevant mutant forms of the receptor (Tiulpakov et al., 2016). The Venus fused subcellular compartment markers used in this assay included: K-ras (plasma membrane); Rab5 (early endosomes); Rab4 (fast recycling endosomes); Rab11a/b (slow recycling endosomes); Rab7 (late endosomes/lysosomes); Rab9 (late endosomes to TGN); Vsp29 (endosomes to TGN); Rab1a (ER to Golgi); Rab6 (Golgi to TGN); and Rab8 (TGN to plasma membrane) (Tiulpakov et al., 2016).

To investigate the localisation and trafficking profile of the FFAR4, a similar methodology was employed, however NLuc was fused to the FFAR4 rather than RLuc8. Basal BRET measurements between FFAR4-NLuc and Venus fused subcellular compartment marker indicated that, prior to stimulation, in addition to the plasma membrane (K-ras) the FFAR4 is present at various subcellular compartments, including the recycling endosomes (Rab11), late endosomes (Rab7 & Rab9) and the TGN (Rab8 & Rab9) (Figure 3.8B).

.
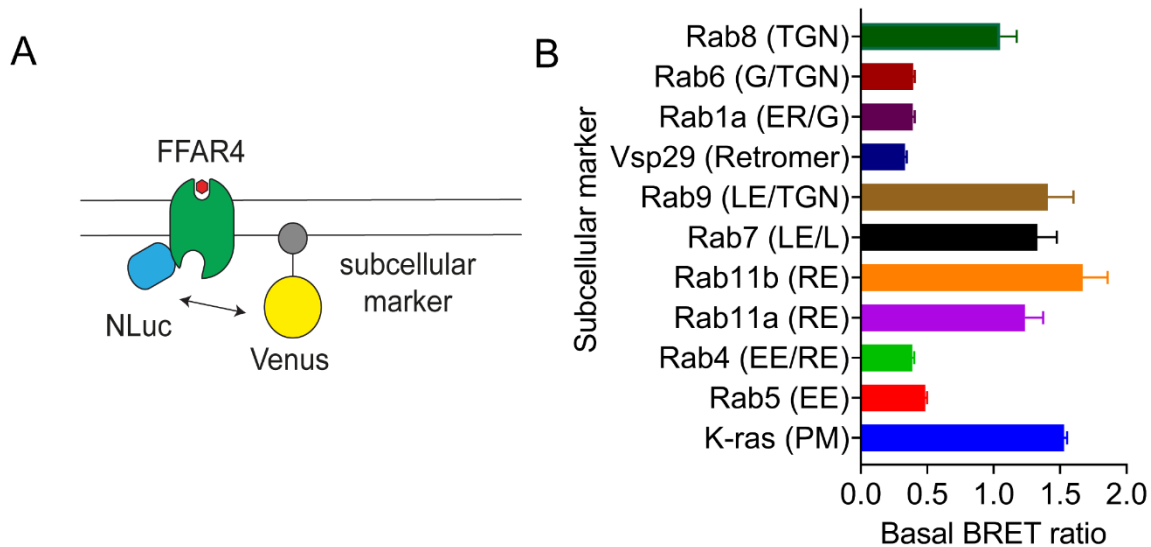
Figure 3. 8: The FFAR4 is present at the PM, LE, RE, and TGN prior to agonist stimulation.

(**A**) Schematic to illustrate the BRET assay used to detect FFAR4 localisation and trafficking by measuring the bystander BRET between NLuc fused FFAR4 and Venus fused subcellular compartment marker. (**B**) Results of basal BRET measurements between FFAR4-NLuc and Venus fused subcellular compartment markers (K-ras, Rab5, Rab4, Rab11a, Rab11b, Rab7, Rab9, Vsp29, Rab1a, Rab6, or Rab8) in HEK293 cells. Data represent mean ± S.E.M. compiled from three independent experiments performed in triplicate. PM = plasma membrane, EE = early endosome, RE = recycling endosome, LE = late endosome, L = lysosome, TGN = trans-Golgi network, G = Golgi, ER = endoplasmic reticulum.

TUG-891 stimulation induced a rapid redistribution of the FFAR4 from the plasma membrane (K-ras) and recycling endosomes (Rab11a/b), into early endosomes (Rab5), late endosomes (Rab7 & Rab9), Golgi/TGN (Rab6 & Rab9), recycling endosomes (Rab4), and the ER (Rab1a). No significant changes in BRET were detected using the retromer marker (Vsp29) or using the TGN to plasma membrane trafficking marker (Rab8) (Figure 3.9A&B). Overall, similar FFAR4 trafficking profiles were obtained with CpdA and α-linolenic acid, even though α-linolenic acid was less

efficient than CpdA and TUG-891 in inducing FFAR4 internalisation and subcellular redistribution (Figure 3.9A&B). These results indicate that, in a simple cell system, the FFAR4 is localised at the plasma membrane, late endosomes, slow recycling endosomes, and the TGN under basal conditions, and efficiently internalises and accumulates in the endosomal network and the ER/Golgi complex after agonist stimulation.
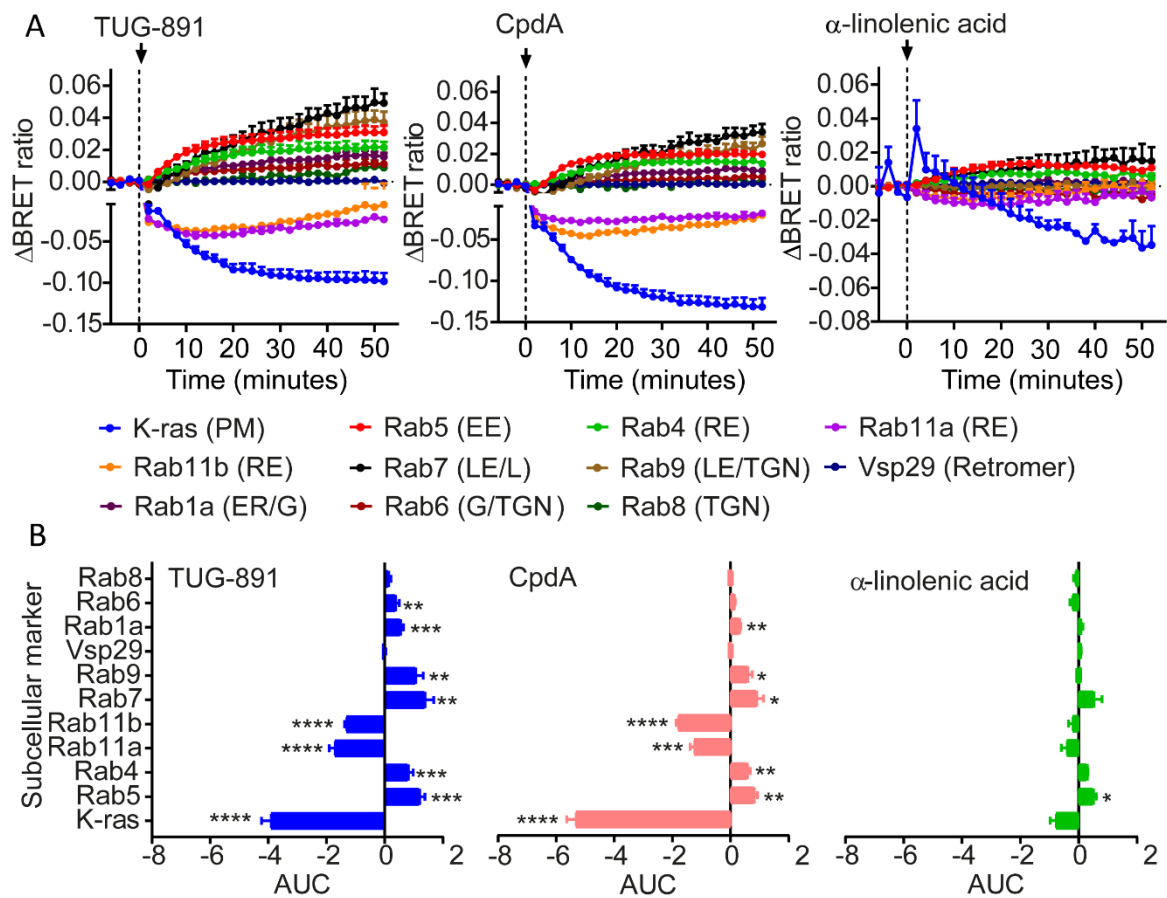
Figure 3. 9: The FFAR4 rapidly internalises into the endosomal network and ER/Golgi upon agonist stimulation.

(**A**) BRET approach monitoring real-time FFAR4 trafficking to subcellular compartments. Shown are the real-time BRET measurements between FFAR4-NLuc and Venus fused compartment markers (K-ras, Rab5, Rab4, Rab11a, Rab11b, Rab7, Rab9, Vsp29, Rab1a, Rab6, or Rab8) after stimulation with TUG-891 (10 μM), CpdA (10 μM), or α-linolenic acid (10 μM). (**B**) Corresponding AUC values. Differences are statistically significant by one-way ANOVA. **** p<0.0001, *** p<0.001, ** p<0.01, *

p<0.05 vs vehicle control by Dunnett's post hoc test at each compartment. Data represent mean ± S.E.M. compiled from three independent experiments performed in triplicate. PM = plasma membrane, EE = early endosome, RE = recycling endosome, LE = late endosome, L = lysosome, TGN = trans-Golgi network, G = Golgi, ER = endoplasmic reticulum.

To determine whether the FFAR4 enters the endosomal network after internalisation, or whether the receptor is directed there via another route, the same assay was repeated in the presence of a dynamin inhibitor, Dyngo-4a (McCluskey et al., 2013). Firstly, the basal receptor localisation was measured after dynamin inhibition. Basal BRET measurements between FFAR4-NLuc and Venus fused compartment marker indicated again that, prior to stimulation, the FFAR4 is present at various compartments, including the plasma membrane (K-ras), recycling endosomes (Rab11), late endosomes (Rab7 & Rab9), and the TGN (Rab8 & Rab9) (Figure 3.10A&B). Upon stimulation with TUG-891, the FFAR4 no longer redistributed into the endosomal network from the plasma membrane. Instead, agonist stimulation efficiently redistributed FFAR4 away from slow recycling endosomes (Rab11a), which seemingly began to accumulate FFAR4 at the plasma membrane (K-ras) (Figure 3.11A&B), although this effect was not significant. Again, similar FFAR4 trafficking profiles were obtained with CpdA and α-linolenic acid, even though α-linolenic acid was less efficient than CpdA and TUG-891 in inducing FFAR4 redistribution (Figure 3.11)

These results suggest that, in a simple cell system, FFAR4 internalisation into the endosomal network occurs via dynamin-dependent mechanisms. In addition, they suggest that there is an intracellular pool of FFAR4 which is already present in slow

recycling endosomes, primed to redistribute to the plasma membrane upon FFAR4 stimulation.
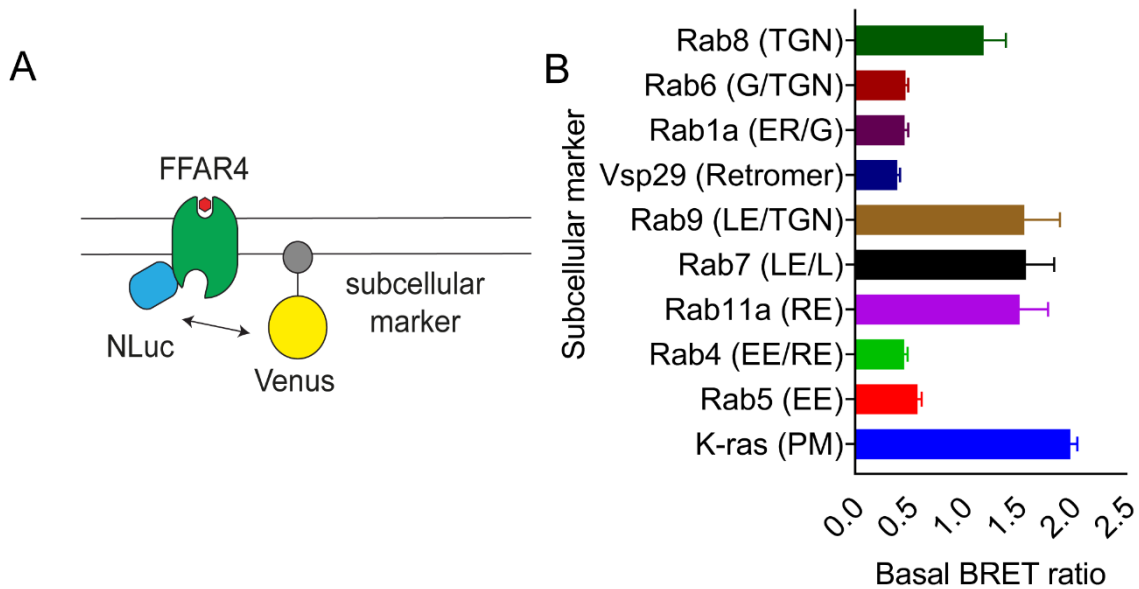
Figure 3. 10: After dynamin inhibition, the FFAR4 remains localised at the PM, LE, RE, and TGN prior to agonist stimulation.

FFAR4-NLuc and Venus fused compartment marker were transiently transfected into HEK293 cells and the basal BRET ratio was calculated. The raw BRET ratios are plotted on a bar graph. Data represent mean ± S.E.M. compiled from three independent experiments performed in triplicate. PM = plasma membrane, EE = early endosome, RE = recycling endosome, LE = late endosome, L = lysosome, TGN = trans-Golgi network, G = Golgi, ER = endoplasmic reticulum.
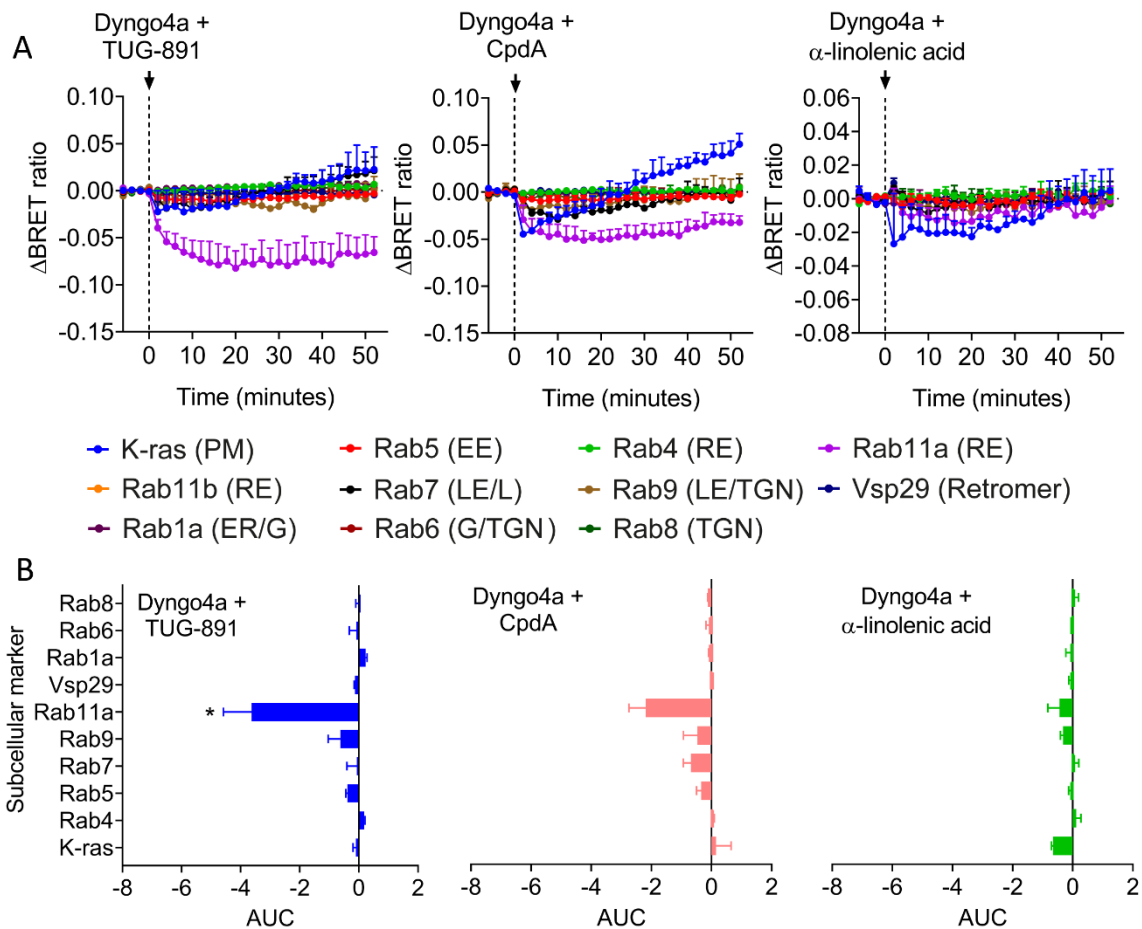
Figure 3. 11: FFAR4 internalisation is blocked by the inhibition of dynamin.
(**A**) BRET-based approach to monitor FFAR4-NLuc trafficking to Venus fused intracellular compartments in real-time in the presence of dynamin inhibitor. FFAR4-NLuc and Venus fused compartment markers (K-ras, Rab4, Rab5, Rab7, Rab9, Rab11a, Rab11b, Vsp29, Rab1a, Rab6, or Rab8) were co-transfected into HEK293 cells and stimulated with TUG-891 (10 μM), CpdA (10 μM), or α-linolenic acid (10 μM). Cells were pre-treated with Dynamin inhibitor, Dyngo-4a (50 μM), for 30 minutes prior to stimulation. (**B**) Corresponding AUC values. Differences are statistically significant by one-way ANOVA. P<0.05 = * vs vehicle control by Dunnett's post hoc test at each compartment. Data represent mean ± S.E.M. compiled from three independent experiments performed in triplicate. PM = plasma membrane, EE = early endosome, RE = recycling endosome, LE = late endosome, L = lysosome, TGN = trans-Golgi network, G = Golgi, ER = endoplasmic reticulum.

3.2.6 Agonist stimulation initiates FFAR4 activation from the endosomal network, TGN, and ER in a simple cell model

After the investigation of FFAR4 localisation and trafficking in a simple cell model, mini-G probes were used to determine sites of FFAR4 activation after agonist stimulation using an imaging-based approach. By co-transfecting Venus fused mini-G probe (mGα_q, mGα_i, mGα_o, mGα_s) with WT FFAR4 in HEK293 cells, mini-G probe translocation was visualised after TUG-891 stimulation using HILO microscopy (Figure 3.12). Prior to FFAR4 activation, all mini-G probe subtypes were observed to be diffuse throughout the cytoplasm. After TUG-891 stimulation, only mGα_i and mGα_o probe translocation was detectable. Despite the ability of the FFAR4 to couple to G$\alpha_{q/11}$, little translocation was observable using mGα_q probes. This could be due to the limitation of the microscope in detecting modest levels of mini-G probe translocation. Stimulation of the FFAR4 with TUG-891 induced mGα_i and mGα_o translocation into punctate spots and vesicular structures – reminiscent of the endosome compartment (Figure 3.12). This observation was further validated using an imaging-based approach. Within this assay, WT FFAR4 was transfected in combination with mGα_i (Figure 3.13A) or mGα_o (Figure 3.13B) and a marker of the early endosomes (mCherry-Rab5). Again, TUG-891 stimulation induced mGα_i and mGα_o translocation to intracellular compartments, which indeed co-localised with the early endosome marker, Rab5.
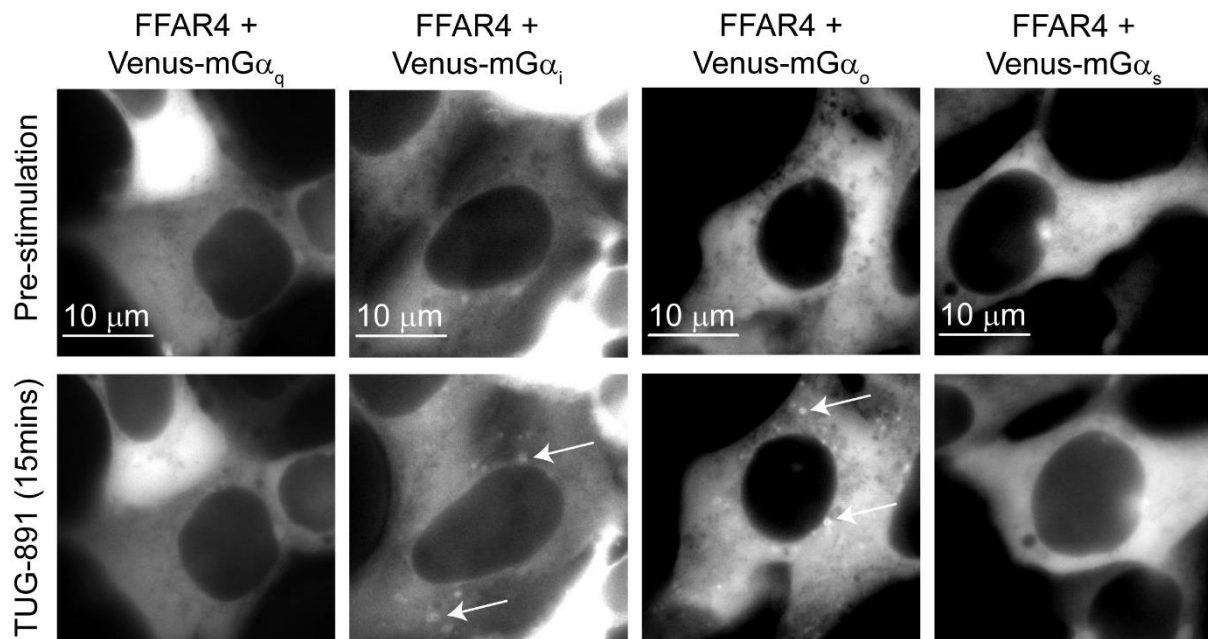
Figure 3. 12: The FFAR4 is active from intracellular compartments in a simple cell model.

Effect of TUG-891 stimulation on Venus fused mini-G probe (mGα_q, mGα_i, mGα_o, mGα_s) translocation into HEK293 cells. Shown are selective frames representative of mini-G translocation after TUG-891 (10 μM) stimulation in the presence of WT FFAR4. Exemplary mini-G probe translocations are indicated by arrows. Data are representative of at least three independent experiments.

A

| | No Stimulation | 5min TUG-891 | 10min TUG-891 | 20min TUG-891 |

Venus-mGα$_i$

mCherry-Rab5

Composite

B

| | No Stimulation | 5min TUG-891 | 10min TUG-891 | 20min TUG-891 |

Venus-mGα$_o$

mCherry-Rab5

Composite

10 μm
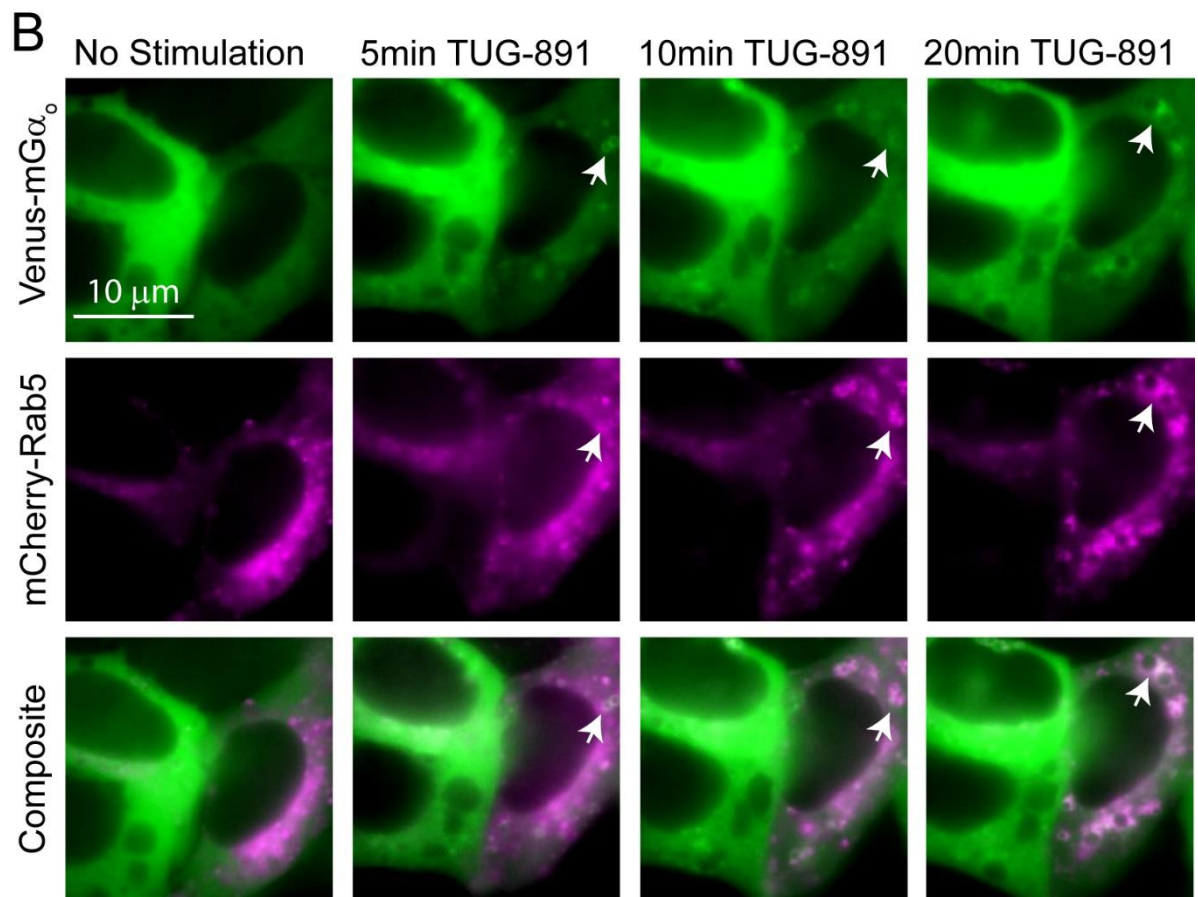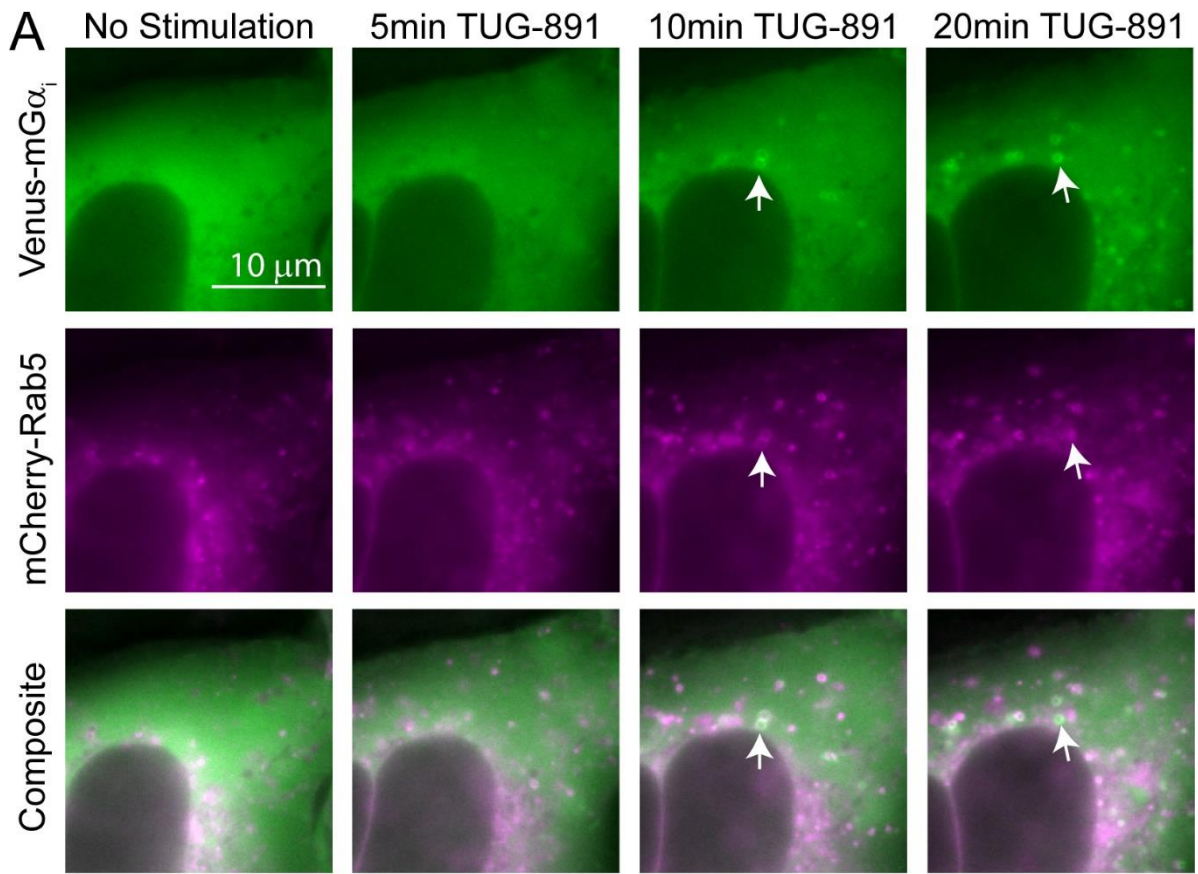
Figure 3. 13: The FFAR4 is active from the early endosomes in a simple cell model.

Effect of TUG-891 stimulation on Venus fused mini-G probe translocation to the early endosomes in HEK293 cells. Shown are selective frames representative of (**A**) mGα_i or (**B**) mGα_o translocation after TUG-891 (10 μM) stimulation in the presence of WT FFAR4 and a marker of the early endosomes (mCherry-Rab5). Displayed are Venus fused mini-G probe (green pseudocolour, top), mCherry-Rab5 (magenta pseudocolour, middle), and a composite of the two channels (bottom) at select time points. Exemplary co-localisations (white colourisation) between mini-G probe and early endosome marker are indicated by arrows. Data are representative of at least three independent experiments.

A BRET-based approach was subsequently designed to monitor compartment specific FFAR4 activation in real-time. In this assay, bystander BRET measurements were performed, in the presence of WT FFAR4, between NLuc fused mini-G probes and the same panel of Venus fused intracellular compartment markers used previously to investigate FFAR4 trafficking (Tiulpakov et al., 2016) (Figure 3.14A).

TUG-891 stimulation induced robust mG$\alpha_{i/o}$ recruitment to the plasma membrane (K-ras) and, to a lesser extent, recycling endosomes (Rab11b), early endosomes (Rab5), late endosomes (Rab7 & Rab9), and the ER (Rab1a). A very small increase in BRET was also detectable at the Golgi/TGN (Rab6/Rab8/Rab9). No increase in BRET was detectable at the retromer compartment (Vsp29). CpdA and α-linolenic acid induced similar mini-G recruitment profiles, albeit with smaller maximal responses (CpdA > α-linolenic acid). In comparison, FFAR4 stimulation with the tested agonists caused a much smaller plasma membrane recruitment of mGα_q than mG$\alpha_{i/o}$, with negligible recruitment to intracellular compartments (Figure 3.14B&C).
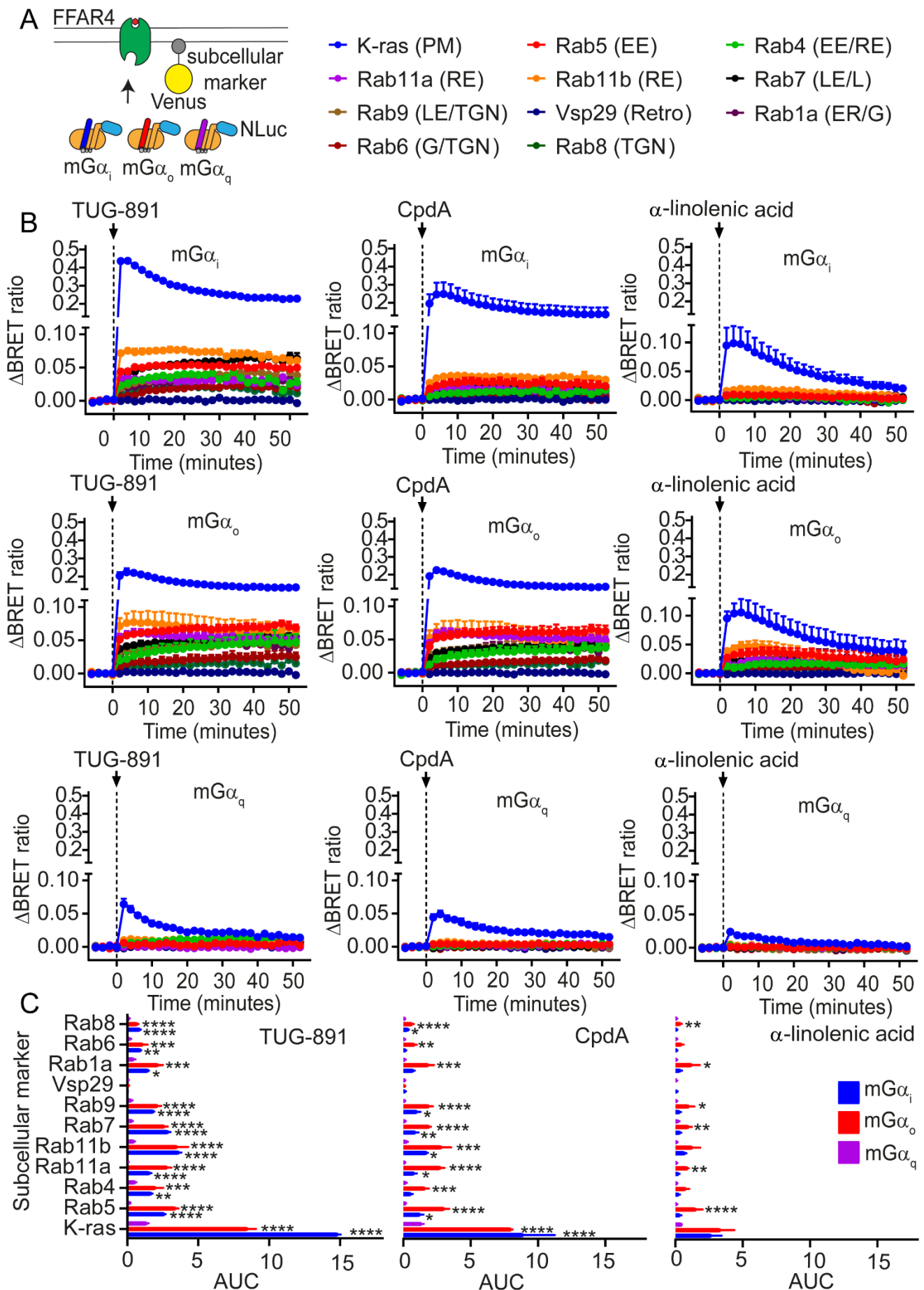
Figure 3. 14: The FFAR4 is active at both the plasma membrane and intracellular compartments in a simple cell model.

(**A**) Schematic of the bystander BRET assay used to detect FFAR4 activation at intracellular compartments. (**B**) Agonist-dependent increases in NLuc-mGα_i, NLuc-mGα_o, NLuc-mGα_q recruitment to Venus fused compartment markers (K-ras, Rab4, Rab5, Rab7, Rab9, Rab11a, Rab11b, Vsp29, Rab1a, Rab6, or Rab8) upon stimulation with TUG-891 (left panel), CpdA (middle panel), α-linolenic acid (right panel) (all 10 μM), monitored by real-time BRET measurements in HEK293 cells. (**C**) Corresponding AUC values. Differences are statistically significant by two-way ANOVA. **** $p<0.0001$, *** $p<0.001$, ** $p<0.01$, * $p<0.05$ vs mini-Gα_q by Dunnett's post hoc test. Data represent mean + S.E.M. compiled from three to four independent experiments performed in duplicate. PM = plasma membrane, EE = early endosome, RE = recycling endosome, LE = late endosome, L = lysosome, TGN = trans-Golgi network, G = Golgi, ER = endoplasmic reticulum.

Furthermore, an assay was performed without overexpression of the FFAR4, to ensure that ligand induced BRET changes were specific to the FFAR4 activation since the FFAR4 is not highly expressed in HEK293 cells (Eclov et al., 2015). For this assay, the recruitment of NLuc-mG$_o$ to Venus fused compartments (K-ras, Rab5, Rab7, Rab9, Rab11b, Rab1a, and Rab8) was measured after stimulation with TUG-891, CpdA, and α-linolenic acid. Such markers were chosen since the largest BRET responses were recorded at these compartments. In this control assay, little translocation of mini-G was detectable (Figure 3.15).

Altogether, these results indicate that, in a simple cell model, FFAR4 stimulation with both endogenous and synthetic agonists induces FFAR4 activation at both the plasma membrane and at various intracellular compartments.
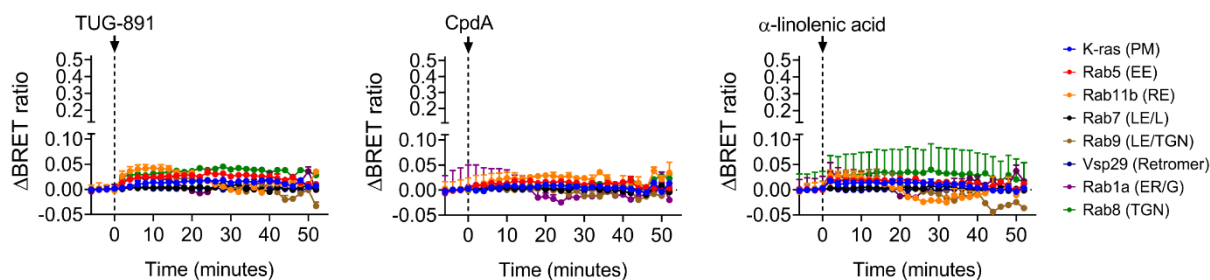
Figure 3. 15: Control BRET assay between mini-G probe and Venus fused compartment markers in the absence of WT FFAR4 overexpression.

Real-time BRET assay detecting mini-G probe translocation to intracellular compartments without FFAR4 overexpression. Shown are the real-time BRET results between Venus fused compartment marker (K-ras, Rab5, Rab11b, Rab7, Rab9, Rab1a, or Rab8), and NLuc fused mini-G probe (mGα$_o$) in HEK293 cells stimulated with TUG-891 (10 μM), CpdA (10 μM), or α-linolenic acid (10 μM). Data represent mean + S.E.M. compiled from one independent experiment performed in triplicate. PM = plasma membrane, EE = early endosome, RE = recycling endosome, LE = late endosome, L = lysosome, TGN = trans-Golgi network, G = Golgi, ER = endoplasmic reticulum.

3.2.7 FFAR4 overexpression inhibits cAMP production

Owing to the robust recruitment of mGα_i and mGα_o following FFAR4 agonist stimulation, suggesting that the FFAR4 is predominantly G$\alpha_{i/o}$ coupled, it was important to determine the downstream action of the FFAR4 on cAMP production. Therefore, a BRET-based sensor was chosen to enable the real-time detection of cAMP changes in live cells. This sensor, named CAMYEL, was used within a simple cell model to determine changes in cAMP production after agonist stimulation (Jiang et al., 2007). In brief, upon cAMP binding to the Epac domain of CAMYEL, a conformational change occurs leading to a reduction in BRET between donor (RLuc) and acceptor (YFP). In this way, the change in intracellular cAMP concentration can be measured in live cells upon agonist stimulation. Initially, the sensor's functionality was tested by measuring changes in cAMP production after stimulation with 8-pCPT-2-O-Me-cAMP-AM, a highly membrane permeable precursor of 8-CPT-2Me-cAMP (cAMP analogue) (Vliem et al., 2008), or forskolin, a direct activator of AC (Qi et al., 2022) (Figure 3.16). After both 8-pCPT-2-O-Me-cAMP-AM stimulation (Figure 3.16A) and forskolin stimulation (Figure 3.16B), cAMP production was detectable. Furthermore, EC$_{50}$ values were subsequently calculated for 8-pCPT-2-O-Me-cAMP-AM and forskolin: 1.708×10^{-7} M and 1.955×10^{-6} M, respectively (Figure 3.16C&D).
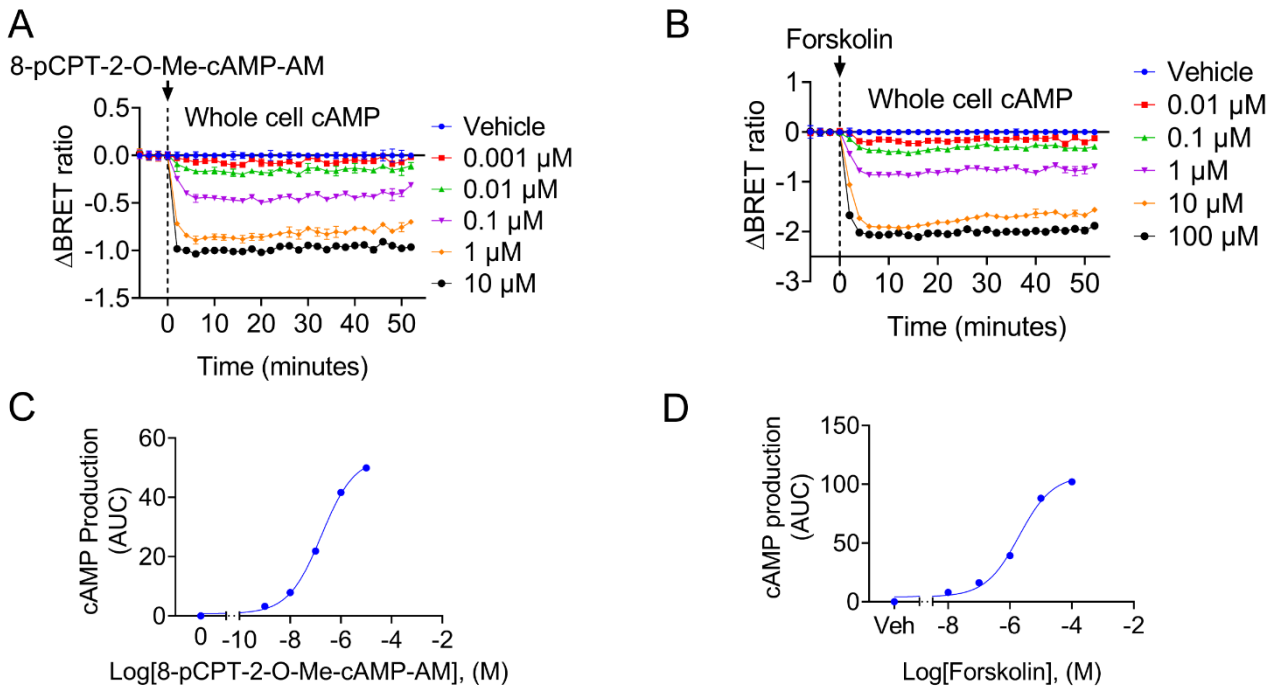
Figure 3. 16: CAMYEL is applicable for the measurement of cAMP production in a simple cell model.

BRET assay using CAMYEL to detect cAMP production. Shown are the real-time BRET measurements detecting cAMP production after stimulation with increasing concentrations of (**A**) 8-pCT-2-Ome-cAMP-AM or (**B**) forskolin. (**C&D**) Corresponding AUCs were used to create dose response curves. Data represent mean ± S.E.M compiled from one independent experiment performed in triplicate.

To understand the overall influence of the FFAR4 on cAMP production, the receptor was over-expressed in increasing amounts in HEK293 cells (0 ng, 50 ng, 100 ng, 250 ng, 500 ng and 1000 ng) (Figure 3.17A&B). The change in cAMP production was subsequently measured after stimulation with forskolin. When no FFAR4 was overexpressed, a greater increase in cAMP was induced. However, in the presence of the FFAR4, cAMP production was inhibited. This inhibition occurred to similar levels in all quantities of FFAR4 overexpression (Figure 3.17A&B).
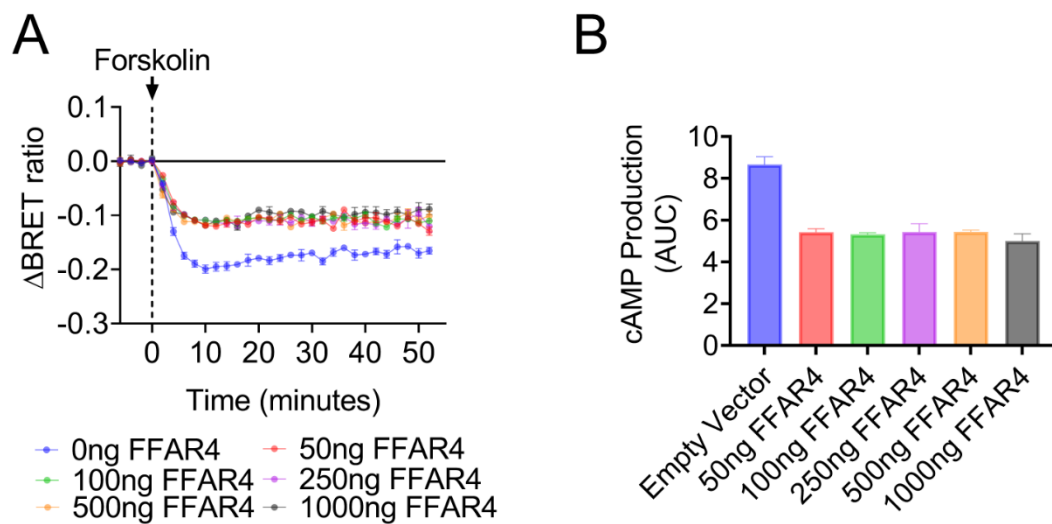
Figure 3. 17: FFAR4 overexpression inhibits cAMP production.
BRET-based assay to detect the effect of FFAR4 overexpression on cAMP production. (**A**) Shown are the real-time BRET measurements detecting cAMP production by CAMYEL in the presence or absence of the FFAR4. FFAR4 was overexpressed (0ng, 50ng, 100ng, 250ng, 500ng, and 1000ng) and equalized with pcDNA3 (empty vector) and stimulated with forskolin (1 μM). (**B**) Corresponding AUC values. Data represent mean ± S.E.M from one independent experiment performed in triplicate.

Since FFAR4 overexpression reduced cAMP production after forskolin stimulation without need for FFAR4 agonist, the effect of the FFAR4 on cAMP production was evaluated in the presence and absence of AH7614 (FFAR4 NAM) (Figure 3.18). Within

this assay, both forskolin and isoproterenol were used as two distinct activators of cAMP production. As observed in the previous assay, the presence of the FFAR4 reduced forskolin-stimulated cAMP production (Figure 3.18A). The same effect was also observed after isoproterenol stimulation (Figure 3.18B). FFAR4 NAM (AH7614) reversed the inhibitory effect of the FFAR4 on cAMP production. When the FFAR4 was not overexpressed, AH7614 had no effect. This is indicative that the FFAR4 inhibits cAMP production in a simple cell model which can be reversed after the inhibition of FFAR4 with AH7614 (Figure 3.18C&D).
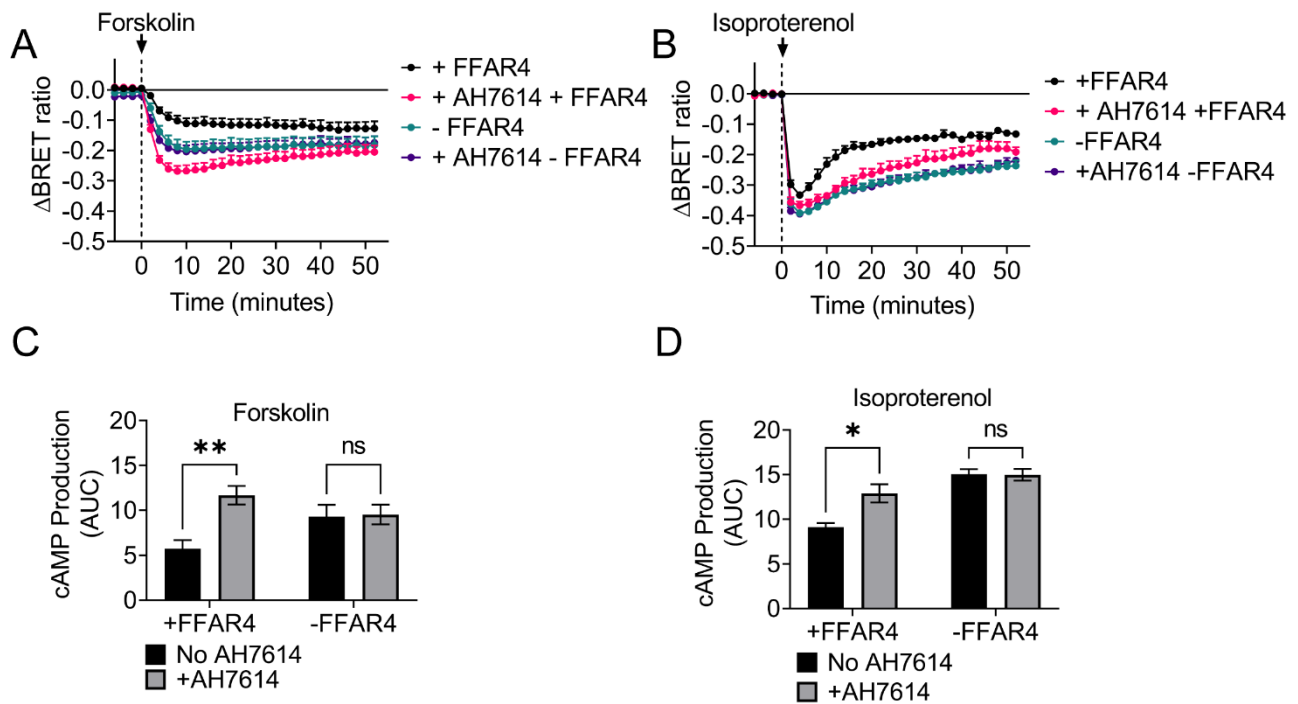
Figure 3. 18: FFAR4 overexpression inhibits cAMP production and is reversible with AH7614.

Real-time BRET assay detecting the effect of FFAR4 overexpression on cAMP production using CAMYEL. (**A&B**) Shown are the real-time BRET measurements of ligand induced changes in cAMP production measured by CAMYEL in the presence of FFAR4 overexpression (+FFAR4), or pcDNA3 overexpression (-FFAR4). HEK293 cells were preincubated with vehicle or AH7614 (10 μM) for 15 minutes and stimulated with (**A**) forskolin (1 μM) or (**B**) isoproterenol (1 μM). (**C&D**) Corresponding AUC values. Differences are statistically significant by two-way ANOVA. ** $p < 0.01$, * $p < 0.05$ by Sidak's multiple comparison test. Data represent mean ± S.E.M. compiled from three to five independent experiments performed in triplicate.

3.2.8 The FFAR4 inhibits cAMP production more greatly from intracellular compartments than from the plasma membrane

Considering that the FFAR4 was found to recruit $mG\alpha_i$ and $mG\alpha_o$ probes strongly to intracellular compartments in a simple cell model, the role of the FFAR4 on local cAMP production was investigated by tethering CAMYEL to specific compartments. In the literature, similar methods have been used to investigate local GPCR signalling. For example, a cAMP sensor was tethered to the Golgi to detect local TSHR signalling in subdomains of the TGN (Godbole et al., 2017). However, in this study, local signals were measured using FRET-based cAMP sensors rather than BRET-based cAMP sensors.

To investigate compartmentalised FFAR4 signalling, CAMYEL has been tethered to the plasma membrane using PDE2A splice variant 3 (PDE2A3) to study the activity of PDE subtypes at the plasma membrane compared to the whole cell PDE activity (Matthiesen and Nielsen, 2011). In order to tether CAMYEL to the plasma membrane, the first 196 N-terminal amino acids of PDE2A3 were fused to the N-terminus of CAMYEL (Matthiesen and Nielsen, 2011). This sensor was used in combination with two new CAMYEL sensors to investigate FFAR4 dependent compartmentalised cAMP production. New sensors were created by tethering CAMYEL to the ER using Sec61β, a Sec61 translocon subunit commonly used as a marker of the ER (Greenfield and High, 1999), or Rab1a – a protein involved in ER to Golgi trafficking as used in previous mini-G translocation, and FFAR4 trafficking, assays (Tiulpakov et al., 2016). The cAMP sensor was targeted to the ER since the FFAR4 was found activated at this compartment after agonist stimulation (Rab1a) (Figure 3.14). Tethering CAMYEL to the ER compartment was supposed to have a sufficiently different localisation from

the plasma membrane to detect predominantly intracellular FFAR4 activity rather than detecting FFAR4 activity at the plasma membrane.

Firstly, the localisation of the new sensors were validated in HEK293 cells. PDE2A3-CAMYEL has been previously validated to localise to the plasma membrane, therefore, its localisation was not further validated with a plasma membrane marker (Matthiesen and Nielsen, 2011). However, the sensor was observed to have a characteristic plasma membrane localisation in HEK293 cells (Figure 3.19A). The localisation of CAMYEL-Sec61β and CAMYEL-Rab1a were validated by assessing the co-localisation between the cAMP sensor and mCherry-Sec61β. CAMYEL-Sec61b clearly localised to the ER (Figure 3.19B&D), however, CAMYEL-Rab1a localised to ER subdomains (Figure 3.19C&D).
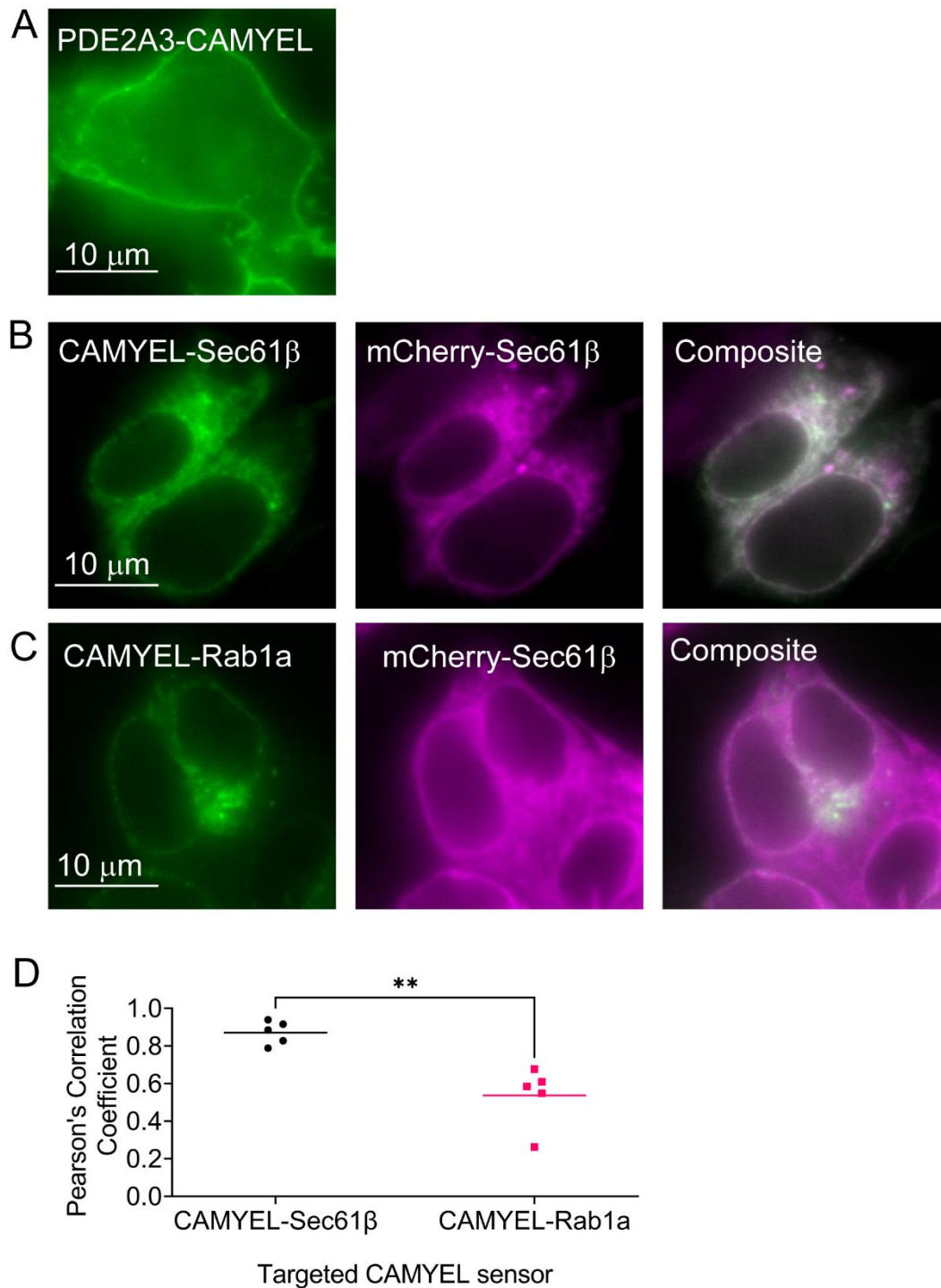
Figure 3. 19: Validation of targeted CAMYEL sensor localisation.

HILO images validating plasma membrane and ER-directed CAMYEL sensors. Shown are representative images of (**A**) PDE2A3-CAMYEL, (**B**) CAMYEL-Sec61β, and (**C**) CAMYEL-Rab1a in HEK293 cells. (**B**) CAMYEL-Sec61β, and (**C**) CAMYEL-Rab1a were co-transfected with mCherry-Sec61β to validate their localisation to the ER. (**D**) Corresponding pearson's correlation coefficient determining co-localisation between

CAMYEL-Sec61β and CAMYEL-Rab1a with mCherry-Sec61β using the JAcoP colocalization plug-in in ImageJ. Differences are statistically significant by t-test, ** p<0.01.

The functionality of the targeted cAMP sensors was subsequently evaluated in HEK293 cells. For this purpose, a BRET assay was employed to detect forskolin stimulated cAMP production (Figure 3.20). From this assay, the sensitivity of the sensors to forskolin stimulated cAMP production (EC$_{50}$) was found to be comparable: PDE2A3-CAMYEL, EC$_{50}$: 2.307×10^{-6} M; CAMYEL-Sec61β, EC$_{50}$: 2.320×10^{-6} M; and CAMYEL-Rab1a, EC$_{50}$: 2.073×10^{-6} M. EC$_{50}$ values were also comparable to whole cell CAMYEL (Figure 3.16).
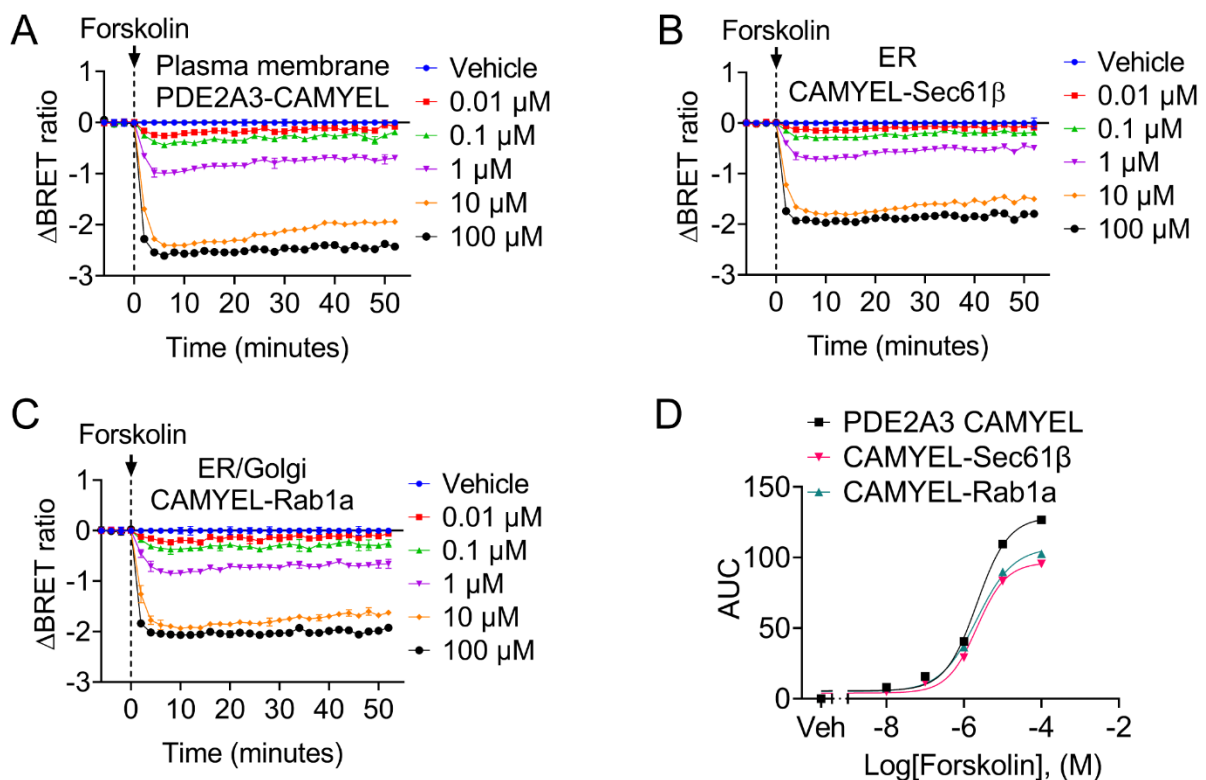
Figure 3. 20: BRET assay to confirm functionality of targeted cAMP sensors.
Real-time BRET assay detecting cAMP production using plasma membrane and ER-directed CAMYEL sensors. Shown are the real-time BRET measurements of (**A**)

PDE2A3-CAMYEL, (**B**) CAMYEL-Sec61β, and (**C**) CAMYEL-Rab1a upon increasing forskolin stimulations in HEK293 cells. (**D**) Corresponding AUC values plotted on a dose response curve. Data represent mean ± S.E.M. compiled from one independent experiment performed in duplicate.

The effect of FFAR4 overexpression on cAMP production was subsequently evaluated in HEK293 cells using whole cell CAMYEL. PDE2A3 CAMYEL, and CAMYEL-Sec61β. CAMYEL-Sec61β was used over CAMYEL-Rab1a because the sensor had improved localisation to the ER.

For each targeted sensor, FFAR4 was overexpressed or corresponding amount of pcDNA3 (empty vector) was overexpressed (Figure 3.21). Real-time BRET was measured by each sensor after stimulation with isoproterenol. By examination of the raw BRET graphs, the FFAR4 seemed to have a greater inhibitory effect using the ER and whole cell directed cAMP sensors compared to the plasma membrane directed cAMP sensor. This observation was further evaluated by either calculating the AUC in the presence of the FFAR4, or the overall change in BRET ratio (ΔBRET) in the presence of the FFAR4 and normalizing to the corresponding response in the presence of empty vector. When measuring overall cAMP production using the AUC, the FFAR4 significantly inhibited ligand-induced cAMP production at all tested compartments (Figure 3.21D). However, when measuring ΔBRET compared to empty vector, the FFAR4 only had significant inhibitory effects using whole cell and ER sensors, and not the plasma membrane directed sensor (Figure 3.21E). These data indicate, that in a simple cell model, the FFAR4 has a greater inhibitory effect on intracellular cAMP production rather than cAMP production at the plasma membrane.
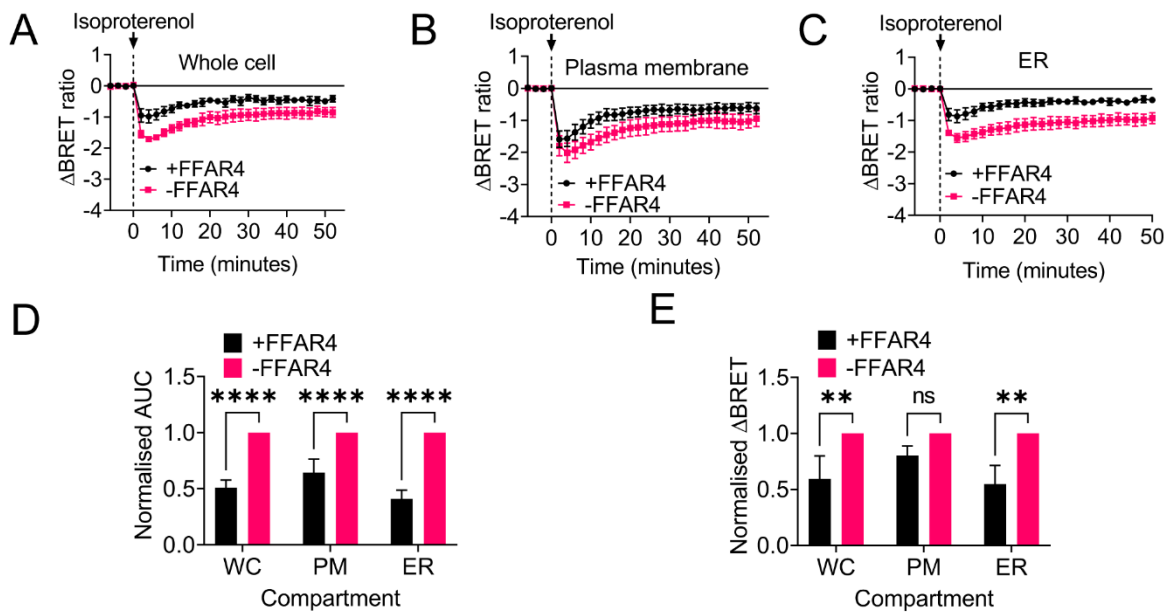
Figure 3. 21: FFAR4 overexpression inhibits cAMP production more greatly at intracellular compartments than at the plasma membrane.

Real-time BRET assay to detect the effect of FFAR4 overexpression on local cAMP production. Shown are the results of ligand induced cAMP production using (**A**) whole cell, (**B**) plasma membrane, and (**C**) ER CAMYEL sensors. FFAR4 or corresponding amount of empty vector were transfected into HEK293 cells and stimulated with isoproterenol (100 nM). (**D**) Corresponding normalised AUC (**E**) or normalised ΔBRET measurements. Differences are statistically significant by two-way ANOVA. **** $p<0.0001$, ** $p<0.01$ with Sidak's post hoc analysis. Data represent mean ± S.E.M. compiled from three independent experiments performed in duplicate.

3.2.9 The FFAR4 increases intracellular [Ca^{2+}] in a simple cell model

Since the FFAR4 has also been shown a G$\alpha_{q/11}$ coupled receptor (Milligan et al., 2017a), and the FFAR4 was found within this study to recruit to mGα_q probes, FFAR4 dependent changes in intracellular [Ca^{2+}] were also investigated in HEK293 cells. For this purpose, CalFlux, a BRET-based Ca^{2+} biosensor, was used to measure ligand induced changes in intracellular [Ca^{2+}] (Yang et al., 2016). In brief, upon Ca^{2+} binding to the troponin-C domain of the sensor, an increase in BRET is detectable (Yang et al., 2016). FFAR4 significantly increased intracellular Ca^{2+} levels after TUG-891 stimulation compared to the empty vector control. Ionomycin was used as a positive control to increase intracellular [Ca^{2+}] levels independently of the FFAR4 (Figure 3.22). The increase in intracellular calcium levels mediated by the FFAR4 was transient.
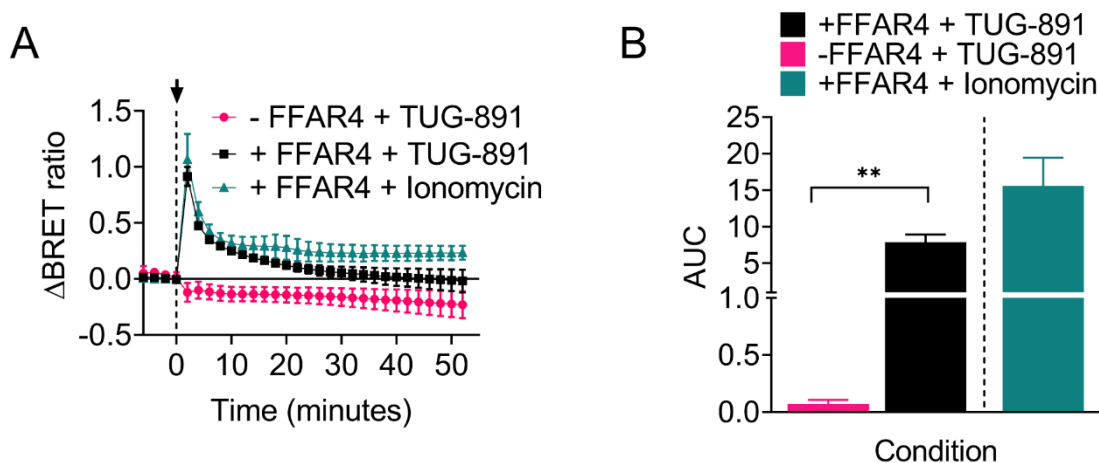
Figure 3. 22: FFAR4 activation increases intracellular [Ca^{2+}].
BRET-based assay to detect the effect of FFAR4 activation on intracellular Ca^{2+} levels. (**A**) Shown are the real-time BRET measurements detecting ligand induced changes in intracellular [Ca^{2+}] using CalFlux BRET sensor in the presence (+FFAR4) or absence (-FFAR4) of FFAR4 overexpression. HEK293 cells were stimulated with TUG-891 (10 μM) and ionomycin (1 μM) was used as a positive control. (**B**) Corresponding AUC values. Differences are statistically significant by t-test, ** p<0.01. Data represent mean ± S.E.M. compiled from three independent experiments performed in triplicate.

3.2.10 The FFAR4 strongly couples to β-arrestin-2 in a simple cell model

Finally, the FFAR4 has been proposed to strongly couple to β-arrestin-2 after its activation – a phenomenon believed to be involved in the regulation of FFAR4 internalisation (Zhang and Leung, 2014). This finding was further validated in HEK293 cells and was performed to gain further insight into subtype specific β-arrestin recruitment to the FFAR4. For this purpose, a BRET-based assay was designed to measure the recruitment of NLuc fused β-arrestin-1 and NLuc fused β-arrestin-2 to the FFAR4-YFP after stimulation with TUG-891 (Figure 3.23A), CpdA (Figure 3.23B), and α-linolenic acid (Figure 3.23C). The recruitment of NLuc fused $mG\alpha_i$ or NLuc fused $mG\alpha_q$ was also measured to the FFAR4 as a positive and a negative control, respectively. After stimulation with all three agonists, FFAR4-YFP most strongly recruited β-arrestin-2 followed by β-arrestin-1 (Figure 3.23D). $mG\alpha_i$ was recruited to the FFAR4-YFP at a comparable amount to β-arrestin-1, and no recruitment of $mG\alpha_s$ was detectable to the FFAR4. In keeping with previous data, the strongest recruitment of β-arrestin to the FFAR4 was observed after stimulation with TUG-891, followed by CpdA, and then α-linolenic acid. From this data, the FFAR4 was confirmed to strongly couple to β-arrestin-2, and to a lesser extent β-arrestin-1, in a simple cell model.
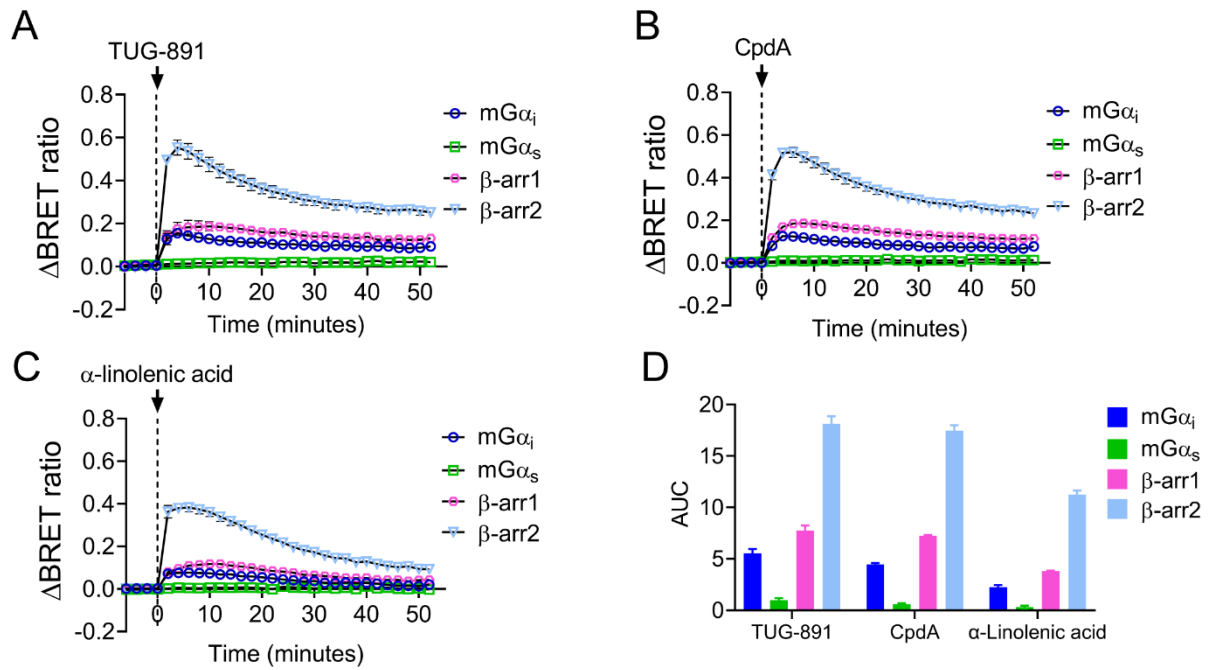
Figure 3. 23: The FFAR4 is strongly coupled to β-arrestin-2.

Real-time BRET assay detecting β-arrestin-1 and β-arrestin-2 recruitment to the FFAR4. Shown are the real-time BRET measurements between NLuc fused β-arrestin (β-arr1 and β-arr2), or NLuc fused mini-G probe subtype (mGα_i or mGα_s) to the FFAR4-YFP upon (**A**) TUG-891, (**B**) CpdA, or (**C**) α-linolenic acid (all 10 μM) stimulation. (**C**) Corresponding AUC values. Data represent mean ± S.E.M. compiled from one independent experiment performed in triplicate.

3.3 Discussion

3.3.1 Summary of key findings

3.3.1.1 G protein coupling

In literature, the FFAR4 has been proposed predominantly coupled to $G\alpha_{q/11}$ proteins in a simple cell model (Milligan et al., 2017b, Miyamoto et al., 2016, Oh and Walenta, 2014), however studies with this conclusion classify G protein coupling selectivity by measuring changes in intracellular calcium/cAMP levels. Despite this, the inhibitory effect of the FFAR4 on cAMP production has been detected in physiologically relevant cell types, suggesting coupling to $G\alpha_{i/o}$ (Husted et al., 2020).

Within this investigation, a BRET-based methodology (Wan et al., 2018) was used to determine the predominant coupling specificity of the FFAR4 in a simple cell model. This assay investigated the recruitment of mini-$G\alpha$ probe subtypes to the FFAR4 to facilitate fair comparison between the G protein families. Using this BRET-based approach, it was demonstrated that the FFAR4 couples predominantly with $G\alpha_{i/o}$ and to a lesser extent $G\alpha_{q/11}$. Importantly, this coupling could be blocked by FFAR4 inhibition using AH7614, confirming the specificity of mini-G probe recruitment to the FFAR4. In addition, the AT_1R, believed to be predominantly coupled to $G\alpha_{q/11}$ and partially coupled to $G\alpha_i$ (Galandrin et al., 2016), more strongly recruited $mG\alpha_q$ than $mG\alpha_i$ – indicating the ability of mini-$G\alpha$ probes to identify the predominant coupling specificity of different GPCRs – including those that couple to both $G\alpha_{q/11}$ and $G\alpha_i$ proteins.

The activity of the FFAR4 has been shown in the literature as both pertussis toxin insensitive (Watson et al., 2012) and pertussis toxin sensitive (Egerod et al., 2015),

therefore, it is possible that the FFAR4 signals through pertussis toxin insensitive members of the $G\alpha_{i/o}$ protein family in some cells and not others (Jimenez-Vargas et al., 2020), however this would require further investigation. Two recent studies, which used high-throughput methods to detect the direct G protein coupling specificity of many GPCRs, including the FFAR4, agree that the FFAR4 couples to $G\alpha_{i/o}$ in a simple cell model (Avet et al., 2022, Inoue et al., 2019). It is likely that this coupling is often missed by methods that only detect changes in second messengers rather than those that detect direct G protein recruitment. In this way, mini-G probes are applicable for the identification of the predominant G protein coupling specificity of GPCRs, and were used to success within this study to identify that the FFAR4 strongly couples to $G\alpha_{i/o}$.

3.3.1.2 FFAR4 trafficking and compartmentalised signalling

Trafficking is regarded as an essential component of compartmentalised GPCR signalling (Caengprasath and Hanyaloglu, 2019). The ability of a GPCR to redistribute to specific subcellular compartments is thought of as a mechanism for GPCRs to fine-tune their activity with subcellular resolution (Calebiro and Koszegi, 2019). Therefore, the trafficking profile of the FFAR4 was investigated within this study using HILO microscopy and BRET-based methods.

Initially, the trafficking profile of the FFAR4 was investigated via HILO microscopy, where it was found that the FFAR4 rapidly internalises, in a dynamin dependent manner, into the early endosome compartment. However, identifying the trafficking profile of GPCRs using microscopy approaches is often time-consuming and does not easily produce quantitative data of large cell populations. Therefore, a more high-throughput BRET-based assay was employed to monitor FFAR4 trafficking to a

selection of compartment markers (Tiulpakov et al., 2016). Using this method, the FFAR4 was demonstrated present at various subcellular compartments, including the plasma membrane (K-ras), recycling endosomes (Rab11a/b), late endosomes (Rab7 & Rab9), and TGN (Rab8 & Rab9). FFAR4 stimulation induced its rapid redistribution from the plasma membrane (K-ras) and slow recycling endosomes (Rab11a/b) into early endosomes (Rab5), fast recycling endosomes (Rab4), late endosomes (Rab7 & Rab9), Golgi/TGN (Rab6 & Rab9), and the Golgi/ER (Rab1a)

Inhibition of FFAR4 internalisation with a dynamin inhibitor (Dyngo-4a) blocked the majority of FFAR4 trafficking into endosomal compartments. This is indicative that the receptor internalises from the plasma membrane in a dynamin dependent manner into the endosomal network and that there is little internalisation independent FFAR4 trafficking after agonist stimulation. However, dynamin inhibitors have also been reported to inhibit anterograde trafficking e.g. trafficking through Rab1a/6 compartments (Preta et al., 2015). Therefore, it is possible that anterograde receptor trafficking (i.e., movement of the FFAR4 from the ER to the Golgi compartments and onto the plasma membrane) might also inhibited after dynamin inhibition and thus may still occur in the absence of receptor internalisation. Intriguingly, the movement of the FFAR4 away from the slow recycling endosome compartment (Rab11a) was not blocked by dynamin inhibition, and under these conditions, FFAR4 had enhanced redistribution to the plasma membrane, albeit not significant. This may indicate that a pool of FFAR4 sits in slow recycling endosomes under basal conditions ready to be directed to the plasma membrane as required.

Once the localisation and trafficking profile of the FFAR4 was investigated, both imaging and BRET-based methods were used to detect sites of ligand induced FFAR4 activation in real-time. It was thought that using methods to detect FFAR4 trafficking in combination with methods that could detect spatiotemporal FFAR4 activity might be used together to piece together sites of FFAR4 localisation and sites of FFAR4 activation. Using HILO imaging, TUG-891 activation of the FFAR4 caused the recruitment of mini-G$\alpha_{i/o}$ probes to intracellular sites, some of which were validated to be early endosomes. Since the FFAR4 was found to localise and traffic to many other subcellular compartments using BRET approaches, including the late endosomes, recycling endosomes, ER, and Golgi compartments, a BRET assay was designed to further characterise additional sites of FFAR4 activation in a simple cell model.

FFAR4 stimulation induced robust mG$\alpha_{i/o}$ recruitment to the plasma membrane (K-ras) and, to a lesser extent, recycling endosomes (Rab11a/b), early endosomes (Rab5), late endosomes (Rab7 & Rab9), and the ER (Rab1a). A small increase in BRET was also detectable at the Golgi/TGN (Rab6/Rab8/Rab9). No increase in BRET was detectable at the retromer compartment (Vsp29). To fully assess the functional relevance of active FFAR4 at specific intracellular compartments, it would be useful to locally block FFAR4 signalling from specific intracellular compartments. This would help to determine the most important signalling locations of the FFAR4 in a simple cell model (Wright et al., 2021).

Taken together with trafficking data, these data suggest that there are two mechanisms of compartmentalised FFAR4 activation. One where the FFAR4 is first activated from the plasma membrane and subsequently internalises and continues to

recruit G proteins in the endosomal network. And another, where the FFAR4 is activated in slow recycling endosomes (Rab11a/b), *en route* to the plasma membrane.

3.3.1.3 FFAR4 activity on cAMP production

Since the FFAR4 was demonstrated $G\alpha_{i/o}$ coupled, BRET-based biosensors were used to determine the impact of FFAR4 signalling in real-time on cAMP production in a simple cell model. Unexpectedly, overexpression of the FFAR4 was found to have a strong inhibitory effect on cAMP production after stimulation with both forskolin and isoproterenol without the addition of selective FFAR4 agonist. This might suggest that either the FFAR4 has some constitutive activity, or that isoproterenol/forskolin might activate the FFAR4 through an unappreciated crosstalk mechanism? The mechanism behind this inhibition requires further examination in HEK293 cells. In the presence of FFAR4 NAM (AH7614), the inhibitory effects of the FFAR4 over cAMP production were reversed. This AH7614-dependent reversal was greater after forskolin stimulation than isoproterenol stimulation. A reason for this phenomenon could be due to differences in the activation of AC pools after stimulation with isoproterenol vs forskolin. For example, forskolin is thought to only weakly activate AC9, whereas isoproterenol (and $G\alpha_s$ activation) is required for full AC9 activation (Qi et al., 2022). It would be interesting to investigate which pools of cyclases are regulated by the FFAR4 most greatly. The subcellular localisation of these pools is most likely to have functional relevance on intracellular FFAR4 signalling (Lazar et al., 2020). In addition, different cell types express different AC isoforms, which is again likely to impact FFAR4 signalling mechanisms.

Considering the FFAR4 was found to recruit mini-G probes to intracellular compartments, the compartmentalised effects of FFAR4 signalling on cAMP production were evaluated in a simple cell model. This was achieved by using plasma membrane, whole cell, or ER directed CAMYEL. After stimulation of cAMP production with isoproterenol, the FFAR4 was found to have greater inhibitory effects on cAMP production from intracellular compartments than from the plasma membrane. In addition, the inhibitory effects of the FFAR4 were sustained and not transient, a hallmark of certain intracellularly active GPCRs (Calebiro et al., 2009, Ferrandon et al., 2009). It would be interesting to further investigate the effects of compartmentalised FFAR4 inhibition after forskolin stimulation to identify if the same is true after GPCR independent cyclase activation in a simple cell model.

3.3.1.4 FFAR4 effects on intracellular [Ca^{2+}] and β-arrestins

Whilst the FFAR4 inhibits cAMP production, the receptor also increases intracellular [Ca^{2+}] upon activation. Using the CalFlux biosensor, FFAR4 activation mediated a transient increase in intracellular [Ca^{2+}]. Taken with the finding that mGα_q recruitment to the FFAR4 was only detectable at the plasma membrane and not from intracellular compartments, it is unlikely that there is functional relevance to intracellular FFAR4-dependent G$\alpha_{q/11}$ signalling, however, this requires further validation.

Finally, within this chapter, the FFAR4 was detected to couple more strongly to β-arrestin-2 than to β-arrestin-1. It would be interesting to evaluate whether β-arrestin-2 helps to mediate the intracellular, G protein-dependent, signalling component of the FFAR4. Or whether β-arrestin simply aids the internalisation of the FFAR4 into the endosomal network. For example, β-arrestins have been found to facilitate sustained

endosomal G protein signalling in a 'megaplex' of GPCR, G protein, and β-arrestin – with β--arrestin in its 'tail' conformation (Nguyen et al., 2019). Evaluating the interplay between β-arrestin and G proteins might be relevant in the further investigation of compartmentalised FFAR4 signalling.

3.3.2 Potential relevance of compartmentalised FFAR4 signalling in adipocytes

Since the FFAR4 is highly expressed in adipocytes (Kimura et al., 2020, Oh et al., 2010), compartmentalised FFAR4 signalling may be of relevance to adipocyte metabolism. Rab proteins are known to have association with the lipid droplets (Zehmer et al., 2009). This includes, but is not limited to, Rab1a, Rab5, Rab7, and Rab11. For example, the expression of dominant negative Rab1a inhibits lipid droplet formation (Nevo-Yassaf et al., 2012). Rab5 is known to regulate the interaction between early endosomes and the lipid droplets, and has been demonstrated involved in the fusion of endosomes and lipid droplets (Liu et al., 2007). Rab5 has also been found on the surface of isolated lipid droplets along with Rab11 (Liu et al., 2007). Finally, Rab7 has been implicated in the control of lipolysis. For example, β_2-AR stimulation enhances the localisation of Rab7 to the lipid droplet compartment (Lizaso et al., 2013). Since the FFAR4 traffics to compartments marked by the above listed Rab proteins and was also found to recruit mini-G probes to these compartments, it might be hypothesised that intracellular FFAR4 signalling has a regulatory role in the control of lipid droplet anabolism and catabolism. It might be further hypothesised that the interplay between the β-ARs, the major activators of lipolysis, and the FFAR4 might be involved in this regulation.

3.3.3 Conclusions

In conclusion, this chapter gives evidence that the FFAR4 is a predominantly $G\alpha_{i/o}$ coupled receptor, with a secondary coupling to $G\alpha_{q/11}$, enabling the receptor to both inhibit cAMP production and increase intracellular $[Ca^{2+}]$ in a simple cell model.

In addition, this chapter gives evidence that FFAR4 activation provokes its internalisation and trafficking into the endosomes, recycling endosomes, late endosomes, and to the ER/Golgi. Furthermore, the FFAR4 was found to recruit mini-G probes to multiple intracellular compartments upon its activation and to inhibit cAMP production more strongly from intracellular sites than from the plasma membrane. Overall, these data suggest that the FFAR4 signals from intracellular compartments to facilitate its local inhibitory control of cAMP production along the endosomal network.

4.0 Chapter Four: Evaluation of FFAR4 signalling in

adipocytes

4.1 Aims of this study

The FFAR4 is intimately involved in adipocyte metabolism and has physiologically relevant effects. Therefore, the signalling mechanisms of the FFAR4 were evaluated in an adipocyte model.

Within this study, mini-G probes were used to investigate the coupling specificity of the FFAR4 in adipocytes, using both imaging and BRET-based approaches. In addition, such methods were further used to investigate the receptor's ability to signal from intracellular compartments. Additionally, the effect of the FFAR4 was assessed on cAMP production using BRET-based methods. Finally, to further investigate the functional relevance of intracellular FFAR4 signalling, a method to inhibit compartmentalised FFAR4 signalling in adipocytes was explored.

4.2 Results

4.2.1 The FFAR4 predominantly couples to G$\alpha_{i/o}$ proteins in pre-adipocytes

Like-to the simple cell model, to investigate the coupling specificity of the FFAR4 in adipocytes, mini-G probes, engineered GTPase domains of the Gα subunit of a G protein (Nehme et al., 2017, Wan et al., 2018), were utilised. The coupling specificity of the FFAR4 was first investigated in two undifferentiated immortalised pre-adipocyte cell lines using a BRET-based approach. Both 3T3-L1 pre-adipocytes and immortalised brown mouse preadipocytes (Harms et al., 2014) were investigated. 3T3-L1 pre-adipocytes are differentiated into adipocytes for use as an *in vitro* adipocyte model which display characteristics of white, beige, and brown adipocytes (Morrison and McGee, 2015). Whereas immortalised brown mouse preadipocytes are differentiated into adipocytes and commonly used as an *in vitro* brown adipocyte model (Sustarsic et al., 2018).

Initially, the BRET was measured between FFAR4-NLuc and Venus fused mini-G probe (mGα_i, mGα_o, mGα_s, mGα_q, or mGα_{12}) in 3T3-L1 pre-adipocytes. Both TUG-891 (Figure 4.1A) and CpdA (Figure 4.1B) were used as activators of the FFAR4 in the presence and absence of FFAR4 antagonist (AH7614). Agonist stimulation induced a major increase in BRET between the FFAR4 and mGα_i and mGα_o (Figure 4.1). A minor increase in BRET was also detectable between the FFAR4 and mGα_q. (Figure 4.1). A virtually negligible response was detectable between the FFAR4 and mGα_s and Gα_{12} subtypes. After both TUG-891 and CpdA stimulation, the presence of AH7614 significantly reduced mGα_i and mGα_o recruitment to the FFAR4, however, did not significantly inhibit mGα_q recruitment – although the response was reduced.

This suggested a preference of the FFAR4 for $G\alpha_{i/o}$ proteins, with a secondary $G\alpha_q$ coupling in pre-adipocyte 3T3-L1 cells.
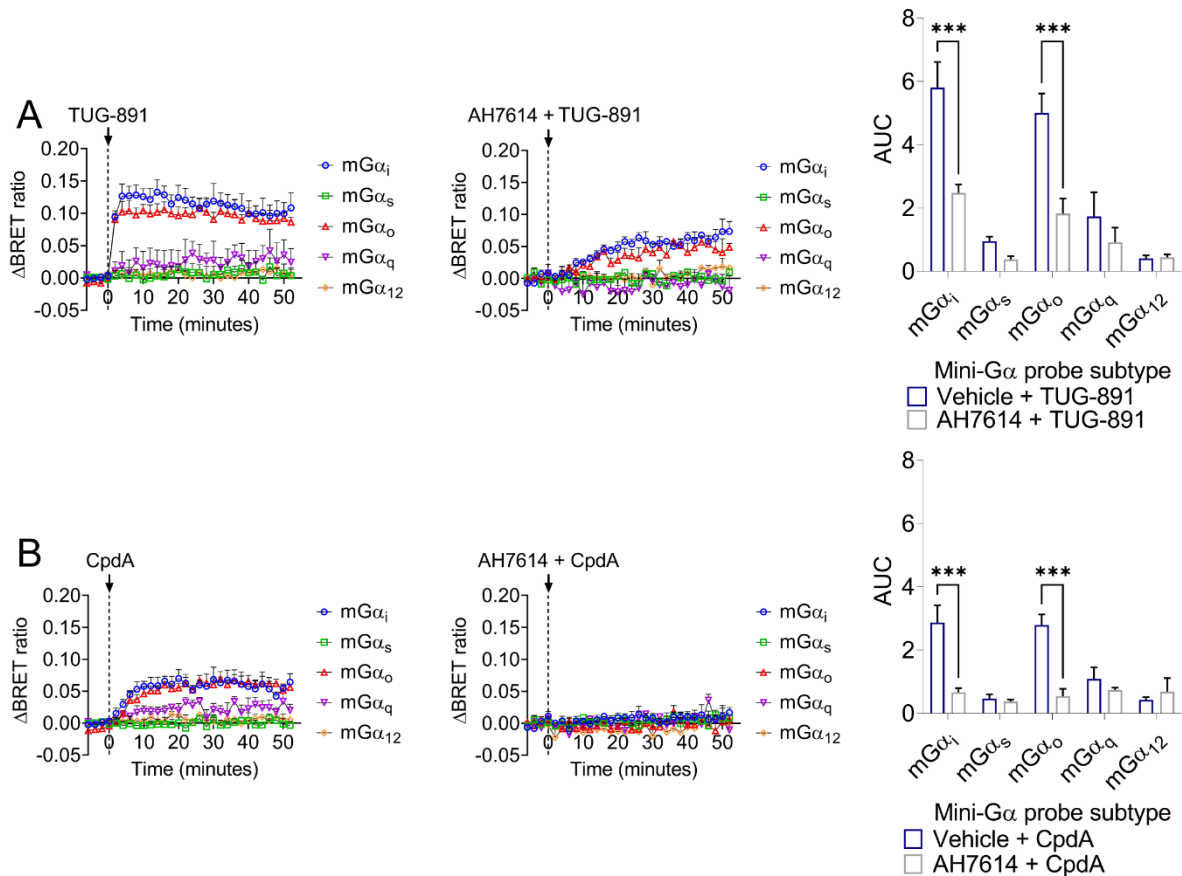
Figure 4. 1: BRET assay to confirm the specificity of Venus fused mini-G probe recruitment to FFAR4-NLuc in 3T3-L1 preadipocytes.

Real-time BRET measurements detecting Venus fused mini-G probe ($mG\alpha_i$, $mG\alpha_o$, $mG\alpha_s$, $mG\alpha_q$, or $mG\alpha_{12}$) recruitment to the FFAR4-NLuc. Shown are the kinetic BRET responses and corresponding AUC values upon (**A**) TUG-891 (10 μM) stimulation (left) with and without AH7614 (10 μM) preincubation (15 mins) or (**B**) CpdA (1 μM) stimulation (left) with and without AH7614 (10 μM) preincubation (15 mins) (middle). Differences are statistically significant by two-way ANOVA. $P<0.001$ = *** by Sidak's post hoc analysis. Data represent mean + S.E.M. compiled from three independent experiments performed in triplicate.

The coupling specificity of the FFAR4 was further evaluated in immortalised brown preadipocytes (Harms et al., 2014). Immortalised brown preadipocytes were transfected with FFAR4-NLuc and Venus fused mini-G probe (mGα_i, mGα_o, mGα_s, and mGα_q). The coupling specificity was examined after stimulation with TUG-891 to evaluate whether these cells were suitable for BRET assays (Figure 4.2). A robust increase in BRET was detectable between FFAR4 and mGα_i and mGα_o probes after TUG-891 stimulation. A small increase in mGα_q was also recruited to the FFAR4. A virtually negligible response was detectable between the FFAR4 and mGα_s. The recruitment of mGα_q to the FFAR4 was more pronounced within this cell type than within 3T3-L1 preadipocytes, and the assay itself had smaller error. Therefore, immortalised brown preadipocyte cells were established as the more appropriate adipocyte model for further BRET-based analysis.
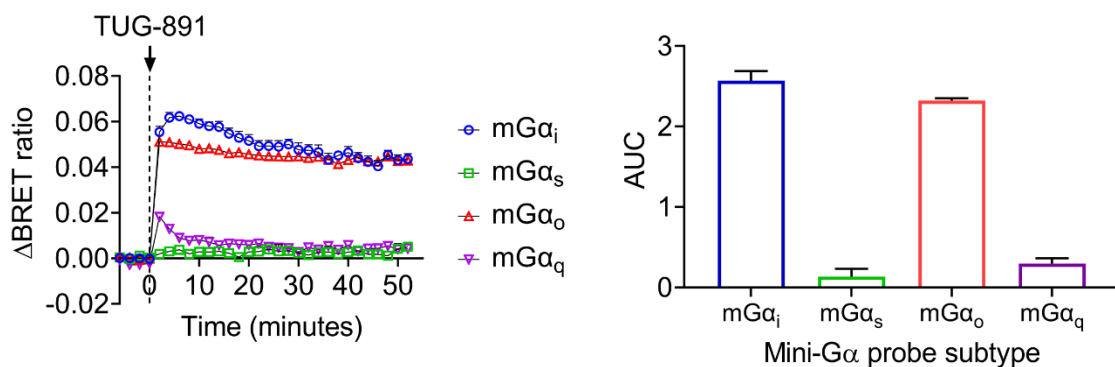
Figure 4. 2: BRET assay to confirm the specificity of Venus tagged mini-G probe recruitment to FFAR4-NLuc in immortalised brown preadipocytes.
Real-time BRET measurements detecting Venus tagged mini-G probe (mGα_i, mGα_o, mGα_s, mGα_q, or mGα_{12}) recruitment to the FFAR4-NLuc. Shown are the kinetic BRET responses and corresponding AUC values upon TUG-891 (10 μM) stimulation. Data represents mean ± S.E.M. compiled from one independent experiment performed in triplicate.

4.2.2 The FFAR4 couples to $G\alpha_{i/o}$ proteins in differentiated adipocytes

Furthermore, BRET assays were optimised in cells expressing lipid droplets. Differentiated immortalised brown adipocytes were transfected with FFAR4-NLuc and Venus fused mini-G probe ($mG\alpha_i$, $mG\alpha_o$, $mG\alpha_s$, $mG\alpha_q$, or $mG\alpha_{12}$). The ligand induced BRET was measured upon stimulation with TUG-891 (Hudson et al., 2013), CpdA (Oh et al., 2014), and α-linolenic acid (Hirasawa et al., 2005, Sanchez-Reyes et al., 2014). Agonist stimulation induced a major increase in BRET between the FFAR4 and $mG\alpha_i$ and $mG\alpha_o$ (Figure 4.3). A minor increase in BRET was also detectable between the FFAR4 and $mG\alpha_q$. (Figure 4.3). A virtually negligible response was detectable between the FFAR4 and $mG\alpha_s$ and $G\alpha_{12}$ subtypes. These results suggest that the FFAR4 is predominantly $G\alpha_{i/o}$ coupled in a differentiated adipocyte model.
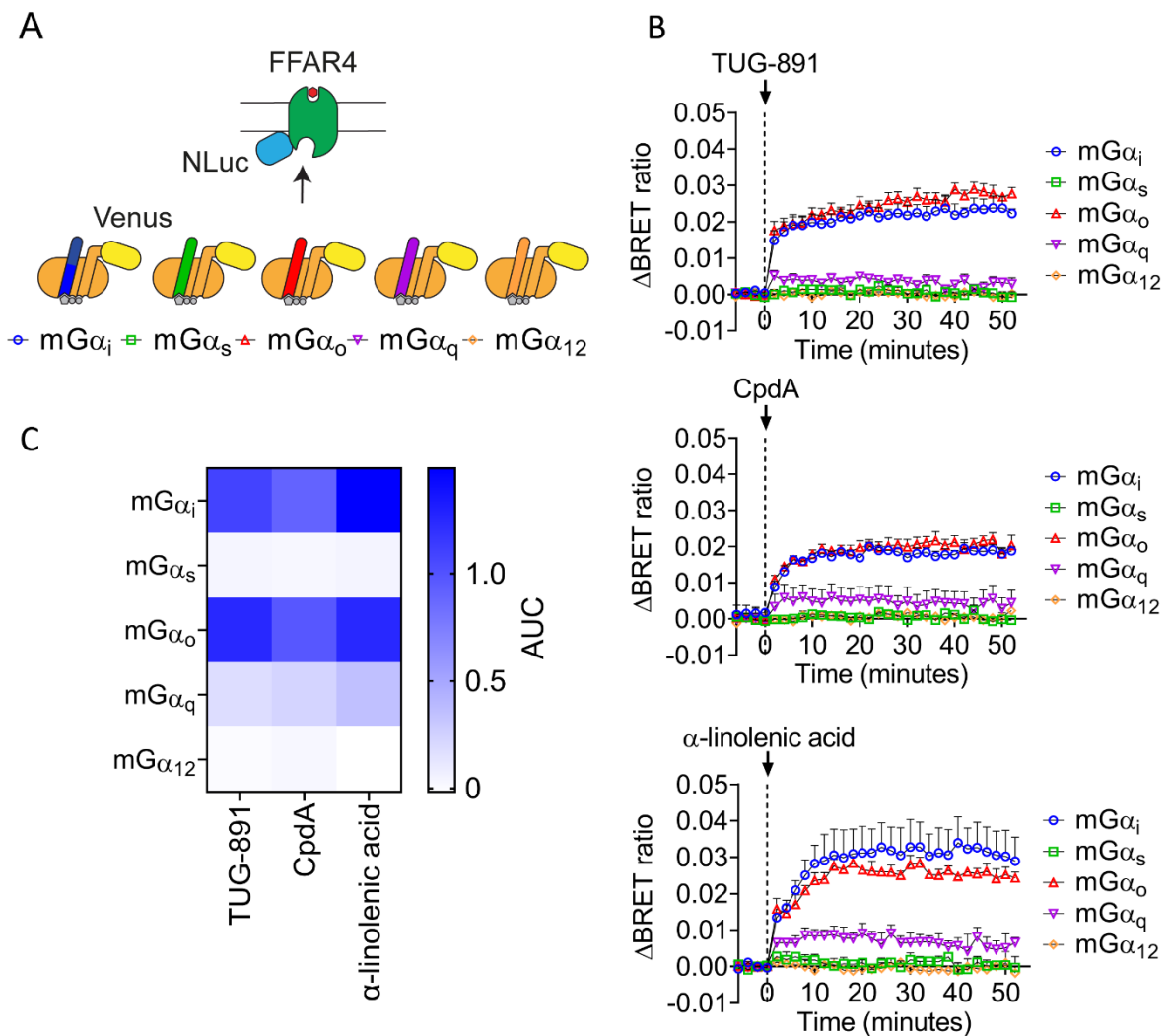
Figure 4. 3: The FFAR4 couples to Gα$_{i/o}$ in differentiated adipocytes.

(**A**) Schematic to illustrate the BRET assay to detect FFAR4 in differentiated immortalised brown adipocytes. (**B**) Real-time BRET measurements of Venus fused mini-G probe (mGα$_i$, mGα$_s$, mGα$_o$, mGα$_q$, or mGα$_{12}$) recruitment to the FFAR4-NLuc upon TUG-891 (top), CpdA (middle), α-linolenic acid (bottom) (10 μM) stimulation. (**C**) Corresponding AUC values are presented on a heat map. Data represent mean ± S.E.M. compiled from three independent experiments performed in triplicate.

4.2.3 The FFAR4 has an enhanced intracellular localisation in 3T3-L1 pre-adipocytes

Having demonstrated that the FFAR4 remains strongly $G\alpha_{i/o}$ coupled in differentiated adipocytes, the localisation of the receptor was further evaluated in adipocyte models. Initially, FFAR4-YFP was transfected into undifferentiated 3T3-L1 preadipocytes. Within these cells, the FFAR4 seemed to have enhanced intracellular localisation compared to plasma membrane localisation. In addition, the FFAR4 had an increased perinuclear localisation. After stimulation with FFAR4 agonist TUG-891, the FFAR4 rapidly accumulated into an endosomal-like compartment (Figure 4.4).
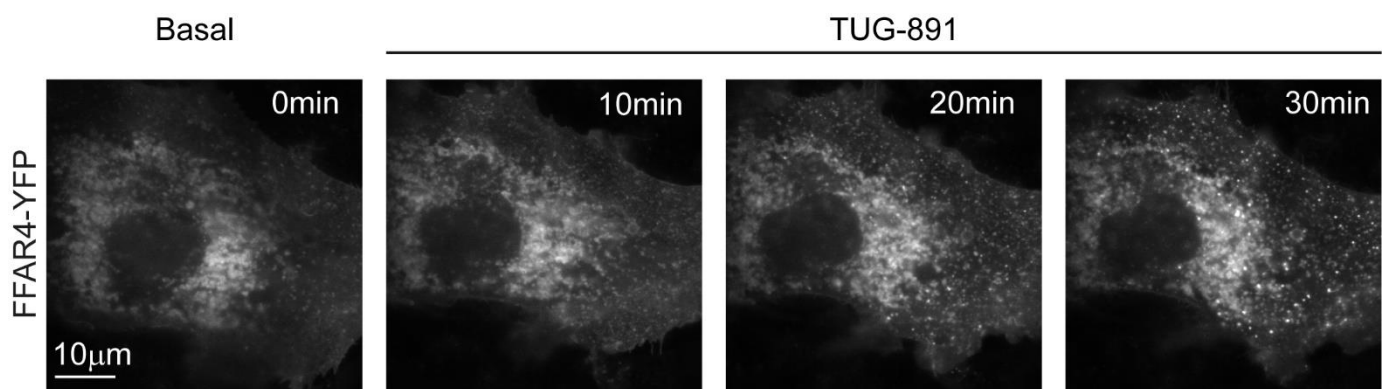
Figure 4. 4: TUG-891 initiates FFAR4 trafficking into an endosome-like compartment in 3T3-L1 pre-adipocytes.

Effect of TUG-891 stimulation on FFAR4 localisation. Shown are selective images of live cell HILO imaging of 3T3-L1 preadipocytes transfected with FFAR4-YFP. Cells were stimulated with TUG-891 (10 μM), selective FFAR4 agonist. Data are representative of at least three independent experiments.

The subcellular localisation of the FFAR4 was evaluated within undifferentiated 3T3-L1 cells after TUG-891 stimulation. Within this investigation, the subcellular localisation of the FFAR4 was initially investigated using markers of early endosomes (mCherry-Rab5), Golgi compartment (ST-RFP), and mitochondria (MitoTracker™ Red) (Figure 4.5). Using such an approach, stimulation with TUG-891 induced receptor recruitment to the early endosome compartment – indicated by FFAR4-YFP co-localisation with mCherry-Rab5. In addition, the FFAR4 was also observed to localise closely to the Golgi compartment and to the mitochondria prior to stimulation.
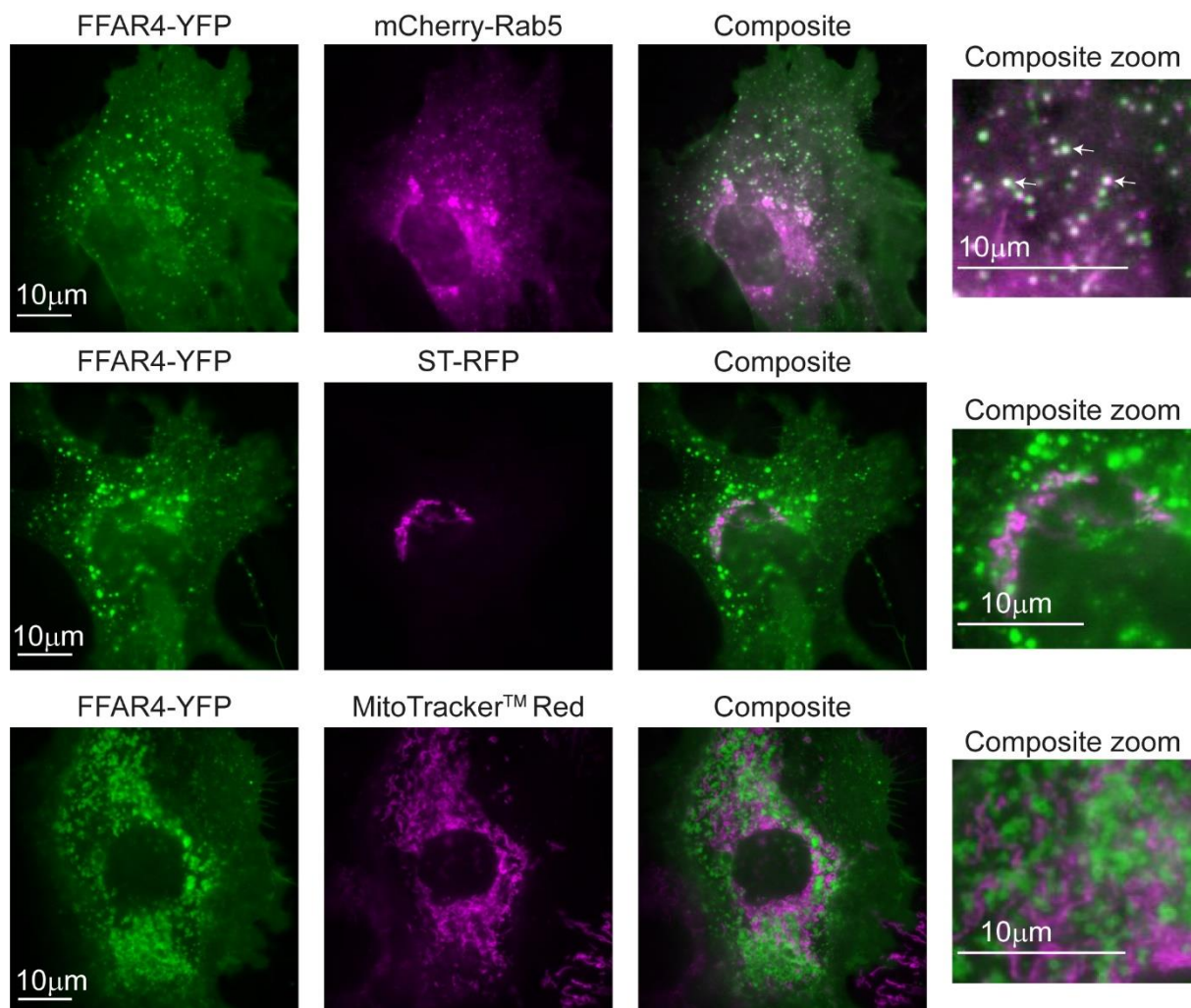
Figure 4. 5: TUG-891 stimulation initiates FFAR4 trafficking into the endosome compartment in 3T3-L1 pre-adipocytes.

Effect of TUG-891 stimulation on FFAR4 localisation in 3T3-L1 pre-adipocytes. Shown are selective frames representative of FFAR4 localisation after TUG-891 (10 μM) stimulation (20 minutes). The localisation of FFAR4-YFP was evaluated in combination with mCherry-Rab5 (early endosome marker), ST-RFP (Golgi marker), or mitochondria (stained with MitoTracker™ Red). Green pseudocolour indicates FFAR4-YFP and magenta pseudocolour indicates mCherry-Rab5 (top), ST-RFP (middle), or MitoTracker Red (bottom). White colouration indicates co-localisation. Images are representative of at least three independent experiments.

4.2.4 The FFAR4 is localised closely to lipid stores in 3T3-L1 adipocytes

Having assessed the localisation of the FFAR4 in 3T3-L1 preadipocytes, the localisation of the FFAR4 was further evaluated in differentiated 3T3-L1 cells – cells containing better developed lipid stores. 3T3-L1 cells were transfected with FFAR4-YFP and subsequently differentiated into adipocytes. On day five of differentiation, the lipid droplets were stained with LipidSpot™ 610 nm and the cells were taken for imaging. Within these cells, the FFAR4 was found to closely localise with lipid stores (Figure 4.6). This was further confirmed by overexpression of the FFAR4 in combination with PLIN1-mCherry, a protein which localises to the surface of lipid droplets (Skinner et al., 2013). Since lipid droplets have a single phospholipid monolayer, unlike other subcellular organelles, which is unlikely to accommodate GPCRs, it was reasoned that the FFAR4 might be localised on membranes of another, closely associated, organelle. Given the known intimate association of the ER with lipid droplets (Olzmann and Carvalho, 2019) and the pattern observed in the images, the ER appeared as a good candidate. This hypothesis was tested by observing the localisation of the FFAR4-YFP in combination with an ER stain (ER Tracker™ Red).

Within differentiated 3T3-L1 adipocytes, the FFAR4-YFP was detected to colocalise with domains of the ER (Figure 4.6).
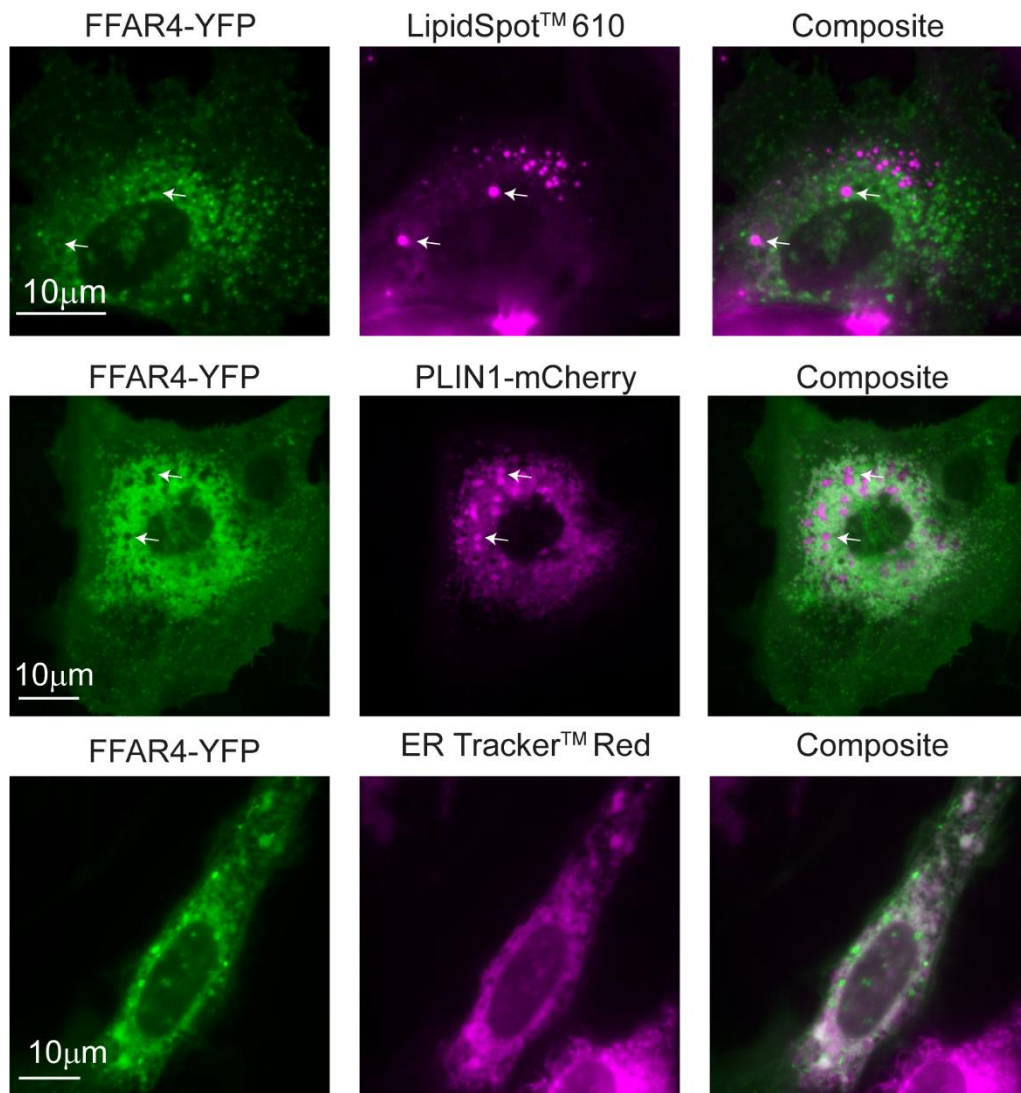
Figure 4. 6: The FFAR4 localises closely to lipid stores in 3T3-L1 adipocytes. Localisation of FFAR4 in 3T3-L1 adipocytes. Shown are selective frames representative of FFAR4-YFP localisation in 3T3-L1 adipocytes in combination with LipidSpot™ (top), PLIN1-mCherry (middle), or ER tracker™ red (bottom). Green pseudocolour indicates FFAR4-YFP and magenta pseudocolour indicates subcellular compartment. White colouration indicates co-localisation.

4.2.5 The FFAR4 is localised closely to lipid stores in immortalised brown adipocytes.

Furthermore, the localisation of the FFAR4 was examined in immortalised brown adipocytes. In cells transfected with FFAR4-YFP, there seemed a relevant fraction of receptor located at intracellular compartments under basal conditions. The relative amount of cell surface and intracellular FFAR4 was variable from cell to cell, which might correlate with their degree of differentiation. In cells with well-developed lipid droplets, the FFAR4 was observed in proximity to structures thought to be lipid droplets (Figure 4.7). Comparably to 3T3-L1 cells, upon TUG-891 stimulation, the FFAR4 trafficked into an endosomal-like compartment.
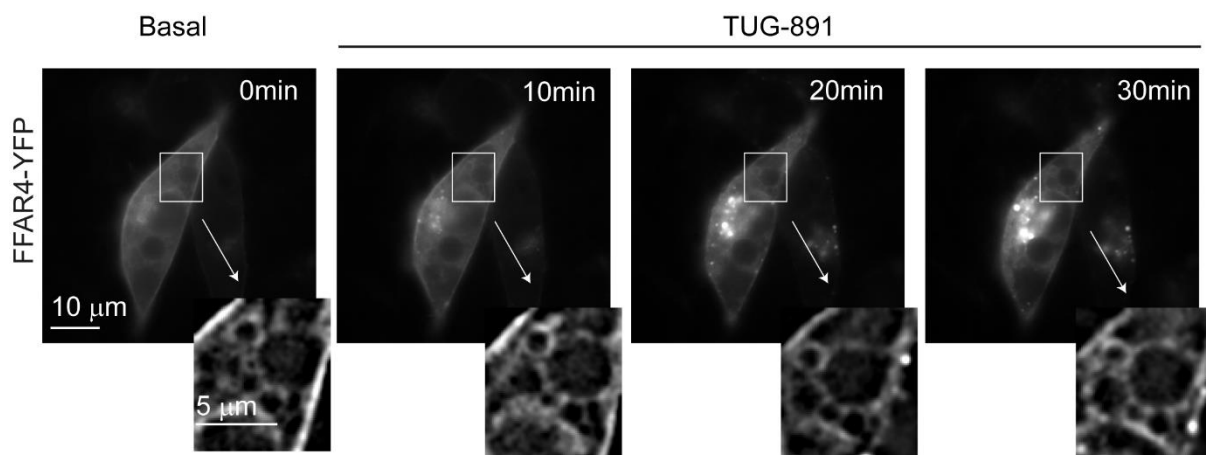
Figure 4. 7: The FFAR4 internalises to intracellular compartments after TUG-891 stimulation and is present at intracellular compartments under basal conditions in immortalised brown adipocytes.

Effect of TUG-891 stimulation on FFAR4 localisation in immortalised brown adipocytes. Shown are selective images of live cell HILO imaging in immortalised brown adipocytes transfected with FFAR4-YFP and stimulated with TUG-891 (10 μM), selective FFAR4 agonist. A Fast Fourier transformation was applied to reduce cytoplasmic signal and facilitate the observation of subcellular structures. Images are representative of at least three independent experiments.

To further investigate the subcellular localization of the FFAR4, SIM was employed. Like-to 3T3-L1 adipocytes, within differentiated immortalised brown adipocytes, in cells co-transfected with FFAR4-YFP and a lipid droplet membrane marker (PLIN1-mCherry), FFAR4 was found closely associated with lipid droplets (Figure 4.8A). Furthermore, the FFAR4 partially colocalised with the ER (Sec61β), indicating that a portion of intracellular FFAR4 is present in the ER in adipocytes (Figure 4.8B). These data could be better appreciated using 3D reconstructions from SIM image stacks (Figure 4.8C&D).
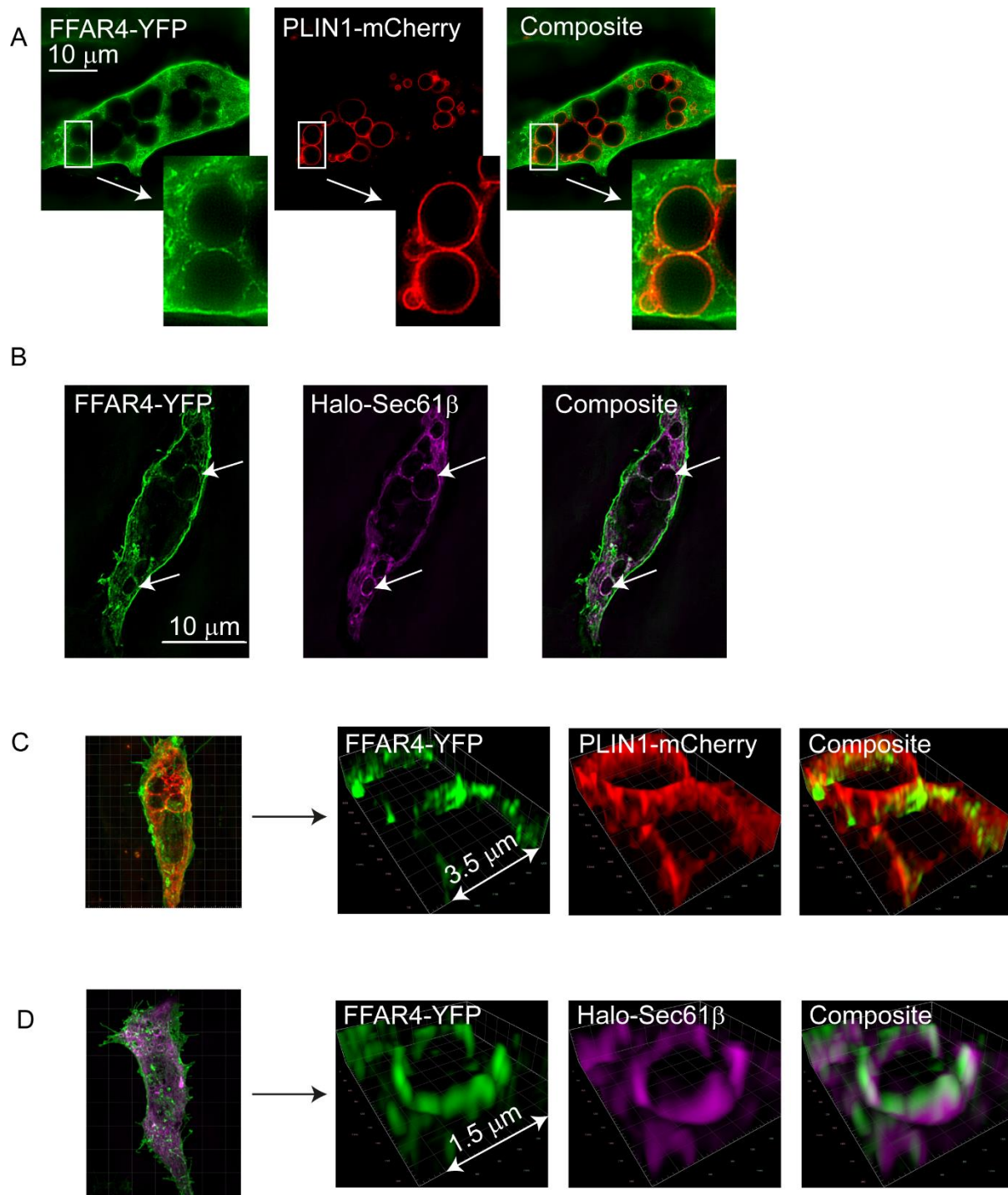
Figure 4. 8: The FFAR4 is localised closely to lipid stores in immortalised brown adipocytes.

Localisation of FFAR4 in immortalised brown adipocytes. (**A&B**) Shown are selective frames representative of 2D FFAR4-YFP localisation in immortalised brown adipocytes in combination with (**A**) PLIN1-mCherry, or (**B**) Halo-Sec61β. (**C&D**) Shown are selective frames representative of 3D FFAR4-YFP localisation in immortalised brown adipocytes in combination with (**C**) PLIN1-mCherry, or (**D**) Halo-Sec61β.

4.2.6 The FFAR4 has enhanced localisation at the ER in immortalised brown adipocytes compared to the β_2AR

To further validate the subcellular localisation of the FFAR4 in immortalised brown adipocytes, a BRET-based assay was designed. For this purpose, the basal BRET ratio was measured between FFAR4-NLuc or β_2AR-NLuc and subcellular compartment markers. These markers included Venus tagged compartment markers: K-ras (plasma membrane); Rab5 (early endosomes); Vsp29 (endosomes to TGN); Rab8 (TGN to plasma membrane) or alternatively, GFP/mEmerald tagged markers: PLIN1/2 (lipid droplets, GFP tagged); and Sec61β (ER, mEmerald tagged) (Figure 4.9).

An increased basal BRET ratio was detectable between the FFAR4 and the ER marker (Sec61β) compared to the β_2AR, indicating enhanced ER localisation. A slightly decreased BRET ratio was detectable between the FFAR4, and the plasma membrane compared to the β_2AR. The basal BRET ratio between the two receptors at other compartments was comparable. This indicates that the FFAR4 has enhanced localisation at the ER and slightly decreased plasma membrane localisation compared to the β_2AR (Figure 4.9). To truly interrogate the basal localisation of the FFAR4 in immortalised brown adipocytes using BRET, the fluorophores tethered to intracellular compartments would need to be identical (e.g., all Venus fused) and be compared to improved controls (e.g., cytosolic NLuc (negative control) or even NLuc fused to subcellular compartments (positive control). This would facilitate the improved quantification of receptor localisation to subcellular compartments with high spatial resolution.
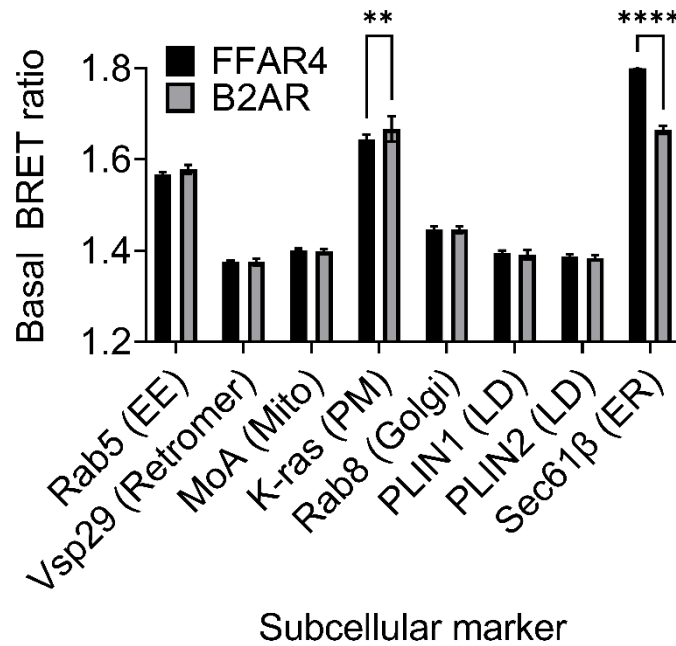
Figure 4. 9: BRET assay comparing FFAR4 and β_2-AR distribution at subcellular compartments in immortalised brown adipocytes.

Subcellular distribution of the FFAR4 compared to the β_2AR. Shown are the basal BRET measurements between FFAR4-NLuc or β_2AR-NLuc, in combination with Venus, GFP, or mEmerald tagged compartment markers. Differences are statistically significant by two-way ANOVA. $P < 0.0001$ = ****, $p < 0.01$ = ** by Sidak's post hoc analysis. Data represents mean ± S.E.M. of one independent experiment performed in sextuplicate.

4.2.7 The FFAR4 has a greater inhibitory effect on cAMP production from intracellular compartments than the plasma membrane in adipocytes

Having observed that a relevant portion of FFAR4 is located intracellularly in adipocytes in close association with lipid droplets, it was hypothesised that intracellular FFAR4 might be able to locally control cAMP production. To test this hypothesis, a BRET sensor sensitive to cAMP was employed: NLuc-Epac-VV (Masuho et al., 2015). This sensor was found to have a superior signal in immortalised adipocytes compared to CAMYEL (used in the simple cell model), likely since NLuc is brighter than RLuc (Dale et al., 2019). The sensor was targeted to the plasma membrane, ER or lipid droplets via fusion to the first 196 N-terminal amino acids of PDE2A3 (Matthiesen and Nielsen, 2011), to Sec61β, (Moore et al., 2021), or to PLIN1 (Rowe et al., 2016), respectively. Like to CAMYEL, a reduction of BRET is indicative of an increase in the local cAMP concentration.

Firstly, the functionality of the new targeted sensors was tested after increasing isoproterenol stimulations in immortalised brown adipocytes. The sensors were found to have similar sensitivity to isoproterenol-induced cAMP production: plasma membrane, EC$_{50}$: 5.453×10^{-8} M; ER, EC$_{50}$: 6.416×1010^{-8} M; and lipid droplet, EC$_{50}$: 4.027×10^{-8} M (Figure 4.10A). Furthermore, the localisation of the targeted sensors was validated. The plasma membrane sensor had a distinctive plasma membrane-like localisation (Figure 4.11B). Both ER and lipid droplet sensors were assessed in combination with mCherry-Sec61β (Figure 4.11C) and PLIN1-mCherry (Figure 4.11D), respectively, to confirm localisation. The new ER and lipid droplet sensors were found to co-localise well with the ER and lipid droplet markers.
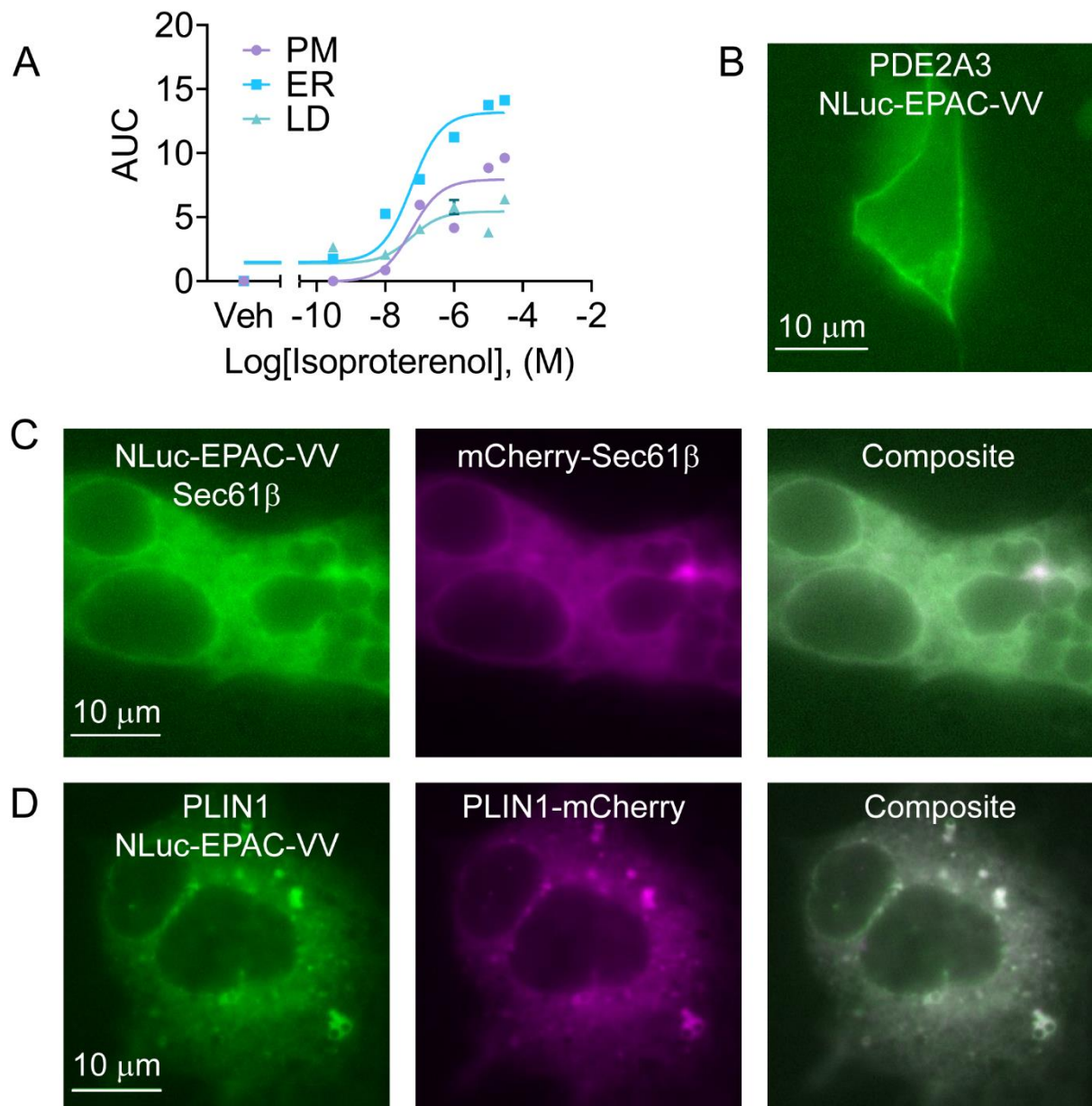
Figure 4. 10: Functionality and localisation of targeted cAMP sensors in immortalised brown adipocytes.

(**A**) Dose response curve detecting cAMP production after increasing isoproterenol stimulations in immortalised brown adipocytes with plasma membrane (PM), ER, and lipid droplet (LD) directed NLuc-Epac-VV cAMP. (**B**) Localisation of plasma membrane directed PDE2A3-NLuc-Epac-VV localisation. (**C**) Localisation of ER directed NLuc-Epac-VV-Sec61β. Shown are selective frames representative of NLuc-Epac-VV-Sec61β (left) in combination with mCherry-Sec61β (middle), and composite of the two

channels (right). (**D**) Localisation of lipid droplet directed PLIN1-NLuc-Epac-VV. Shown are selective frames representative of PLIN1-NLuc-Epac-VV (left) in combination with PLIN1-mCherry (middle), and composite of the two channels (right). White colour indicates co-localisation.

Furthermore, the effect of FFAR4 overexpression, compared to pcDNA3 overexpression (empty vector), on cAMP production was examined at each compartment in immortalised brown adipocytes. As expected, activation of ACs, either via the β-adrenergic agonist isoproterenol (Figure 4.11A) or direct stimulation with forskolin (Figure 4.11B), resulted in a reduction of BRET at all compartments, indicative of local increases in cAMP production. Co-transfection of FFAR4 attenuated the BRET response, consistent with FFAR4-mediated activation of $G\alpha_{i/o}$-proteins (Figure 4.11). Interestingly, the inhibitory effect of FFAR4 overexpression on cAMP production was more pronounced after stimulation with isoproterenol compared to forskolin. This could be due to differences in the activation of cyclase pools after stimulation with each agonist.

When comparing the AUC in the presence or absence of the FFAR4, no significant effect was detectable between compartments. However, when comparing the total change in BRET (ΔBRET), in the presence or the absence of the FFAR4, the effect of FFAR4 expression on cAMP levels was more pronounced when measured at lipid droplets and the ER compared to the plasma membrane (LD>ER>PM) (Figure 4.11C&D), consistent with FFAR4 exerting local effects on cAMP production near the lipid droplets. These data indicate that the FFAR4 exerts greater inhibitory effects on cAMP production from intracellular compartments than from the plasma membrane in adipocytes.
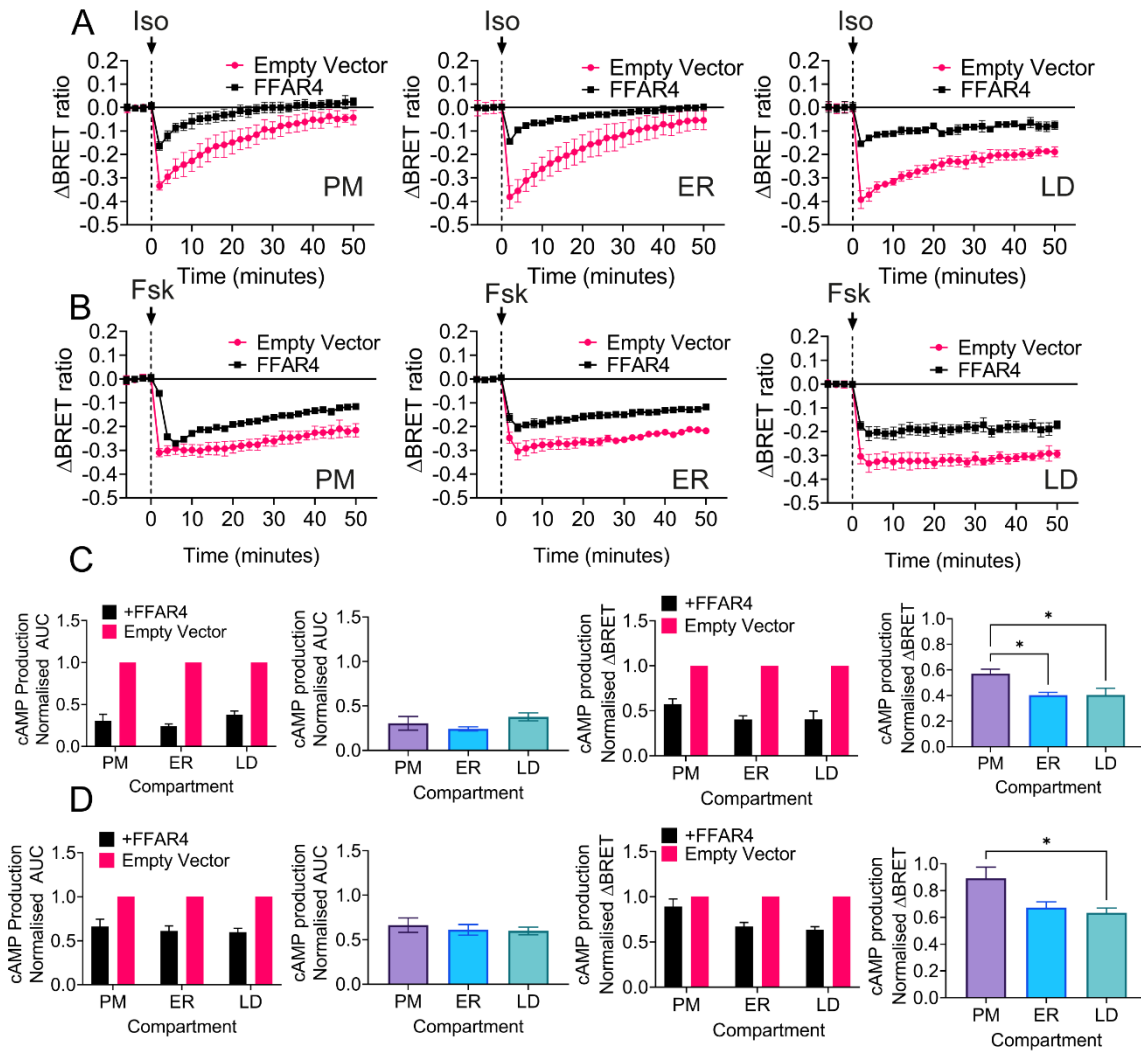
Figure 4. 11: FFAR4 overexpression inhibits cAMP production more greatly from intracellular compartments than from the plasma membrane.

Real-time BRET measurements of local cAMP levels in immortalised brown adipocytes with or without FFAR4 overexpression. (**A&B**) Shown are the real-time BRET measurements after stimulation with (**A**) isoproterenol (Iso) (10 μM) or (**B**) forskolin (Fsk) (10 μM). (**C&D**) AUC or total change in BRET ratio (ΔBRET) in the presence of the FFAR4 was normalised to the AUC or total change in BRET (ΔBRET) in the absence of the FFAR4 (compensated with empty vector). Shown are the resulting calculations after (**C**) isoproterenol or (**D**) forskolin stimulation. Differences are statistically significant by one-way ANOVA. * $p<0.05$ by Sidak's multiple comparison post hoc test. Data represent mean ± S.E.M. from three independent experiments performed in duplicate.

4.2.8 The FFAR4 inhibits lipolysis in immortalised brown adipocytes

In the literature, the FFAR4 has been shown to have an inhibitory role on adipocyte lipolysis (Satapati et al., 2017), however, the mechanism behind this inhibition has not been fully understood. Since the FFAR4 was observed to inhibit cAMP production (Figure 4.11), it was hypothesised that the FFAR4 would inhibit lipolysis in immortalised brown adipocytes.

In previous assays, isoproterenol and forskolin were used to detect FFAR4 provoked changes in cAMP production (Figure 4.11). However, since forskolin and isoproterenol raise the concentration of intracellular cAMP, PKA is activated, and in adipocytes, lipolysis is stimulated (Duncan et al., 2007). Therefore, both compounds are commonly used as lipolysis activators.

To test the effect of endogenous FFAR4 on lipolysis, immortalised brown adipocytes were pre-treated with vehicle or AH7614 (FFAR4 NAM) and stimulated with isoproterenol to initiate lipolysis (Figure 4.12). A low concentration of isoproterenol was used so that the effect of endogenous FFAR4 was not oversaturated. After stimulation with isoproterenol, the extracellular concentration of glycerol was quantified. Lipolysis stimulation significantly increased glycerol release compared to the vehicle control. This increase was only significant after 30 minutes stimulation, and not after 10 minutes stimulation. After 30 minutes, FFAR4 inhibition with AH7614 significantly increased isoproterenol-stimulated glycerol release. Since FFAR4 inhibition increased glycerol release, these data indeed indicate that the FFAR4 has

an inhibitory role on lipolysis, confirming evidence from the literature (Satapati et al., 2017).
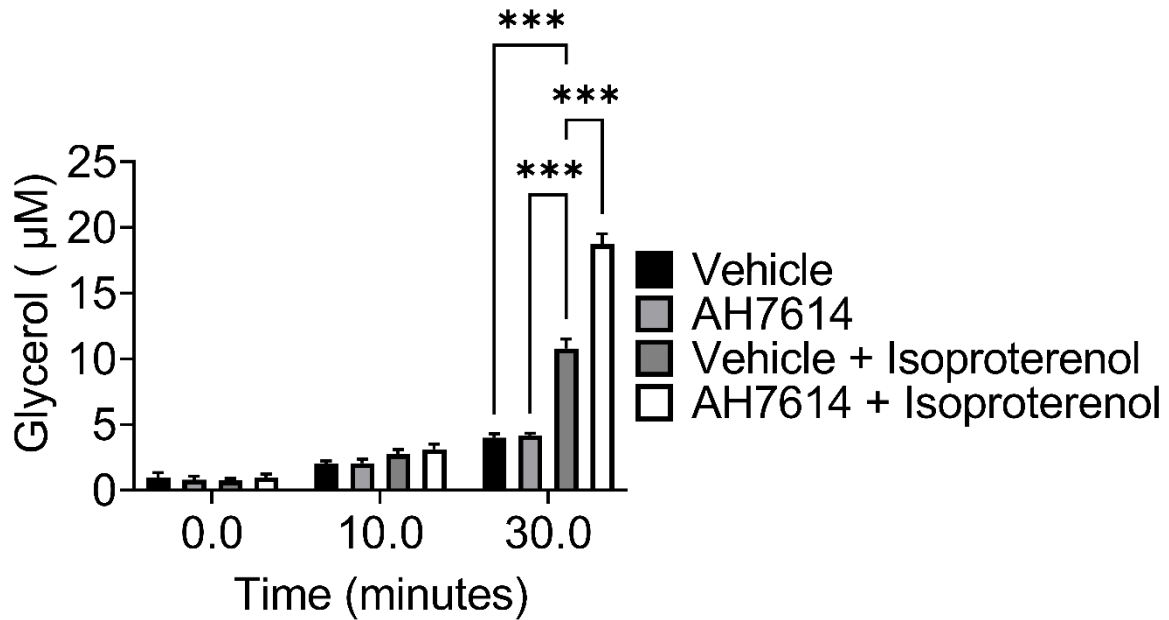
Figure 4. 12: The FFAR4 inhibits lipolysis in immortalised brown adipocytes.
Effect of FFAR4 inhibition on lipolysis. Shown are the results of extracellular glycerol quantification, after adipocytes were pre-incubated with AH7614 (10 μM for 15 minutes), or vehicle, and stimulated with isoproterenol (500 ρM) in the presence or absence of AH7614 (10 μM). The assay was conducted in Krebs-Ringer buffer supplemented with BSA (10 μM). Media samples (50 μL) were taken after 0-, 10-, and 30-minute time points and the total glycerol concentration was quantified using the Glycerol-Glo^{TM} quantification kit (Promega). Differences are statistically significant by two-way ANOVA. $P<0.001 = ***$ by Dunnett's post hoc analysis. Data represent mean $\pm$S.E.M. and are compiled from two independent experiments performed in triplicate.

4.2.9 The FFAR4 is activated in response to lipolysis in immortalised brown adipocytes

Confirming that the FFAR4 inhibits glycerol release (Figure 4.12), and thus lipolysis, in immortalised brown adipocytes, and that overexpression of the FFAR4 inhibits cAMP production without application of specific FFAR4 agonist (Figure 4.11), the mechanism of activation of the FFAR4 in response to lipolysis activation was further investigated. It was hypothesised that lipolysis promotes the release of FFAs, which bind and activate the FFAR4 (Husted et al., 2020).

To test this hypothesis, a BRET assay was designed to detect FFAR4 activation upon lipolysis induction. Initially, this phenomenon was investigated in immortalised brown pre-adipocytes. In this assay, FFAR4-NLuc was transiently transfected, in combination with Venus fused $mG\alpha_i$ or Venus fused $mG\alpha_o$ and pre-adipocytes were stimulated with forskolin or isoproterenol, as lipolysis activators, or with specific FFAR4 activator, TUG-891, as a positive control. Within pre-adipocyte cells, although FFAR4 activation was detectable after TUG-891 stimulation by a robust increase in BRET between $mG\alpha_i$ and $mG\alpha_o$ to the FFAR4, no activation was detectable after stimulation with isoproterenol or forskolin. This indicated that in pre-adipocytes, cells with minimal lipid stores, the FFAR4 is not activated after lipolysis induction.

This assay was subsequently repeated in immortalised brown adipocytes – where the cells now expressed lipid droplets. After stimulation with TUG-891, like to the pre-adipocyte cells, a robust increase in BRET was detectable between $mG\alpha_i$ and $mG\alpha_o$ to the FFAR4. However, now, after stimulation of lipolysis with isoproterenol and forskolin, a major BRET increase was detectable between $mG\alpha_i$ and $mG\alpha_o$ and the

FFAR4. Stimulation of lipolysis generated FFAR4 activation nearly to the same level as TUG-891 stimulation. This indicated that the FFAR4 is indeed directly and rapidly activated upon the induction of lipolysis in adipocytes.
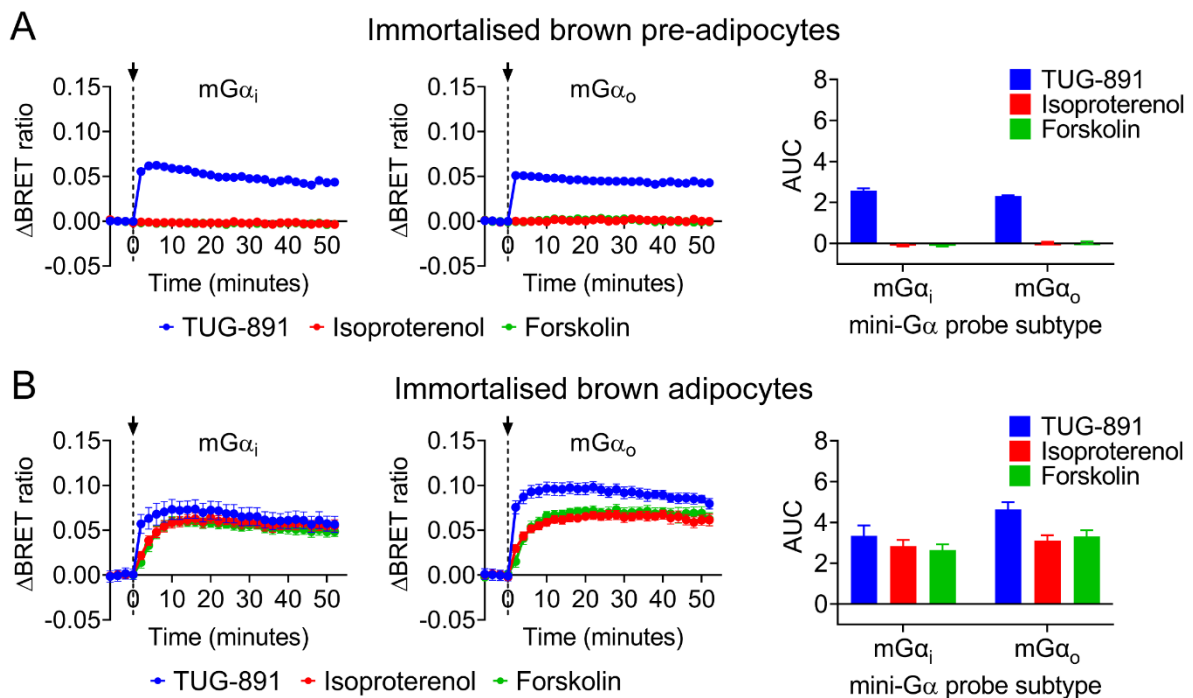
Figure 4. 13: Lipolysis activates the FFAR4 in immortalised brown adipocytes. (**A**) BRET assay detecting FFAR4 activation upon lipolysis stimulation in immortalised brown pre-adipocytes. Shown are the real-time BRET measurements between FFAR4-NLuc and Venus fused mGα_i (left) or Venus fused mGα_o (middle) after stimulation with specific FFAR4 agonist (TUG-891, 10 μM), or lipolysis activator (forskolin/isoproterenol, 10 μM) and corresponding AUC values (right). (**B**) BRET assay detecting FFAR4 activation upon lipolysis stimulation in immortalised brown adipocytes. Shown are the real-time BRET measurements between FFAR4-NLuc and Venus fused mGα_i (left) or Venus fused mGα_o (middle) after stimulation with specific FFAR4 agonist (TUG-891, 10 μM), or lipolysis activator (forskolin/isoproterenol, 10 μM) and corresponding AUC values (right). Data represents mean ±S.E.M. and are compiled from three independent experiments performed in triplicate.

4.2.10 FFAR4 activation is specific to FFA release

To further confirm that FFAR4 activation upon stimulation of lipolysis is specific to fatty acid release and not due to upstream cAMP/PKA activation, lipase inhibitors (HSL or ATGL inhibitors) were used to inhibit lipolysis. BAY 59-9435 (BAY) was used as an inhibitor of HSL whereas atglistatin (Ai) was used as an inhibitor of ATGL (Mottillo et al., 2019).

Firstly, to validate that the lipase inhibitors were able to inhibit lipolysis, the effects of BAY and Ai were tested on glycerol release (Figure 4.14). Prior to lipolysis activation, lipase inhibitors were found to have little effect on glycerol release. However, after stimulation of lipolysis with isoproterenol, inhibition of ATGL robustly reduced glycerol release, whereas inhibition of HSL only partially reduced glycerol release. A combination of both lipase inhibitors together was most successful at blocking extracellular glycerol release and thus lipolysis.
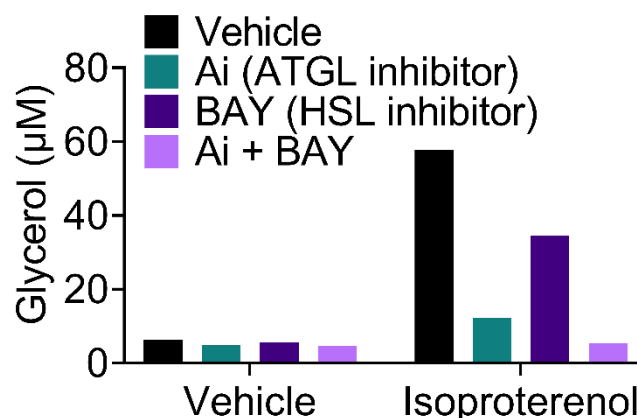
Figure 4. 14: HSL and ATGL inhibitors reduce isoproterenol stimulated lipolysis in immortalised brown adipocytes.

Extracellular glycerol quantification after stimulation of lipolysis in the presence and absence of lipolysis inhibitors. Shown are the results of extracellular glycerol

quantification after preincubation of immortalised brown adipocytes with Atglistatin (Ai, ATGL inhibitor, 10 μM), BAY 59-9435 (BAY, HSL inhibitor, 5 μM) or a combination of Ai and BAY (10 μM and 5 μM, respectively), for 30-minutes. Adipocytes were stimulated with lipolysis activator (isoproterenol, 100 nM) in Krebs-ringer buffer supplemented with BSA (10 μM) in the presence or absence of corresponding antagonist. Media samples were collected, and total glycerol concentration was quantified using Glycerol-Glo luminescence kit (Promega) by comparing to a Glycerol standard of known concentration. Data shows the raw values of one independent experiment

Furthermore, lipolysis-induced FFAR4 activation was tested in the presence and absence of lipolysis inhibitors (BAY and Ai) and FFAR4 inhibitor (AH7614). For this purpose, the BRET between FFAR4-NLuc and Venus fused mini-G probe (mGα_i and mGα_o) was measured after forskolin and isoproterenol stimulation in the presence and absence of HSL inhibitor (BAY), ATGL inhibitor (Ai), HSL inhibitor and ATGL inhibitor in combination, or FFAR4 inhibitor (AH7614) in immortalised brown adipocytes (Figure 4.15).

As hypothesised, inhibition of ATGL with Ai attenuated the BRET between FFAR4 and mGα_i or mGα_o after forskolin and isoproterenol stimulation, but not TUG-891 stimulation. Inhibition of HSL with BAY delayed the onset of BRET between FFAR4 and mini-G probes, but had little effect on the overall BRET response. The addition of both lipase inhibitors in combination had the greatest inhibitory effect on FFAR4 activation. Finally, treatment with AH7614 inhibited early recruitment of mini-G probe to the FFAR4, but was less effective at later time points in the assay. These data indicate that FFAR4 activation after isoproterenol and forskolin stimulation in

immortalised brown adipocytes is both specific to FFA release by lipolysis and also specific to FFAR4 activation.
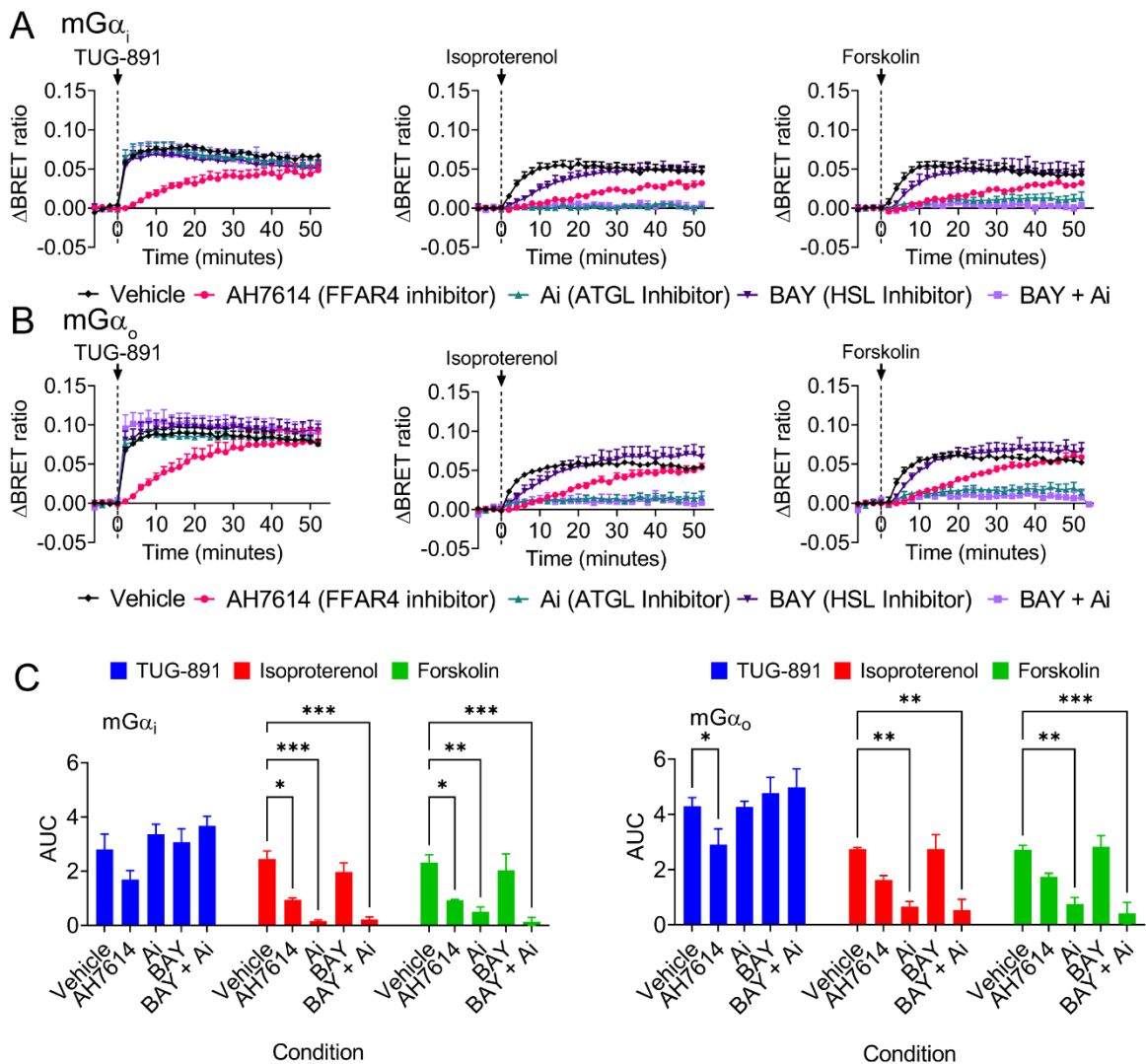
Figure 4. 15: Activation of the FFAR4 after forskolin and isoproterenol stimulation is specific to lipolysis.

BRET assay detecting FFAR4 activation after specific FFAR4 stimulation or stimulation of lipolysis in the presence or absence of FFAR4 inhibitors or lipase inhibitors. (**A**&**B**) Shown are the real-time BRET measurements between FFAR4-NLuc and (**A**) Venus-mGα_i or (**B**) Venus-mGα_o preincubated (30 minutes) with vehicle, FFAR4 inhibitor (AH7614, 10 μM), ATGL inhibitor (Ai, 10 μM), HSL inhibitor (BAY, 5 μM), or both lipase inhibitors together (Ai, 10 μM and BAY, 5 μM). Adipocytes were stimulated with TUG-891 (left, 10 μM), isoproterenol (middle, 10 μM), or forskolin

(right, 10 μM). (**C**) Corresponding AUC values. Differences are statistically significant by two-way ANOVA. P<0.001 = ***, P<0.01 = **, P<0.05 = * by Dunnett's post-hoc analysis. Data represents mean +S.E.M. and are compiled from three independent experiments performed in duplicate.

Within the literature, small molecules have been created to activate lipolysis downstream of cAMP and PKA activation e.g. SR-3420. SR-3420 is described to activate lipolysis by inducing CGI-58 release from PLIN leading to activation of ATGL (Rondini et al., 2017). To further confirm that FFAR4 activation occurs downstream of cAMP/PKA activation, FFAR4 activation was tested after SR-3420 stimulation. For this purpose, the BRET was measured between FFAR4-NLuc and Venus fused mini-G probes (mGα_i, mGα_s, mGα_o, mGα_q, mGα_{12}) (Figure 4.16). Stimulation of lipolysis with SR-3420 induced a robust BRET increase between FFAR4 and mGα_i or mGα_o. A small increase in the BRET between FFAR4 and mGα_q was also detectable. This again gives direct evidence that the FFAR4 is activated after lipolysis-stimulated FFA release.
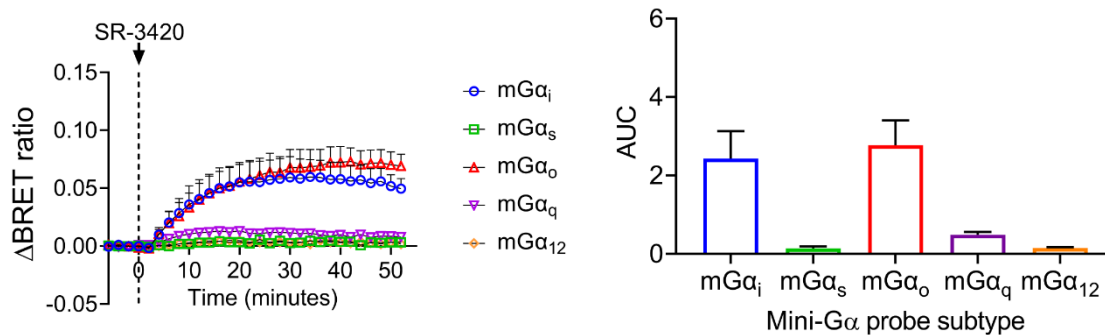
Figure 4. 16: BRET assay confirming FFAR4 activation after specific induction of lipolysis with SR-3420.

Kinetics and AUC of Venus fused mini-G probe (mGα$_i$, mGα$_s$, mGα$_o$, mGα$_{12}$) recruitment to FFAR4-NLuc upon SR-3420 (40 μM) stimulation. Data represent mean +S.E.M. compiled from three independent experiments performed in triplicate.

4.2.11 The FFAR4 is activated under conditions where extracellular FFA is undetectable

Since the FFAR4 was activated in response to lipolysis, the extracellular fatty acid concentration was examined in response to lipolysis activation. Surprisingly, after stimulation with isoproterenol and forskolin, extracellular fatty acid release was undetectable (Figure 4.17A). In the literature, it has been shown that eliminating BSA from extracellular media leads to intracellular fatty acid accumulation in adipocytes, whereas BSA addition to extracellular media enhances fatty acid export (Mottillo and Granneman, 2011, Mottillo et al., 2019). To enable detectable extracellular fatty acid quantification, the cell media was supplemented with BSA. Now, extracellular fatty acid release after lipolysis stimulation was easily detectable (Figure 4.17A).

Since major lipolysis specific FFAR4 activation occurred in conditions where BSA was not present (Figure 4.13, 4.15, and 4.16), and thus under conditions where extracellular FFA was so far undetectable, the concentration of extracellular FFA in

the absence of BSA was further investigated. The fatty acid quantification kit used in Figure 4.17A was only suggested sensitive to fatty acid concentrations between 2-200 μM. Therefore, extracellular fatty acid release after isoproterenol and forskolin stimulation in immortalised brown adipocytes was scaled up from a 96-well plate into a 6-well plate. Extracellular media samples were collected in a larger volume, extracted for fatty acids, and concentrated into a smaller volume. The same was achieved for palmitic acid standards of known concentrations. Using this approach, fatty acid detection in the absence of BSA was increased into the nanomolar range – somewhere between 400 nM and 700 nM. However, fatty acid release was still undetectable after forskolin and isoproterenol stimulation (Figure 4.13D). Once again, supplementation of cell media with BSA led to detectable fatty acid release, however, the addition of BSA seemed to interfere with the sensitivity of the assay (Figure 4.13C&D). These data again indicated that fatty acid release after the induction of lipolysis in the absence of BSA was minimal.
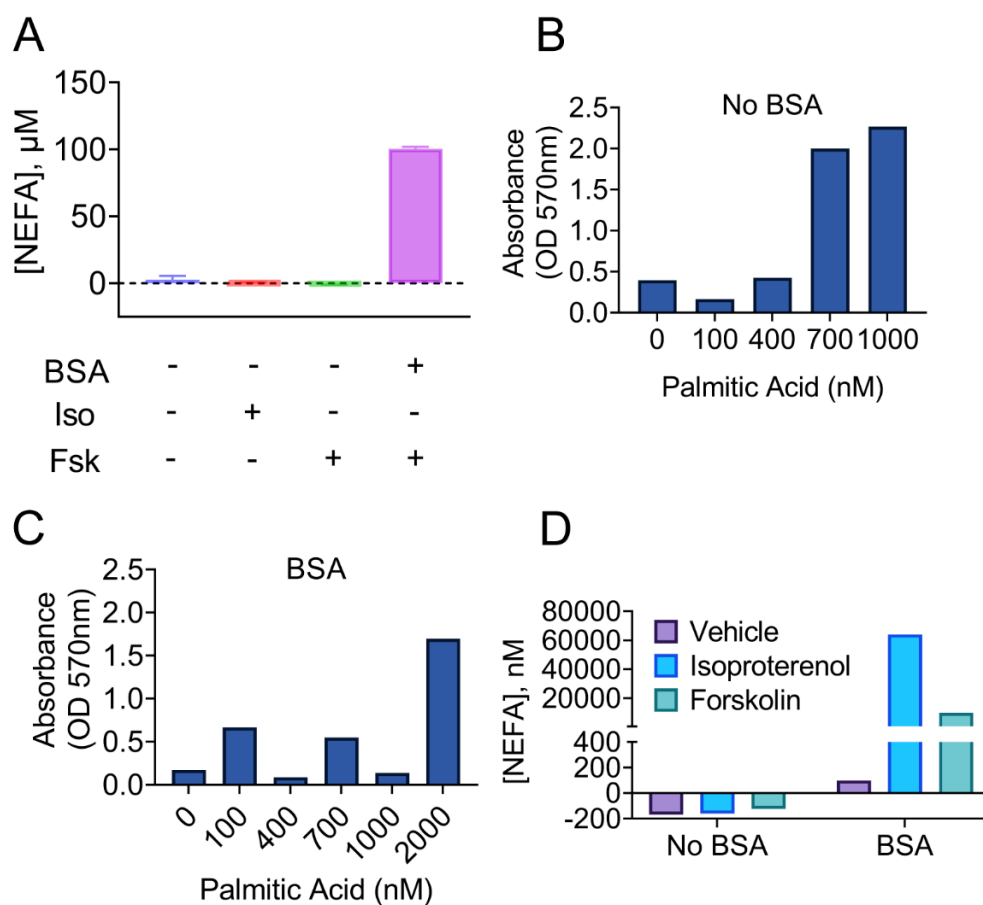
Figure 4. 17: Extracellular fatty acid release from immortalised brown adipocytes is undetectable in the absence of BSA using fatty acid quantification kit.

Effect of BSA supplementation on extracellular fatty acid release after stimulation of lipolysis. (**A**) Lipolysis induced fatty acid release in the absence of BSA. Shown are the results of fatty acid quantification after isoproterenol (10 μM) and forskolin (10 μM) stimulation for 1 hr. Forskolin (1 hr, 10 μM) stimulation in the presence of BSA (100 μM) is included as a positive control. (**B**, **C**, **D**) Assay designed to enhance the sensitivity of the fatty acid quantification kit. Shown are the results of fatty acid quantification of palmitic acid standards (0-, 0.1-, 0.4-, 0.7-, 1-, and 2 μM standards in 1 mL Krebs-ringer buffer) in the absence (**B**) and presence (**C**) of BSA. (**D**) Fatty acid quantification after isoproterenol (10 μM) and forskolin (10 μM) stimulation using enhanced sensitivity fatty acid detection method. Data shows raw values from one independent experiment.

Furthermore, GCMS was used to both identify the specific species of LCFA released after lipolysis stimulation and also to increase the sensitivity of fatty acid quantification. Within this assay, media samples were taken after lipolysis stimulation with forskolin and isoproterenol in the presence and absence of BSA supplementation (Figure 4.18). In the absence of BSA, extracellular fatty acid release was below the lower limit of quantification – however fatty acid standards were detectable in the picomolar range (Figure 4.18A). This suggests fatty acid release in response to lipolysis activation in the absence of BSA might be less than the picomolar range. In the presence of BSA, the most prevalent extracellular LCFAs detectable were palmitoleic acid (C16:1n-7), palmitic acid (C16:0), oleic acid (C18:1n-9), vaccenic acid (C18:1n-7), and myristic acid (C14:0) (Figure 4.18B). Of these fatty acids, palmitoleic acid (C16:1n-7), palmitic acid (C16:0), oleic acid (C18:1n-90), and vaccenic acid (C18:1n-7) significantly increased after forskolin and isoproternol stimulation. These fatty acids are believed activators of the FFAR4.
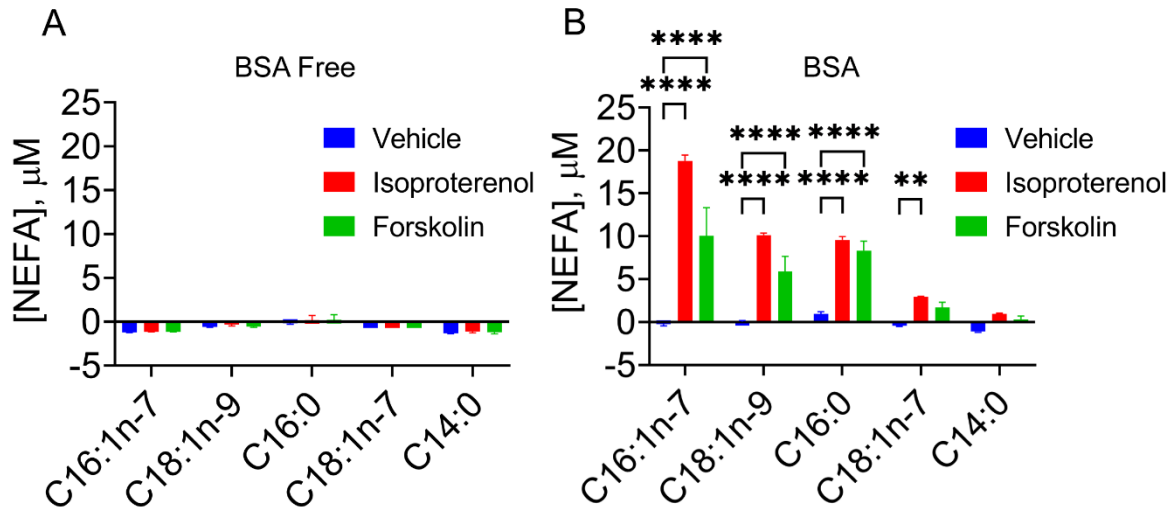
Figure 4. 18: Extracellular fatty acid release is undetectable in the absence of BSA using GCMS.

Effect of BSA supplementation on extracellular fatty acid release after stimulation of lipolysis detected by GCMS. (**A&B**) Shown are the results of extracellular fatty acid quantification by GCMS after isoproterenol (10 μM) and forskolin (10 μM) stimulation in the (**A**) absence and (**B**) presence BSA (100 μM). Differences are statistically significant by two-way ANOVA. $P < 0.001$ = *******, $p < 0.01$ = ******, * $p < 0.05$ by Dunnett's post hoc analysis. Data represent mean ±S.E.M. and are compiled from two independent experiments performed in quadruplicate. Lower limit of quantification of each fatty acid species: C16:1n-7 = 373 ρM; C18:1n-9/n-7 = 359 ρM; C16:0 = 390 ρM; C14:0 =348 ρM.

Since extracellular fatty acid release was undetectable in the absence of BSA, and the FFAR4 is strongly activated under the same conditions, the concentration of extracellular fatty acid required to activate the FFAR4 was further investigated. Within this assay, FFAR4-NLuc and Venus-mGα_o were transfected into immortalised brown adipocytes and stimulated with increasing concentrations of α-linolenic acid, oleic acid, palmitoleic acid, and palmitic acid (Figure 4.19). FFAR4 activation was detectable after micromolar stimulations of palmitoleic acid, oleic acid, and α-linolenic

acid. The results of this assay suggest that FFAR4 activation requires extracellular fatty acid concentrations in the micromolar range. Intriguingly, no FFAR4 activation was detectable after stimulation with palmitic acid. Two different stocks of palmitic acid were used in attempt to activate the FFAR4 without success (data not shown). Either this is indicative that palmitic acid is not a FFAR4 agonist, or that under these conditions, the solubility of palmitic acid was too low to activate the receptor. The other fatty acids had similar potencies to initiate FFAR4 activation: palmitoleic acid EC_{50}: 6.127×10^{-5} M; oleic acid EC_{50}:2.848×10^{-6} M; and α-linolenic acid: 4.831×10^{-6} M.
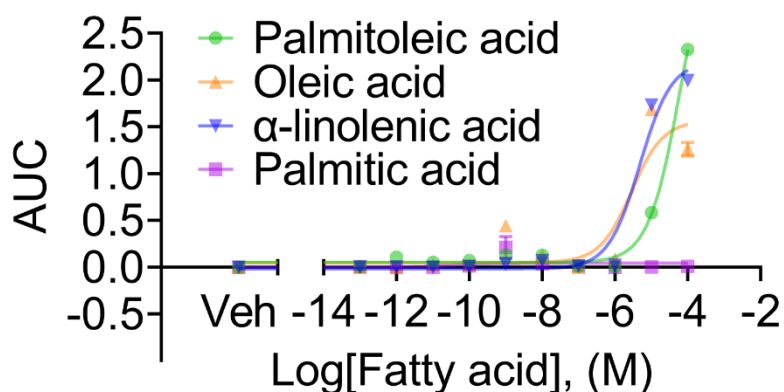
Figure 4. 19: FFAR4 activation requires extracellular fatty acid concentrations in the micromolar range.

Real-time BRET assay detecting FFAR4 activation upon stimulation with increasing concentrations of fatty acid. Shown are the results of BRET measurements between FFAR4-NLuc and Venus fused mini-$G\alpha_o$ after stimulation with increasing concentrations of α-linolenic acid (C18:3n-3), palmitoleic acid (C16:1n7), oleic acid (C18:1n-9), and palmitic acid (C16:0). The corresponding AUC is plotted on a dose response curve. Data represent mean ±S.E.M. and are compiled from one independent experiment performed in duplicate.

Given that FFAR4 activation was only detectable after stimulation of fatty acid concentrations in the micromolar range (Figure 4.19) – a concentration of fatty acid

much higher than released after lipolysis activation in the absence of BSA – it was rationalised that FFAR4 activation detected in response to lipolysis induction was most likely due to intracellular FFAR4 activation rather than FFAR4 activation at the plasma membrane.

To further understand the effects of BSA supplementation on FFAR4 activation, a BRET assay was designed to measure FFAR4 activation upon increasing stimulations of isoproterenol or α-linolenic acid in the presence or absence of BSA. In the absence of BSA, isoproterenol dose-dependently enhanced the activation of the FFAR4. In the presence of 100 μM BSA, FFAR4 activation was reduced (Figure 4.20A). Similar observations were observed after α-linolenic acid stimulation. In the absence of BSA, α-linolenic acid dose-dependently enhanced the activation of the FFAR4. In the presence of 100 μM BSA, the effects of α-linolenic acid were largely attenuated (Figure 4.20B).

Additionally, the effects of BSA supplementation and FFAR4 inhibition were investigated on lipolysis. In this assay, glycerol release was measured as a read-out of lipolysis. Lipolysis was stimulated with isoproterenol in the presence and absence of FFAR4 NAM (AH7614) and in the presence and absence of BSA addition. Without BSA addition, isoproterenol stimulation largely did not effect glycerol release. (Figure 4.20C). In addition, FFAR4 inhibiton did not effect glycerol release under basal or under isoproterenol-stimulated conditions. In the presence of BSA (100 μM), isoproterenol stimulation was now able to facilitate extracellular glycerol release (Figure 4.20D). In addition, FFAR4 inhibition with AH7614 enhanced glycerol release

after isoproterenol stimulation but not under basal conditions – similar observations were observed in figure 4.12 where 10 μM BSA (rather than 100 μM BSA) was used.

From these data, it could be speculated that in the presence of 100 μM BSA, FFA is exported extracellularly, decreasing the intracellular pool of FFA able to activate the FFAR4 and causing a reduction in its activation. Since 100 μM BSA also largely blocks FFAR4 activation after stimulation of α-linolenic acid (up to 100 μM), it is also likely that in the presence of 100 μM BSA, when extracellular fatty acid release is under 100 μM, that the predominant mode of FFAR4 activation is from intracellular compartments and not from the plasma membrane.
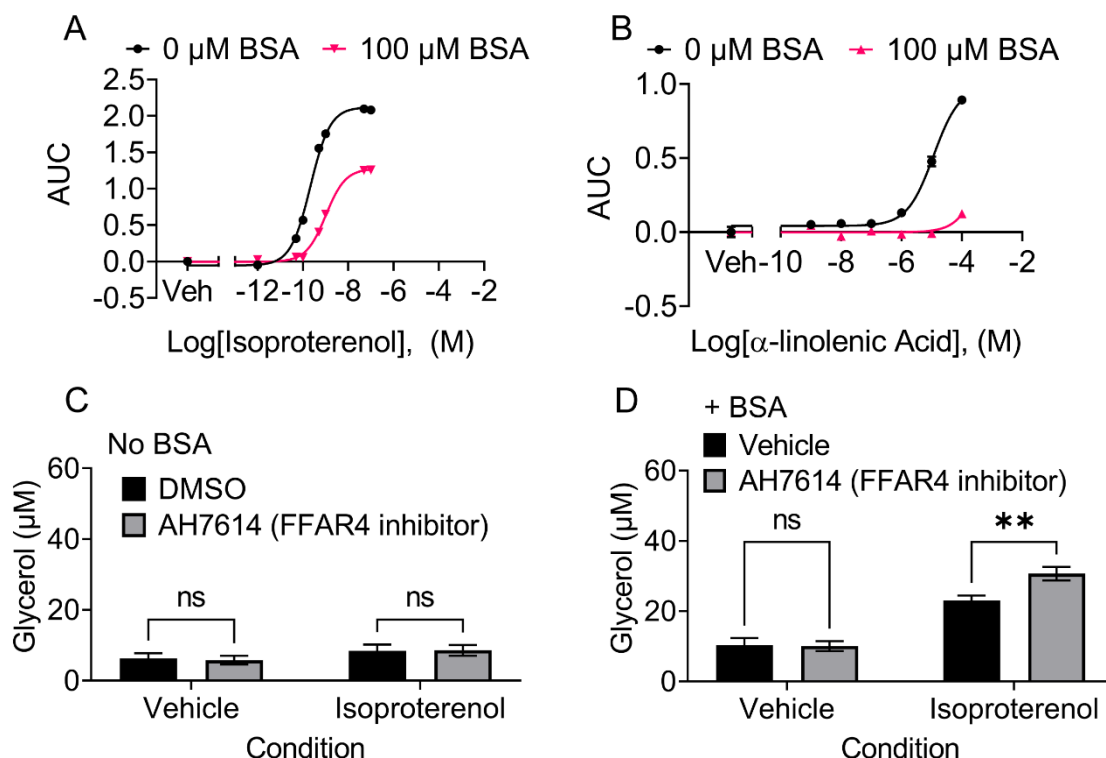
Figure 4. 20: BSA supplementation affects FFAR4 activation.
(**A&B**) BRET assay detecting FFAR4 activation upon stimulation with increasing concentrations of (**A**) isoproterenol or (**B**) α-linolenic acid. Shown are dose response

curves of the resulting AUC values calculated from BRET measurements between FFAR4-NLuc and Venus fused mini-Gα_o probe in the absence and presence of BSA (100 μM) in immortalised brown adipocytes. (**C&D**) Effect of FFAR4 inhibition on extracellular glycerol quantification in the (**C**) absence or (**D**) presence of BSA (100 μM) after stimulation of lipolysis. Immortalised brown adipocytes were preincubated with FFAR4 inhibitor (AH7614, 10μM) or vehicle for 15-minutes and stimulated with vehicle or lipolysis activator (isoproterenol, 10μM) in the presence or absence of FFAR4 inhibitor (AH7614, 10μM). The concentration of total extracellular glycerol was quantified using Glycerol-Glo luminescence kit (Promega). Differences are statistically significant by two-way ANOVA. $P < 0.01$ =** by Sidak's post hoc analysis. Data represent mean ± S.E.M. and are compiled from three independent experiments performed in triplicate.

4.2.12 The FFAR4 is activated from intracellular compartments after stimulation of lipolysis

Spatiotemporal activation of the FFAR4 was subsequently evaluated to investigate the location of FFAR4 activation in adipocytes upon the induction of lipolysis. For this purpose, mini-G probes were used to visualise FFAR4 activation in immortalised brown adipocytes upon the induction of lipolysis. These experiments were performed in the absence of BSA to reduce fatty acid export.

FFAR4-YFP and Halo-mGα_o. were transfected into immortalised brown adipocytes and stimulated with isoproterenol, forskolin, and SR-3420 (Figure 4.21). Prior to lipolysis activation, mGα_o was occasionally already recruited to the FFAR4 at intracellular compartments – this indicated some basal intracellular FFAR4 activation. Upon stimulation with lipolysis activator (Figure 4.21A,B&C), mGα_o rapidly recruited to intracellular FFAR4. To assess if intracellular receptor internalises from the plasma membrane after lipolysis activation to exert its effect at intracellular compartments, a

dynamin inhibitor (Dyngo-4a) was used to prevent receptor internalisation (Figure 4.21D). In the presence of Dyngo-4a, mini-G probe was still recruited to intracellular FFAR4 after activation of lipolysis. Unfortunately, Dyngo-4a is coloured and partially interfered with the imaging assay. Despite some limitations of the experimental set-up, these data indicate that there is indeed an intracellular pool of FFAR4 activated in response to intracellular FFA.
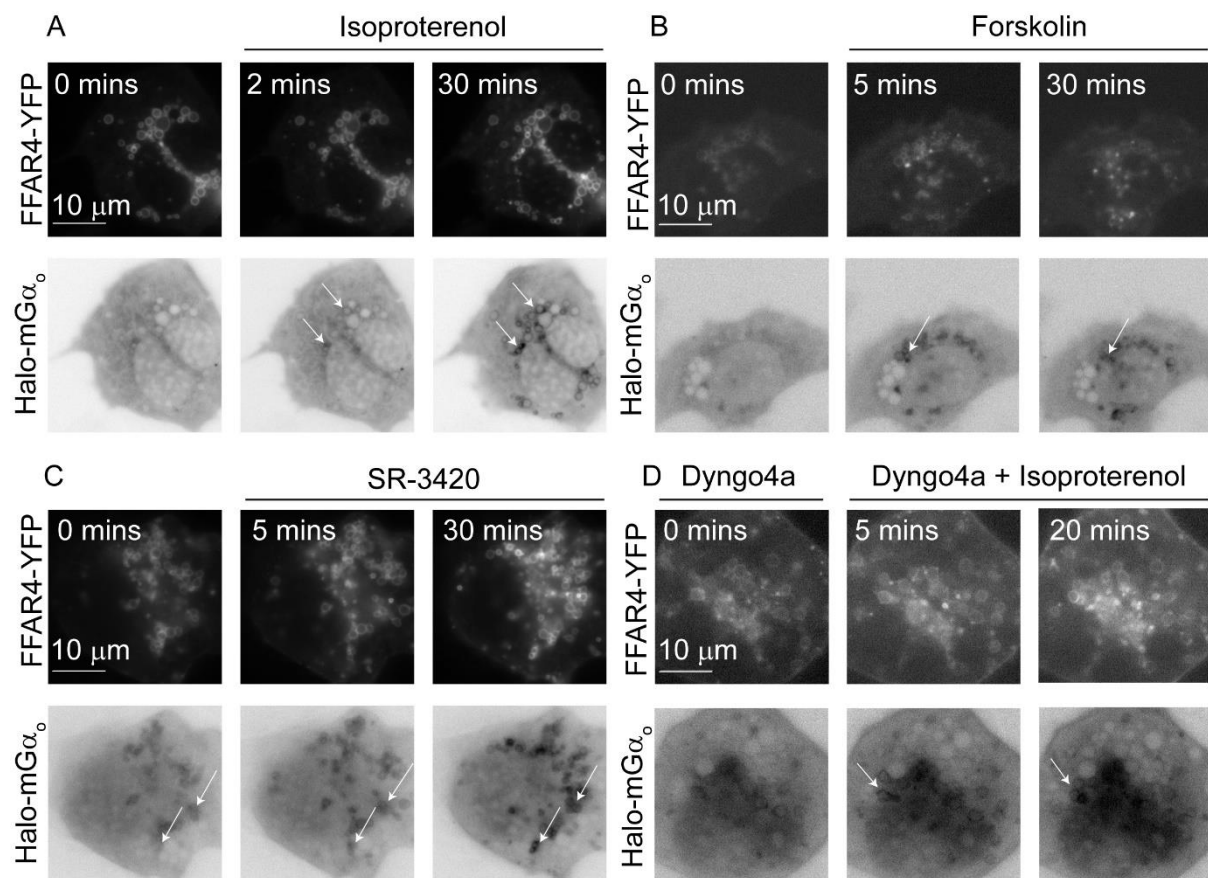
Figure 4. 21: Intracellular FFAR4 is activated upon induction of lipolysis.
Effect of lipolysis activation on Venus fused mini-$G\alpha_o$ probe translocation to FFAR4-YFP in immortalised brown adipocytes. Shown are selective frames representative of (**A**) isoproterenol (10 μM), (**B**) forskolin (10 μM), or (**C**) specific lipolysis activator (SR-3420, 40 μM) stimulation. (**D**) Effect of Dyngo-4a pre-treatment (30 minutes, 50 μM) on mini-$G\alpha_o$ translocation after isoproterenol (10 μM) stimulation. Images are representative of at least three independent experiments.

4.2.13 Attempt to locally inhibit FFAR4 signalling in adipocytes

Having observed intracellular FFAR4 activation after the induction of lipolysis, an effort was made to block local intracellular FFAR4 signalling. It was considered that mini-G probes might be applicable for use as a tool to inhibit downstream GPCR signalling, likely through steric occlusion of WT Gα proteins, in a manner similar to nanobodies (Irannejad et al., 2017).

To assess this hypothesis, cAMP production was measured after overexpressing mGα_s, mGα_i, or mGα_o in the presence and absence of the FFAR4 (Figure 4.22). Since the FFAR4 was found strongly coupled to G$\alpha_{i/o}$ proteins, mGα_i and mGα_o were speculated to block FFAR4 signalling, whereas mGα_s was speculated to have no effect on FFAR4 signalling. cAMP production was measured using whole cell cAMP sensor NLuc-Epac-VV after stimulation with both isoproterenol (Figure 4.22A) and forskolin (Figure 4.22B). In the presence of the FFAR4, upon isoproterenol stimulation, overexpression of mGα_i and mGα_o increased cAMP production, whereas overexpression of mGα_s reduced cAMP production (Figure 4.22A). A similar trend was detectable after forskolin stimulation and overexpression of mGα_i and mGα_o increased cAMP production, however, overexpression of mGα_s no longer inhibited cAMP production (Figure 4.22B).

Without FFAR4 overexpression (empty vector), slight increases in cAMP production were detectable after overexpression of mGα_i or mGα_o upon both forskolin and isoproterenol stimulation, however these changes were very subtle – this is likely to be due to the inhibition of endogenously expressed FFAR4 activity (Figure 4.22A&B). After mGα_s overexpression, cAMP production was reduced after isoproterenol

stimulation and not forskolin stimulation. This inhibition is likely to be through the inhibition of β-ARs since it occurred after isoproterenol, and not forskolin, stimulation. Importantly, this effect was not mediated by the FFAR4. From this data, mini-G probes were confirmed applicable as tools to partially block downstream FFAR4 signalling.
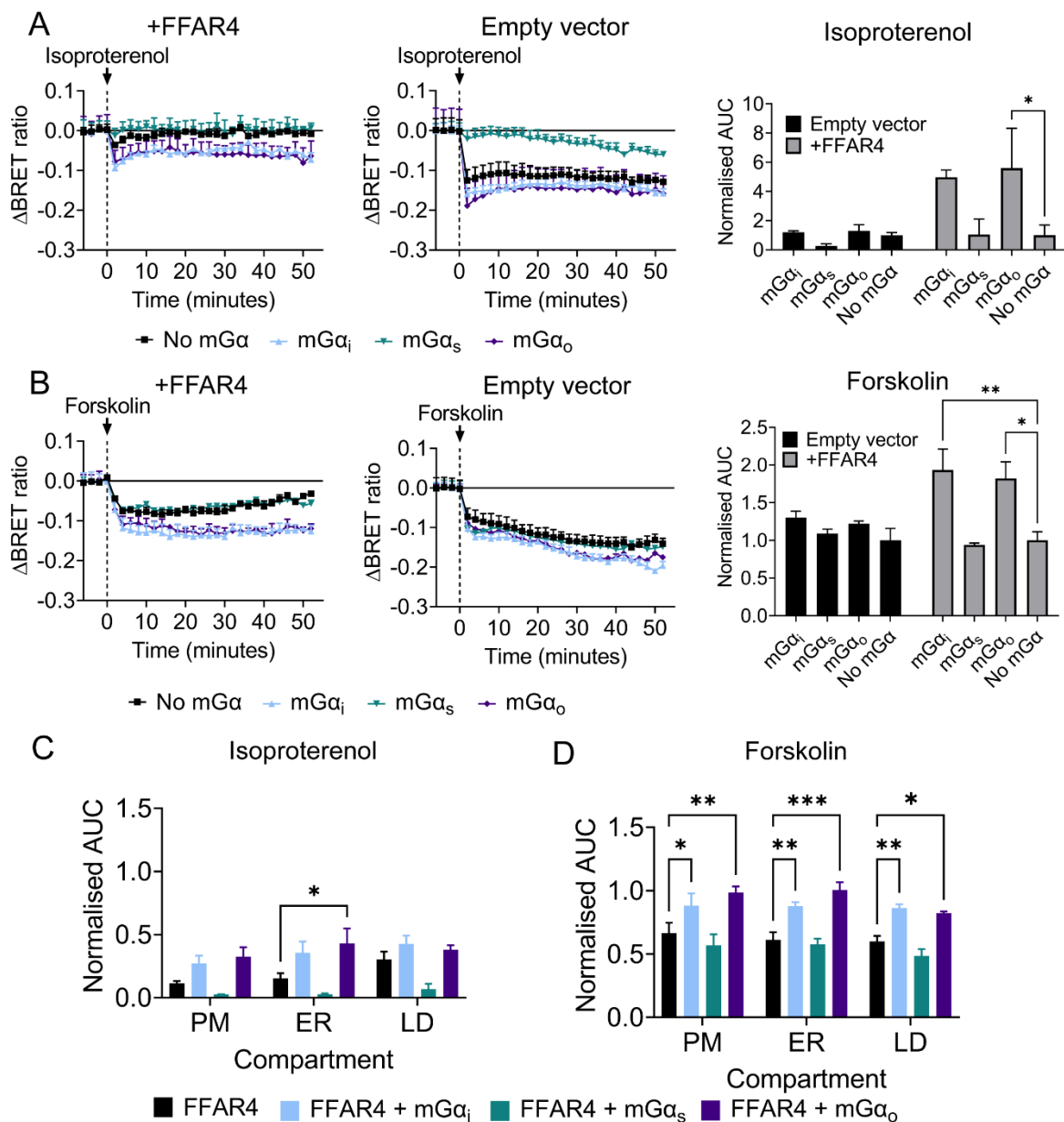
Figure 4. 22: Mini-G probes can be used as inhibitors of GPCR regulated cAMP production.

BRET assay detecting effect of FFAR4 overexpression on cAMP production in the presence of mini-G probe (mGα_i, mGα_s, mGα_o, or empty vector) overexpression. Shown are the real-time BRET measurements by NLuc-Epac-VV after (**A**) isoproterenol (10 μM) or (**B**) forskolin (10 μM) stimulation in the presence (left) or absence (middle) of FFAR4, and corresponding AUC values (right) normalised to empty vector. The assay was further repeated using targeted NLuc-Epac-VV directed to the plasma membrane (PM), ER, and lipid droplets (LD) after (**C**) isoproterenol (10 μM) or (**D**) forskolin (10 μM) stimulation. Shown are corresponding AUC values normalised to the maximum response of forskolin calculated from real-time BRET measurements. Differences are statistically significant by two-way ANOVA. $P<0.001$ = ***, $P<0.01$ = **, $P<0.05$ = * by Dunnett's post hoc analysis. Data represents mean ±S.E.M. from three independent experiments performed in duplicate.

The effect of mini-G overexpression in the presence of the FFAR4 was further evaluated using the plasma membrane, lipid droplet, and ER directed NLuc-Epac-VV cAMP sensors to gain further insight into local FFAR4 signalling after lipolysis activation. Within this assay, forskolin and isoproterenol were used to stimulate cAMP production (and lipolysis) in the presence and absence of mini-G probe overexpression (mGα_i, mGα_o, mGα_s) and changes in cAMP production were measured using PDE2A3-NLuc-Epac-VV (plasma membrane), NLuc-Epac-VV-Sec61b (ER), or PLIN1-NLuc-Epac-VV (lipid droplets) (Figure 4.22C&D). As seen with the whole cell cAMP sensor, mGα_i and mGα_o overexpression enhanced cAMP production in both isoproterenol (Figure 4.22C) and forskolin (Figure 4.22D) stimulated conditions using all targeted cAMP sensors. On average, this enhancement of cAMP production was most pronounced at the ER compared to the plasma membrane and

lipid droplets, however, there were no major differences detectable between compartments.

Since no major differences in cAMP production was found between compartments by inhibiting FFAR4 signalling using mini-G$\alpha_{i/o}$ overexpression, a method was designed to attenuate compartment specific FFAR4 signalling. In the literature, by taking advantage of the FRB and FKBP inducible protein system, nanobodies have been directed to specific subcellular compartments to block intracellular GPCR signalling (Irannejad et al., 2017). Upon stimulation with rapamycin, a protein fused with FRB and a protein fused with FKBP dimerise (Choi et al., 1996). By fusion of FRB to the N-terminus of Halo-mini-Gα probes and fusion of FKBP to the N-terminus of intracellular compartment markers, Sec61β, PLIN1, and K-ras, a system was created to facilitate rapamycin induced mini-Gα probe recruitment to the ER, lipid droplets, and plasma membrane, respectively. Firstly, FFAR4 activation was evaluated in response to rapamycin stimulation. This was achieved to ensure that rapamycin did not activate the FFAR4 e.g., via an effect on lipolysis. For this purpose, the BRET was measured between Venus-mGα probe (mGα_i, mGα_s, mGα_o, mGα_q, or mGα_{12}) and FFAR4-NLuc in immortalised brown adipocytes after rapamycin, isoproterenol, and TUG-891 stimulation (Figure 4.23A). Isoproterenol and TUG-891 stimulated a robust recruitment of mGα_i, mGα_o, and to a lesser extent mGα_q, to the FFAR4, indicating FFAR4 activation. However, rapamycin had no effect on FFAR4 activation, suggesting that rapamycin does not induce FFAR4 activation.

Subsequently, rapamycin induced FRB-Halo-mGα translocation was validated using an imaging-based approach. FKBP-compartment and FRB-Halo-mGα were

transfected into immortalised brown adipocytes. After stimulation with rapamycin, subcellular FRB-Halo-mGα probe translocation was detectable to the ER, lipid droplets, and plasma membrane (Figure 4.23B,C&D). To validate that FRB-Halo-mGα probes recruited to the correct subcellular compartments upon stimulation with rapamycin, the Halo tag of FRB-Halo-mGα was replaced with NLuc. The rapamycin induced bystander BRET could then be measured between Venus/GFP fused compartment marker and FRB-NLuc-mGα probe in the presence of overexpressed FFAR4 (Figure 4.23E). Rapamycin induced detectable mini-G recruitment to the plasma membrane (Venus-K-ras) and lipid droplets (GFP-PLIN1). No BRET increase was detectable at the ER (Venus-Rab1a). TUG-891 was also used to activate the FFAR4 to stimulate mini-G recruitment to sites of FFAR4 activation as a positive control. TUG-891 induced FRB-NLuc-mGα recruitment was only detectable to the plasma membrane. Since rapamycin and TUG-891 induced mini-G translocation was not easily detectable via BRET to subcellular compartments in immortalised brown adipocytes, the FRB/FKBP inducible system was further validated using a simple cell model (HEK293) (Figure 4.23F). This was achieved to facilitate the detection of smaller BRET responses. Now rapamycin stimulation induced detectable mini-G translocation to the plasma membrane (K-ras), lipid droplets (PLIN1), and ER (Rab1a). TUG-891 induced detectable FRB-NLuc-mini-Gα probe recruitment to the plasma membrane (K-ras), and the ER (Rab1a), but not to the lipid droplets (PLIN1). With these data in mind, the FRB FKBP system was found able to direct mini-Gα probes to the plasma membrane, ER, and lipid droplets in immortalised brown adipocytes.
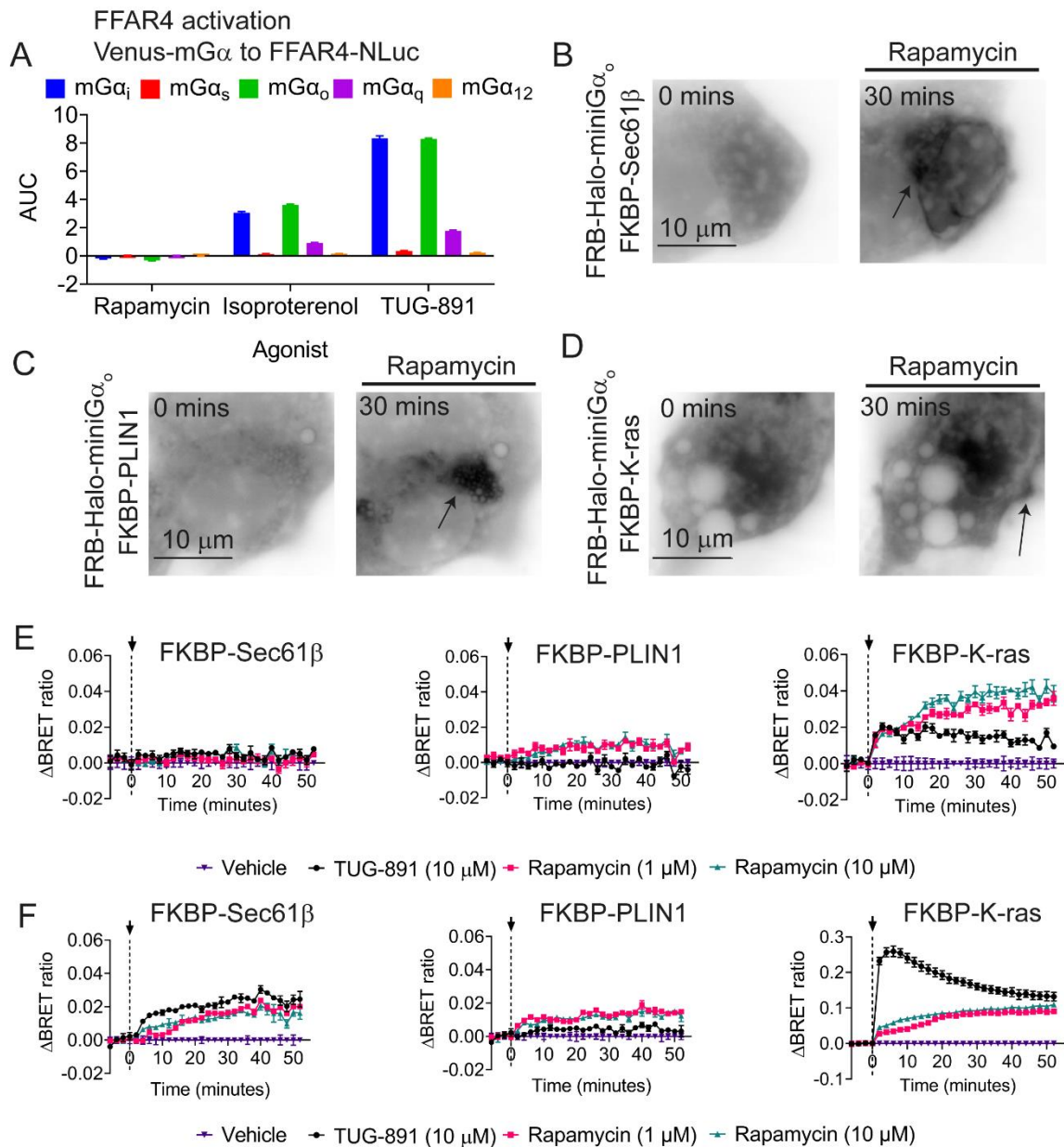
Figure 4. 23: Optimisation of rapamycin induced FRB-mini-Gα translocation to the ER, lipid droplets, and the plasma membrane.

(**A**) Detection of FFAR4 activation. Shown are the resulting AUC values calculated from real-time BRET measurements between FFAR4-NLuc and Venus tagged mini-Gα$_o$ upon rapamycin (1 μM), isoproterenol (10 μM), and TUG-891 (10 μM) stimulation in immortalised brown adipocytes. (**B, C, D**) Rapamycin induced mini-Gα probe translocation. Shown are selective frames representative of FRB-Halo-mGα translocation in the presence of (**B**) FKBP-Sec61β, (**C**) FKBP-PLIN1, and (**D**) FKBP-K-ras in immortalised brown adipocytes. Arrows indicate mini-Gα probe translocation.

(**E&F**) Real-time bystander BRET assay detecting rapamycin induced mini-Gα probe translocation to the ER, lipid droplets, and the plasma membrane in (**E**) immortalised brown adipocytes or (**F**) HEK293 cells. Shown are the resulting BRET measurements between FRB-NLuc-mGα and Venus fused Rab1a (left), GFP fused PLIN1 (middle), or Venus fused K-ras (right) in the presence of FFAR4 and FKBP-Sec61β (left), FKBP-PLIN1 (middle), or FKBP-K-ras (right) after stimulation with TUG-891 (10μM), or rapamycin (1 μM and 10 μM).

Subsequently, the inducible FRB/FKBP system was employed in an attempt to block local FFAR4 signalling at the plasma membrane, lipid droplets, and ER. Halo-FRB-mGα_o, in combination with FKBP-K-ras, FKBP-PLIN1, or FKBP-Sec61β, were transfected into immortalised brown adipocytes in the presence of overexpressed FFAR4. cAMP production was measured in each condition using plasma membrane directed NLuc-Epac-VV (PDE2A3-NLuc-Epac-VV) (Figure 4.24A) or ER directed NLuc-Epac-VV (NLuc-Epac-VV-Sec61β) (Figure 4.24B). The adipocytes were pre-treated with rapamycin (40 minutes) and subsequently stimulated with forskolin or isoproterenol, in the presence of rapamycin, to stimulate cAMP production/lipolysis activation (Figure 4.24). Isoproterenol and forskolin induced a robust increase in cAMP production, however, rapamycin treatment had minimal effect on cAMP production in all tested conditions. Thus, although the inducible system was able to direct mini-G probes to specific compartments upon rapamycin stimulation, this recruitment was not efficient enough to attenuate the inhibitory effect of the FFAR4 on cAMP production under current experimental conditions.
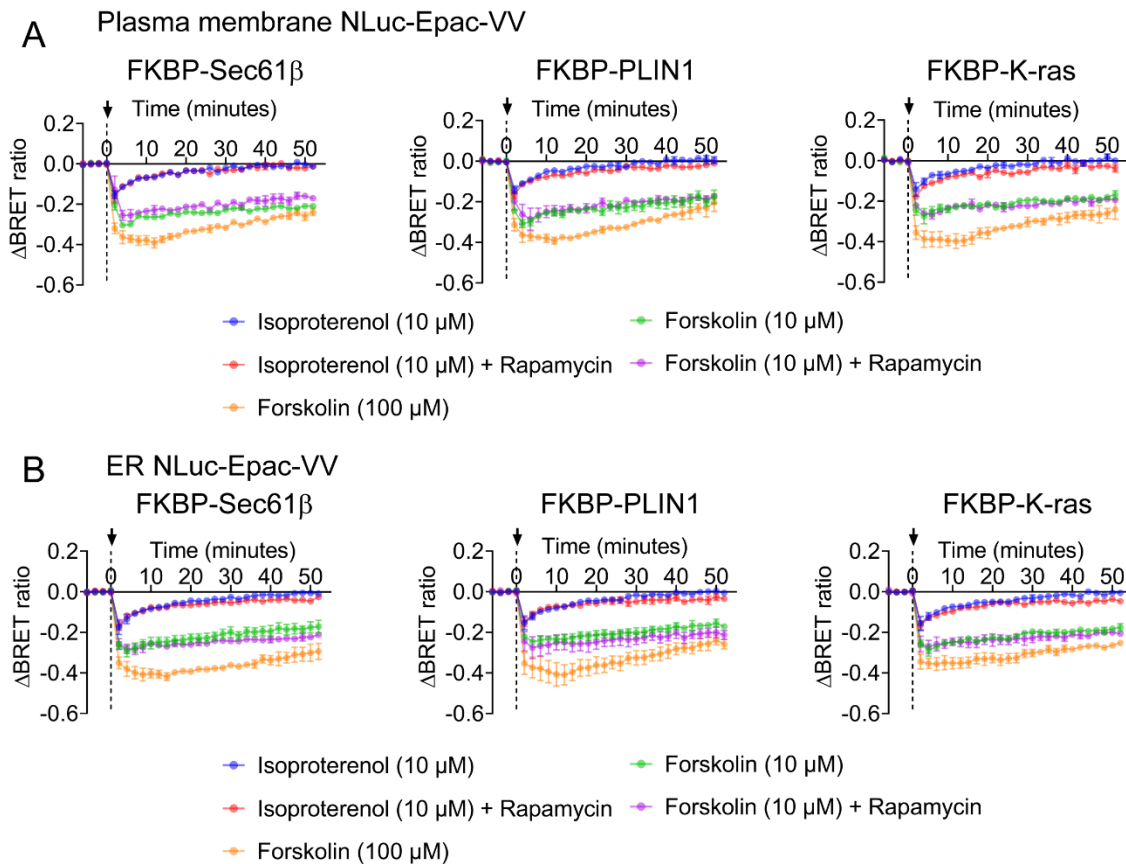
Figure 4. 24: Rapamycin induced FRB-mini-Gα_o translocation to the ER, lipid droplets, or plasma membrane has negligible effect on FFAR4 inhibited cAMP production.

Real-time BRET assay detecting cAMP production after rapamycin induced FRB-mini-Gα_o probe translocation to the ER, lipid droplets, or plasma membrane in the presence of the FFAR4. (**A&B**) Shown are the real-time BRET measurements detected by (**A**) plasma membrane targeted NLuc-Epac-VV or (**B**) ER targeted NLuc-Epac-VV in the presence of FFAR4, FRB-Halo-mGα_o, and FKBP-Sec61b (left), FKBP-PLIN1 (middle), or FKBP-K-ras (right). Adipocytes were preincubated with or without rapamycin (1 μM, 40 minutes) and stimulated with isoproterenol (10 μM) or forskolin (10 μM and 100 μM) in the presence or absence of rapamycin (1 μM). Data represents mean ± S.E.M. and are compiled from three independent experiments performed in duplicate.

4.3 Discussion

4.3.1 Summary and discussion of key findings

4.3.1.1 Rationale

This investigation was performed to study the spatiotemporal signalling profile of the FFAR4 in adipocyte models to give further insight into the mechanisms controlling FFAR4 signalling and the receptor's potential role in adipocyte metabolism. Within this study, both imaging and BRET-based approaches were employed to permit the investigation of FFAR4 coupling, localisation, and function in adipocytes.

4.3.1.2 The FFAR4 is predominantly G$\alpha_{i/o}$ coupled in adipocytes

Firstly, using a BRET-based approach, it was demonstrated in 3T3-L1 preadipocytes, immortalised brown preadipocytes, and immortalised brown adipocytes (cells with abundant lipid stores), that activation of the FFAR4 induces strong recruitment of mGα_i and mGα_o probes, and weak recruitment of mGα_q probes, to the FFAR4. This is suggestive that the FFAR4 is predominantly coupled to G$\alpha_{i/o}$ proteins, with a secondary coupling to G$\alpha_{q/11}$ proteins, in adipocytes. In addition, in immortalised brown adipocytes, selective FFAR4 agonists (TUG-891 and CpdA), and physiologically relevant α-linolenic acid, were found to effectively activate the receptor – consistent with the data acquired from the simple cell (HEK293) model. To my knowledge, this is the first direct evidence – by measuring mini-G probe recruitment to the FFAR4 – that the FFAR4 couples strongly to G$\alpha_{i/o}$ proteins in differentiated adipocytes.

4.3.1.3 A significant intracellular pool of FFAR4 exists in adipocytes

Having established the coupling specificity of the receptor in adipocyte cell lines, the localisation of the FFAR4 was evaluated in adipocyte models. In 3T3-L1 preadipocytes/adipocytes and immortalised brown adipocytes, a significant intracellular pool of FFAR4 was detected. The amount of intracellular receptor was variable from cell to cell, which might be due to differences between cell-to-cell differentiation, or even cell-to-cell differences in the basal activation of lipolysis.

Using an imaging-based approach, the FFAR4 was found to localise closely to lipid stores in both 3T3-L1 adipocytes and in immortalised brown adipocytes. Since lipid droplets have a single phospholipid monolayer (Olzmann and Carvalho, 2019), it was believed unlikely that the FFAR4 would reside in this membrane. Some of the intracellular pool of FFAR4 was later confirmed to reside in subdomains of the ER. It is also plausible that the intracellular pool of FFAR4 is not just at the ER but also at other subcellular compartments. A BRET-based assay was designed to measure basal FFAR4 localisation in immortalised brown adipocytes prior to agonist stimulation to gain further insight into the distribution of FFAR4 at subcellular compartments. Using this approach, the FFAR4 was found present at the plasma membrane, early endosomes, Golgi, and ER. To truly identify subcellular FFAR4 locations further, intracellular compartment markers would require fusion to the same fluorophore (e.g., Venus) in combination with more appropriate controls. It would also be beneficial to evaluate endogenous receptor localisation, and not overexpressed FFAR4, to confirm that these observations are physiologically relevant.

Furthermore, after agonist stimulation, the FFAR4 was also found to traffic to endosomal-like compartments in both adipocyte cell lines – this was confirmed by observing co-localisation between the receptor and a marker of the early endosomes (mCherry-Rab5) in undifferentiated 3T3-L1 cells. It might be of importance to further investigate FFAR4 trafficking in adipocytes, however, again it would be more beneficial to evaluate endogenous receptor trafficking within these cells. Despite this, it is likely that the trafficking profile of the FFAR4 in adipocytes is similar to the trafficking profile observed in HEK293 cells.

4.3.1.4 The FFAR4 exerts compartmentalised effects on cAMP production in adipocytes

Since intracellular FFAR4 was localised closely to lipid droplets in adipocyte models, compartmentalised cAMP production was measured using BRET-based biosensor: NLuc-Epac-VV. For this purpose, NLuc-Epac-VV was targeted to the plasma membrane, lipid droplets, and ER. Upon measurement of cAMP production with these directed sensors, FFAR4 overexpression was found to strongly inhibit cAMP production in immortalised brown adipocytes. Intriguingly, the inhibitory effect of the FFAR4 was greatest at sites close to the ER and the lipid droplets, compared to the plasma membrane. In addition, the FFAR4 seemed to exert a greater inhibitory effect on cAMP production after stimulation with isoproterenol compared to stimulation with forskolin. The reason for this effect is not yet understood. It could be due to differences in the activation of cyclase pools after isoproterenol vs forskolin stimulation, or fatty acid independent effects on FFAR4 internalisation after stimulation of β-ARs. It could be anticipated that the FFAR4 and β-ARs exist in close association/complexes that allow FFAR4 to better inhibit β_2AR-mediated effects? Additionally, the two receptors

might internalise together after β-AR, and not FFAR4, stimulation. This would facilitate the activation of the correct cyclase pools for the FFAR4 to inhibit, whilst increasing the amount of intracellular FFAR4 able to respond to intracellular fatty acids.

4.3.1.5 The FFAR4 is activated in response to lipolysis

Since FFAR4 inhibitory effects on cAMP production were most pronounced when measured at the lipid droplets, it was hypothesised that the receptor might have a role in the regulation of lipolysis i.e., lipolysis drives FFA release from lipid stores to activate intracellular FFAR4 and inhibit cAMP production. Initially, the overall effect of the FFAR4 was tested on lipolysis. Since isoproterenol and forskolin increase the level of cAMP production, they also stimulate lipolysis. By inhibiting the FFAR4 with AH7614, and stimulating lipolysis with isoproterenol, endogenous FFAR4 was found to have an inhibitory effect on isoproterenol-stimulated glycerol release. This gave a basic indication that the FFAR4 inhibits lipolysis in adipocytes, confirming evidence from the literature.

Direct FFAR4 activation was subsequently tested after stimulation of lipolysis with both forskolin and isoproterenol. In immortalised brown adipocytes (cells expressing lipid droplets), the FFAR4 was strongly activated. This effect was not observed in immortalised brown preadipocytes. This is important on two levels. Firstly, the FFAR4 is not expressed in pre-adipocyte cell lines (Oh et al., 2010, Yamada et al., 2017), but also, pre-adipocytes do not have large lipid stores. This suggests that FFAR4 activation upon lipolysis induction is specific to lipid droplet abundance. In addition, lipolysis activation strongly induced mG$\alpha_{i/o}$ probe recruitment to the FFAR4, indicating

that the FFAR4 most likely recruits G$\alpha_{i/o}$ proteins to inhibit cAMP production in response to FFAs released from lipolysis.

To further confirm that lipolysis dependent FFAR4 activation is specific to FFA release, and lies downstream of cAMP/PKA activation, ATGL and HSL, two key lipases known to regulate lipolysis (Mottillo et al., 2019), were inhibited. Both inhibition of ATGL and HSL affected FFAR4 activation. ATGL inhibition largely attenuated FFAR4 activation, whereas HSL inhibition seemed to delay FFAR4 activation. ATGL is the lipase required for the first step of lipolysis – the break-down of TAG into DAG (Wilson et al., 2006). As such, ATGL is considered to be the rate limiting lipase in lipolysis (Mottillo et al., 2019). Furthermore, HSL is considered the rate limiting lipase for the second step of lipolysis – DAG into MAG (Brejchova et al., 2021). Without ATGL inhibition, FFAs are likely still released upon the stimulation of lipolysis after HSL inhibition, facilitating FFAR4 activation. This is the most logical reason as to why HSL inhibition has a lesser effect on FFAR4 activation than ATGL inhibition. Furthermore, specific lipolysis activator SR-3420, a compound indicated to act downstream of cAMP/PKA signalling by releasing CGI-58 from PLIN to initiate ATGL activation (Rondini et al., 2017), was found to activate the FFAR4. In this way, FFAR4 activation upon lipolysis induction can be attributed to FFA release and activation of the FFAR4 and not via upstream second messengers.

4.3.1.6 Lipolysis-induced FFAR4 activation occurs under conditions where extracellular FFA is undetectable

Subsequently, the concentration of extracellular FFA released was investigated after lipolysis activation. Surprisingly, it was found that in the absence of BSA

supplementation, lipolysis stimulated extracellular FFA release was undetectable – even when increasing the sensitivity of the fatty acid detection assay into the picomolar range by GCMS. In the presence of BSA, lipolysis dependent FFA release was easily detectable. This confirmed that FFAR4 agonists – in particular palmitoleic acid and oleic acid – are released from lipid stores upon stimulation of lipolysis in immortalised brown adipocytes. Using BRET to detect FFAR4 activation, the application of extracellular fatty acids, including palmitoleic acid and oleic acid, were found to activate the FFAR4 in the micromolar range. Since the concentration of extracellular fatty acid required to activate the FFAR4 was much higher than the concentration of fatty acid released by lipolysis activation, it was rationalised that the majority of FFAR4 activation detected via BRET was due to intracellular FFAR4, and not FFAR4 at the plasma membrane.

Further evidence in support of this finding was obtained by investigating the effect of BSA supplementation on FFAR4 activation. BSA supplementation reduced lipolysis-stimulated FFAR4 activation by isoproterenol, and attenuated FFAR4 activation by α-linolenic acid. It is likely that two mechanisms are occuring here. Firstly, BSA supplementation increases lipolysis-induced FFA export, decreasing the concentration of intracellular FFA available to bind to the FFAR4, thus reducing intracellular FFAR4 activation. Secondly, extracellular BSA may bind and sequester extracellular fatty acid (e.g. α-linolenic acid) from activating the FFAR4. This is likely to occur until the concentration of fatty acid exceeds the buffering capacity of BSA.
To further investigate these findings, it would be of relevance to both visualise and quantify the trafficking and concentration of intracellular FFA released upon lipolysis stimulation in the absence of BSA supplementation (Mottillo et al., 2019).

4.3.1.7 Intracellular FFAR4 is activated by lipolysis

To give insight on the location and speed of FFAR4 activation after the induction of lipolysis, the recruitment of mini-G probe was measured to the FFAR4 upon stimulation with isoproterenol, forskolin, and SR-3420. Using this approach, basally present intracellular FFAR4 was rapidly activated from intracellular compartments (mini-G recruitment was detectable in under five minutes). This activation also occurred in the presence of Dyngo4a, preventing FFAR4 internalisation, and indicating that some of the intracellular pool of FFAR4 signals in response to lipolysis induction without the requirement of internalisation. However, under physiological conditions, the FFAR4 is also likely to have a role to inhibit cAMP production from the plasma membrane. The two locations of FFAR4 signalling are likely activated by two different mechanisms. For example, plasma membrane FFAR4 might be activated in response to the degradation of TAGs contained in postprandial chylomicrons which arrive to act at the FFAR4 by adipose capillaries (Husted et al., 2017). On the other hand, intracellular FFAR4 is most likely activated in response to lipolysis, facilitating the receptor to play a role in the control over fatty acid flux (Zechner et al., 2012).

4.3.1.8 Mini-G probes can be used as inhibitors of FFAR4-regulated cAMP inhibition

Mini-G probes were demonstrated applicable for use as inhibitors of FFAR4 signalling. Overexpression of $mG\alpha_i$ and $mG\alpha_o$, and not $mG\alpha_s$, partially blocked the inhibitory effect of the FFAR4 on cAMP production (observed by an increase in cAMP). In the absence of the FFAR4, overexpression of $mG\alpha_s$ blocked isoproterenol induced cAMP production, and not forskolin induced cAMP production. This is indicative that mini-

Gα_s might be able to block β-AR signalling. Consequently, mini-G probes may be useful tools to block downstream signalling of other GPCRs.

Despite creating a model capable of inducing mini-G probe recruitment to subcellular compartments, this induction was not great enough to block compartment specific FFAR4 signalling. Modifications to this approach might facilitate the inhibition of compartment specific FFAR4 signalling and thus help to investigate the functional relevance of intracellular FFAR4 signalling. Such methods may even help to investigate the functional relevance of other intracellularly active GPCRs.

4.3.2 Conclusions

In conclusion, these data give evidence that the induction of adipocyte lipolysis releases FFAs which bind to, and activate, intracellular FFAR4. The intracellular pool of receptor seems important for the inhibition of local cAMP production closely to lipid droplets, and this action is expected to be due to receptor localised in subdomains of the ER or indeed at other subcellular locations. In addition, this chapter demonstrates the applicability of mini-G probes for use as inhibitors of GPCR activity – in a manner similar to nanobodies (Irannejad et al., 2017). Unfortunately, intracellular FFAR4 activity was unable to be effectively inhibited using an inducible FKBP/FRB system under current conditions. This is ongoing work and hopefully tools will be available to fully interrogate the intracellular vs plasma membrane dependent activity of the FFAR4 in the near future.

5.0 Chapter Five: General discussion

5.1 Discussion

5.1.1 Implications of my research

Compartmentalised GPCR signalling can be initiated by extracellular ligand application, facilitating GPCR internalisation, and subsequent intracellular signalling in the endosomal network (Ferrandon et al., 2009, Irannejad et al., 2013), or in the TGN after arrival by retrograde trafficking (Calebiro et al., 2009, Godbole et al., 2017). GPCRs have also been found active in the Golgi, without requirement for internalisation, mechanically distinct from classical intracellular GPCR signalling (Irannejad et al., 2017, Nash et al., 2019). Furthermore, growing evidence supports the concept that certain GPCRs can signal from other subcellular organelles, including mitochondria (Benard et al., 2012, Suofu et al., 2017, Wang et al., 2016), the nucleus (Di Benedetto et al., 2014, Joyal et al., 2014, Kinsey et al., 2007, Re et al., 2010), the ER (Revankar et al., 2005), and late endosomes/lysosomes (Kunselman et al., 2021, Rozenfeld and Devi, 2008). Analogous GPCR signals from different subcellular compartments are likely to produce distinct biological responses, furthering the complexity of GPCR signalling.

My research provides evidence that in adipocytes, there is a pool of subcellular FFAR4 which can fine-tune lipolysis as part of an 'intracrine' feedback system. Intracellular FFAR4 is rapidly activated in response to lipolysis activation, and this effect is mediated by intracellular FFAs (Figure 5.1). Interestingly, a similar concept has been suggested for the MT_1R which has been proposed to signal on the OMM in response to mitochondrially produced melatonin (Suofu et al., 2017). My findings add further complexity to what is known about intracellular GPCR signalling. They suggest that some intracellularly active GPCRs might fine-tune cellular responses in reply to

intracellularly produced metabolites, enabling signalling proximally to their downstream effectors.
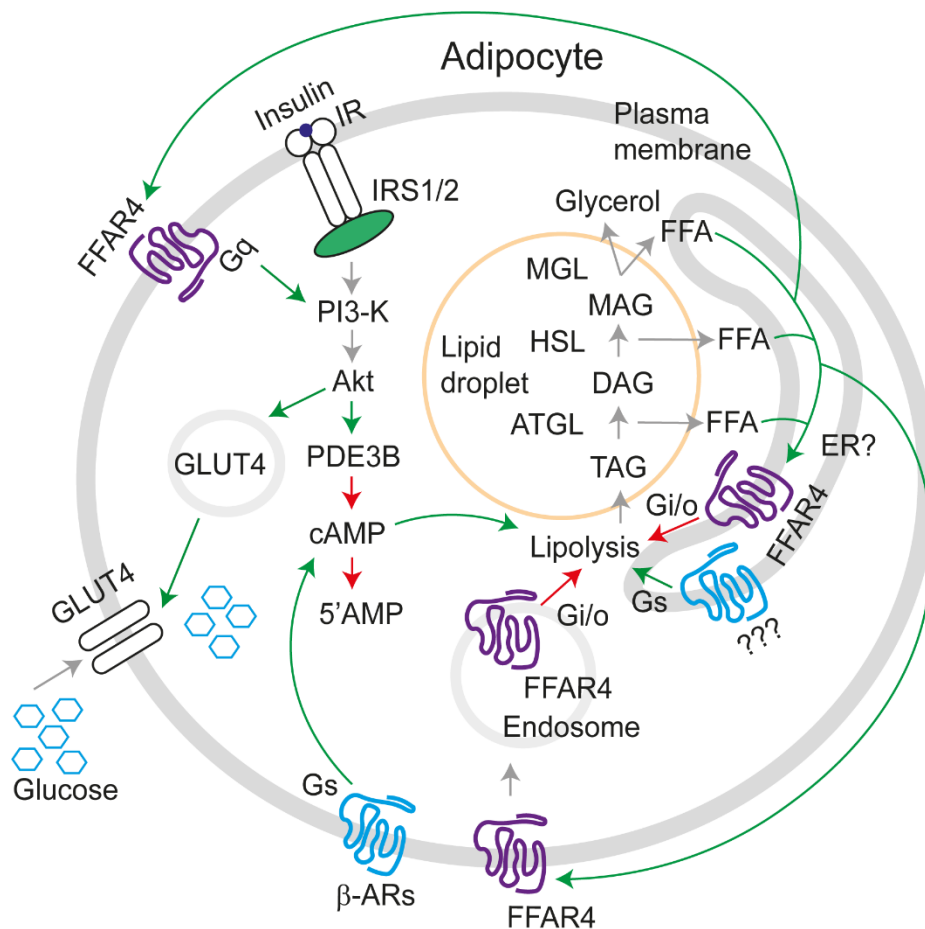
Figure 5. 1: Schematic to indicate the potential physiological relevance of FFAR4 activation in response to lipolysis.

Upon the activation of lipolysis through activation of $G\alpha_s$ and thus cAMP and PKA, FFAs are released from lipid droplets which bind and activate the FFAR4. Firstly, intracellular FFAR4 is rapidly activated to inhibit lipolysis from a compartment residing closely to the lipid droplets. Plasma membrane FFAR4 is then likely activated once the concentration of extracellular FFA is of physiological relevance. It is likely that plasma membrane localised FFAR4 subsequently internalises, to further enhance inhibitory effects on lipolysis in close proximity to lipid droplets. The FFAR4 also signals through $G\alpha_q$, which aids glucose uptake. The relevance of intracellular FFAR4 signalling through $G\alpha q$ is unknown. The FFAR4 is likely to work synergistically with the IR to enhance glucose uptake and inhibit lipolysis

In adipocytes, this 'intracrine' signalling phenomenon is likely to be of particular relevance to other GPCRs that mediate their effects by metabolite ligands. For example, GPR84, FFAR2, HCAR1, adenosine receptors, and GPR91. GPR84, a receptor sensitive to MCFAs that is expressed in adipose tissue (Montgomery et al., 2019, Nagasaki et al., 2012), has also been found to signal from intracellular compartments (Peters et al., 2020). Considering this, it might be hypothesized that GPR84 is activated intracellularly after lipolysis activation in adipocytes in an analogous way to the FFAR4, but in response to MCFAs. In addition, SCFAs (Tang et al., 2015) and lactate (Ahmed et al., 2010) are produced intracellularly in states of nutritional surplus, therefore the FFAR2 and the HCAR1 might also be activated intracellularly to control TAG storage (Ahmed et al., 2010, Ge et al., 2008). Furthermore, since adenosine is persistently produced intracellularly and extracellularly through the dephosphorylation of AMP (Pardo et al., 2017), intracellular adenosine receptors might also be involved in the regulation of lipolysis. Intriguingly, GPR91, a GPCR that is activated by mitochondrially produced succinate, has recently been found localised at the mitochondria in human umbilical vein endothelial cells (Atallah et al., 2021). Since succinate only reaches physiologically relevant extracellular concentrations during metabolic stress (McCreath et al., 2015), it could be hypothesised that GPR91 is active subcellularly in the mitochondria in response to mitochondrially produced succinate to regulate adipocyte metabolism. Metabolite-driven intracellular GPCR signalling is likely to support the intimate control of adipocyte metabolism, as well as the metabolism of other metabolically active tissues.

Endosomal GPCR signalling has been suggested important in the regulation of various physiological processes, including nociception (Jensen et al., 2017, Yarwood et al.,

2017), insulin secretion (Girada et al., 2017, Kuna et al., 2013), neuronal excitability (Merriam et al., 2013), oocyte meiosis resumption (Lyga et al., 2016), and lipid droplet formation (Sayers et al., 2021, Sposini et al., 2020). In the case of the FFAR4, subcellular receptor signalling would inhibit TAG catabolism in response to the local concentration of intracellular FFAs. This signalling would facilitate direct lipolytic inhibition to prevent excessive accumulation of intracellular FFAs, or excessive FFA release into the systemic circulation (Lee et al., 2022). This activity is also likely to play a role in the regulation of additional intracellular negative feedback mechanisms of lipolysis, for example FFA re-esterification (Reshef et al., 2003). In addition, the FFAR4 has been implicated in the control of lipid droplet formation (Rohwedder et al., 2014) and adipogenesis (Song et al., 2016). It might be hypothesised that the FFAR4 is initially expressed at the plasma membrane and binds extracellular FFAs as they arrive to cells via transport by the blood, initiating FFAR4 internalisation and intracellular signalling. It is likely that this intracellular FFAR4 signalling is involved in the control of lipid droplet formation, as has been recently proposed for the follicle stimulating hormone receptor (FSHR) (Sayers et al., 2021). However, since mature endosomes have been demonstrated to have contact with the ER (Friedman et al., 2013, Olzmann and Carvalho, 2019), and the ER is intimately associated with lipid droplets (Olzmann and Carvalho, 2019), internalised FFAR4 would subsequently be in position to respond to local intracellular FFAs released during lipolysis. This mechanism would enable the FFAR4 to have different localisations in different tissues – dependent on the fatty acid concentration that reaches the tissue.

Since evidence suggests that endosomal GPCR signalling is of pathophysiological relevance (Gorvin et al., 2018, Nash et al., 2019), and as the FFAR4 has been

implicated in type 2 diabetes and obesity (Bonnefond et al., 2015, Ichimura et al., 2012, Lamri et al., 2016), loss of subcellular FFAR4 signalling might be involved in the development of metabolic diseases. For example, if the FFAR4 is unable to signal intracellularly to inhibit lipolysis, FFA release from TAG would be enhanced, leading to the intracellular accumulation of FFA metabolites, as well as ectopic accumulation of TAG in surrounding tissues (Lee et al., 2022). Such a loss of intracellular FFAR4 signalling may be involved in the development of insulin resistance (Figure 5.1).

Intracellular GPCR signalling might be exploited therapeutically to develop more effective pharmaceuticals. In the case of the FFAR4, an obvious example would be to ensure that FFAR4 agonists designed for the treatment of excessive FFA release into the systemic circulation are cell permeable to facilitate their access to subcellular pools of FFAR4. A possible approach would be the addition of a lipophilic moiety to a ligand, facilitating its endosomal accumulation (Jensen et al., 2017). Or, a drug could be incorporated into pH-sensitive nanoparticles, which once taken up intracellularly, would mediate the controlled release of a drug in acidic endosomes (Jimenez-Vargas et al., 2020, Jimenez-Vargas et al., 2018). Additional research is required to develop methods which will direct ligands to specific subcellular compartments, and to further understand whether subcellular GPCR signals are of therapeutic value and might be pharmacologically exploited.

5.1.2 Other research implications

The FFAR4 is not only expressed within adipocytes, but also across a variety of other tissue types, including the intestine, the hypothalamus, lungs, immune cells, pancreatic delta cells, and taste buds (Kimura et al., 2020). An evident consequence

of my research is that the measurement of BRET between FFAR4-NLuc and Venus fused mini-G$\alpha_{i/o}$ probes is likely to be applicable for the investigation of FFAR4 activation in other cell types. Similar methods could also be applicable for the investigation of other adipose expressed GPCRs to help investigate their effects on adipocyte metabolism.

Another intriguing idea is that the recruitment of Venus fused mG$\alpha_{i/o}$ to the FFAR4-NLuc, which can be used as a read-out of intracellular lipolysis activation in live cells, might be a useful method to identify novel compounds which can activate or inhibit lipolysis. This could be a useful method since current approaches to detect intracellular lipolysis activation typically involve cell lysis (Mottillo and Granneman, 2022). The measurement of mG$\alpha_{i/o}$ recruitment to the FFAR4 after modulation of lipolysis would bypass this limitation. This could be performed in adipocytes, but such methods might also be applicable to other lipid droplet expressing cell types.

In addition, mini-G probes were found applicable as inhibitors of GPCR-mediated cAMP signalling. A current limitation in the GPCR field, particularly for those who are studying location specific signalling events, is the ability to either activate/inhibit local pools of receptor. In our hands, the ability to locally inhibit FFAR4 will be advantageous to demonstrate that this subcellular pool of receptor drives the FFAR4 described anti-lipolytic effects. Preliminary data suggests that subtype specific mini-G probe overexpression might be a useful tool to investigate the functional relevance of intracellular FFAR4 signalling, but also to investigate compartment specific signalling of other GPCRs. Such methods may also be applicable for the inhibition of endogenous intracellular GPCR activity, however appropriate controls would be

needed (e.g., KO/knock-down cells) to ensure the specificity of mini-G inhibition to the receptor in question. It is likely that mini-G probes will also be applicable for the inhibition of $G\alpha_q/G\alpha_{12}$ signalling, however this was not explored further within the realms of this thesis.

Finally, I targeted BRET-based cAMP sensors (CAMYEL or NLuc-Epac-VV) to the plasma membrane, the ER, and the lipid droplets. Whilst useful for detecting compartment specific effects on cAMP signalling mediated by the FFAR4, these sensors may also be useful for the investigation of compartmentalised cAMP signalling in adipocytes or in other cell types.

5.1.3 Controversies

The main controversy of this thesis is that I demonstrate that the FFAR4 is a predominantly $G\alpha_{i/o}$ coupled receptor. This coupling has been indicated in the literature; however, it is of common opinion that the FFAR4 does not couple to the $G\alpha_{i/o}$ protein family (Kimura et al., 2020, Watson et al., 2012). Three recent studies challenge this notion by using read-outs that measure direct FFAR4 activation, rather than those that measure second messenger production, to confirm that the FFAR4 is coupled to $G\alpha_{i/o}$ (Avet et al., 2022, Husted et al., 2020, Inoue et al., 2019). Within this thesis, I used methods that directly measure the coupling specificity of the FFAR4, in combination with methods capable of detecting cAMP production, to confirm that the FFAR4 exerts inhibitory effects on cAMP signalling in both a simple cell, and a more complex adipocyte cell, model. No FFAR4 specific agonist was required to detect FFAR4-dependent effects on cAMP inhibition. Therefore, the addition of FFAR4 agonist after stimulation of AC activation is likely to have no effect on cAMP production

or might even increase cAMP production – an effect observed sometimes after the persistent activation of $G\alpha_{i/o}$ proteins (Watts and Neve, 2005). This is the most logical explanation as to why the FFAR4 has sometimes been thought unable to couple to $G\alpha_{i/o}$ proteins in the literature. Although mini-G probes, and not WT G proteins, were used to detect FFAR4 activation in this thesis, the FFAR4 coupling specificity has recently been evaluated with WT G proteins – where the receptor was again demonstrated to couple to the $G\alpha_{i/o}$ protein family (Avet et al., 2022).

Another controversial finding is that when stimulating the FFAR4 with different FFAs, palmitic acid (C16:0) was unable to activate the FFAR4 – despite evidence that palmitic acid is a FFAR4 agonist (Suckow et al., 2014). My findings indicate that palmitic acid might not be a true FFAR4 agonist. This result is in agreement with another study that demonstrates, by comparing to FFAR4 knock-down cells, that the FFAR4 mediates ERK phosphorylation through α-linolenic acid and docosahexaenoic acid stimulation, and not through palmitic acid stimulation (Oh et al., 2010). This result is especially intriguing since palmitoleic acid (C16:1n-7) was able to efficiently activate the FFAR4. Both palmitoleic acid and palmitic acid are of the same carbon length, however palmitoleic acid is monounsaturated whereas palmitic acid is saturated. Furthermore, palmitoleic acid is a metabolite of palmitic acid (Carta et al., 2017). It is remarkable that the FFAR4 seems to have selectivity over the two molecules. This finding also highlights the specificity of BRET methods in detecting GPCR activation.

5.1.4 Limitations of investigation and recommendations for further study

Despite the information gained from this study, there are a few potential limitations associated with my employed methods and several areas where more research would be beneficial to further investigate the role of the FFAR4 and its control over lipolysis.

Firstly, this research used immortalised cell lines (HEK293 cells or adipocyte cell lines) to evaluate the mechanism of action of the FFAR4 *in vitro*. Whilst such approaches are especially useful for basic mechanism of action studies, and the use of adipocyte cell lines offers improved understanding of GPCR activity compared to HEK293 cells, the use of immortalised cell lines is not necessarily predictive of *in vivo* GPCR activity. Future studies should therefore investigate the role of compartmentalised FFAR4 signalling in primary cells or *in vivo.*

In addition, the BRET/imaging-based approaches used in this investigation required overexpression of the FFAR4, and other proteins, to assess the activity and functionality of the receptor in both a simple cell, and a more complex adipocyte cell, model. To give further information regarding FFAR4 signalling in adipocytes, it would be beneficial to investigate the role of the FFAR4 *in vitro* and *in vivo* with endogenous levels of FFAR4 expression. However, such an approach might require engineered cell-lines, knock-in animals, or better antibodies than are currently available for the FFAR4, to facilitate the improved understanding of endogenous intracellular FFAR4 signalling mechanisms. For example, White et al. used clustered regularly interspaced short palindromic repeat (CRISPR) techniques, fusing NLuc to the C-X-C chemokine receptor type 4 (CXCR4), to detect endogenous CXCR4 internalisation, trafficking, and β-arrestin recruitment, in a simple HEK293 cell model (White et al., 2017). By

fusing endogenous FFAR4 with NLuc (at its C-terminus), endogenous FFAR4 coupling, signalling, and trafficking might be detectable using BRET-based methods in live cells. In addition, the endogenous localisation of the FFAR4 could then be further interrogated using immunofluorescence, or even cell fractionation, methods e.g., by using an antibody directed against NLuc. This could be achieved in human adipocyte derived stem cells (Mandl et al., 2020) which would then be differentiated into adipocytes, or by the creation of a knock-in mouse (Merkle et al., 2015). Considering that FFAR4 expression increases after adipocyte differentiation and the receptor is not expressed in preadipocytes (Oh et al., 2010), it would also be of interest to monitor the localisation of endogenous FFAR4 over the time course of adipocyte differentiation. This might help to evaluate the mechanisms behind FFAR4 presence at intracellular compartments e.g., does the localisation of the FFAR4 change in response to adipocyte differentiation? Or is intracellular FFAR4 there by an alternative mechanism?

Furthermore, if the FFAR4 is active and localises on intracellular membranes in adipocytes, are other GPCRs also present at intracellular compartments in adipocytes? And are these GPCRs capable of signalling from intracellular compartments in response to intracellular ligands? This research would be especially relevant for other metabolite sensing GPCRs, for example GPR84, FFAR2, HCAR1, adenosine receptors, and GPR91. However, it is likely to also be of relevance to the β-ARs which are already known to have intracellular signalling roles (Irannejad et al., 2017, Irannejad et al., 2013, Nash et al., 2019), and are the main activators of adipocyte lipolysis (Duncan et al., 2007). This could be investigated by using similar

methods used in this thesis for a first initial screen and moved into primary cells/mouse models for receptors found to signal in adipocytes from intracellular compartments. Secondly, this investigation relied on the rationale that the majority of FFAR4 activation upon the induction of lipolysis is due to intracellular FFAR4 activation rather than FFAR4 activation at the plasma membrane. This was reasoned since extracellular FFA accumulation after lipolysis stimulation was undetectable and lower than the concentration of extracellular FFA required to activate the FFAR4. To give further evidence for this observation, it would be relevant to measure the concentration of intracellular FFA after lipolysis stimulation in the presence and absence of FFAR4 NAM (AH7614) or using compartment specific mini-G$\alpha_{i/o}$ overexpression. An alternative method to investigate intracellular FFAR4 activation would be to create an agonist that is only active intracellularly and not extracellularly (Tadevosyan et al., 2016). Or even by comparing FFAR4 activation after the application of cell permeable and cell impermeable FFAR4 agonists (Jong et al., 2018).

Thirdly, this thesis did not explore AC localisation in adipocytes and whether the FFAR4 has subtype specific bias over the regulation of AC activation. It would be important to investigate the localisation of AC isoforms in adipocytes as it may give an indication of the intracellular compartments where the FFAR4, and other relevant GPCRs, might exert intracellular effects. In addition, since additional downstream signalling pathways seem important to the FFAR4 (Burns et al., 2014), it would be relevant to further evaluate intracellular FFAR4 signalling and its effects on intracellular [Ca^{2+}] accumulation, β-arrestin signalling, and G$\beta\gamma$ activation. Considering β-arrestin has been found capable of forming a megaplex with G protein and GPCR, and is thought to have a role in persistent intracellular signalling of select GPCRs

(Nguyen et al., 2019), the investigation of β-arrestin could be of relevance in the FFAR4's control of lipolysis. Furthermore, as FFAR4 inhibitory effects on cAMP production have been demonstrated undetectable in the presence of PDE inhibitor IBMX, a compound used in some cAMP assays to raise cAMP production (Husted et al., 2020), the FFAR4 may also be involved in the regulation of PDEs? Since PDE3B is involved in insulin resistance and has been discovered subcellularly localised in the lipid droplet compartment (DiPilato et al., 2015), it is tempting to hypothesise that intracellular FFAR4 pools might activate lipid-droplet associated PDE3B in response to intracellular FFAs to inhibit lipolysis (Wang et al., 2017). This might be facilitated by β−arrestin, since β−arrestin has been implicated in the regulation of PDEs (Perry et al., 2002).

Fourthly, further research is required to develop tools capable of detecting subcellular GPCR signalling. For example, BERKY (BRET sensors based on an ER/K linker and YFP) sensors (Maziarz et al., 2020), might be applicable since they can detect endogenous G protein activation. BERKY sensors consist of a NLuc donor module and a YFP acceptor module separated by an ER/K linker (10 nm). The sensor is fused to the plasma membrane via a membrane anchoring sequence at its N-terminus and has a G protein detector peptide at its C-terminus. The biosensor assumes a bent conformation when it binds to an active G protein, which can be measured by an increase in BRET. Fusing BERKY sensors to subcellular compartments might facilitate the detection of endogenous G protein activity with subtype specific and subcellular resolution.

In addition to the detection of subcellular GPCR activation, it is of importance to develop tools capable of blocking subcellular GPCR signalling. In the past, this has been achieved by directing nanobodies to subcellular compartments using an inducible FRB FKBP dimerization system (Irannejad et al., 2017, Nash et al., 2019). Or, more recently, by tethering the RGS domain of GRK2 to the plasma membrane or the early endosomes to block compartment specific Gα_q signalling (Wright et al., 2021). The development of these, or similar, methods may help to determine the functional relevance of subcellular GPCR signalling.

Within this thesis, mini-G probes were found applicable to block GPCR-specific effects on cAMP signalling in a manner similar to nanobodies (Irannejad et al., 2017). However, by harnessing the FRB-FKBP inducible dimerization system to target mini-G probes to specific compartments, this method was unable to efficiently block compartment-specific FFAR4-dependent effects on cAMP. A better approach might be to directly fuse mini-G probes to subcellular compartments to block subcellular FFAR4 signalling. If successful, these methods might enable a robust interrogation of intracellular GPCR activity and subsequently, the assessment of their physiological relevance.

Finally, having investigated the FFAR4S within my studies, similar approaches could be applied to investigate the mutant version of the FFAR4 (p.R270H) which has been associated with an increased risk of type 2 diabetes in combination with a high fat diet (Bonnefond et al., 2015), or even FFAR4L, the FFAR4 variant supposed not to couple to G proteins (Watson et al., 2012). It would be intriguing to investigate physiologically relevant FFAR4 mutations and variants, and their impact on FFAR4 coupling,

trafficking, and intracellular signalling. This could be achieved via similar methods to those that have been applied in this thesis.

5.1.5 Final conclusions

In conclusion, experiments from this thesis give evidence that the FFAR4 is a predominantly $G\alpha_{i/o}$ coupled receptor which inhibits cAMP production from subcellular compartments in response to intracellular FFAs released upon the induction of lipolysis.

In a simple cell model, mini-G probes were used to demonstrate spatiotemporal FFAR4 activation. Specific FFAR4 stimulation was found first to initiate FFAR4 activation at the plasma membrane, and subsequently, to initiate FFAR4 activation from intracellular compartments, including the early endosomes, late endosomes, recycling endosomes, and subdomains of the ER/Golgi, in a $G\alpha_{i/o}$ dependent manner. It is likely that most of this activation is dependent on receptor internalisation considering that FFAR4 trafficking to these compartments was able to be blocked after inhibition of GPCR internalisation with the dynamin inhibitor, Dyngo4a.

In an adipocyte model, whilst mini-G probes were not applicable to detect intracellular activation of the FFAR4 via BRET, imaging-based methods could detect spatiotemporal FFAR4 activation. Within these experiments, the FFAR4 was found to rapidly recruit mini-G probes to intracellular compartments after lipolysis induction – indicating FFAR4 activation from intracellular compartments in response to intracellular FFAs. Considering the speed of FFAR4 activation, and the low abundance of extracellular FFA released under applied experimental conditions, it is most likely

that the activation of the FFAR4 in differentiated adipocytes predominantly occurs from intracellular compartments, rather than from the plasma membrane.

Finally, this investigation demonstrated the applicability of mini-G probes to measure GPCR coupling and spatiotemporal GPCR activation in an adipocyte model. Such methods may also be applicable for the investigation of subcellular signalling of other GPCRs expressed in adipocytes. In addition, this thesis demonstrates a use for mini-G probes to inhibit downstream GPCR regulated cAMP signalling detected by the BRET-based cAMP sensor, NLuc-Epac-VV. Further work is required to confirm the localisation of endogenous FFAR4 in adipocytes, and the functional relevance of intracellular FFAR4 signalling and its control over adipocyte lipolysis.

6.0 Chapter six: References

6.1 References

ADAMS, S. R., HAROOTUNIAN, A. T., BUECHLER, Y. J., TAYLOR, S. S. & TSIEN, R. Y. 1991. Fluorescence ratio imaging of cyclic AMP in single cells. *Nature,* 349**,** 694-7.

AHMED, K., TUNARU, S., LANGHANS, C. D., HANSON, J., MICHALSKI, C. W., KOLKER, S., JONES, P. M., OKUN, J. G. & OFFERMANNS, S. 2009. Deorphanization of GPR109B as a receptor for the beta-oxidation intermediate 3-OH-octanoic acid and its role in the regulation of lipolysis. *J Biol Chem,* 284**,** 21928-21933.

AHMED, K., TUNARU, S., TANG, C., MULLER, M., GILLE, A., SASSMANN, A., HANSON, J. & OFFERMANNS, S. 2010. An autocrine lactate loop mediates insulin-dependent inhibition of lipolysis through GPR81. *Cell Metab,* 11**,** 311-9.

AHN, S., SHENOY, S. K., WEI, H. & LEFKOWITZ, R. J. 2004. Differential kinetic and spatial patterns of beta-arrestin and G protein-mediated ERK activation by the angiotensin II receptor. *J Biol Chem,* 279**,** 35518-25.

ALEXANDER, N. S., PREININGER, A. M., KAYA, A. I., STEIN, R. A., HAMM, H. E. & MEILER, J. 2014. Energetic analysis of the rhodopsin-G-protein complex links the alpha5 helix to GDP release. *Nat Struct Mol Biol,* 21**,** 56-63.

AMISTEN, S., NEVILLE, M., HAWKES, R., PERSAUD, S. J., KARPE, F. & SALEHI, A. 2015. An atlas of G-protein coupled receptor expression and function in human subcutaneous adipose tissue. *Pharmacol Ther,* 146**,** 61-93.

ATALLAH, R., GINDLHUBER, J., PLATZER, W., BARNTHALER, T., TATZL, E., TOLLER, W., STRUTZ, J., RITTCHEN, S., LUSCHNIG, P., BIRNER-GRUENBERGER, R., WADSACK, C. & HEINEMANN, A. 2021. SUCNR1 Is Expressed in Human Placenta and Mediates Angiogenesis: Significance in Gestational Diabetes. *Int J Mol Sci,* 22.

ATTWOOD, T. K. & FINDLAY, J. B. C. 1994. Fingerprinting G-protein-coupled receptors. *Protein Engineering,* 7**,** 195-203.

AUGUSTE, S., FISETTE, A., FERNANDES, M. F., HRYHORCZUK, C., POITOUT, V., ALQUIER, T. & FULTON, S. 2016. Central Agonism of GPR120 Acutely Inhibits Food Intake and Food Reward and Chronically Suppresses Anxiety-Like Behavior in Mice. *Int J Neuropsychopharmacol,* 19.

AVET, C., MANCINI, A., BRETON, B., LE GOUILL, C., HAUSER, A. S., NORMAND, C., KOBAYASHI, H., GROSS, F., HOGUE, M., LUKASHEVA, V., ST-ONGE, S., CARRIER, M., HEROUX, M., MORISSETTE, S., FAUMAN, E. B., FORTIN, J. P., SCHANN, S., LEROY, X., GLORIAM, D. E. & BOUVIER, M. 2022. Effector membrane translocation biosensors reveal G protein and betaarrestin coupling profiles of 100 therapeutically relevant GPCRs. *Elife,* 11.

BACSKAI, B. J., HOCHNER, B., MAHAUT-SMITH, M., ADAMS, S. R., KAANG, B. K., KANDEL, E. R. & TSIEN, R. Y. 1993. Spatially resolved dynamics of cAMP and protein kinase A subunits in Aplysia sensory neurons. *Science,* 260**,** 222-6.

BARAGLI, A., GHE, C., ARNOLETTI, E., GRANATA, R., GHIGO, E. & MUCCIOLI, G. 2011. Acylated and unacylated ghrelin attenuate isoproterenol-induced lipolysis in isolated rat visceral adipocytes through activation of phosphoinositide 3-kinase gamma and phosphodiesterase 3B. *Biochim Biophys Acta,* 1811**,** 386-96.

BARAK, L. S., SALAHPOUR, A., ZHANG, X., MASRI, B., SOTNIKOVA, T. D., RAMSEY, A. J., VIOLIN, J. D., LEFKOWITZ, R. J., CARON, M. G. & GAINETDINOV, R. R. 2008. Pharmacological characterization of membrane-expressed human trace amine-associated receptor 1 (TAAR1) by a bioluminescence resonance energy transfer cAMP biosensor. *Mol Pharmacol,* 74**,** 585-594.

BENARD, G., MASSA, F., PUENTE, N., LOURENCO, J., BELLOCCHIO, L., SORIA-GOMEZ, E., MATIAS, I., DELAMARRE, A., METNA-LAURENT, M., CANNICH, A., HEBERT-CHATELAIN, E., MULLE, C., ORTEGA-GUTIERREZ, S., MARTIN-FONTECHA, M., KLUGMANN, M., GUGGENHUBER, S., LUTZ, B., GERTSCH, J., CHAOULOFF, F., LOPEZ-RODRIGUEZ, M. L., GRANDES, P., ROSSIGNOL, R. &

MARSICANO, G. 2012. Mitochondrial CB(1) receptors regulate neuronal energy metabolism. *Nat Neurosci,* 15**,** 558-64.

BERG, K. A. & CLARKE, W. P. 2018. Making Sense of Pharmacology: Inverse Agonism and Functional Selectivity. *Int J Neuropsychopharmacol,* 21**,** 962-977.

BERMAN, D. M., KOZASA, T. & GILMAN, A. G. 1996. The GTPase-activating protein RGS4 stabilizes the transition state for nucleotide hydrolysis. *J Biol Chem,* 271**,** 27209-12.

BLAD, C. C., AHMED, K., AP, I. J. & OFFERMANNS, S. 2011. Biological and pharmacological roles of HCA receptors. *Adv Pharmacol,* 62**,** 219-50.

BLONDIN, D. P., NIELSEN, S., KUIPERS, E. N., SEVERINSEN, M. C., JENSEN, V. H., MIARD, S., JESPERSEN, N. Z., KOOIJMAN, S., BOON, M. R., FORTIN, M., PHOENIX, S., FRISCH, F., GUERIN, B., TURCOTTE, E. E., HAMAN, F., RICHARD, D., PICARD, F., RENSEN, P. C. N., SCHEELE, C. & CARPENTIER, A. C. 2020. Human Brown Adipocyte Thermogenesis Is Driven by beta2-AR Stimulation. *Cell Metab,* 32**,** 287-300 e7.

BLUMER, J. B. & LANIER, S. M. 2014. Activators of G protein signaling exhibit broad functionality and define a distinct core signaling triad. *Mol Pharmacol,* 85**,** 388-96.

BOIVIN, B., LAVOIE, C., VANIOTIS, G., BARAGLI, A., VILLENEUVE, L. R., ETHIER, N., TRIEU, P., ALLEN, B. G. & HEBERT, T. E. 2006. Functional beta-adrenergic receptor signalling on nuclear membranes in adult rat and mouse ventricular cardiomyocytes. *Cardiovasc Res,* 71**,** 69-78.

BOKOCH, M. P., ZOU, Y., RASMUSSEN, S. G., LIU, C. W., NYGAARD, R., ROSENBAUM, D. M., FUNG, J. J., CHOI, H. J., THIAN, F. S., KOBILKA, T. S., PUGLISI, J. D., WEIS, W. I., PARDO, L., PROSSER, R. S., MUELLER, L. & KOBILKA, B. K. 2010. Ligand-specific regulation of the extracellular surface of a G-protein-coupled receptor. *Nature,* 463**,** 108-12.

BONNEFOND, A., LAMRI, A., LELOIRE, A., VAILLANT, E., ROUSSEL, R., LEVY-MARCHAL, C., WEILL, J., GALAN, P., HERCBERG, S., RAGOT, S., HADJADJ, S., CHARPENTIER, G., BALKAU, B., MARRE, M., FUMERON, F. & FROGUEL, P. 2015. Contribution of the low-frequency, loss-of-function p.R270H mutation in FFAR4 (GPR120) to increased fasting plasma glucose levels. *J Med Genet,* 52**,** 595-8.

BRAUN, K., OECKL, J., WESTERMEIER, J., LI, Y. & KLINGENSPOR, M. 2018. Non-adrenergic control of lipolysis and thermogenesis in adipose tissues. *J Exp Biol,* 221.

BREJCHOVA, K., RADNER, F. P. W., BALAS, L., PALUCHOVA, V., CAJKA, T., CHODOUNSKA, H., KUDOVA, E., SCHRATTER, M., SCHREIBER, R., DURAND, T., ZECHNER, R. & KUDA, O. 2021. Distinct roles of adipose triglyceride lipase and hormone-sensitive lipase in the catabolism of triacylglycerol estolides. *Proc Natl Acad Sci U S A,* 118.

BRISCOE, C. P., TADAYYON, M., ANDREWS, J. L., BENSON, W. G., CHAMBERS, J. K., EILERT, M. M., ELLIS, C., ELSHOURBAGY, N. A., GOETZ, A. S., MINNICK, D. T., MURDOCK, P. R., SAULS, H. R., JR., SHABON, U., SPINAGE, L. D., STRUM, J. C., SZEKERES, P. G., TAN, K. B., WAY, J. M., IGNAR, D. M., WILSON, S. & MUIR, A. I. 2003. The orphan G protein-coupled receptor GPR40 is activated by medium and long chain fatty acids. *J Biol Chem,* 278**,** 11303-11.

BROWN, A. J., GOLDSWORTHY, S. M., BARNES, A. A., EILERT, M. M., TCHEANG, L., DANIELS, D., MUIR, A. I., WIGGLESWORTH, M. J., KINGHORN, I., FRASER, N. J., PIKE, N. B., STRUM, J. C., STEPLEWSKI, K. M., MURDOCK, P. R., HOLDER, J. C., MARSHALL, F. H., SZEKERES, P. G., WILSON, S., IGNAR, D. M., FOORD, S. M., WISE, A. & DOWELL, S. J. 2003. The Orphan G protein-coupled receptors GPR41 and GPR43 are activated by propionate and other short chain carboxylic acids. *J Biol Chem,* 278**,** 11312-9.

BURNS, R. N., SINGH, M., SENATOROV, I. S. & MONIRI, N. H. 2014. Mechanisms of homologous and heterologous phosphorylation of FFA receptor 4 (GPR120): GRK6 and PKC mediate phosphorylation of Thr(3)(4)(7), Ser(3)(5)(0), and Ser(3)(5)(7) in the C-terminal tail. *Biochem Pharmacol,* 87**,** 650-9.

BURNS, T. W., LANGLEY, P. E., TERRY, B. E. & ROBINSON, G. A. 1978. The role of free fatty acids in the regulation of lipolysis by human adipose tissue cells. *Metabolism,* 27**,** 1755-1762.

CAENGPRASATH, N. & HANYALOGLU, A. C. 2019. Hardwiring wire-less networks: spatially encoded GPCR signaling in endocrine systems. *Curr Opin Cell Biol,* 57**,** 77-82.

CAHILL, T. J., 3RD, THOMSEN, A. R., TARRASCH, J. T., PLOUFFE, B., NGUYEN, A. H., YANG, F., HUANG, L. Y., KAHSAI, A. W., BASSONI, D. L., GAVINO, B. J., LAMERDIN, J. E., TRIEST, S., SHUKLA, A. K., BERGER, B., LITTLE, J. T., ANTAR, A., BLANC, A., QU, C. X., CHEN, X., KAWAKAMI, K., INOUE, A., AOKI, J., STEYAERT, J., SUN, J. P., BOUVIER, M., SKINIOTIS, G. & LEFKOWITZ, R. J. 2017. Distinct conformations of GPCR-beta-arrestin complexes mediate desensitization, signaling, and endocytosis. *Proc Natl Acad Sci U S A,* 114**,** 2562-2567.

CALEBIRO, D. & GODBOLE, A. 2018. Internalization of G-protein-coupled receptors: Implication in receptor function, physiology and diseases. *Best Pract Res Clin Endocrinol Metab,* 32**,** 83-91.

CALEBIRO, D. & KOSZEGI, Z. 2019. The subcellular dynamics of GPCR signaling. *Molecular and Cellular Endocrinology,* 483**,** 24-30.

CALEBIRO, D., KOSZEGI, Z., LANOISELEE, Y., MILJUS, T. & O'BRIEN, S. 2021. G protein-coupled receptor-G protein interactions: a single-molecule perspective. *Physiol Rev,* 101**,** 857-906.

CALEBIRO, D. & MAIELLARO, I. 2014. cAMP signaling microdomains and their observation by optical methods. *Front Cell Neurosci,* 8**,** 350.

CALEBIRO, D., NIKOLAEV, V. O., GAGLIANI, M. C., DE FILIPPIS, T., DEES, C., TACCHETTI, C., PERSANI, L. & LOHSE, M. J. 2009. Persistent cAMP-signals triggered by internalized G-protein-coupled receptors. *PLoS Biol,* 7**,** e1000172.

CAMPS, M., HOU, C., SIDIROPOULOS, D., STOCK, J. B., JAKOBS, K. H. & GIERSCHIK, P. 1992. Stimulation of phospholipase C by guanine-nucleotide-binding protein beta gamma subunits. *Eur J Biochem,* 206**,** 821-31.

CAO, A. M., QUAST, R. B., FATEMI, F., RONDARD, P., PIN, J. P. & MARGEAT, E. 2021. Allosteric modulators enhance agonist efficacy by increasing the residence time of a GPCR in the active state. *Nat Commun,* 12**,** 5426.

CARPENE, C., BOUSQUET-MELOU, A., GALITZKY, J., BERLAN, M. & LAFONTAN, M. 1998. Lipolytic effects of beta 1-, beta 2-, and beta 3-adrenergic agonists in white adipose tissue of mammals. *Ann N Y Acad Sci,* 839**,** 186-9.

CARTA, G., MURRU, E., BANNI, S. & MANCA, C. 2017. Palmitic Acid: Physiological Role, Metabolism and Nutritional Implications. *Front Physiol,* 8**,** 902.

CARTONI, C., YASUMATSU, K., OHKURI, T., SHIGEMURA, N., YOSHIDA, R., GODINOT, N., LE COUTRE, J., NINOMIYA, Y. & DAMAK, S. 2010. Taste preference for fatty acids is mediated by GPR40 and GPR120. *J Neurosci,* 30**,** 8376-82.

CASSIER, E., GALLAY, N., BOURQUARD, T., CLAEYSEN, S., BOCKAERT, J., CREPIEUX, P., POUPON, A., REITER, E., MARIN, P. & VANDERMOERE, F. 2017. Phosphorylation of beta-arrestin2 at Thr(383) by MEK underlies beta-arrestin-dependent activation of Erk1/2 by GPCRs. *Elife,* 6.

CERF, M. E. 2013. Beta cell dysfunction and insulin resistance. *Front Endocrinol (Lausanne),* 4**,** 37.

CERIONE, R. A., CODINA, J., BENOVIC, J. L., LEFKOWITZ, R. J., BIRNBAUMER, L. & CARON, M. G. 1984. The mammalian beta 2-adrenergic receptor: reconstitution of functional interactions between pure receptor and pure stimulatory nucleotide binding protein of the adenylate cyclase system. *Biochemistry,* 23**,** 4519-25.

CHANG, L., CHIANG, S. H. & SALTIEL, A. R. 2004. Insulin signaling and the regulation of glucose transport. *Mol Med,* 10**,** 65-71.

CHE, T., ENGLISH, J., KRUMM, B. E., KIM, K., PARDON, E., OLSEN, R. H. J., WANG, S., ZHANG, S., DIBERTO, J. F., SCIAKY, N., CARROLL, F. I., STEYAERT, J., WACKER, D. & ROTH, B. L. 2020. Nanobody-enabled monitoring of kappa opioid receptor states. *Nat Commun,* 11**,** 1145.

CHEREZOV, V., ROSENBAUM, D. M., HANSON, M. A., RASMUSSEN, S. G., THIAN, F. S., KOBILKA, T. S., CHOI, H. J., KUHN, P., WEIS, W. I., KOBILKA, B. K. & STEVENS, R. C. 2007. High-resolution crystal structure of an engineered human beta2-adrenergic G protein-coupled receptor. *Science,* 318**,** 1258-65.

CHEUNG, P., YANG, G. & BODEN, G. 2003. Milrinone, a selective phosphodiesterase 3 inhibitor, stimulatesl lipolysis, endogenous glucose production, and insulin secretion. *Metabolism,* 52**,** 1496-1500.

CHOE, S. S., HUH, J. Y., HWANG, I. J., KIM, J. I. & KIM, J. B. 2016. Adipose Tissue Remodeling: Its Role in Energy Metabolism and Metabolic Disorders. *Front Endocrinol (Lausanne),* 7**,** 30.

CHOI, J., CHEN, J., SCHREIBER, S. L. & CLARDY, J. 1996. Structure of the FKBP12-rapamycin complex interacting with the binding domain of human FRAP. *Science,* 273**,** 239-42.

CHRISTIAN, M. 2020. Elucidation of the roles of brown and brite fat genes: GPR120 is a modulator of brown adipose tissue function. *Exp Physiol,* 105**,** 1201-1205.

CHRISTIANSEN, E., WATTERSON, K. R., STOCKER, C. J., SOKOL, E., JENKINS, L., SIMON, K., GRUNDMANN, M., PETERSEN, R. K., WARGENT, E. T., HUDSON, B. D., KOSTENIS, E., EJSING, C. S., CAWTHORNE, M. A., MILLIGAN, G. & ULVEN, T. 2015. Activity of dietary fatty acids on FFA1 and FFA4 and characterisation of pinolenic acid as a dual FFA1/FFA4 agonist with potential effect against metabolic diseases. *Br J Nutr,* 113**,** 1677-88.

COBURN, C. T., KNAPP, F. F., JR., FEBBRAIO, M., BEETS, A. L., SILVERSTEIN, R. L. & ABUMRAD, N. A. 2000. Defective uptake and utilization of long chain fatty acids in muscle and adipose tissues of CD36 knockout mice. *J Biol Chem,* 275**,** 32523-9.

COELHO, M., OLIVEIRA, T. & FERNANDES, R. 2013. Biochemistry of adipose tissue: an endocrine organ. *Arch Med Sci,* 9**,** 191-200.

CORNALL, L. M., MATHAI, M. L., HRYCIW, D. H. & MCAINCH, A. J. 2011. Diet-induced obesity up-regulates the abundance of GPR43 and GPR120 in a tissue specific manner. *Cell Physiol Biochem,* 28**,** 949-58.

CROZE, M. L., FLISHER, M. F., GUILLAUME, A., TREMBLAY, C., NOGUCHI, G. M., GRANZIERA, S., VIVOT, K., CASTILLO, V. C., CAMPBELL, S. A., GHISLAIN, J., HUISING, M. O. & POITOUT, V. 2021. Free fatty acid receptor 4 inhibitory signaling in delta cells regulates islet hormone secretion in mice. *Mol Metab,* 45**,** 101166.

CUCCHI, D., CAMACHO-MUNOZ, D., CERTO, M., PUCINO, V., NICOLAOU, A. & MAURO, C. 2019. Fatty acids - from energy substrates to key regulators of cell survival, proliferation and effector function. *Cell Stress,* 4**,** 9-23.

DA SILVA ROSA, S. C., NAYAK, N., CAYMO, A. M. & GORDON, J. W. 2020. Mechanisms of muscle insulin resistance and the cross-talk with liver and adipose tissue. *Physiol Rep,* 8**,** e14607.

DALE, N. C., JOHNSTONE, E. K. M., WHITE, C. W. & PFLEGER, K. D. G. 2019. NanoBRET: The Bright Future of Proximity-Based Assays. *Front Bioeng Biotechnol,* 7**,** 1-13.

DE MUTSERT, R., GAST, K., WIDYA, R., DE KONING, E., JAZET, I., LAMB, H., LE CESSIE, S., DE ROOS, A., SMIT, J., ROSENDAAL, F. & DEN HEIJER, M. 2018. Associations of Abdominal Subcutaneous and Visceral Fat with Insulin Resistance and Secretion Differ Between Men and Women: The Netherlands Epidemiology of Obesity Study. *Metab Syndr Relat Disord,* 16**,** 54-63.

DE WAARD, M., LIU, H., WALKER, D., SCOTT, V. E., GURNETT, C. A. & CAMPBELL, K. P. 1997. Direct binding of G-protein betagamma complex to voltage-dependent calcium channels. *Nature,* 385**,** 446-50.

DEFEA, K. A., ZALEVSKY, J., THOMA, M. S., DERY, O., MULLINS, R. D. & BUNNETT, N. W. 2000. beta-arrestin-dependent endocytosis of proteinase-activated receptor 2 is required for intracellular targeting of activated ERK1/2. *J Cell Biol,* 148**,** 1267-81.

DEL CASTILLO, J. & KATZ, B. 1957. Interaction at end-plate receptors between different choline derivatives. *Proc R Soc Lond B Biol Sci,* 146**,** 369-81.

DESPRES, J. P. 2007. Cardiovascular disease under the influence of excess visceral fat. *Crit Pathw Cardiol,* 6**,** 51-9.

DEVREE, B. T., MAHONEY, J. P., VELEZ-RUIZ, G. A., RASMUSSEN, S. G., KUSZAK, A. J., EDWALD, E., FUNG, J. J., MANGLIK, A., MASUREEL, M., DU, Y., MATT, R. A., PARDON, E., STEYAERT, J., KOBILKA, B. K. & SUNAHARA, R. K. 2016. Allosteric coupling from G protein to the agonist-binding pocket in GPCRs. *Nature,* 535**,** 182-6.

DI BENEDETTO, A., SUN, L., ZAMBONIN, C. G., TAMMA, R., NICO, B., CALVANO, C. D., COLAIANNI, G., JI, Y., MORI, G., GRANO, M., LU, P., COLUCCI, S., YUEN, T., NEW, M. I., ZALLONE, A. & ZAIDI, M. 2014. Osteoblast regulation via ligand-activated nuclear trafficking of the oxytocin receptor. *Proc Natl Acad Sci U S A,* 111**,** 16502-7.

DIPILATO, L. M., AHMAD, F., HARMS, M., SEALE, P., MANGANIELLO, V. & BIRNBAUM, M. J. 2015. The Role of PDE3B Phosphorylation in the Inhibition of Lipolysis by Insulin. *Mol Cell Biol,* 35**,** 2752-60.

DIPILATO, L. M., CHENG, X. & ZHANG, J. 2004. Fluorescent indicators of cAMP and Epac activation reveal differential dynamics of cAMP signaling within discrete subcellular compartments. *Proc Natl Acad Sci U S A,* 101**,** 16513-8.

DOHERTY, G. J. & MCMAHON, H. T. 2009. Mechanisms of endocytosis. *Annu Rev Biochem,* 78**,** 857-902.

DOWNES, G. B. & GAUTAM, N. 1999. The G protein subunit gene families. *Genomics,* 62**,** 544-52.

DRAKE, M. T., VIOLIN, J. D., WHALEN, E. J., WISLER, J. W., SHENOY, S. K. & LEFKOWITZ, R. J. 2008. beta-arrestin-biased agonism at the beta2-adrenergic receptor. *J Biol Chem,* 283**,** 5669-76.

DROR, R. O., MILDORF, T. J., HILGER, D., MANGLIK, A., BORHANI, D. W., ARLOW, D. H., PHILIPPSEN, A., VILLANUEVA, N., YANG, Z., LERCH, M. T., HUBBELL, W. L., KOBILKA, B. K., SUNAHARA, R. K. & SHAW, D. E. 2015. SIGNAL TRANSDUCTION. Structural basis for nucleotide exchange in heterotrimeric G proteins. *Science,* 348**,** 1361-5.

DRUBE, J., HAIDER, R. S., MATTHEES, E. S. F., REICHEL, M., ZEINER, J., FRITZWANKER, S., ZIEGLER, C., BARZ, S., KLEMENT, L., FILOR, J., WEITZEL, V., KLIEWER, A., MIESS-TANNEBERG, E., KOSTENIS, E., SCHULZ, S. & HOFFMANN, C. 2022. GPCR kinase knockout cells reveal the impact of individual GRKs on arrestin binding and GPCR regulation. *Nat Commun,* 13**,** 540.

DUNCAN, R. E., AHMADIAN, M., JAWORSKI, K., SARKADI-NAGY, E. & SUL, H. S. 2007. Regulation of lipolysis in adipocytes. *Annu Rev Nutr,* 27**,** 79-101.

DUPRE, D. J., ROBITAILLE, M., ETHIER, N., VILLENEUVE, L. R., MAMARBACHI, A. M. & HEBERT, T. E. 2006. Seven transmembrane receptor core signaling complexes are assembled prior to plasma membrane trafficking. *J Biol Chem,* 281**,** 34561-73.

ECLOV, J. A., QIAN, Q., REDETZKE, R., CHEN, Q., WU, S. C., HEALY, C. L., ORTMEIER, S. B., HARMON, E., SHEARER, G. C. & O'CONNELL, T. D. 2015. EPA, not DHA, prevents fibrosis in pressure overload-induced heart failure: potential role of free fatty acid receptor 4. *J Lipid Res,* 56**,** 2297-308.

EGEROD, K. L., ENGELSTOFT, M. S., LUND, M. L., GRUNDDAL, K. V., ZHAO, M., BARIR-JENSEN, D., NYGAARD, E. B., PETERSEN, N., HOLST, J. J. & SCHWARTZ, T. W. 2015. Transcriptional and Functional Characterization of the G Protein-Coupled Receptor Repertoire of Gastric Somatostatin Cells. *Endocrinology,* 156**,** 3909-23.

EICHEL, K. & VON ZASTROW, M. 2018. Subcellular Organization of GPCR Signaling. *Trends Pharmacol Sci,* 39**,** 200-208.

EL KHAMLICHI, C., REVERCHON-ASSADI, F., HERVOUET-COSTE, N., BLOT, L., REITER, E. & MORISSET-LOPEZ, S. 2019. Bioluminescence Resonance Energy Transfer as a Method to Study Protein-Protein Interactions: Application to G Protein Coupled Receptor Biology. *Molecules,* 24.

ELLIS, J. M., LI, L. O., WU, P.-C., KOVES, T. R., ILKAYEVA, O., STEVENS, R. D., WATKINS, S. M., MUOIO, D. M. & COLEMAN, R. A. 2010. Adipose Acyl-CoA Synthetase-1 Directs Fatty Acids toward β-Oxidation and Is Required for Cold Thermogenesis. *Cell Metabolism,* 12**,** 53-64.

ENGELSTOFT, M. S., PARK, W. M., SAKATA, I., KRISTENSEN, L. V., HUSTED, A. S., OSBORNE-LAWRENCE, S., PIPER, P. K., WALKER, A. K., PEDERSEN, M. H., NOHR, M. K., PAN, J., SINZ, C. J., CARRINGTON, P. E., AKIYAMA, T. E., JONES, R. M., TANG, C., AHMED, K., OFFERMANNS, S., EGEROD, K. L., ZIGMAN, J. M. & SCHWARTZ, T. W. 2013. Seven transmembrane G protein-coupled receptor repertoire of gastric ghrelin cells. *Mol Metab,* 2**,** 376-92.

FAIN, J. N. & SHEPHERD, R. E. 1975. Free fatty acids as feedback regulators of adenylate cyclase and cyclic 3':5'-AMP accumulation in rat fat cells. *Journal of Biological Chemistry,* 250**,** 6586-6592.

FENZL, A. & KIEFER, F. W. 2014. Brown adipose tissue and thermogenesis. *Horm Mol Biol Clin Investig,* 19**,** 25-37.

FERRANDON, S., FEINSTEIN, T. N., CASTRO, M., WANG, B., BOULEY, R., POTTS, J. T., GARDELLA, T. J. & VILARDAGA, J. P. 2009. Sustained cyclic AMP production by parathyroid hormone receptor endocytosis. *Nat Chem Biol,* 5**,** 734-42.

FILIPEANU, C. M., ZHOU, F., CLAYCOMB, W. C. & WU, G. 2004. Regulation of the cell surface expression and function of angiotensin II type 1 receptor by Rab1-mediated endoplasmic reticulum-to-Golgi transport in cardiac myocytes. *J Biol Chem,* 279**,** 41077-84.

FILIPEANU, C. M., ZHOU, F., FUGETTA, E. K. & WU, G. 2006. Differential regulation of the cell-surface targeting and function of beta- and alpha1-adrenergic receptors by Rab1 GTPase in cardiac myocytes. *Mol Pharmacol,* 69**,** 1571-8.

FLOCK, T., RAVARANI, C. N. J., SUN, D., VENKATAKRISHNAN, A. J., KAYIKCI, M., TATE, C. G., VEPRINTSEV, D. B. & BABU, M. M. 2015. Universal allosteric mechanism for Galpha activation by GPCRs. *Nature,* 524**,** 173-179.

FLORES-ESPINOZA, E., MEIZOSO-HUESCA, A., VILLEGAS-COMONFORT, S., REYES-CRUZ, G. & GARCIA-SAINZ, J. A. 2020. Effect of docosahexaenoic acid, phorbol myristate acetate, and insulin on the interaction of the FFA4 (short isoform) receptor with Rab proteins. *Eur J Pharmacol,* 889**,** 173595.

FOSTER, D. J. & CONN, P. J. 2017. Allosteric Modulation of GPCRs: New Insights and Potential Utility for Treatment of Schizophrenia and Other CNS Disorders. *Neuron,* 94**,** 431-446.

FREDRIKSSON, R., LAGERSTROM, M. C., LUNDIN, L. G. & SCHIOTH, H. B. 2003. The G-protein-coupled receptors in the human genome form five main families. Phylogenetic analysis, paralogon groups, and fingerprints. *Mol Pharmacol,* 63**,** 1256-72.

FRIEDMAN, J. R., DIBENEDETTO, J. R., WEST, M., ROWLAND, A. A. & VOELTZ, G. K. 2013. Endoplasmic reticulum-endosome contact increases as endosomes traffic and mature. *Mol Biol Cell,* 24**,** 1030-40.

GALANDRIN, S., DENIS, C., BOULARAN, C., MARIE, J., M'KADMI, C., PILETTE, C., DUBROCA, C., NICAISE, Y., SEGUELAS, M. H., N'GUYEN, D., BANERES, J. L., PATHAK, A., SENARD, J. M. & GALES, C. 2016. Cardioprotective Angiotensin-(1-7) Peptide Acts as a Natural-Biased Ligand at the Angiotensin II Type 1 Receptor. *Hypertension,* 68**,** 1365-1374.

GALLARDO-MONTEJANO, V. I., YANG, C., HAHNER, L., MCAFEE, J. L., JOHNSON, J. A., HOLLAND, W. L., FERNANDEZ-VALDIVIA, R. & BICKEL, P. E. 2021. Perilipin 5 links mitochondrial uncoupled respiration in brown fat to healthy white fat remodeling and systemic glucose tolerance. *Nat Commun,* 12**,** 3320.

GANDOTRA, S., LE DOUR, C., BOTTOMLEY, W., CERVERA, P., GIRAL, P., REZNIK, Y., CHARPENTIER, G., AUCLAIR, M., DELEPINE, M., BARROSO, I., SEMPLE, R. K., LATHROP, M., LASCOLS, O., CAPEAU, J., O'RAHILLY, S., MAGRE, J., SAVAGE, D. B. & VIGOUROUX, C. 2011a. Perilipin deficiency and autosomal dominant partial lipodystrophy. *N Engl J Med,* 364**,** 740-8.

GANDOTRA, S., LIM, K., GIROUSSE, A., SAUDEK, V., O'RAHILLY, S. & SAVAGE, D. B. 2011b. Human frame shift mutations affecting the carboxyl terminus of perilipin increase lipolysis by failing to sequester the adipose triglyceride lipase (ATGL) coactivator AB-hydrolase-containing 5 (ABHD5). *J Biol Chem,* 286**,** 34998-5006.

GARGIULO, C. E., STUHLSATZ-KROUPER, S. M. & SCHAFFER, J. E. 1999. Localization of adipocyte long-chain fatty acyl-CoA synthetase at the plasma membrane. *Journal of Lipid Research,* 40**,** 881-892.

GE, H., LI, X., WEISZMANN, J., WANG, P., BARIBAULT, H., CHEN, J. L., TIAN, H. & LI, Y. 2008. Activation of G protein-coupled receptor 43 in adipocytes leads to inhibition of lipolysis and suppression of plasma free fatty acids. *Endocrinology,* 149**,** 4519-26.

GENTRY, P. R., SEXTON, P. M. & CHRISTOPOULOS, A. 2015. Novel Allosteric Modulators of G Protein-coupled Receptors. *J Biol Chem,* 290**,** 19478-88.

GIBSON, D. G., YOUNG, L., CHUANG, R. Y., VENTER, J. C., HUTCHISON, C. A., 3RD & SMITH, H. O. 2009. Enzymatic assembly of DNA molecules up to several hundred kilobases. *Nat Methods,* 6**,** 343-5.

GIRADA, S. B., KUNA, R. S., BELE, S., ZHU, Z., CHAKRAVARTHI, N. R., DIMARCHI, R. D. & MITRA, P. 2017. Galphas regulates Glucagon-Like Peptide 1 Receptor-mediated cyclic AMP generation at Rab5 endosomal compartment. *Mol Metab,* 6**,** 1173-1185.

GIUBILARO, J., SCHUETZ, D. A., STEPNIEWSKI, T. M., NAMKUNG, Y., KHOURY, E., LARA-MARQUEZ, M., CAMPBELL, S., BEAUTRAIT, A., ARMANDO, S., RADRESA, O., DUCHAINE, J., LAMARCHE-VANE, N., CLAING, A., SELENT, J., BOUVIER, M., MARINIER, A. & LAPORTE, S. A. 2021. Discovery of a dual Ras and ARF6 inhibitor from a GPCR endocytosis screen. *Nat Commun,* 12**,** 4688.

GNAD, T., SCHEIBLER, S., VON KUGELGEN, I., SCHEELE, C., KILIC, A., GLODE, A., HOFFMANN, L. S., REVERTE-SALISA, L., HORN, P., MUTLU, S., EL-TAYEB, A., KRANZ, M., DEUTHER-CONRAD, W., BRUST, P., LIDELL, M. E., BETZ, M. J., ENERBACK, S., SCHRADER, J., YEGUTKIN, G. G., MULLER, C. E. & PFEIFER, A. 2014. Adenosine activates brown adipose tissue and recruits beige adipocytes via A2A receptors. *Nature,* 516**,** 395-9.

GODBOLE, A., LYGA, S., LOHSE, M. J. & CALEBIRO, D. 2017. Internalized TSH receptors en route to the TGN induce local Gs-protein signaling and gene transcription. *Nat Commun,* 8**,** 443.

GODDARD, A. D. & WATTS, A. 2012. Regulation of G protein-coupled receptors by palmitoylation and cholesterol. *BMC Biol,* 10**,** 27.

GOLDBERG, I. J., ECKEL, R. H. & ABUMRAD, N. A. 2009. Regulation of fatty acid uptake into tissues: lipoprotein lipase- and CD36-mediated pathways. *J Lipid Res,* 50 Suppl**,** S86-90.

GONG, Z., YOSHIMURA, M., AIZAWA, S., KUROTANI, R., ZIGMAN, J. M., SAKAI, T. & SAKATA, I. 2014. G protein-coupled receptor 120 signaling regulates ghrelin secretion in vivo and in vitro. *Am J Physiol Endocrinol Metab,* 306**,** E28-35.

GOODMAN, O. B., JR., KRUPNICK, J. G., SANTINI, F., GUREVICH, V. V., PENN, R. B., GAGNON, A. W., KEEN, J. H. & BENOVIC, J. L. 1996. Beta-arrestin acts as a clathrin adaptor in endocytosis of the beta2-adrenergic receptor. *Nature,* 383**,** 447-50.

GORVIN, C. M., ROGERS, A., HASTOY, B., TARASOV, A. I., FROST, M., SPOSINI, S., INOUE, A., WHYTE, M. P., RORSMAN, P., HANYALOGLU, A. C., BREITWIESER, G. E. & THAKKER, R. V. 2018. AP2sigma Mutations Impair Calcium-Sensing Receptor Trafficking and Signaling, and Show an Endosomal Pathway to Spatially Direct G-Protein Selectivity. *Cell Rep,* 22**,** 1054-1066.

GOTOH, C., HONG, Y. H., IGA, T., HISHIKAWA, D., SUZUKI, Y., SONG, S. H., CHOI, K. C., ADACHI, T., HIRASAWA, A., TSUJIMOTO, G., SASAKI, S. & ROH, S. G. 2007. The regulation of adipogenesis through GPR120. *Biochem Biophys Res Commun,* 354**,** 591-7.

GREENFIELD, J. J. & HIGH, S. 1999. The Sec61 complex is located in both the ER and the ER-Golgi intermediate compartment. *J Cell Sci,* 112 (Pt 10)**,** 1477-86.

GREGORY, K. J., SEXTON, P. M. & CHRISTOPOULOS, A. 2010. Overview of receptor allosterism. *Curr Protoc Pharmacol,* Chapter 1**,** Unit 1 21.

GRUNDMANN, M., MERTEN, N., MALFACINI, D., INOUE, A., PREIS, P., SIMON, K., RUTTIGER, N., ZIEGLER, N., BENKEL, T., SCHMITT, N. K., ISHIDA, S., MULLER, I., REHER, R., KAWAKAMI, K., INOUE, A., RICK, U., KUHL, T., IMHOF, D., AOKI, J., KONIG, G. M., HOFFMANN, C., GOMEZA, J., WESS, J. & KOSTENIS, E. 2018. Lack of beta-arrestin signaling in the absence of active G proteins. *Nat Commun,* 9**,** 341.

GRUNDY, S. M. 2004. Obesity, metabolic syndrome, and cardiovascular disease. *J Clin Endocrinol Metab,* 89**,** 2595-600.

GUREVICH, V. V. & GUREVICH, E. V. 2019. GPCR Signaling Regulation: The Role of GRKs and Arrestins. *Front Pharmacol,* 10**,** 125.

HAEMMERLE, G., ZIMMERMANN, R., HAYN, M., THEUSSL, C., WAEG, G., WAGNER, E., SATTLER, W., MAGIN, T. M., WAGNER, E. F. & ZECHNER, R. 2002. Hormone-sensitive lipase deficiency in

mice causes diglyceride accumulation in adipose tissue, muscle, and testis. *J Biol Chem,* 277**,** 4806-15.

HALL, M. P., UNCH, J., BINKOWSKI, B. F., VALLEY, M. P., BUTLER, B. L., WOOD, M. G., OTTO, P., ZIMMERMAN, K., VIDUGIRIS, G., MACHLEIDT, T., ROBERS, M. B., BENINK, H. A., EGGERS, C. T., SLATER, M. R., MEISENHEIMER, P. L., KLAUBERT, D. H., FAN, F., ENCELL, L. P. & WOOD, K. V. 2012. Engineered luciferase reporter from a deep sea shrimp utilizing a novel imidazopyrazinone substrate. *ACS Chem Biol,* 7**,** 1848-57.

HAMDAN, F. F., PERCHERANCIER, Y., BRETON, B. & BOUVIER, M. 2006. Monitoring protein-protein interactions in living cells by bioluminescence resonance energy transfer (BRET). *Curr Protoc Neurosci,* Chapter 5**,** Unit 5 23.

HAMM, H. E., DERETIC, D., ARENDT, A., HARGRAVE, P. A., KOENIG, B. & HOFMANN, K. P. 1988. Site of G protein binding to rhodopsin mapped with synthetic peptides from the alpha subunit. *Science,* 241**,** 832-5.

HARMS, M. J., ISHIBASHI, J., WANG, W., LIM, H. W., GOYAMA, S., SATO, T., KUROKAWA, M., WON, K. J. & SEALE, P. 2014. Prdm16 is required for the maintenance of brown adipocyte identity and function in adult mice. *Cell Metab,* 19**,** 593-604.

HASHIMOTO, T., SEGAWA, H., OKUNO, M., KANO, H., HAMAGUCHI, H. O., HARAGUCHI, T., HIRAOKA, Y., HASUI, S., YAMAGUCHI, T., HIROSE, F. & OSUMI, T. 2012. Active involvement of micro-lipid droplets and lipid-droplet-associated proteins in hormone-stimulated lipolysis in adipocytes. *J Cell Sci,* 125**,** 6127-36.

HAUSER, A. S., ATTWOOD, M. M., RASK-ANDERSEN, M., SCHIOTH, H. B. & GLORIAM, D. E. 2017. Trends in GPCR drug discovery: new agents, targets and indications. *Nat Rev Drug Discov,* 16**,** 829-842.

HE, W., MIAO, F. J., LIN, D. C., SCHWANDNER, R. T., WANG, Z., GAO, J., CHEN, J. L., TIAN, H. & LING, L. 2004. Citric acid cycle intermediates as ligands for orphan G-protein-coupled receptors. *Nature,* 429**,** 188-93.

HEID, H., RICKELT, S., ZIMBELMANN, R., WINTER, S., SCHUMACHER, H., DORFLINGER, Y., KUHN, C. & FRANKE, W. W. 2014. On the formation of lipid droplets in human adipocytes: the organization of the perilipin-vimentin cortex. *PLoS One,* 9**,** e90386.

HEMPEL, C. M., VINCENT, P., ADAMS, S. R., TSIEN, R. Y. & SELVERSTON, A. I. 1996. Spatio-temporal dynamics of cyclic AMP signals in an intact neural circuitm. *Nature,* 384**,** 166-9.

HENQUIN, J. C. 2000. Triggering and amplifying pathways of regulation of insulin secretion by glucose. *Diabetes,* 49**,** 1751-60.

HERLITZE, S., GARCIA, D. E., MACKIE, K., HILLE, B., SCHEUER, T. & CATTERALL, W. A. 1996. Modulation of Ca2+ channels by G-protein beta gamma subunits. *Nature,* 380**,** 258-62.

HILGENDORF, K. I., JOHNSON, C. T., MEZGER, A., RICE, S. L., NORRIS, A. M., DEMETER, J., GREENLEAF, W. J., REITER, J. F., KOPINKE, D. & JACKSON, P. K. 2019. Omega-3 Fatty Acids Activate Ciliary FFAR4 to Control Adipogenesis. *Cell,* 179**,** 1289-1305 e21.

HIRASAWA, A., TSUMAYA, K., AWAJI, T., KATSUMA, S., ADACHI, T., YAMADA, M., SUGIMOTO, Y., MIYAZAKI, S. & TSUJIMOTO, G. 2005. Free fatty acids regulate gut incretin glucagon-like peptide-1 secretion through GPR120. *Nat Med,* 11**,** 90-4.

HOLM, C. 2003. Molecular mechanisms regulating hormone-sensitive lipase and lipolysis. *Biochem Soc Trans,* 31**,** 1120-4.

HOUTHUIJZEN, J. M., OOSTEROM, I., HUDSON, B. D., HIRASAWA, A., DAENEN, L. G. M., MCLEAN, C. M., HANSEN, S. V. F., VAN JAARSVELD, M. T. M., PEEPER, D. S., JAFARI SADATMAND, S., ROODHART, J. M. L., VAN DE LEST, C. H. A., ULVEN, T., ISHIHARA, K., MILLIGAN, G. & VOEST, E. E. 2017. Fatty acid 16:4(n-3) stimulates a GPR120-induced signaling cascade in splenic macrophages to promote chemotherapy resistance. *FASEB J,* 31**,** 2195-2209.

HUDSON, B. D., SHIMPUKADE, B., MACKENZIE, A. E., BUTCHER, A. J., PEDIANI, J. D., CHRISTIANSEN, E., HEATHCOTE, H., TOBIN, A. B., ULVEN, T. & MILLIGAN, G. 2013. The pharmacology of TUG-891, a potent and selective agonist of the free fatty acid receptor 4 (FFA4/GPR120),

demonstrates both potential opportunity and possible challenges to therapeutic agonism. *Mol Pharmacol,* 84**,** 710-25.

HUSTED, A. S., EKBERG, J. H., TRIPP, E., NISSEN, T. A. D., MEIJNIKMAN, S., O'BRIEN, S. L., ULVEN, T., ACHERMAN, Y., BRUIN, S. C., NIEUWDORP, M., GERHART-HINES, Z., CALEBIRO, D., DRAGSTED, L. O. & SCHWARTZ, T. W. 2020. Autocrine negative feedback regulation of lipolysis through sensing of NEFAs by FFAR4/GPR120 in WAT. *Mol Metab,* 42**,** 101103.

HUSTED, A. S., TRAUELSEN, M., RUDENKO, O., HJORTH, S. A. & SCHWARTZ, T. W. 2017. GPCR-Mediated Signaling of Metabolites. *Cell Metab,* 25**,** 777-796.

HUTAGALUNG, A. H. & NOVICK, P. J. 2011. Role of Rab GTPases in membrane traffic and cell physiology. *Physiol Rev,* 91**,** 119-49.

HWANG, I. & KIM, J. B. 2019. Two Faces of White Adipose Tissue with Heterogeneous Adipogenic Progenitors. *Diabetes Metab J,* 43**,** 752-762.

ICHIMURA, A., HIRASAWA, A., POULAIN-GODEFROY, O., BONNEFOND, A., HARA, T., YENGO, L., KIMURA, I., LELOIRE, A., LIU, N., IIDA, K., CHOQUET, H., BESNARD, P., LECOEUR, C., VIVEQUIN, S., AYUKAWA, K., TAKEUCHI, M., OZAWA, K., TAUBER, M., MAFFEIS, C., MORANDI, A., BUZZETTI, R., ELLIOTT, P., POUTA, A., JARVELIN, M. R., KORNER, A., KIESS, W., PIGEYRE, M., CAIAZZO, R., VAN HUL, W., VAN GAAL, L., HORBER, F., BALKAU, B., LEVY-MARCHAL, C., ROUSKAS, K., KOUVATSI, A., HEBEBRAND, J., HINNEY, A., SCHERAG, A., PATTOU, F., MEYRE, D., KOSHIMIZU, T. A., WOLOWCZUK, I., TSUJIMOTO, G. & FROGUEL, P. 2012. Dysfunction of lipid sensor GPR120 leads to obesity in both mouse and human. *Nature,* 483**,** 350-4.

ILLENBERGER, D., WALLISER, C., NURNBERG, B., DIAZ LORENTE, M. & GIERSCHIK, P. 2003. Specificity and structural requirements of phospholipase C-beta stimulation by Rho GTPases versus G protein beta gamma dimers. *J Biol Chem,* 278**,** 3006-14.

INOUE, A., RAIMONDI, F., KADJI, F. M. N., SINGH, G., KISHI, T., UWAMIZU, A., ONO, Y., SHINJO, Y., ISHIDA, S., ARANG, N., KAWAKAMI, K., GUTKIND, J. S., AOKI, J. & RUSSELL, R. B. 2019. Illuminating G-Protein-Coupling Selectivity of GPCRs. *Cell,* 177**,** 1933-1947 e25.

IRANNEJAD, R., PESSINO, V., MIKA, D., HUANG, B., WEDEGAERTNER, P. B., CONTI, M. & VON ZASTROW, M. 2017. Functional selectivity of GPCR-directed drug action through location bias. *Nat Chem Biol,* 13**,** 799-806.

IRANNEJAD, R., TOMSHINE, J. C., TOMSHINE, J. R., CHEVALIER, M., MAHONEY, J. P., STEYAERT, J., RASMUSSEN, S. G., SUNAHARA, R. K., EL-SAMAD, H., HUANG, B. & VON ZASTROW, M. 2013. Conformational biosensors reveal GPCR signalling from endosomes. *Nature,* 495**,** 534-8.

ITABE, H., YAMAGUCHI, T., NIMURA, S. & SASABE, N. 2017. Perilipins: a diversity of intracellular lipid droplet proteins. *Lipids Health Dis,* 16**,** 83.

IWASAKI, K., HARADA, N., SASAKI, K., YAMANE, S., IIDA, K., SUZUKI, K., HAMASAKI, A., NASTESKA, D., SHIBUE, K., JOO, E., HARADA, T., HASHIMOTO, T., ASAKAWA, Y., HIRASAWA, A. & INAGAKI, N. 2015. Free fatty acid receptor GPR120 is highly expressed in enteroendocrine K cells of the upper small intestine and has a critical role in GIP secretion after fat ingestion. *Endocrinology,* 156**,** 837-46.

JANETOPOULOS, C., JIN, T. & DEVREOTES, P. 2001. Receptor-mediated activation of heterotrimeric G-proteins in living cells. *Science,* 291**,** 2408-11.

JENKINS, C. M., MANCUSO, D. J., YAN, W., SIMS, H. F., GIBSON, B. & GROSS, R. W. 2004. Identification, cloning, expression, and purification of three novel human calcium-independent phospholipase A2 family members possessing triacylglycerol lipase and acylglycerol transacylase activities. *J Biol Chem,* 279**,** 48968-75.

JENSEN, D. D., LIEU, T., HALLS, M. L., VELDHUIS, N. A., IMLACH, W. L., MAI, Q. N., POOLE, D. P., QUACH, T., AURELIO, L., CONNER, J., HERENBRINK, C. K., BARLOW, N., SIMPSON, J. S., SCANLON, M. J., GRAHAM, B., MCCLUSKEY, A., ROBINSON, P. J., ESCRIOU, V., NASSINI, R., MATERAZZI, S., GEPPETTI, P., HICKS, G. A., CHRISTIE, M. J., PORTER, C. J. H., CANALS, M. &

BUNNETT, N. W. 2017. Neurokinin 1 receptor signaling in endosomes mediates sustained nociception and is a viable therapeutic target for prolonged pain relief. *Sci Transl Med,* 9.

JIANG, L. I., COLLINS, J., DAVIS, R., LIN, K. M., DECAMP, D., ROACH, T., HSUEH, R., REBRES, R. A., ROSS, E. M., TAUSSIG, R., FRASER, I. & STERNWEIS, P. C. 2007. Use of a cAMP BRET sensor to characterize a novel regulation of cAMP by the sphingosine 1-phosphate/G13 pathway. *J Biol Chem,* 282**,** 10576-84.

JIMENEZ-VARGAS, N. N., GONG, J., WISDOM, M. J., JENSEN, D. D., LATORRE, R., HEGRON, A., TENG, S., DICELLO, J. J., RAJASEKHAR, P., VELDHUIS, N. A., CARBONE, S. E., YU, Y., LOPEZ-LOPEZ, C., JARAMILLO-POLANCO, J., CANALS, M., REED, D. E., LOMAX, A. E., SCHMIDT, B. L., LEONG, K. W., VANNER, S. J., HALLS, M. L., BUNNETT, N. W. & POOLE, D. P. 2020. Endosomal signaling of delta opioid receptors is an endogenous mechanism and therapeutic target for relief from inflammatory pain. *Proc Natl Acad Sci U S A,* 117**,** 15281-15292.

JIMENEZ-VARGAS, N. N., PATTISON, L. A., ZHAO, P., LIEU, T., LATORRE, R., JENSEN, D. D., CASTRO, J., AURELIO, L., LE, G. T., FLYNN, B., HERENBRINK, C. K., YEATMAN, H. R., EDGINGTON-MITCHELL, L., PORTER, C. J. H., HALLS, M. L., CANALS, M., VELDHUIS, N. A., POOLE, D. P., MCLEAN, P., HICKS, G. A., SCHEFF, N., CHEN, E., BHATTACHARYA, A., SCHMIDT, B. L., BRIERLEY, S. M., VANNER, S. J. & BUNNETT, N. W. 2018. Protease-activated receptor-2 in endosomes signals persistent pain of irritable bowel syndrome. *Proc Natl Acad Sci U S A,* 115**,** E7438-E7447.

JOHANSSON, S. M., LINDGREN, E., YANG, J. N., HERLING, A. W. & FREDHOLM, B. B. 2008. Adenosine A1 receptors regulate lipolysis and lipogenesis in mouse adipose tissue-interactions with insulin. *Eur J Pharmacol,* 597**,** 92-101.

JONG, Y. I., HARMON, S. K. & O'MALLEY, K. L. 2018. GPCR signalling from within the cell. *Br J Pharmacol,* 175**,** 4026-4035.

JOYAL, J. S., NIM, S., ZHU, T., SITARAS, N., RIVERA, J. C., SHAO, Z., SAPIEHA, P., HAMEL, D., SANCHEZ, M., ZANIOLO, K., ST-LOUIS, M., OUELLETTE, J., MONTOYA-ZAVALA, M., ZABEIDA, A., PICARD, E., HARDY, P., BHOSLE, V., VARMA, D. R., GOBEIL, F., JR., BEAUSEJOUR, C., BOILEAU, C., KLEIN, W., HOLLENBERG, M., RIBEIRO-DA-SILVA, A., ANDELFINGER, G. & CHEMTOB, S. 2014. Subcellular localization of coagulation factor II receptor-like 1 in neurons governs angiogenesis. *Nat Med,* 20**,** 1165-73.

KANG, Y., ZHOU, X. E., GAO, X., HE, Y., LIU, W., ISHCHENKO, A., BARTY, A., WHITE, T. A., YEFANOV, O., HAN, G. W., XU, Q., DE WAAL, P. W., KE, J., TAN, M. H., ZHANG, C., MOELLER, A., WEST, G. M., PASCAL, B. D., VAN EPS, N., CARO, L. N., VISHNIVETSKIY, S. A., LEE, R. J., SUINO-POWELL, K. M., GU, X., PAL, K., MA, J., ZHI, X., BOUTET, S., WILLIAMS, G. J., MESSERSCHMIDT, M., GATI, C., ZATSEPIN, N. A., WANG, D., JAMES, D., BASU, S., ROY-CHOWDHURY, S., CONRAD, C. E., COE, J., LIU, H., LISOVA, S., KUPITZ, C., GROTJOHANN, I., FROMME, R., JIANG, Y., TAN, M., YANG, H., LI, J., WANG, M., ZHENG, Z., LI, D., HOWE, N., ZHAO, Y., STANDFUSS, J., DIEDERICHS, K., DONG, Y., POTTER, C. S., CARRAGHER, B., CAFFREY, M., JIANG, H., CHAPMAN, H. N., SPENCE, J. C., FROMME, P., WEIERSTALL, U., ERNST, O. P., KATRITCH, V., GUREVICH, V. V., GRIFFIN, P. R., HUBBELL, W. L., STEVENS, R. C., CHEREZOV, V., MELCHER, K. & XU, H. E. 2015. Crystal structure of rhodopsin bound to arrestin by femtosecond X-ray laser. *Nature,* 523**,** 561-7.

KANNABIRAN, S. A., GOSEJACOB, D., NIEMANN, B., NIKOLAEV, V. O. & PFEIFER, A. 2020. Real-time monitoring of cAMP in brown adipocytes reveals differential compartment of beta1 and beta3-adrenoceptor signalling. *Mol Metab,* 37**,** 100986.

KAYA, A. I., LOKITS, A. D., GILBERT, J. A., IVERSON, T. M., MEILER, J. & HAMM, H. E. 2014. A conserved phenylalanine as a relay between the alpha5 helix and the GDP binding region of heterotrimeric Gi protein alpha subunit. *J Biol Chem,* 289**,** 24475-87.

KERSHAW, E. E. & FLIER, J. S. 2004. Adipose tissue as an endocrine organ. *J Clin Endocrinol Metab,* 89**,** 2548-56.

KHANDELIA, H., DUELUND, L., PAKKANEN, K. I. & IPSEN, J. H. 2010. Triglyceride blisters in lipid bilayers: implications for lipid droplet biogenesis and the mobile lipid signal in cancer cell membranes. *PLoS One,* 5**,** e12811.

KIM, C., CHENG, C. Y., SALDANHA, S. A. & TAYLOR, S. S. 2007. PKA-I holoenzyme structure reveals a mechanism for cAMP-dependent activation. *Cell,* 130**,** 1032-43.

KIM, S. J., TANG, T., ABBOTT, M., VISCARRA, J. A., WANG, Y. & SUL, H. S. 2016. AMPK Phosphorylates Desnutrin/ATGL and Hormone-Sensitive Lipase To Regulate Lipolysis and Fatty Acid Oxidation within Adipose Tissue. *Mol Cell Biol,* 36**,** 1961-76.

KIM, T. H., CHUNG, K. Y., MANGLIK, A., HANSEN, A. L., DROR, R. O., MILDORF, T. J., SHAW, D. E., KOBILKA, B. K. & PROSSER, R. S. 2013. The role of ligands on the equilibria between functional states of a G protein-coupled receptor. *J Am Chem Soc,* 135**,** 9465-74.

KIMURA, I., ICHIMURA, A., OHUE-KITANO, R. & IGARASHI, M. 2020. Free Fatty Acid Receptors in Health and Disease. *Physiol Rev,* 100**,** 171-210.

KINNEY, B. P., QIAO, L., LEVAUGH, J. M. & SHAO, J. 2010. B56alpha/protein phosphatase 2A inhibits adipose lipolysis in high-fat diet-induced obese mice. *Endocrinology,* 151**,** 3624-32.

KINSEY, C. G., BUSSOLATI, G., BOSCO, M., KIMURA, T., PIZZORNO, M. C., CHERNIN, M. I., CASSONI, P. & NOVAK, J. F. 2007. Constitutive and ligand-induced nuclear localization of oxytocin receptor. *J Cell Mol Med,* 11**,** 96-110.

KITAMURA, T., KITAMURA, Y., KURODA, S., HINO, Y., ANDO, M., KOTANI, K., KONISHI, H., MATSUZAKI, H., KIKKAWA, U., OGAWA, W. & KASUGA, M. 1999. Insulin-induced phosphorylation and activation of cyclic nucleotide phosphodiesterase 3B by the serine-threonine kinase Akt. *Mol Cell Biol,* 19**,** 6286-96.

KLARENBEEK, J. B., GOEDHART, J., HINK, M. A., GADELLA, T. W. & JALINK, K. 2011. A mTurquoise-based cAMP sensor for both FLIM and ratiometric read-out has improved dynamic range. *PLoS One,* 6**,** e19170.

KOCH, W. J., INGLESE, J., STONE, W. C. & LEFKOWITZ, R. J. 1993. The binding site for the beta gamma subunits of heterotrimeric G proteins on the beta-adrenergic receptor kinase. *J Biol Chem,* 268**,** 8256-60.

KOFUKU, Y., UEDA, T., OKUDE, J., SHIRAISHI, Y., KONDO, K., MAEDA, M., TSUJISHITA, H. & SHIMADA, I. 2012. Efficacy of the beta(2)-adrenergic receptor is determined by conformational equilibrium in the transmembrane region. *Nat Commun,* 3**,** 1045.

KOREN, S., DIPILATO, L. M., EMMETT, M. J., SHEARIN, A. L., CHU, Q., MONKS, B. & BIRNBAUM, M. J. 2015. The role of mouse Akt2 in insulin-dependent suppression of adipocyte lipolysis in vivo. *Diabetologia,* 58**,** 1063-70.

KOTOWSKI, S. J., HOPF, F. W., SEIF, T., BONCI, A. & VON ZASTROW, M. 2011. Endocytosis promotes rapid dopaminergic signaling. *Neuron,* 71**,** 278-90.

KRUPNICK, J. G. & BENOVIC, J. L. 1998. The role of receptor kinases and arrestins in G protein-coupled receptor regulation. *Annu Rev Pharmacol Toxicol,* 38**,** 289-319.

KUNA, R. S., GIRADA, S. B., ASALLA, S., VALLENTYNE, J., MADDIKA, S., PATTERSON, J. T., SMILEY, D. L., DIMARCHI, R. D. & MITRA, P. 2013. Glucagon-like peptide-1 receptor-mediated endosomal cAMP generation promotes glucose-stimulated insulin secretion in pancreatic beta-cells. *Am J Physiol Endocrinol Metab,* 305**,** E161-70.

KUNSELMAN, J. M., GUPTA, A., GOMES, I., DEVI, L. A. & PUTHENVEEDU, M. A. 2021. Compartment-specific opioid receptor signaling is selectively modulated by different dynorphin peptides. *Elife,* 10.

LAGERSTROM, M. C. & SCHIOTH, H. B. 2008. Structural diversity of G protein-coupled receptors and significance for drug discovery. *Nat Rev Drug Discov,* 7**,** 339-57.

LAMRI, A., BONNEFOND, A., MEYRE, D., BALKAU, B., ROUSSEL, R., MARRE, M., FROGUEL, P., FUMERON, F. & GROUP, D. E. S. I. R. S. 2016. Interaction between GPR120 p.R270H loss-of-function variant and dietary fat intake on incident type 2 diabetes risk in the D.E.S.I.R. study. *Nutr Metab Cardiovasc Dis,* 26**,** 931-6.

LAN, T. H., KURAVI, S. & LAMBERT, N. A. 2011. Internalization dissociates beta2-adrenergic receptors. *PLoS One,* 6**,** e17361.

LAN, T. H., LIU, Q., LI, C., WU, G. & LAMBERT, N. A. 2012. Sensitive and high resolution localization and tracking of membrane proteins in live cells with BRET. *Traffic,* 13**,** 1450-6.

LASS, A., ZIMMERMANN, R., HAEMMERLE, G., RIEDERER, M., SCHOISWOHL, G., SCHWEIGER, M., KIENESBERGER, P., STRAUSS, J. G., GORKIEWICZ, G. & ZECHNER, R. 2006. Adipose triglyceride lipase-mediated lipolysis of cellular fat stores is activated by CGI-58 and defective in Chanarin-Dorfman Syndrome. *Cell Metab,* 3**,** 309-19.

LAZAR, A. M., IRANNEJAD, R., BALDWIN, T. A., SUNDARAM, A. B., GUTKIND, J. S., INOUE, A., DESSAUER, C. W. & VON ZASTROW, M. 2020. G protein-regulated endocytic trafficking of adenylyl cyclase type 9. *Elife,* 9.

LEBON, G., WARNE, T., EDWARDS, P. C., BENNETT, K., LANGMEAD, C. J., LESLIE, A. G. & TATE, C. G. 2011. Agonist-bound adenosine A2A receptor structures reveal common features of GPCR activation. *Nature,* 474**,** 521-5.

LEE, S. H., PARK, S. Y. & CHOI, C. S. 2022. Insulin Resistance: From Mechanisms to Therapeutic Strategies. *Diabetes Metab J,* 46**,** 15-37.

LEITNER, B. P., HUANG, S., BRYCHTA, R. J., DUCKWORTH, C. J., BASKIN, A. S., MCGEHEE, S., TAL, I., DIECKMANN, W., GUPTA, G., KOLODNY, G. M., PACAK, K., HERSCOVITCH, P., CYPESS, A. M. & CHEN, K. Y. 2017. Mapping of human brown adipose tissue in lean and obese young men. *Proc Natl Acad Sci U S A,* 114**,** 8649-8654.

LI, H., LI, H. F., FELDER, R. A., PERIASAMY, A. & JOSE, P. A. 2008. Rab4 and Rab11 coordinately regulate the recycling of angiotensin II type I receptor as demonstrated by fluorescence resonance energy transfer microscopy. *J Biomed Opt,* 13**,** 031206.

LI, L. O., KLETT, E. L. & COLEMAN, R. A. 2010a. Acyl-CoA synthesis, lipid metabolism and lipotoxicity. *Biochim Biophys Acta,* 1801**,** 246-51.

LI, Y., LI, Z., NGANDIRI, D. A., LLERINS PEREZ, M., WOLF, A. & WANG, Y. 2022. The Molecular Brakes of Adipose Tissue Lipolysis. *Front Physiol,* 13**,** 826314.

LI, Y., WANG, G., LIN, K., YIN, H., ZHOU, C., LIU, T., WU, G. & QIAN, G. 2010b. Rab1 GTPase promotes expression of beta-adrenergic receptors in rat pulmonary microvascular endothelial cells. *Int J Biochem Cell Biol,* 42**,** 1201-1209.

LISSANDRON, V., TERRIN, A., COLLINI, M., D'ALFONSO, L., CHIRICO, G., PANTANO, S. & ZACCOLO, M. 2005. Improvement of a FRET-based indicator for cAMP by linker design and stabilization of donor-acceptor interaction. *J Mol Biol,* 354**,** 546-55.

LIU, D., WANG, L., MENG, Q., KUANG, H. & LIU, X. 2012a. G-protein coupled receptor 120 is involved in glucose metabolism in fat cells. *Cellular and Molecular Biology,* 58**,** 1757-62.

LIU, J. J., HORST, R., KATRITCH, V., STEVENS, R. C. & WUTHRICH, K. 2012b. Biased signaling pathways in beta2-adrenergic receptor characterized by 19F-NMR. *Science,* 335**,** 1106-10.

LIU, P., BARTZ, R., ZEHMER, J. K., YING, Y. S., ZHU, M., SERRERO, G. & ANDERSON, R. G. 2007. Rab-regulated interaction of early endosomes with lipid droplets. *Biochim Biophys Acta,* 1773**,** 784-93.

LIZASO, A., TAN, K. T. & LEE, Y. H. 2013. beta-adrenergic receptor-stimulated lipolysis requires the RAB7-mediated autolysosomal lipid degradation. *Autophagy,* 9**,** 1228-43.

LOGOTHETIS, D. E., KURACHI, Y., GALPER, J., NEER, E. J. & CLAPHAM, D. E. 1987. The beta gamma subunits of GTP-binding proteins activate the muscarinic K+ channel in heart. *Nature,* 325**,** 321-6.

LUCEY, M., ASHIK, T., MARZOOK, A., WANG, Y., GOULDING, J., OISHI, A., BROICHHAGEN, J., HODSON, D. J., MINNION, J., ELANI, Y., JOCKERS, R., BRIDDON, S. J., BLOOM, S. R., TOMAS, A. & JONES, B. 2021. Acylation of the Incretin Peptide Exendin-4 Directly Impacts Glucagon-Like Peptide-1 Receptor Signaling and Trafficking. *Mol Pharmacol,* 100**,** 319-334.

LUO, L. & LIU, M. 2016. Adipose tissue in control of metabolism. *J Endocrinol,* 231**,** R77-R99.

LUTTRELL, L. M., DELLA ROCCA, G. J., VAN BIESEN, T., LUTTRELL, D. K. & LEFKOWITZ, R. J. 1997. Gbetagamma subunits mediate Src-dependent phosphorylation of the epidermal growth factor receptor. A scaffold for G protein-coupled receptor-mediated Ras activation. *J Biol Chem,* 272**,** 4637-44.

LUTTRELL, L. M., FERGUSON, S. S., DAAKA, Y., MILLER, W. E., MAUDSLEY, S., DELLA ROCCA, G. J., LIN, F., KAWAKATSU, H., OWADA, K., LUTTRELL, D. K., CARON, M. G. & LEFKOWITZ, R. J. 1999. Beta-arrestin-dependent formation of beta2 adrenergic receptor-Src protein kinase complexes. *Science,* 283**,** 655-61.

LYGA, S., VOLPE, S., WERTHMANN, R. C., GOTZ, K., SUNGKAWORN, T., LOHSE, M. J. & CALEBIRO, D. 2016. Persistent cAMP Signaling by Internalized LH Receptors in Ovarian Follicles. *Endocrinology,* 157**,** 1613-21.

MAHMUD, Z. A., JENKINS, L., ULVEN, T., LABEGUERE, F., GOSMINI, R., DE VOS, S., HUDSON, B. D., TIKHONOVA, I. G. & MILLIGAN, G. 2017. Three classes of ligands each bind to distinct sites on the orphan G protein-coupled receptor GPR84. *Sci Rep,* 7**,** 17953.

MAHONEY, J. P. & SUNAHARA, R. K. 2016. Mechanistic insights into GPCR-G protein interactions. *Curr Opin Struct Biol,* 41**,** 247-254.

MAI, Q. N., SHENOY, P., QUACH, T., RETAMAL, J. S., GONDIN, A. B., YEATMAN, H. R., AURELIO, L., CONNER, J. W., POOLE, D. P., CANALS, M., NOWELL, C. J., GRAHAM, B., DAVIS, T. P., BRIDDON, S. J., HILL, S. J., PORTER, C. J. H., BUNNETT, N. W., HALLS, M. L. & VELDHUIS, N. A. 2021. A lipid-anchored neurokinin 1 receptor antagonist prolongs pain relief by a three-pronged mechanism of action targeting the receptor at the plasma membrane and in endosomes. *J Biol Chem,* 296**,** 100345.

MANDL, M., RITTHAMMER, H., EJAZ, A., WAGNER, S. A., HATZMANN, F. M., BAUMGARTEN, S., VIERTLER, H. P., ZWIERZINA, M. E., MATTESICH, M., SCHILLER, V., RAUCHENWALD, T., PLONER, C., WALDEGGER, P., PIERER, G. & ZWERSCHKE, W. 2020. CRISPR/Cas9-mediated gene knockout in human adipose stem/progenitor cells. *Adipocyte,* 9**,** 626-635.

MANGLIK, A., KIM, T. H., MASUREEL, M., ALTENBACH, C., YANG, Z., HILGER, D., LERCH, M. T., KOBILKA, T. S., THIAN, F. S., HUBBELL, W. L., PROSSER, R. S. & KOBILKA, B. K. 2015. Structural Insights into the Dynamic Process of beta2-Adrenergic Receptor Signaling. *Cell,* 161**,** 1101-11.

MANOLOPOULOS, K. N., KARPE, F. & FRAYN, K. N. 2010. Gluteofemoral body fat as a determinant of metabolic health. *Int J Obes (Lond),* 34**,** 949-59.

MASUHO, I., OSTROVSKAYA, O., KRAMER, G. M., JONES, C. D., XIE, K. & MARTEMYANOV, K. A. 2015. Distinct profiles of functional discrimination among G proteins determine the actions of G protein-coupled receptors. *Sci Signal,* 8**,** ra123.

MATTHEES, E. S. F., HAIDER, R. S., HOFFMANN, C. & DRUBE, J. 2021. Differential Regulation of GPCRs-Are GRK Expression Levels the Key? *Front Cell Dev Biol,* 9**,** 687489.

MATTHIESEN, K. & NIELSEN, J. 2011. Cyclic AMP control measured in two compartments in HEK293 cells: phosphodiesterase K(M) is more important than phosphodiesterase localization. *PLoS One,* 6**,** e24392.

MAURIEGE, P., GALITZKY, J., BERLAN, M. & LAFONTAN, M. 1987. Heterogeneous distribution of beta and alpha-2 adrenoceptor binding sites in human fat cells from various fat deposits: functional consequences. *Eur J Clin Invest,* 17**,** 156-65.

MAZIARZ, M., PARK, J. C., LEYME, A., MARIVIN, A., GARCIA-LOPEZ, A., PATEL, P. P. & GARCIA-MARCOS, M. 2020. Revealing the Activity of Trimeric G-proteins in Live Cells with a Versatile Biosensor Design. *Cell,* 182**,** 770-785 e16.

MCCLUSKEY, A., DANIEL, J. A., HADZIC, G., CHAU, N., CLAYTON, E. L., MARIANA, A., WHITING, A., GORGANI, N. N., LLOYD, J., QUAN, A., MOSHKANBARYANS, L., KRISHNAN, S., PERERA, S., CHIRCOP, M., VON KLEIST, L., MCGEACHIE, A. B., HOWES, M. T., PARTON, R. G., CAMPBELL, M., SAKOFF, J. A., WANG, X., SUN, J. Y., ROBERTSON, M. J., DEANE, F. M., NGUYEN, T. H.,

MEUNIER, F. A., COUSIN, M. A. & ROBINSON, P. J. 2013. Building a better dynasore: the dyngo compounds potently inhibit dynamin and endocytosis. *Traffic,* 14**,** 1272-89.

MCCREATH, K. J., ESPADA, S., GALVEZ, B. G., BENITO, M., DE MOLINA, A., SEPULVEDA, P. & CERVERA, A. M. 2015. Targeted disruption of the SUCNR1 metabolic receptor leads to dichotomous effects on obesity. *Diabetes,* 64**,** 1154-67.

MERKLE, F. T., NEUHAUSSER, W. M., SANTOS, D., VALEN, E., GAGNON, J. A., MAAS, K., SANDOE, J., SCHIER, A. F. & EGGAN, K. 2015. Efficient CRISPR-Cas9-mediated generation of knockin human pluripotent stem cells lacking undesired mutations at the targeted locus. *Cell Rep,* 11**,** 875-883.

MERRIAM, L. A., BARAN, C. N., GIRARD, B. M., HARDWICK, J. C., MAY, V. & PARSONS, R. L. 2013. Pituitary adenylate cyclase 1 receptor internalization and endosomal signaling mediate the pituitary adenylate cyclase activating polypeptide-induced increase in guinea pig cardiac neuron excitability. *J Neurosci,* 33**,** 4614-22.

MILLIGAN, G., ALVAREZ-CURTO, E., HUDSON, B. D., PRIHANDOKO, R. & TOBIN, A. B. 2017a. FFA4/GPR120: Pharmacology and Therapeutic Opportunities. *Trends Pharmacol Sci,* 38**,** 809-821.

MILLIGAN, G., SHIMPUKADE, B., ULVEN, T. & HUDSON, B. D. 2017b. Complex Pharmacology of Free Fatty Acid Receptors. *Chem Rev,* 117**,** 67-110.

MISTRY, J. J., HELLMICH, C., MOORE, J. A., JIBRIL, A., MACAULAY, I., MORENO-GONZALEZ, M., DI PALMA, F., BERAZA, N., BOWLES, K. M. & RUSHWORTH, S. A. 2021. Free fatty-acid transport via CD36 drives beta-oxidation-mediated hematopoietic stem cell response to infection. *Nat Commun,* 12**,** 7130.

MIYAMOTO, J., HASEGAWA, S., KASUBUCHI, M., ICHIMURA, A., NAKAJIMA, A. & KIMURA, I. 2016. Nutritional Signaling via Free Fatty Acid Receptors. *Int J Mol Sci,* 17**,** 450.

MONTGOMERY, M. K., OSBORNE, B., BRANDON, A. E., O'REILLY, L., FIVEASH, C. E., BROWN, S. H. J., WILKINS, B. P., SAMSUDEEN, A., YU, J., DEVANAPALLI, B., HERTZOG, A., TOLUN, A. A., KAVANAGH, T., COOPER, A. A., MITCHELL, T. W., BIDEN, T. J., SMITH, N. J., COONEY, G. J. & TURNER, N. 2019. Regulation of mitochondrial metabolism in murine skeletal muscle by the medium-chain fatty acid receptor Gpr84. *FASEB J,* 33**,** 12264-12276.

MOORE, A. S., COSCIA, S. M., SIMPSON, C. L., ORTEGA, F. E., WAIT, E. C., HEDDLESTON, J. M., NIRSCHL, J. J., OBARA, C. J., GUEDES-DIAS, P., BOECKER, C. A., CHEW, T. L., THERIOT, J. A., LIPPINCOTT-SCHWARTZ, J. & HOLZBAUR, E. L. F. 2021. Actin cables and comet tails organize mitochondrial networks in mitosis. *Nature,* 591**,** 659-664.

MOORE, B. S., STEPANCHICK, A. N., TEWSON, P. H., HARTLE, C. M., ZHANG, J., QUINN, A. M., HUGHES, T. E. & MIRSHAHI, T. 2016. Cilia have high cAMP levels that are inhibited by Sonic Hedgehog-regulated calcium dynamics. *Proc Natl Acad Sci U S A,* 113**,** 13069-13074.

MORRISON, S. & MCGEE, S. L. 2015. 3T3-L1 adipocytes display phenotypic characteristics of multiple adipocyte lineages. *Adipocyte,* 4**,** 295-302.

MOTTILLO, E. P. & GRANNEMAN, J. G. 2011. Intracellular fatty acids suppress beta-adrenergic induction of PKA-targeted gene expression in white adipocytes. *Am J Physiol Endocrinol Metab,* 301**,** E122-31.

MOTTILLO, E. P. & GRANNEMAN, J. G. 2022. Fluorescent and Luminescent Methods to Detect Lipolysis. *Methods Mol Biol,* 2448**,** 97-106.

MOTTILLO, E. P., ZHANG, H., YANG, A., ZHOU, L. & GRANNEMAN, J. G. 2019. Genetically-encoded sensors to detect fatty acid production and trafficking. *Mol Metab,* 29**,** 55-64.

MUCCIOLI, G., PONS, N., GHE, C., CATAPANO, F., GRANATA, R. & GHIGO, E. 2004. Ghrelin and des-acyl ghrelin both inhibit isoproterenol-induced lipolysis in rat adipocytes via a non-type 1a growth hormone secretagogue receptor. *Eur J Pharmacol,* 498**,** 27-35.

MUNK, C., MUTT, E., ISBERG, V., NIKOLAJSEN, L. F., BIBBE, J. M., FLOCK, T., HANSON, M. A., STEVENS, R. C., DEUPI, X. & GLORIAM, D. E. 2019. An online resource for GPCR structure determination and analysis. *Nat Methods,* 16**,** 151-162.

NAGASAKI, H., KONDO, T., FUCHIGAMI, M., HASHIMOTO, H., SUGIMURA, Y., OZAKI, N., ARIMA, H., OTA, A., OISO, Y. & HAMADA, Y. 2012. Inflammatory changes in adipose tissue enhance expression of GPR84, a medium-chain fatty acid receptor: TNFalpha enhances GPR84 expression in adipocytes. *FEBS Lett,* 586**,** 368-72.

NAGY, H. M., PAAR, M., HEIER, C., MOUSTAFA, T., HOFER, P., HAEMMERLE, G., LASS, A., ZECHNER, R., OBERER, M. & ZIMMERMANN, R. 2014. Adipose triglyceride lipase activity is inhibited by long-chain acyl-coenzyme A. *Biochim Biophys Acta,* 1841**,** 588-94.

NASH, C. A., WEI, W., IRANNEJAD, R. & SMRCKA, A. V. 2019. Golgi localized beta1-adrenergic receptors stimulate Golgi PI4P hydrolysis by PLCepsilon to regulate cardiac hypertrophy. *Elife,* 8.

NEHME, R., CARPENTER, B., SINGHAL, A., STREGE, A., EDWARDS, P. C., WHITE, C. F., DU, H., GRISSHAMMER, R. & TATE, C. G. 2017. Mini-G proteins: Novel tools for studying GPCRs in their active conformation. *PLoS One,* 12**,** e0175642.

NELSON, C. D., PERRY, S. J., REGIER, D. S., PRESCOTT, S. M., TOPHAM, M. K. & LEFKOWITZ, R. J. 2007. Targeting of diacylglycerol degradation to M1 muscarinic receptors by beta-arrestins. *Science,* 315**,** 663-6.

NEVO-YASSAF, I., YAFFE, Y., ASHER, M., RAVID, O., EIZENBERG, S., HENIS, Y. I., NAHMIAS, Y., HIRSCHBERG, K. & SKLAN, E. H. 2012. Role for TBC1D20 and Rab1 in hepatitis C virus replication via interaction with lipid droplet-bound nonstructural protein 5A. *J Virol,* 86**,** 6491-502.

NGUYEN, A. H., THOMSEN, A. R. B., CAHILL, T. J., 3RD, HUANG, R., HUANG, L. Y., MARCINK, T., CLARKE, O. B., HEISSEL, S., MASOUDI, A., BEN-HAIL, D., SAMAAN, F., DANDEY, V. P., TAN, Y. Z., HONG, C., MAHONEY, J. P., TRIEST, S., LITTLE, J. T., CHEN, X., SUNAHARA, R., STEYAERT, J., MOLINA, H., YU, Z., DES GEORGES, A. & LEFKOWITZ, R. J. 2019. Structure of an endosomal signaling GPCR-G protein-beta-arrestin megacomplex. *Nat Struct Mol Biol,* 26**,** 1123-1131.

NIKOLAEV, V. O., BUNEMANN, M., HEIN, L., HANNAWACKER, A. & LOHSE, M. J. 2004. Novel single chain cAMP sensors for receptor-induced signal propagation. *J Biol Chem,* 279**,** 37215-8.

NISHI, H., HIGASHIHARA, T. & INAGI, R. 2019. Lipotoxicity in Kidney, Heart, and Skeletal Muscle Dysfunction. *Nutrients,* 11.

NOEL, J. P., HAMM, H. E. & SIGLER, P. B. 1993. The 2.2 A crystal structure of transducin-alpha complexed with GTP gamma S. *Nature,* 366**,** 654-63.

NYGAARD, R., ZOU, Y., DROR, R. O., MILDORF, T. J., ARLOW, D. H., MANGLIK, A., PAN, A. C., LIU, C. W., FUNG, J. J., BOKOCH, M. P., THIAN, F. S., KOBILKA, T. S., SHAW, D. E., MUELLER, L., PROSSER, R. S. & KOBILKA, B. K. 2013. The dynamic process of beta(2)-adrenergic receptor activation. *Cell,* 152**,** 532-42.

O'BRIEN, S. L., JOHNSTONE, E. K. M., DEVOST, D., CONROY, J., REICHELT, M. E., PURDUE, B. W., AYOUB, M. A., KAWAI, T., INOUE, A., EGUCHI, S., HEBERT, T. E., PFLEGER, K. D. G. & THOMAS, W. G. 2018. BRET-based assay to monitor EGFR transactivation by the AT1R reveals Gq/11 protein-independent activation and AT1R-EGFR complexes. *Biochem Pharmacol,* 158**,** 232-242.

O'HAYRE, M., EICHEL, K., AVINO, S., ZHAO, X., STEFFEN, D. J., FENG, X., KAWAKAMI, K., AOKI, J., MESSER, K., SUNAHARA, R., INOUE, A., VON ZASTROW, M. & GUTKIND, J. S. 2017. Genetic evidence that beta-arrestins are dispensable for the initiation of beta2-adrenergic receptor signaling to ERK. *Sci Signal,* 10.

OH, D. Y., TALUKDAR, S., BAE, E. J., IMAMURA, T., MORINAGA, H., FAN, W., LI, P., LU, W. J., WATKINS, S. M. & OLEFSKY, J. M. 2010. GPR120 is an omega-3 fatty acid receptor mediating potent anti-inflammatory and insulin-sensitizing effects. *Cell,* 142**,** 687-98.

OH, D. Y. & WALENTA, E. 2014. Omega-3 Fatty Acids and FFAR4. *Front Endocrinol (Lausanne),* 5**,** 115.

OH, D. Y., WALENTA, E., AKIYAMA, T. E., LAGAKOS, W. S., LACKEY, D., PESSENTHEINER, A. R., SASIK, R., HAH, N., CHI, T. J., COX, J. M., POWELS, M. A., DI SALVO, J., SINZ, C., WATKINS, S. M., ARMANDO, A. M., CHUNG, H., EVANS, R. M., QUEHENBERGER, O., MCNELIS, J., BOGNER-

STRAUSS, J. G. & OLEFSKY, J. M. 2014. A Gpr120-selective agonist improves insulin resistance and chronic inflammation in obese mice. *Nat Med,* 20**,** 942-7.

OKASHAH, N., WAN, Q., GHOSH, S., SANDHU, M., INOUE, A., VAIDEHI, N. & LAMBERT, N. A. 2019. Variable G protein determinants of GPCR coupling selectivity. *Proceedings of the National Academy of Sciences*.

OKUMURA, T., HARADA, K., OUE, K., ZHANG, J., ASANO, S., HAYASHIUCHI, M., MIZOKAMI, A., TANAKA, H., IRIFUNE, M., KAMATA, N., HIRATA, M. & KANEMATSU, T. 2014. Phospholipase C-related catalytically inactive protein (PRIP) regulates lipolysis in adipose tissue by modulating the phosphorylation of hormone-sensitive lipase. *PLoS One,* 9**,** e100559.

OLDHAM, W. M., VAN EPS, N., PREININGER, A. M., HUBBELL, W. L. & HAMM, H. E. 2006. Mechanism of the receptor-catalyzed activation of heterotrimeric G proteins. *Nat Struct Mol Biol,* 13**,** 772-7.

OLZMANN, J. A. & CARVALHO, P. 2019. Dynamics and functions of lipid droplets. *Nat Rev Mol Cell Biol,* 20**,** 137-155.

PAKHARUKOVA, N., MASOUDI, A., PANI, B., STAUS, D. P. & LEFKOWITZ, R. J. 2020. Allosteric activation of proto-oncogene kinase Src by GPCR-beta-arrestin complexes. *J Biol Chem,* 295**,** 16773-16784.

PALCZEWSKI, K., KUMASAKA, T., HORI, T., BEHNKE, C. A., MOTOSHIMA, H., FOX, B. A., LE TRONG, I., TELLER, D. C., OKADA, T., STENKAMP, R. E., YAMAMOTO, M. & MIYANO, M. 2000. Crystal structure of rhodopsin: A G protein-coupled receptor. *Science,* 289**,** 739-45.

PAPACKOVA, Z. & CAHOVA, M. 2015. Fatty acid signaling: the new function of intracellular lipases. *Int J Mol Sci,* 16**,** 3831-55.

PARAMONOV, V. M., MAMAEVA, V., SAHLGREN, C. & RIVERO-MULLER, A. 2015. Genetically-encoded tools for cAMP probing and modulation in living systems. *Front Pharmacol,* 6**,** 196.

PARDO, F., VILLALOBOS-LABRA, R., CHIARELLO, D. I., SALSOSO, R., TOLEDO, F., GUTIERREZ, J., LEIVA, A. & SOBREVIA, L. 2017. Molecular implications of adenosine in obesity. *Mol Aspects Med,* 55**,** 90-101.

PERRY, S. J., BAILLIE, G. S., KOHOUT, T. A., MCPHEE, I., MAGIERA, M. M., ANG, K. L., MILLER, W. E., MCLEAN, A. J., CONTI, M., HOUSLAY, M. D. & LEFKOWITZ, R. J. 2002. Targeting of cyclic AMP degradation to beta 2-adrenergic receptors by beta-arrestins. *Science,* 298**,** 834-6.

PETERS, A., RABE, P., KRUMBHOLZ, P., KALWA, H., KRAFT, R., SCHONEBERG, T. & STAUBERT, C. 2020. Natural biased signaling of hydroxycarboxylic acid receptor 3 and G protein-coupled receptor 84. *Cell Commun Signal,* 18**,** 31.

PFLEGER, K. D. G., SEEBER, R. M. & EIDNE, K. A. 2006. Bioluminescence resonance energy transfer (BRET) for the real-time detection of protein-protein interactions. *Nature Protocols,* 1**,** 337-345.

PIERCE, K. L., PREMONT, R. T. & LEFKOWITZ, R. J. 2002. Seven-transmembrane receptors. *Nat Rev Mol Cell Biol,* 3**,** 639-50.

PINKOSKY, S. L., SCOTT, J. W., DESJARDINS, E. M., SMITH, B. K., DAY, E. A., FORD, R. J., LANGENDORF, C. G., LING, N. X. Y., NERO, T. L., LOH, K., GALIC, S., HOQUE, A., SMILES, W. J., NGOEI, K. R. W., PARKER, M. W., YAN, Y., MELCHER, K., KEMP, B. E., OAKHILL, J. S. & STEINBERG, G. R. 2020. Long-chain fatty acyl-CoA esters regulate metabolism via allosteric control of AMPK beta1 isoforms. *Nat Metab,* 2**,** 873-881.

PITCHER, J., LOHSE, M. J., CODINA, J., CARON, M. G. & LEFKOWITZ, R. J. 1992a. Desensitization of the isolated beta 2-adrenergic receptor by beta-adrenergic receptor kinase, cAMP-dependent protein kinase, and protein kinase C occurs via distinct molecular mechanisms. *Biochemistry,* 31**,** 3193-7.

PITCHER, J. A., INGLESE, J., HIGGINS, J. B., ARRIZA, J. L., CASEY, P. J., KIM, C., BENOVIC, J. L., KWATRA, M. M., CARON, M. G. & LEFKOWITZ, R. J. 1992b. Role of beta gamma subunits of G proteins in targeting the beta-adrenergic receptor kinase to membrane-bound receptors. *Science,* 257**,** 1264-7.

PONSIOEN, B., ZHAO, J., RIEDL, J., ZWARTKRUIS, F., VAN DER KROGT, G., ZACCOLO, M., MOOLENAAR, W. H., BOS, J. L. & JALINK, K. 2004. Detecting cAMP-induced Epac activation by fluorescence resonance energy transfer: Epac as a novel cAMP indicator. *EMBO Rep,* 5**,** 1176-80.

PRETA, G., CRONIN, J. G. & SHELDON, I. M. 2015. Dynasore - not just a dynamin inhibitor. *Cell Commun Signal,* 13**,** 24.

PRIHANDOKO, R., ALVAREZ-CURTO, E., HUDSON, B. D., BUTCHER, A. J., ULVEN, T., MILLER, A. M., TOBIN, A. B. & MILLIGAN, G. 2016. Distinct Phosphorylation Clusters Determine the Signaling Outcome of Free Fatty Acid Receptor 4/G Protein-Coupled Receptor 120. *Mol Pharmacol,* 89**,** 505-20.

PRIHANDOKO, R., KAUR, D., WIEGMAN, C. H., ALVAREZ-CURTO, E., DONOVAN, C., CHACHI, L., ULVEN, T., TYAS, M. R., EUSTON, E., DONG, Z., ALHARBI, A. G. M., KIM, R. Y., LOWE, J. G., HANSBRO, P. M., CHUNG, K. F., BRIGHTLING, C. E., MILLIGAN, G. & TOBIN, A. B. 2020. Pathophysiological regulation of lung function by the free fatty acid receptor FFA4. *Sci Transl Med,* 12.

PRINZ, A., DISKAR, M., ERLBRUCH, A. & HERBERG, F. W. 2006. Novel, isotype-specific sensors for protein kinase A subunit interaction based on bioluminescence resonance energy transfer (BRET). *Cell Signal,* 18**,** 1616-25.

PURI, N. M., ROMANO, G. R., LIN, T. Y., MAI, Q. N. & IRANNEJAD, R. 2022. The organic cation transporter 2 regulates dopamine D1 receptor signaling at the Golgi apparatus. *Elife,* 11.

QI, C., LAVRIHA, P., MEHTA, V., KHANPPNAVAR, B., MOHAMMED, I., LI, Y., LAZARATOS, M., SCHAEFER, J. V., DREIER, B., PLUCKTHUN, A., BONDAR, A. N., DESSAUER, C. W. & KORKHOV, V. M. 2022. Structural basis of adenylyl cyclase 9 activation. *Nat Commun,* 13**,** 1045.

QIAO, L., KINNEY, B., SCHAACK, J. & SHAO, J. 2011. Adiponectin inhibits lipolysis in mouse adipocytes. *Diabetes,* 60**,** 1519-27.

QUESADA-LOPEZ, T., CEREIJO, R., TURATSINZE, J. V., PLANAVILA, A., CAIRO, M., GAVALDA-NAVARRO, A., PEYROU, M., MOURE, R., IGLESIAS, R., GIRALT, M., EIZIRIK, D. L. & VILLARROYA, F. 2016. The lipid sensor GPR120 promotes brown fat activation and FGF21 release from adipocytes. *Nat Commun,* 7**,** 13479.

QUESADA-LOPEZ, T., GAVALDA-NAVARRO, A., MORON-ROS, S., CAMPDERROS, L., IGLESIAS, R., GIRALT, M. & VILLARROYA, F. 2019. GPR120 controls neonatal brown adipose tissue thermogenic induction. *Am J Physiol Endocrinol Metab,* 317**,** E742-E750.

RASMUSSEN, S. G., DEVREE, B. T., ZOU, Y., KRUSE, A. C., CHUNG, K. Y., KOBILKA, T. S., THIAN, F. S., CHAE, P. S., PARDON, E., CALINSKI, D., MATHIESEN, J. M., SHAH, S. T., LYONS, J. A., CAFFREY, M., GELLMAN, S. H., STEYAERT, J., SKINIOTIS, G., WEIS, W. I., SUNAHARA, R. K. & KOBILKA, B. K. 2011. Crystal structure of the beta2 adrenergic receptor-Gs protein complex. *Nature,* 477**,** 549-55.

RE, M., PAMPILLO, M., SAVARD, M., DUBUC, C., MCARDLE, C. A., MILLAR, R. P., CONN, P. M., GOBEIL, F., JR., BHATTACHARYA, M. & BABWAH, A. V. 2010. The human gonadotropin releasing hormone type I receptor is a functional intracellular GPCR expressed on the nuclear membrane. *PLoS One,* 5**,** e11489.

RESHEF, L., OLSWANG, Y., CASSUTO, H., BLUM, B., CRONIGER, C. M., KALHAN, S. C., TILGHMAN, S. M. & HANSON, R. W. 2003. Glyceroneogenesis and the triglyceride/fatty acid cycle. *J Biol Chem,* 278**,** 30413-6.

REVANKAR, C. M., CIMINO, D. F., SKLAR, L. A., ARTERBURN, J. B. & PROSSNITZ, E. R. 2005. A transmembrane intracellular estrogen receptor mediates rapid cell signaling. *Science,* 307**,** 1625-30.

RHEE, S. G. 2001. Regulation of phosphoinositide-specific phospholipase C. *Annu Rev Biochem,* 70**,** 281-312.

ROGNE, M. & TASKEN, K. 2014. Compartmentalization of cAMP signaling in adipogenesis, lipogenesis, and lipolysis. *Horm Metab Res,* 46**,** 833-40.

ROHWEDDER, A., ZHANG, Q., RUDGE, S. A. & WAKELAM, M. J. 2014. Lipid droplet formation in response to oleic acid in Huh-7 cells is mediated by the fatty acid receptor FFAR4. *J Cell Sci,* 127**,** 3104-15.

RONDINI, E. A., MLADENOVIC-LUCAS, L., ROUSH, W. R., HALVORSEN, G. T., GREEN, A. E. & GRANNEMAN, J. G. 2017. Novel Pharmacological Probes Reveal ABHD5 as a Locus of Lipolysis Control in White and Brown Adipocytes. *J Pharmacol Exp Ther,* 363**,** 367-376.

ROSE, A. S., ELGETI, M., ZACHARIAE, U., GRUBMULLER, H., HOFMANN, K. P., SCHEERER, P. & HILDEBRAND, P. W. 2014. Position of transmembrane helix 6 determines receptor G protein coupling specificity. *J Am Chem Soc,* 136**,** 11244-7.

ROSENBAUM, D. M., ZHANG, C., LYONS, J. A., HOLL, R., ARAGAO, D., ARLOW, D. H., RASMUSSEN, S. G., CHOI, H. J., DEVREE, B. T., SUNAHARA, R. K., CHAE, P. S., GELLMAN, S. H., DROR, R. O., SHAW, D. E., WEIS, W. I., CAFFREY, M., GMEINER, P. & KOBILKA, B. K. 2011. Structure and function of an irreversible agonist-beta(2) adrenoceptor complex. *Nature,* 469**,** 236-40.

ROSS, E. M. 2008. Coordinating speed and amplitude in G-protein signaling. *Curr Biol,* 18**,** R777-R783.

ROWE, E. R., MIMMACK, M. L., BARBOSA, A. D., HAIDER, A., ISAAC, I., OUBERAI, M. M., THIAM, A. R., PATEL, S., SAUDEK, V., SINIOSSOGLOU, S. & SAVAGE, D. B. 2016. Conserved Amphipathic Helices Mediate Lipid Droplet Targeting of Perilipins 1-3. *J Biol Chem,* 291**,** 6664-78.

ROZENFELD, R. & DEVI, L. A. 2008. Regulation of CB1 cannabinoid receptor trafficking by the adaptor protein AP-3. *FASEB J,* 22**,** 2311-22.

RUOHONEN, S. T., VALVE, L., TUOMAINEN, K., AILANEN, L., ROYTTA, M., MANZ, G., BAUR, N., JOOS, T. O., SAVONTAUS, E. & SCHEININ, M. 2018. Increased Energy Expenditure, Lipolysis and Hyperinsulinemia Confer Resistance to Central Obesity and Type 2 Diabetes in Mice Lacking Alpha2alpha-Adrenoceptors. *Neuroendocrinology,* 107**,** 324-339.

SANCHEZ-REYES, O. B., ROMERO-AVILA, M. T., CASTILLO-BADILLO, J. A., TAKEI, Y., HIRASAWA, A., TSUJIMOTO, G., VILLALOBOS-MOLINA, R. & GARCIA-SAINZ, J. A. 2014. Free fatty acids and protein kinase C activation induce GPR120 (free fatty acid receptor 4) phosphorylation. *Eur J Pharmacol,* 723**,** 368-74.

SANDERS, M. A., MADOUX, F., MLADENOVIC, L., ZHANG, H., YE, X., ANGRISH, M., MOTTILLO, E. P., CARUSO, J. A., HALVORSEN, G., ROUSH, W. R., CHASE, P., HODDER, P. & GRANNEMAN, J. G. 2015. Endogenous and Synthetic ABHD5 Ligands Regulate ABHD5-Perilipin Interactions and Lipolysis in Fat and Muscle. *Cell Metab,* 22**,** 851-60.

SATAPATI, S., QIAN, Y., WU, M. S., PETROV, A., DAI, G., WANG, S. P., ZHU, Y., SHEN, X., MUISE, E. S., CHEN, Y., ZYCBAND, E., WEINGLASS, A., DI SALVO, J., DEBENHAM, J. S., COX, J. M., LAN, P., SHAH, V., PREVIS, S. F., ERION, M., KELLEY, D. E., WANG, L., HOWARD, A. D. & SHANG, J. 2017. GPR120 suppresses adipose tissue lipolysis and synergizes with GPR40 in antidiabetic efficacy. *J Lipid Res,* 58**,** 1561-1578.

SATO, T., MUSHIAKE, S., KATO, Y., SATO, K., SATO, M., TAKEDA, N., OZONO, K., MIKI, K., KUBO, Y., TSUJI, A., HARADA, R. & HARADA, A. 2007. The Rab8 GTPase regulates apical protein localization in intestinal cells. *Nature,* 448**,** 366-9.

SATOH, A. K., O'TOUSA, J. E., OZAKI, K. & READY, D. F. 2005. Rab11 mediates post-Golgi trafficking of rhodopsin to the photosensitive apical membrane of Drosophila photoreceptors. *Development,* 132**,** 1487-97.

SAYERS, N. S., ANUJAN, P., YU, H. N., PALMER, S. S., NAUTIYAL, J., FRANKS, S. & HANYALOGLU, A. C. 2021. Follicle-Stimulating Hormone Induces Lipid Droplets via Galphai/o and beta-Arrestin in an Endometrial Cancer Cell Line. *Front Endocrinol (Lausanne),* 12**,** 798866.

SCHILPEROORT, M., VAN DAM, A. D., HOEKE, G., SHABALINA, I. G., OKOLO, A., HANYALOGLU, A. C., DIB, L. H., MOL, I. M., CAENGPRASATH, N., CHAN, Y. W., DAMAK, S., MILLER, A. R., COSKUN, T., SHIMPUKADE, B., ULVEN, T., KOOIJMAN, S., RENSEN, P. C. & CHRISTIAN, M. 2018. The GPR120 agonist TUG-891 promotes metabolic health by stimulating mitochondrial respiration in brown fat. *EMBO Mol Med,* 10.

SCHOISWOHL, G., STEFANOVIC-RACIC, M., MENKE, M. N., WILLS, R. C., SURLOW, B. A., BASANTANI, M. K., SITNICK, M. T., CAI, L., YAZBECK, C. F., STOLZ, D. B., PULINILKUNNIL, T., O'DOHERTY, R. M. & KERSHAW, E. E. 2015. Impact of Reduced ATGL-Mediated Adipocyte Lipolysis on Obesity-Associated Insulin Resistance and Inflammation in Male Mice. *Endocrinology,* 156**,** 3610-24.

SEACHRIST, J. L. & FERGUSON, S. S. 2003. Regulation of G protein-coupled receptor endocytosis and trafficking by Rab GTPases. *Life Sci,* 74**,** 225-35.

SEKAR, R. B. & PERIASAMY, A. 2003. Fluorescence resonance energy transfer (FRET) microscopy imaging of live cell protein localizations. *J Cell Biol,* 160**,** 629-33.

SHENOY, S. K., DRAKE, M. T., NELSON, C. D., HOUTZ, D. A., XIAO, K., MADABUSHI, S., REITER, E., PREMONT, R. T., LICHTARGE, O. & LEFKOWITZ, R. J. 2006. beta-arrestin-dependent, G protein-independent ERK1/2 activation by the beta2 adrenergic receptor. *J Biol Chem,* 281**,** 1261-73.

SKINNER, J. R., HARRIS, L. A., SHEW, T. M., ABUMRAD, N. A. & WOLINS, N. E. 2013. Perilipin 1 moves between the fat droplet and the endoplasmic reticulum. *Adipocyte,* 2**,** 80-6.

SLAWIK, M. & VIDAL-PUIG, A. J. 2006. Lipotoxicity, overnutrition and energy metabolism in aging. *Ageing Res Rev,* 5**,** 144-64.

SLESSAREVA, J. E., ROUTT, S. M., TEMPLE, B., BANKAITIS, V. A. & DOHLMAN, H. G. 2006. Activation of the phosphatidylinositol 3-kinase Vps34 by a G protein alpha subunit at the endosome. *Cell,* 126**,** 191-203.

SNYDER, J. C., ROCHELLE, L. K., LYERLY, H. K., CARON, M. G. & BARAK, L. S. 2013. Constitutive internalization of the leucine-rich G protein-coupled receptor-5 (LGR5) to the trans-Golgi network. *J Biol Chem,* 288**,** 10286-97.

SONG, T., YANG, Y., ZHOU, Y., WEI, H. & PENG, J. 2017. GPR120: a critical role in adipogenesis, inflammation, and energy metabolism in adipose tissue. *Cell Mol Life Sci,* 74**,** 2723-2733.

SONG, T., ZHOU, Y., PENG, J., TAO, Y. X., YANG, Y., XU, T., PENG, J., REN, J., XIANG, Q. & WEI, H. 2016. GPR120 promotes adipogenesis through intracellular calcium and extracellular signal-regulated kinase 1/2 signal pathway. *Mol Cell Endocrinol,* 434**,** 1-13.

SORKIN, A. & VON ZASTROW, M. 2009. Endocytosis and signalling: intertwining molecular networks. *Nat Rev Mol Cell Biol,* 10**,** 609-22.

SPIEGEL, A. M., BACKLUND, P. S., BUTRYNSKI, J. E., JONES, T. L. Z. & SIMONDS, W. F. 1991. The G protein connection: molecular basis of membrane association. *Trends in Biochemical Sciences,* 16**,** 338-341.

SPOSINI, S., DE PASCALI, F., RICHARDSON, R., SAYERS, N. S., PERRAIS, D., YU, H. N., PALMER, S., NATARAJA, S., REITER, E. & HANYALOGLU, A. C. 2020. Pharmacological Programming of Endosomal Signaling Activated by Small Molecule Ligands of the Follicle Stimulating Hormone Receptor. *Front Pharmacol,* 11**,** 593492.

SPOSINI, S., JEAN-ALPHONSE, F. G., AYOUB, M. A., OQUA, A., WEST, C., LAVERY, S., BROSENS, J. J., REITER, E. & HANYALOGLU, A. C. 2017. Integration of GPCR Signaling and Sorting from Very Early Endosomes via Opposing APPL1 Mechanisms. *Cell Rep,* 21**,** 2855-2867.

SPRANG, S. R. 1997. G protein mechanisms: insights from structural analysis. *Annu Rev Biochem,* 66**,** 639-78.

SRIRAM, K. & INSEL, P. A. 2018. G Protein-Coupled Receptors as Targets for Approved Drugs: How Many Targets and How Many Drugs? *Mol Pharmacol,* 93**,** 251-258.

STAUS, D. P., WINGLER, L. M., STRACHAN, R. T., RASMUSSEN, S. G., PARDON, E., AHN, S., STEYAERT, J., KOBILKA, B. K. & LEFKOWITZ, R. J. 2014. Regulation of beta2-adrenergic receptor function by conformationally selective single-domain intrabodies. *Mol Pharmacol,* 85**,** 472-81.

STOCKLI, J., ZADOORIAN, A., COOKE, K. C., DESHPANDE, V., YAU, B., HERRMANN, G., KEBEDE, M. A., HUMPHREY, S. J. & JAMES, D. E. 2019. ABHD15 regulates adipose tissue lipolysis and hepatic lipid accumulation. *Mol Metab,* 25**,** 83-94.

STOEBER, M., JULLIE, D., LOBINGIER, B. T., LAEREMANS, T., STEYAERT, J., SCHILLER, P. W., MANGLIK, A. & VON ZASTROW, M. 2018. A Genetically Encoded Biosensor Reveals Location Bias of Opioid Drug Action. *Neuron,* 98**,** 963-976 e5.

STONE, V. M., DHAYAL, S., BROCKLEHURST, K. J., LENAGHAN, C., SORHEDE WINZELL, M., HAMMAR, M., XU, X., SMITH, D. M. & MORGAN, N. G. 2014. GPR120 (FFAR4) is preferentially expressed in pancreatic delta cells and regulates somatostatin secretion from murine islets of Langerhans. *Diabetologia,* 57**,** 1182-91.

STORCH, J. & CORSICO, B. 2008. The emerging functions and mechanisms of mammalian fatty acid-binding proteins. *Annu Rev Nutr,* 28**,** 73-95.

SU, Y., WALKER, J. R., PARK, Y., SMITH, T. P., LIU, L. X., HALL, M. P., LABANIEH, L., HURST, R., WANG, D. C., ENCELL, L. P., KIM, N., ZHANG, F., KAY, M. A., CASEY, K. M., MAJZNER, R. G., COCHRAN, J. R., MACKALL, C. L., KIRKLAND, T. A. & LIN, M. Z. 2020. Novel NanoLuc substrates enable bright two-population bioluminescence imaging in animals. *Nat Methods,* 17**,** 852-860.

SUCKOW, A. T., POLIDORI, D., YAN, W., CHON, S., MA, J. Y., LEONARD, J. & BRISCOE, C. P. 2014. Alteration of the glucagon axis in GPR120 (FFAR4) knockout mice: a role for GPR120 in glucagon secretion. *J Biol Chem,* 289**,** 15751-63.

SUN, D., FLOCK, T., DEUPI, X., MAEDA, S., MATKOVIC, M., MENDIETA, S., MAYER, D., DAWSON, R., SCHERTLER, G. F. X., MADAN BABU, M. & VEPRINTSEV, D. B. 2015. Probing Galphai1 protein activation at single-amino acid resolution. *Nat Struct Mol Biol,* 22**,** 686-694.

SUN, D., OSTERMAIER, M. K., HEYDENREICH, F. M., MAYER, D., JAUSSI, R., STANDFUSS, J. & VEPRINTSEV, D. B. 2013. AAscan, PCRdesign and MutantChecker: a suite of programs for primer design and sequence analysis for high-throughput scanning mutagenesis. *PLoS One,* 8**,** e78878.

SUNAHARA, R. K. & TAUSSIG, R. 2002. Isoforms of mammalian adenylyl cyclase: multiplicities of signaling. *Mol Interv,* 2**,** 168-84.

SUOFU, Y., LI, W., JEAN-ALPHONSE, F. G., JIA, J., KHATTAR, N. K., LI, J., BARANOV, S. V., LERONNI, D., MIHALIK, A. C., HE, Y., CECON, E., WEHBI, V. L., KIM, J., HEATH, B. E., BARANOVA, O. V., WANG, X., GABLE, M. J., KRETZ, E. S., DI BENEDETTO, G., LEZON, T. R., FERRANDO, L. M., LARKIN, T. M., SULLIVAN, M., YABLONSKA, S., WANG, J., MINNIGH, M. B., GUILLAUMET, G., SUZENET, F., RICHARDSON, R. M., POLOYAC, S. M., STOLZ, D. B., JOCKERS, R., WITT-ENDERBY, P. A., CARLISLE, D. L., VILARDAGA, J. P. & FRIEDLANDER, R. M. 2017. Dual role of mitochondria in producing melatonin and driving GPCR signaling to block cytochrome c release. *Proc Natl Acad Sci U S A,* 114**,** E7997-E8006.

SUSTARSIC, E. G., MA, T., LYNES, M. D., LARSEN, M., KARAVAEVA, I., HAVELUND, J. F., NIELSEN, C. H., JEDRYCHOWSKI, M. P., MORENO-TORRES, M., LUNDH, M., PLUCINSKA, K., JESPERSEN, N. Z., GREVENGOED, T. J., KRAMAR, B., PEICS, J., HANSEN, J. B., SHAMSI, F., FORSS, I., NEESS, D., KEIPERT, S., WANG, J., STOHLMANN, K., BRANDSLUND, I., CHRISTENSEN, C., JORGENSEN, M. E., LINNEBERG, A., PEDERSEN, O., KIEBISH, M. A., QVORTRUP, K., HAN, X., PEDERSEN, B. K., JASTROCH, M., MANDRUP, S., KJAER, A., GYGI, S. P., HANSEN, T., GILLUM, M. P., GRARUP, N., EMANUELLI, B., NIELSEN, S., SCHEELE, C., TSENG, Y. H., FAERGEMAN, N. J. & GERHART-HINES, Z. 2018. Cardiolipin Synthesis in Brown and Beige Fat Mitochondria Is Essential for Systemic Energy Homeostasis. *Cell Metab,* 28**,** 159-174 e11.

SYROVATKINA, V., ALEGRE, K. O., DEY, R. & HUANG, X. Y. 2016. Regulation, Signaling, and Physiological Functions of G-Proteins. *J Mol Biol,* 428**,** 3850-68.

SZTALRYD, C. & BRASAEMLE, D. L. 2017. The perilipin family of lipid droplet proteins: Gatekeepers of intracellular lipolysis. *Biochim Biophys Acta Mol Cell Biol Lipids,* 1862**,** 1221-1232.

TADEVOSYAN, A., VILLENEUVE, L. R., FOURNIER, A., CHATENET, D., NATTEL, S. & ALLEN, B. G. 2016. Caged ligands to study the role of intracellular GPCRs. *Methods,* 92**,** 72-7.

TAGGART, A. K., KERO, J., GAN, X., CAI, T. Q., CHENG, K., IPPOLITO, M., REN, N., KAPLAN, R., WU, K., WU, T. J., JIN, L., LIAW, C., CHEN, R., RICHMAN, J., CONNOLLY, D., OFFERMANNS, S.,

WRIGHT, S. D. & WATERS, M. G. 2005. (D)-beta-Hydroxybutyrate inhibits adipocyte lipolysis via the nicotinic acid receptor PUMA-G. *J Biol Chem,* 280**,** 26649-52.

TANAKA, T., YANO, T., ADACHI, T., KOSHIMIZU, T. A., HIRASAWA, A. & TSUJIMOTO, G. 2008. Cloning and characterization of the rat free fatty acid receptor GPR120: in vivo effect of the natural ligand on GLP-1 secretion and proliferation of pancreatic beta cells. *Naunyn Schmiedebergs Arch Pharmacol,* 377**,** 515-22.

TANG, C., AHMED, K., GILLE, A., LU, S., GRONE, H. J., TUNARU, S. & OFFERMANNS, S. 2015. Loss of FFA2 and FFA3 increases insulin secretion and improves glucose tolerance in type 2 diabetes. *Nat Med,* 21**,** 173-7.

TASCHLER, U., RADNER, F. P., HEIER, C., SCHREIBER, R., SCHWEIGER, M., SCHOISWOHL, G., PREISS-LANDL, K., JAEGER, D., REITER, B., KOEFELER, H. C., WOJCIECHOWSKI, J., THEUSSL, C., PENNINGER, J. M., LASS, A., HAEMMERLE, G., ZECHNER, R. & ZIMMERMANN, R. 2011. Monoglyceride lipase deficiency in mice impairs lipolysis and attenuates diet-induced insulin resistance. *J Biol Chem,* 286**,** 17467-77.

TEHAN, B. G., BORTOLATO, A., BLANEY, F. E., WEIR, M. P. & MASON, J. S. 2014. Unifying family A GPCR theories of activation. *Pharmacol Ther,* 143**,** 51-60.

TERRILLON, S. & BOUVIER, M. 2004. Receptor activity-independent recruitment of betaarrestin2 reveals specific signalling modes. *EMBO J,* 23**,** 3950-61.

THOMSEN, A. R. B., PLOUFFE, B., CAHILL, T. J., 3RD, SHUKLA, A. K., TARRASCH, J. T., DOSEY, A. M., KAHSAI, A. W., STRACHAN, R. T., PANI, B., MAHONEY, J. P., HUANG, L., BRETON, B., HEYDENREICH, F. M., SUNAHARA, R. K., SKINIOTIS, G., BOUVIER, M. & LEFKOWITZ, R. J. 2016. GPCR-G Protein-beta-Arrestin Super-Complex Mediates Sustained G Protein Signaling. *Cell,* 166**,** 907-919.

TIULPAKOV, A., WHITE, C. W., ABHAYAWARDANA, R. S., SEE, H. B., CHAN, A. S., SEEBER, R. M., HENG, J. I., DEDOV, I., PAVLOS, N. J. & PFLEGER, K. D. 2016. Mutations of Vasopressin Receptor 2 Including Novel L312S Have Differential Effects on Trafficking. *Mol Endocrinol,* 30**,** 889-904.

TOHGO, A., CHOY, E. W., GESTY-PALMER, D., PIERCE, K. L., LAPORTE, S., OAKLEY, R. H., CARON, M. G., LEFKOWITZ, R. J. & LUTTRELL, L. M. 2003. The stability of the G protein-coupled receptor-beta-arrestin interaction determines the mechanism and functional consequence of ERK activation. *J Biol Chem,* 278**,** 6258-67.

TOHGO, A., PIERCE, K. L., CHOY, E. W., LEFKOWITZ, R. J. & LUTTRELL, L. M. 2002. beta-Arrestin scaffolding of the ERK cascade enhances cytosolic ERK activity but inhibits ERK-mediated transcription following angiotensin AT1a receptor stimulation. *J Biol Chem,* 277**,** 9429-36.

TOWER-GILCHRIST, C., LEE, E. & SZTUL, E. 2011. Endosomal trafficking of the G protein-coupled receptor somatostatin receptor 3. *Biochem Biophys Res Commun,* 413**,** 555-60.

TRAUT, T. W. 1994. Physiological concentrations of purines and pyrimidines. *Mol Cell Biochem,* 140**,** 1-22.

TSVETANOVA, N. G. & VON ZASTROW, M. 2014. Spatial encoding of cyclic AMP signaling specificity by GPCR endocytosis. *Nat Chem Biol,* 10**,** 1061-5.

TUNARU, S., KERO, J., SCHAUB, A., WUFKA, C., BLAUKAT, A., PFEFFER, K. & OFFERMANNS, S. 2003. PUMA-G and HM74 are receptors for nicotinic acid and mediate its anti-lipolytic effect. *Nat Med,* 9**,** 352-5.

UCHIKAWA, E., CHOI, E., SHANG, G., YU, H. & BAI, X. C. 2019. Activation mechanism of the insulin receptor revealed by cryo-EM structure of the fully liganded receptor-ligand complex. *Elife,* 8.

VADAS, O., DBOUK, H. A., SHYMANETS, A., PERISIC, O., BURKE, J. E., ABI SAAB, W. F., KHALIL, B. D., HARTENECK, C., BRESNICK, A. R., NURNBERG, B., BACKER, J. M. & WILLIAMS, R. L. 2013. Molecular determinants of PI3Kgamma-mediated activation downstream of G-protein-coupled receptors (GPCRs). *Proc Natl Acad Sci U S A,* 110**,** 18862-7.

VALM, A. M., COHEN, S., LEGANT, W. R., MELUNIS, J., HERSHBERG, U., WAIT, E., COHEN, A. R., DAVIDSON, M. W., BETZIG, E. & LIPPINCOTT-SCHWARTZ, J. 2017. Applying systems-level spectral imaging and analysis to reveal the organelle interactome. *Nature,* 546**,** 162-167.

VAN EPS, N., PREININGER, A. M., ALEXANDER, N., KAYA, A. I., MEIER, S., MEILER, J., HAMM, H. E. & HUBBELL, W. L. 2011. Interaction of a G protein with an activated receptor opens the interdomain interface in the alpha subunit. *Proc Natl Acad Sci U S A,* 108**,** 9420-4.

VAUGHAN, M., BERGER, J. E. & STEINBERG, D. 1964. Hormone-Sensitive Lipase and Monoglyceride Lipase Activities in Adipose Tissue. *J Biol Chem,* 239**,** 401-9.

VILLENA, J. A., ROY, S., SARKADI-NAGY, E., KIM, K. H. & SUL, H. S. 2004. Desnutrin, an adipocyte gene encoding a novel patatin domain-containing protein, is induced by fasting and glucocorticoids: ectopic expression of desnutrin increases triglyceride hydrolysis. *J Biol Chem,* 279**,** 47066-75.

VINCENT, K., CORNEA, V. M., JONG, Y. I., LAFERRIERE, A., KUMAR, N., MICKEVICIUTE, A., FUNG, J. S. T., BANDEGI, P., RIBEIRO-DA-SILVA, A., O'MALLEY, K. L. & CODERRE, T. J. 2016. Intracellular mGluR5 plays a critical role in neuropathic pain. *Nat Commun,* 7**,** 10604.

VLIEM, M. J., PONSIOEN, B., SCHWEDE, F., PANNEKOEK, W. J., RIEDL, J., KOOISTRA, M. R., JALINK, K., GENIESER, H. G., BOS, J. L. & REHMANN, H. 2008. 8-pCPT-2'-O-Me-cAMP-AM: an improved Epac-selective cAMP analogue. *Chembiochem,* 9**,** 2052-4.

WACKER, D., STEVENS, R. C. & ROTH, B. L. 2017. How Ligands Illuminate GPCR Molecular Pharmacology. *Cell,* 170**,** 414-427.

WAN, Q., OKASHAH, N., INOUE, A., NEHME, R., CARPENTER, B., TATE, C. G. & LAMBERT, N. A. 2018. Mini G protein probes for active G protein-coupled receptors (GPCRs) in live cells. *J Biol Chem,* 293**,** 7466-7473.

WANG, G., WEI, Z. & WU, G. 2018a. Role of Rab GTPases in the export trafficking of G protein-coupled receptors. *Small GTPases,* 9**,** 130-135.

WANG, G. & WU, G. 2012. Small GTPase regulation of GPCR anterograde trafficking. *Trends Pharmacol Sci,* 33**,** 28-34.

WANG, H., SREENIVASAN, U., HU, H., SALADINO, A., POLSTER, B. M., LUND, L. M., GONG, D. W., STANLEY, W. C. & SZTALRYD, C. 2011. Perilipin 5, a lipid droplet-associated protein, provides physical and metabolic linkage to mitochondria. *J Lipid Res,* 52**,** 2159-2168.

WANG, J., WU, X., SIMONAVICIUS, N., TIAN, H. & LING, L. 2006. Medium-chain fatty acids as ligands for orphan G protein-coupled receptor GPR84. *J Biol Chem,* 281**,** 34457-64.

WANG, M., ZHANG, X., MA, L. J., FENG, R. B., YAN, C., SU, H., HE, C., KANG, J. X., LIU, B. & WAN, J. B. 2017. Omega-3 polyunsaturated fatty acids ameliorate ethanol-induced adipose hyperlipolysis: A mechanism for hepatoprotective effect against alcoholic liver disease. *Biochim Biophys Acta Mol Basis Dis,* 1863**,** 3190-3201.

WANG, Q., ZHANG, H., XU, H., GUO, D., SHI, H., LI, Y., ZHANG, W. & GU, Y. 2016. 5-HTR3 and 5-HTR4 located on the mitochondrial membrane and functionally regulated mitochondrial functions. *Sci Rep,* 6**,** 37336.

WANG, Y. M., LIU, H. X. & FANG, N. Y. 2018b. 9-PAHSA promotes browning of white fat via activating G-protein-coupled receptor 120 and inhibiting lipopolysaccharide / NF-kappa B pathway. *Biochem Biophys Res Commun,* 506**,** 153-160.

WATSON, S. J., BROWN, A. J. & HOLLIDAY, N. D. 2012. Differential signaling by splice variants of the human free fatty acid receptor GPR120. *Mol Pharmacol,* 81**,** 631-42.

WATTERSON, K. R., HANSEN, S. V. F., HUDSON, B. D., ALVAREZ-CURTO, E., RAIHAN, S. Z., AZEVEDO, C. M. G., MARTIN, G., DUNLOP, J., YARWOOD, S. J., ULVEN, T. & MILLIGAN, G. 2017. Probe-Dependent Negative Allosteric Modulators of the Long-Chain Free Fatty Acid Receptor FFA4. *Mol Pharmacol,* 91**,** 630-641.

WATTS, V. J. & NEVE, K. A. 2005. Sensitization of adenylate cyclase by Galpha i/o-coupled receptors. *Pharmacol Ther,* 106**,** 405-21.

WEI, Z., ZHANG, M., LI, C., HUANG, W., FAN, Y., GUO, J., KHATER, M., FUKUDA, M., DONG, Z., HU, G. & WU, G. 2019. Specific TBC Domain-Containing Proteins Control the ER-Golgi-Plasma Membrane Trafficking of GPCRs. *Cell Rep,* 28**,** 554-566 e4.

WEIS, W. I. & KOBILKA, B. K. 2018. The Molecular Basis of G Protein-Coupled Receptor Activation. *Annu Rev Biochem,* 87**,** 897-919.

WHITE, A. D., JEAN-ALPHONSE, F. G., FANG, F., PENA, K. A., LIU, S., KONIG, G. M., INOUE, A., ASLANOGLOU, D., GELLMAN, S. H., KOSTENIS, E., XIAO, K. & VILARDAGA, J. P. 2020. Gq/11-dependent regulation of endosomal cAMP generation by parathyroid hormone class B GPCR. *Proc Natl Acad Sci U S A,* 117**,** 7455-7460.

WHITE, C. W., VANYAI, H. K., SEE, H. B., JOHNSTONE, E. K. M. & PFLEGER, K. D. G. 2017. Using nanoBRET and CRISPR/Cas9 to monitor proximity to a genome-edited protein in real-time. *Sci Rep,* 7**,** 3187.

WILSON, P. A., GARDNER, S. D., LAMBIE, N. M., COMMANS, S. A. & CROWTHER, D. J. 2006. Characterization of the human patatin-like phospholipase family. *J Lipid Res,* 47**,** 1940-9.

WRIGHT, S. C., LUKASHEVA, V., LE GOUILL, C., KOBAYASHI, H., BRETON, B., MAILHOT-LAROUCHE, S., BLONDEL-TEPAZ, E., ANTUNES VIEIRA, N., COSTA-NETO, C., HEROUX, M., LAMBERT, N. A., PARREIRAS, E. S. L. T. & BOUVIER, M. 2021. BRET-based effector membrane translocation assay monitors GPCR-promoted and endocytosis-mediated Gq activation at early endosomes. *Proc Natl Acad Sci U S A,* 118.

WRZOSEK, M., ZAWADZKA, Z., SAWICKA, A., BOBROWSKA-KORCZAK, B. & BIALEK, A. 2022. Impact of Fatty Acids on Obesity-Associated Diseases and Radical Weight Reduction. *Obes Surg,* 32**,** 428-440.

WU, G., ZHAO, G. & HE, Y. 2003. Distinct pathways for the trafficking of angiotensin II and adrenergic receptors from the endoplasmic reticulum to the cell surface: Rab1-independent transport of a G protein-coupled receptor. *J Biol Chem,* 278**,** 47062-9.

WU, J., BOSTROM, P., SPARKS, L. M., YE, L., CHOI, J. H., GIANG, A. H., KHANDEKAR, M., VIRTANEN, K. A., NUUTILA, P., SCHAART, G., HUANG, K., TU, H., VAN MARKEN LICHTENBELT, W. D., HOEKS, J., ENERBACK, S., SCHRAUWEN, P. & SPIEGELMAN, B. M. 2012. Beige adipocytes are a distinct type of thermogenic fat cell in mouse and human. *Cell,* 150**,** 366-76.

XIA, W., PESSENTHEINER, A. R., HOFER, D. C., AMOR, M., SCHREIBER, R., SCHOISWOHL, G., EICHMANN, T. O., WALENTA, E., ITARIU, B., PRAGER, G., HACKL, H., STULNIG, T., KRATKY, D., RULICKE, T. & BOGNER-STRAUSS, J. G. 2018. Loss of ABHD15 Impairs the Anti-lipolytic Action of Insulin by Altering PDE3B Stability and Contributes to Insulin Resistance. *Cell Rep,* 23**,** 1948-1961.

XU, F., WU, H., KATRITCH, V., HAN, G. W., JACOBSON, K. A., GAO, Z. G., CHEREZOV, V. & STEVENS, R. C. 2011. Structure of an agonist-bound human A2A adenosine receptor. *Science,* 332**,** 322-7.

YAMADA, H., UMEMOTO, T., KAKEI, M., MOMOMURA, S. I., KAWAKAMI, M., ISHIKAWA, S. E. & HARA, K. 2017. Eicosapentaenoic acid shows anti-inflammatory effect via GPR120 in 3T3-L1 adipocytes and attenuates adipose tissue inflammation in diet-induced obese mice. *Nutr Metab (Lond),* 14**,** 33.

YANG, A. & MOTTILLO, E. P. 2020. Adipocyte lipolysis: from molecular mechanisms of regulation to disease and therapeutics. *Biochem J,* 477**,** 985-1008.

YANG, J., CUMBERBATCH, D., CENTANNI, S., SHI, S. Q., WINDER, D., WEBB, D. & JOHNSON, C. H. 2016. Coupling optogenetic stimulation with NanoLuc-based luminescence (BRET) Ca(++) sensing. *Nat Commun,* 7**,** 13268.

YANG, L., DING, Y., CHEN, Y., ZHANG, S., HUO, C., WANG, Y., YU, J., ZHANG, P., NA, H., ZHANG, H., MA, Y. & LIU, P. 2012. The proteomics of lipid droplets: structure, dynamics, and functions of the organelle conserved from bacteria to humans. *J Lipid Res,* 53**,** 1245-53.

YARWOOD, R. E., IMLACH, W. L., LIEU, T., VELDHUIS, N. A., JENSEN, D. D., KLEIN HERENBRINK, C., AURELIO, L., CAI, Z., CHRISTIE, M. J., POOLE, D. P., PORTER, C. J. H., MCLEAN, P., HICKS, G. A., GEPPETTI, P., HALLS, M. L., CANALS, M. & BUNNETT, N. W. 2017. Endosomal signaling of the

receptor for calcitonin gene-related peptide mediates pain transmission. *Proc Natl Acad Sci U S A,* 114, **12309-12314**.

YIN, H., LI, Q., QIAN, G., WANG, Y., LI, Y., WU, G. & WANG, G. 2011. Rab1 GTPase regulates phenotypic modulation of pulmonary artery smooth muscle cells by mediating the transport of angiotensin II type 1 receptor under hypoxia. *Int J Biochem Cell Biol,* 43, **401-8**.

YUDOWSKI, G. A., PUTHENVEEDU, M. A., HENRY, A. G. & VON ZASTROW, M. 2009. Cargo-mediated regulation of a rapid Rab4-dependent recycling pathway. *Mol Biol Cell,* 20, **2774-84**.

ZACCOLO, M., DE GIORGI, F., CHO, C. Y., FENG, L., KNAPP, T., NEGULESCU, P. A., TAYLOR, S. S., TSIEN, R. Y. & POZZAN, T. 2000. A genetically encoded, fluorescent indicator for cyclic AMP in living cells. *Nat Cell Biol,* 2, **25-9**.

ZACHARIAS, D. A., VIOLIN, J. D., NEWTON, A. C. & TSIEN, R. Y. 2002. Partitioning of lipid-modified monomeric GFPs into membrane microdomains of live cells. *Science,* 296, **913-6**.

ZAIBI, M. S., STOCKER, C. J., O'DOWD, J., DAVIES, A., BELLAHCENE, M., CAWTHORNE, M. A., BROWN, A. J., SMITH, D. M. & ARCH, J. R. 2010. Roles of GPR41 and GPR43 in leptin secretory responses of murine adipocytes to short chain fatty acids. *FEBS Lett,* 584, **2381-6**.

ZECHNER, R., ZIMMERMANN, R., EICHMANN, T. O., KOHLWEIN, S. D., HAEMMERLE, G., LASS, A. & MADEO, F. 2012. FAT SIGNALS--lipases and lipolysis in lipid metabolism and signaling. *Cell Metab,* 15, **279-91**.

ZEHMER, J. K., HUANG, Y., PENG, G., PU, J., ANDERSON, R. G. & LIU, P. 2009. A role for lipid droplets in inter-membrane lipid traffic. *Proteomics,* 9, **914-21**.

ZHANG, D. & LEUNG, P. S. 2014. Potential roles of GPR120 and its agonists in the management of diabetes. *Drug Des Devel Ther,* 8, **1013-27**.

ZHANG, D., ZHAO, Q. & WU, B. 2015. Structural Studies of G Protein-Coupled Receptors. *Mol Cells,* 38, **836-42**.

ZHANG, J. & LIU, F. 2014. Tissue-specific insulin signaling in the regulation of metabolism and aging. *IUBMB Life,* 66, **485-95**.

ZHANG, J., MA, Y., TAYLOR, S. S. & TSIEN, R. Y. 2001. Genetically encoded reporters of protein kinase A activity reveal impact of substrate tethering. *Proc Natl Acad Sci U S A,* 98, **14997-5002**.

ZHANG, X., WANG, G., DUPRE, D. J., FENG, Y., ROBITAILLE, M., LAZARTIGUES, E., FENG, Y. H., HEBERT, T. E. & WU, G. 2009. Rab1 GTPase and dimerization in the cell surface expression of angiotensin II type 2 receptor. *J Pharmacol Exp Ther,* 330, **109-17**.

ZHUANG, X., ADIPIETRO, K. A., DATTA, S., NORTHUP, J. K. & RAY, K. 2010. Rab1 small GTP-binding protein regulates cell surface trafficking of the human calcium-sensing receptor. *Endocrinology,* 151, **5114-23**.

ZIMMERMANN, R., STRAUSS, J. G., HAEMMERLE, G., SCHOISWOHL, G., BIRNER-GRUENBERGER, R., RIEDERER, M., LASS, A., NEUBERGER, G., EISENHABER, F., HERMETTER, A. & ZECHNER, R. 2004. Fat mobilization in adipose tissue is promoted by adipose triglyceride lipase. *Science,* 306, **1383-6**.

7.0 Chapter seven: Appendices

7.1 Cloning primers

Primer sequence	Direction	Template	Features	Reason	Construct	Cloning method
ccgtcaggatccgcc accatggactacaag gac	Forward	FFAR4-eYFP	BamHI EcoRI and stop codon (TAG)	Cloning FFAR4 in pcDNA3	WT FFAR4	Cut and paste
tcgggcgaattccta gccagaaataatcga caagtc	Reverse					
taagcagaattcgcc gccatggtcttcacac tcgaagat	Forward	Nluc-miniGαi	EcoRI XhoI and stop codon (TAA)	Cloning NLuc onto FFAR4 (wild type)	FFAR4-NLuc	Cut and paste
cgacaactcgagtta cgccagaatgcgttc gca	Reverse					
gaattcgccgccatg gtc	Forward	FFAR4-NLuc		Mutate FFAR4 stop codon (TAG-TCG)	FFAR4-NLuc	Mutagen esis
gccagaaataatcga caagtcatttc	Reverse					
accataagcttaagt ttaaacgctagccag cttgg	Forward	PDE2A3-CAMYEL	GGSGG linker	Cloning CAMYEL-Sec61β	Camyel-Sec61β (ER cAMP sensor)	Gibson assembly
gttcgtaggcgccgc tcgagtctagagggc ccgtttaaac	Reverse					
ttaaacttaagcttat ggtgagcaagggcg aggagc	Forward	PDE2A3-CAMYEL				
tgccaccgctgccac cctgctcgttcttcag cactctctcc	Reverse					
tcgagcggcgcctac gaacgagtgtacttg ccccaaatg	Forward	mCherry-Sec61β				
gttcgtaggcgccgc tcgagtctagagggc ccgtttaaac	Reverse					
accataagcttaagt ttaaacgctagccag cttgg	Forward	PDE2A3-CAMYEL	GGSGG linker	Cloning CAMYEL-Rab1a	CAMYEL-Rab1a (ER	Gibson assembly

tgctaagcgccgctc gagtctagagggccc gtttaaac	Reverse			cAMP sensor)	
ttaaacttaagcttat ggtgagcaagggcg aggagc	Forward	PDE2A3-CAMYEL			
atgctggacatgcca ccgctgccaccctgct cgttcttcagcactct ctcc	Reverse				
gcggtggcatgtcca gcatgaatcccgaat atgattatttattcaa gttac	Forward	Venus-Rab1a			
actcgagcggcgctt agcagcaacctccac ctgactgc	Reverse				
gcttccaccatggca gtcaacaaaggcctc accttg	Forward	PLIN1-CAMYEL	GGSGG linker	Cloning PLIN1-NLuc-Epac-VV	PLIN1-NLuc-Epac-VV (Lipid droplet cAMP sensor)	Gibson assembly
agtgtgaagaccatg ccaccgctgccaccg ctc	Reverse				
tgactgccatggtgg aagctgggtctccct atag	Forward	NLuc-Epac-VV			
gtggcatggtcttcac actcgaagatttcgtt gg	Reverse				
gcgcgcctcggtggc agcggtggcatgcct g	Forward	CAMYEL-Sec61β	GGSGG linker	Cloning NLuc-Epac-VV-Sec61β	NLuc-Epac-VV-Sec61β (ER cAMP sensor)	Gibson assembly
gccctctagactacg aacgagtgtacttgc cccaaatg	Reverse				
cgctgccaccgaggc gcgccgcgttaacct c	Forward	NLuc-Epac-VV			
cgttcgtagtctaga gggccctattctatag tgtcacc	Reverse				
caagcttccaccatg gggcaggcatgcgg ccac	Forward	PDE2A3-CAMYEL	GGSGG linker	Cloning PDE2A3-	PDE2A3-NLuc-Epac-VV	Gibson assembly

Primer	Direction					
gtgtgaagaccatgc caccgctgccaccctt gtac	Reverse			NLuc-Epac-VV	(Plasma membrane cAMP sensor)	
gccccatggtggaag cttgggtctccctata g	Forward	NLuc-Epac-VV				
ggtggcatggtcttca cactcgaagatttcgt tgg	Reverse					
ggtatgatcctctggc atgagatgtggcatg aag	Forward	FRB-Nb80	DSAGAGG linker			
gatttctgctccacca gcactaccagcacta tcc	Reverse			Cloning Halo-FRB-mGα	Halo-FRB-mGα	Gibson assembly
gccagaggatcatac cggtagcgctagcgg atc	Forward	Halo-mGαi/o/s/q				
tggtggagcagaaat cggtactggctttcca ttcg	Reverse					
ctggtggaatggtctt cacactcgaagattt cgttgg	Forward	FFAR4-NLuc				
tgagtccggacgcca gaatgcgttcgcaca gc	Reverse			Cloning NLuc-FRB-mGα	NLuc-FRB-mGα	Gibson assembly
gtgaagaccattcca ccagcactaccagca ctatcc	Forward	Halo-mGαi/o/s/q				
attctggcgtccgga ctcagatctcgagct gg	Reverse					
taagcaggatccgcc accatgggagtgcag tgcttatgtacacctc	Forward	FKBP-GalT	BamHI	Cloning FKBP-K-ras	FKBP-K-ras	Cut and paste
cagcttcagcagctc	Reverse		BsrGI-HF			
cactcccatggtgga agcttgggtctcccta tag	Forward	NLuc-Epac-VV-Sec61β	GGSGG linker			
ttccaccatgggagt gcaggtggaaaccat ctcc	Reverse			Cloning FKBP-Sec61β	FKBP-Sec61β	Gibson assembly
cactcccatggtgga agcttgggtctcccta tag	Forward	FKBP-GalT				

agctggagggtggca gcggtggcatgcctg	Reverse					235
ggtggcatggcagtc aacaaaggcctcacc ttg	Forward	PLIN1- NLuc- Epac-VV	GGSGG linker	Cloning FKBP- PLIN1	FKBP- PLIN1	Gibson assembly
gccctctagactagct cttcttgcgcagctgg ctg	Reverse					
tgttgactgccatgcc accgctgccaccctc c	Forward	FKBP- Sec61β				
aagagctagtctaga gggccctattctatag tgtc	Reverse					

Table 7. 1: List of cloning primers